EXPERIMENTAL HYDRODYNAMIC STUDY OF A NOVEL GLOBE-SHAPED SUBMERSIBLE FISH CAGE SYSTEM

WEN JIE ZHENG, B.Eng.

EXPERIMENTAL HYDRODYNAMIC STUDY OF A NOVEL GLOBE-SHAPED SUBMERSIBLE FISH CAGE SYSTEM

BY

©WEN JIE ZHENG, B. ENG.

A THESIS SUBMITTED TO THE SCHOOL OF GRADUATE STUDIES IN PARTIAL FULFILMENT OF THE REQUIREMENTS FOR THE DEGREE OF MASTER OF ENGINEERING

FACULTY OF ENGINEERING AND APPLIED SCIENCE

MEMORIAL UNIVERSITY OF NEWFOUNDLAND

OCTOBER, 1991

ST. JOHN'S NEWFOUNDLAND CANADA

ISBN 0-315-73295-4

ABSTRACT

In order to meet the increasing requirement of farming fish in more exposed offshore sites, a novel globe-shaped submersible fish cage system with two tension mooring lines has been proposed. In normal sea conditions the cage remains on the surface; during storms the cage can be submerged some distance below the water surface to reduce the wave forces and motions of the cage and hence reduce the forces in the mooring system and the stress on the farmed fish. Since the proposed system is a quite new design concept, few theoretical and experimental results can be found to guide the prototype design.

To have a better understanding of the hydrodynamic performance of the proposed system, qualitative analyses were conducted and a series of resistance tests and moored tests were carried out with two globe-shaped cage models, one spherical and the other geodesic, to study the resistance forces of the cages in currents and the motion and mooring force responses of the cage system in waves. In the resistance tests, three orientations of the cage axle to the current direction were tested. In the moored tests, three submerged positions and three orientations were tested and the effects of pretension and axial stiffness of the mooring lines were

investigated in both regular waves and irregular waves.

The study shows that the relationship between the current velocity and the resultant resistance force can be interpolated very well with a quadratic equation regressed from the test results. Provided the Reynolds numbers of the cage elements are still within the range of subcritical flow regime, the regressed equation can also be used to extrapolate the resistance force outside the Reynolds number range tested.

The study also shows that the method of submerging the cage below the water surface to reduce the motions of the cage and the forces in the mooring system is very effective in deep water waves, but becomes less and less effective in intermediate water waves. The pretension of the mooring lines has little effect on the dynamic mooring force and motion responses of the cage system as long as the mooring lines do not go slack. The stiffness of the mooring lines has a significant effect on the responses of mooring force, heave and roll, but has little effect on the responses of surge and sway. When the cage is perpendicular to the wavefront, the vertical displacement and mooring force on one side of the cage may be significantly larger than those on the other side because of the phase difference between the heave and roll motions of the cage.

ACKNOWLEDGEMENTS

First of all, I would like to thank Dr. J.H. Allen for his excellent supervision and guidance throughout my whole study and the support he provided all the time.

I would also like to thank Dr. C.A. Sharpe, the Associate Dean of the School of Graduate Studies; Dr. G.R. Peters, the Dean of Faculty of Engineering and Dr. T.R. Chari, the Associate Dean of Faculty of Engineering for the financial aids of Graduate Fellowship and Teaching Assistantships which made this study possible.

Furthermore, I wish to say special thank you to Dr. D.B. Muggeridge, the Director of Ocean Engineering Research Centre for our long discussions which proved to be very helpful; and to Mr. L. Little and Mr. A. Kuczora of the Ocean Engineering Research Centre for their patience and invaluable assistance all the time during the experiment.

Finally, I wish to thank my parents for their love and encouragement.

CONTENTS

ABSTRACT ii

ACKNOWLEDGEMENTS iv

LIST OF TABLES viii

LIST OF FIGURES ix

DEFINITION OF SYMBOLS USED xvi

1 INTRODUCTION 1

2 REVIEW OF LITERATURE 10

3 THEORETICAL BACKGROUND 15

3.1 Variation of Wave Motion with Depth below Water Surface and its Effect on Submersible Fish Cage 15

3.2 Motion and Mooring Force Responses of the Moored Cage to Wave Action 23

3.2.1 Motion response 23

3.2.2 Mooring force response 32

3.3 Hydraulic Modelling 34

3.3.1 Resistance tests 35

3.3.2 Moored tests 40

3.3.3 Selection of a proper model net 41

4 EXPERIMENTAL STUDY 45

4.1 Test Facility and Models 45

4.1.1 Wave/tow tank 45

4.1.2 Spherical and geodesic models 47
4.1.3 Model net 49
4.1.4 Mooring system 51
4.2 Resistance Tests 52
4.2.1 Experimental arrangement 52
4.2.2 Instrumentation and data acquisition 54
4.2.3 Experimental procedure 56
4.2.4 Method of data analysis 57
4.3 Moored Tests 59
4.3.1 Experimental arrangement 59
4.3.2 Instrumentation and data acquisition 60
4.3.3 Experimental procedure 65
4.3.4 Method of data analysis 68

5 EXPERIMENTAL RESULTS AND DISCUSSIONS 72
5.1 Resistance Tests 72
5.1.1 Resistance forces of the models 72
5.1.2 Application of the model test results to prototype 81
5.2 Moored Tests 88
5.2.1 Motion responses 91
5.2.2 Mooring force responses 118
5.2.3 Application of the model test results to prototype 139

6 CONCLUSIONS 142

7 REFERENCES 148

APPENDICES 150

A Resistance Forces of the models 150

B Measured Results of the Resistance Tests 163

C Motion and Mooring Force Responses of the Spherical Cage Model 175

D Motion and Mooring Force Responses of the Geodesic Cage Model 192

LIST OF TABLES

Table 3.1 - Wave period ranges corresponding to deep, intermediate and shallow water waves 22

Table 3.2 - Scale factors based on Reynolds law 36

Table 3.3 - Scale factors based on Froude law 42

Table 4.1 - Parameters of the spherical cage model 50

Table 4.2 - Parameters of the geodesic cage model 50

Table 4.3 - Wave frequencies used in regular wave tests and corresponding wave periods for model and prototype 65

Table 5.1 - Reynolds number ranges of model testing..... 79

Table 5.2 - Comparison of resistance forces in different orientations 81

Table 5.3 - Example of correction factors K_C for resistance force calculations of spherical and geodesic frames 86

LIST OF FIGURES

Figure 1.1 - Spherical cage in fully submerged position. 3

Figure 1.2 - Geodesic cage in fully submerged position . 4

Figure 1.3 - Geodesic cage in operational position 5

Figure 3.1 - Definition sketch for a progressive wave .. 15

Figure 3.2 - Variation of particle orbits and kinematics with depth by linear theory 20

Figure 3.3 - Ratio of kinetic energy at s/d to kinetic energy at s/d = 1.0 (water surface) 21

Figure 3.4 - Percent kinetic energy concentrated above elevation s/d 21

Figure 3.5 - Six degrees of motion of the cage 24

Figure 3.6 - C_D - Re interaction 38

Figure 4.1 - Elevation and plan view of the wave/tow tank 46

Figure 4.2 - Spherical model 47

Figure 4.3 - Floats of the models 48

Figure 4.4 - Experimental arrangement of the resistance tests 53

Figure 4.5 - Instrumentation and data recording system of the resistance tests 55

Figure 4.6 - Experimental arrangement of the moored tests 61

Figure 4.7 - Instrumentation and data recording system of the moored tests 62

Figure 4.8 - Model submerged positions during testing .. 66

Figure 4.9 - Orientations of the model during testing .. 67

Figure 4.10 - Geodesic model in middle position and parallel orientation 67

Figure 5.1 - Resistance force of the spherical frame with net 74

Figure 5.2 - Resistance force of the spherical frame without net 74

Figure 5.3 - Resistance force of the net on the spherical frame 75

Figure 5.4 - Resistance force of the geodesic frame with net 75

Figure 5.5 - Resistance force of the geodesic frame without net 76

Figure 5.6 - Resistance force of the net on the geodesic frame 76

Figure 5.7 - Resistance force of the model net tested on the 1.0 m × 1.0 m model holding frame 77

Figure 5.8 - Resistance force of the float 77

Figure 5.9 - Comparison between heave responses of two orientations: spherical model, surface position 93

Figure 5.10 - Comparison between heave responses of two orientations: spherical model, middle position 93

Figure 5.11 - Comparison between heave responses of two orientations: spherical model, bottom position 94

Figure 5.12 - Comparison between surge of parallel orientation and sway of perpendicular orientation: spherical model, surface position 94

Figure 5.13 - Comparison between surge of parallel orientation and sway of perpendicular orientation: spherical model, middle position 95

Figure 5.14 - Comparison between surge of parallel orientation and sway of perpendicular orientation: spherical model, bottom position 95

Figure 5.15 - Comparison between heave responses of two orientations: geodesic model, surface position 96

Figure 5.16 - Comparison between heave responses of two orientations: geodesic model, middle position 96

Figure 5.17 - Comparison between heave responses of two orientations: geodesic model, bottom position 97

Figure 5.18 - Comparison between surge of parallel orientation and sway of perpendicular orientation: geodesic model, surface position 97

Figure 5.19 - Comparison between surge of parallel orientation and sway of perpendicular orientation: geodesic model, middle position 98

Figure 5.20 - Comparison between surge of parallel orientation and sway of perpendicular orientation: geodesic model, bottom position 98

Figure 5.21 - Surge responses in different submerged positions: spherical model, parallel orientation 103

Figure 5.22 - Heave responses in different submerged positions: spherical model, parallel orientation 103

Figure 5.23 - Surge responses in different submerged positions: geodesic model, parallel orientation 104

Figure 5.24 - Heave responses in different submerged positions: geodesic model, parallel orientation 104

Figure 5.25 - Surge responses in different submerged positions: geodesic model, parallel orientation, with stiffer mooring lines .. 105

Figure 5.26 - Heave responses in different submerged positions: geodesic model, parallel orientation, with stiffer mooring lines .. 105

Figure 5.27 - Sway responses in different submerged positions: spherical model, perpendicular orientation 106

Figure 5.28 - Heave responses in different submerged positions: spherical model, perpendicular orientation 106

Figure 5.29 - Roll responses in different submerged positions: spherical model, perpendicular orientation 107

Figure 5.30 - Sway responses in different submerged positions: spherical model, perpendicular orientation 107

Figure 5.31 - Heave responses in different submerged positions: geodesic model, perpendicular orientation 108

Figure 5.32 - Roll responses in different submerged positions: geodesic model, perpendicular orientation 108

Figure 5.33 - Heave and sway responses in different submerged positions: geodesic model, perpendicular orientation, with stiffer mooring lines 109

Figure 5.34 - Roll responses in different submerged positions: geodesic model, perpendicular orientation, with stiffer mooring lines .. 109

Figure 5.35 - Effect of mooring line pretension on heave response: middle position, parallel orientation 112

Figure 5.36 - Effect of mooring line pretension on surge response: middle position, parallel orientation 112

Figure 5.37 - Effect of mooring line pretension on heave response: bottom position, parallel orientation 113

Figure 5.38 - Effect of mooring line pretension on surge response: bottom position, parallel orientation 113

Figure 5.39 - Effect of mooring line stiffness on surge response: middle position, parallel orientation 114

Figure 5.40 - Effect of mooring line stiffness on heave response: middle position, parallel orientation 114

Figure 5.41 - Effect of mooring line stiffness on surge response: bottom position, parallel orientation 115

Figure 5.42 - Effect of mooring line stiffness on heave response: bottom position, parallel orientation 115

Figure 5.43 - Effect of mooring line stiffness on heave and sway responses: middle position, perpendicular orientation 116

Figure 5.44 - Effect of mooring line stiffness on roll response: middle position, perpendicular orientation 116

Figure 5.45 - Effect of mooring line stiffness on heave and sway responses: bottom position, perpendicular orientation 117

Figure 5.46 - Effect of mooring line stiffness on roll response: bottom position, perpendicular orientation 117

Figure 5.47 - Comparison among force responses of both mooring lines in parallel orientation, sea side and lee side mooring lines in perpendicular orientation: spherical model, surface position 121

Figure 5.48 - Comparison among force responses of both mooring lines in parallel orientation, sea side and lee side mooring lines in perpendicular orientation: spherical model, middle position 121

Figure 5.49 - Comparison among force responses of both mooring lines in parallel orientation, sea side and lee side mooring lines in perpendicular orientation: spherical model, bottom position 122

Figure 5.50 - Comparison among force responses of both mooring lines in parallel orientation, sea side and lee side mooring lines in perpendicular orientation: geodesic model, surface position 122

Figure 5.51 - Comparison among force responses of both mooring lines in parallel orientation, sea side and lee side mooring lines in perpendicular orientation: geodesic model, middle position 123

Figure 5.52 - Comparison among force responses of both mooring lines in parallel orientation, sea side and lee side mooring lines in perpendicular orientation: geodesic model, bottom position 123

Figure 5.53 - Effect of phase difference between heave and roll on vertical displacements at the ends of sea side and lee side mooring lines 124

Figure 5.54 - Force responses of both mooring lines in different submerged positions: spherical model, parallel orientation 131

Figure 5.55 - Force responses of both mooring lines in different submerged positions: geodesic model, parallel orientation 131

Figure 5.56 - Force responses of both mooring lines in different submerged positions: geodesic model, parallel orientation, with stiffer mooring lines 132

Figure 5.57 - Force responses of sea side mooring line in different submerged positions: spherical model, perpendicular orientation 132

Figure 5.58 - Force responses of lee side mooring line in different submerged positions: spherical model, perpendicular orientation 133

Figure 5.59 - Force responses of sea side mooring line in different submerged positions: geodesic model, perpendicular orientation 133

Figure 5.60 - Force responses of lee side mooring line in different submerged positions: geodesic model, perpendicular orientation 134

Figure 5.61 - Force responses of sea side and lee side mooring lines in different submerged positions: geodesic model, perpendicular orientation, with stiffer mooring lines .. 134

Figure 5.62 - Effect of mooring line pretension on force responses of both mooring lines: middle position, parallel orientation 135

Figure 5.63 - Effect of mooring line pretension on force responses of both mooring lines: bottom position, parallel orientation 135

Figure 5.64 - Effect of mooring line stiffness on force responses of both mooring lines: middle position, parallel orientation 136

Figure 5.65 - Effect of mooring line stiffness on force response of sea side mooring line: middle position, perpendicular orientation 136

Figure 5.66 - Effect of mooring line stiffness on force response of lee side mooring line: middle position, perpendicular orientation 137

Figure 5.67 - Effect of mooring line stiffness on force responses of both mooring lines: bottom position, parallel orientation 137

Figure 5.68 - Effect of mooring line stiffness on force responses of sea side mooring line: bottom position, perpendicular orientation 138

Figure 5.69 - Effect of mooring line stiffness on force response of lee side mooring line: bottom position, perpendicular orientation 138

DEFINITION OF SYMBOLS USED

Symbol	Description
A	Amplitude or semiaxis in x direction
B	Semiaxis in z direction
C	Damping coefficient
C_D	Drag coefficient of cylinder
C_r	Resistance force coefficient
D	Diameter of cylinder
f	Wave frequency (= 1/T)
F	Force
F_M	Dynamic mooring force
F_r	Resistance force obtained from model test
Fr	Froude number
d	Water depth or distance between the centres of two floatation chambers (also distance between two mooring lines)
g	Gravity acceleration
H	Wave height
H(f)	Frequency transfer function
I	Moment of inertia
I_A	Added moment of inertia
k	Wave number or constant regressed from series of resistance tests
K	Axial spring constant of mooring line
K_c	Correction factor
K_M	Spring constant of mooring system
K_R	Hydrostatic restoring force coefficient
l	Length of tension mooring line or length of wave tank
L	Length or wave length
m	Mass of cage
M	Added mass of cage
RAO	Response Amplitude Operator
Re	Reynolds number
s	Elevation from ocean floor or cage motion
S_F	Section area of floatation chamber in water line
$S_x(f)$	Spectral density of incident wave
$S_{yy}(f)$	Spectral density of respcnse
SWL	Still water level
t	time
T	Wave period or pretension in mooring line
T_n	Natural oscillating period of wave tank
u	Horizontal water particle velocity
v	Vertical water particle velocity
V	Current velocity

Symbol	Description
x	Horizontal coordinate
y	Transverse coordinate
z	Vertical coordinate or instantaneous heave motion of cage
ϕ	Instantaneous roll motion of cage
ε_1	Phase angle of wave force
ε_2	Phase angle between motion response and wave force
λ	Model scale (= prototype value/model value)
ω	Angular wave frequency (= $2\pi/T$)
ω_n	Natural frequency (angular)
η	Vertical water particle displacement
ν	Kinematic viscosity
ρ	Density of water
θ	Angle between cylinder element and current direction
ξ	Horizontal water particle displacement
π	3.14159

Subscripts

p	prototype
m	model

1 INTRODUCTION

With the decrease of fish stocks in oceans because of overfishing in offshore waters, aquaculture has become more and more important and is one of the world's rapid growth resource industries among Western nations. The use of cages is felt to be the most economically feasible method of intensively rearing fish such as salmonids, yellowtail and grouper in marine waters, and can be a comparatively profitable means of producing other species (Beveridge, 1987).

There are four basic types of fish cage: fixed, floating, submersible and submerged (Beveridge, 1987). Floating cages are by far the most widely used and research has been carried out mainly on this type of cage. With the increasing requirement of farming fish in more exposed offshore sites, more and more attention will be focused on submersible cages. The advantage of this type of cage is that its position in the water column can be adjusted to take advantage of prevailing environmental conditions. In normal conditions the cage remains on the surface; during storms the cage can be submerged below the water surface to reduce the wave forces and motions of the cage and hence the stress on the farmed fish. The cage can also be submerged to avoid supercooled surface water and surface ice damage during winter periods,

and to avoid exceptional toxic plankton blooms in the surface water layer which may cause catastrophic loss of fish. Up to now, few submersible cages have been built and tested and few research papers can be found.

The proposed globe-shaped submersible fish cage system and two kinds of cage frames which are studied in this thesis are shown in Figures 1.1, 1.2 and 1.3. Figure 1.1 shows the spherical cage and Figure 1.2 shows the geodesic cage in a fully submerged position. Figure 1.3 shows the geodesic cage in the normal operational position. The diameters of the prototype cages would be about 12 m. The spherical cage consists of 8 half bows and two bow reinforcements (not shown in the Figure). The geodesic cage consists of short bars and joint elements. Therefore, the geodesic is much easier to manufacture, transport and assemble, and has a stronger cage structure than the spherical cage, but it may also have larger resistance forces in currents. Both cages have an axle in the middle of the cage which can also be used as a food feeder.

For the proposed cage system, the cage can be raised or submerged along the cables by adjusting the buoyancy of the floatation chambers. The operational position of the cage system is when the axle of the cage is about 1/3 diameter below the water surface (this may vary with tidal level). The

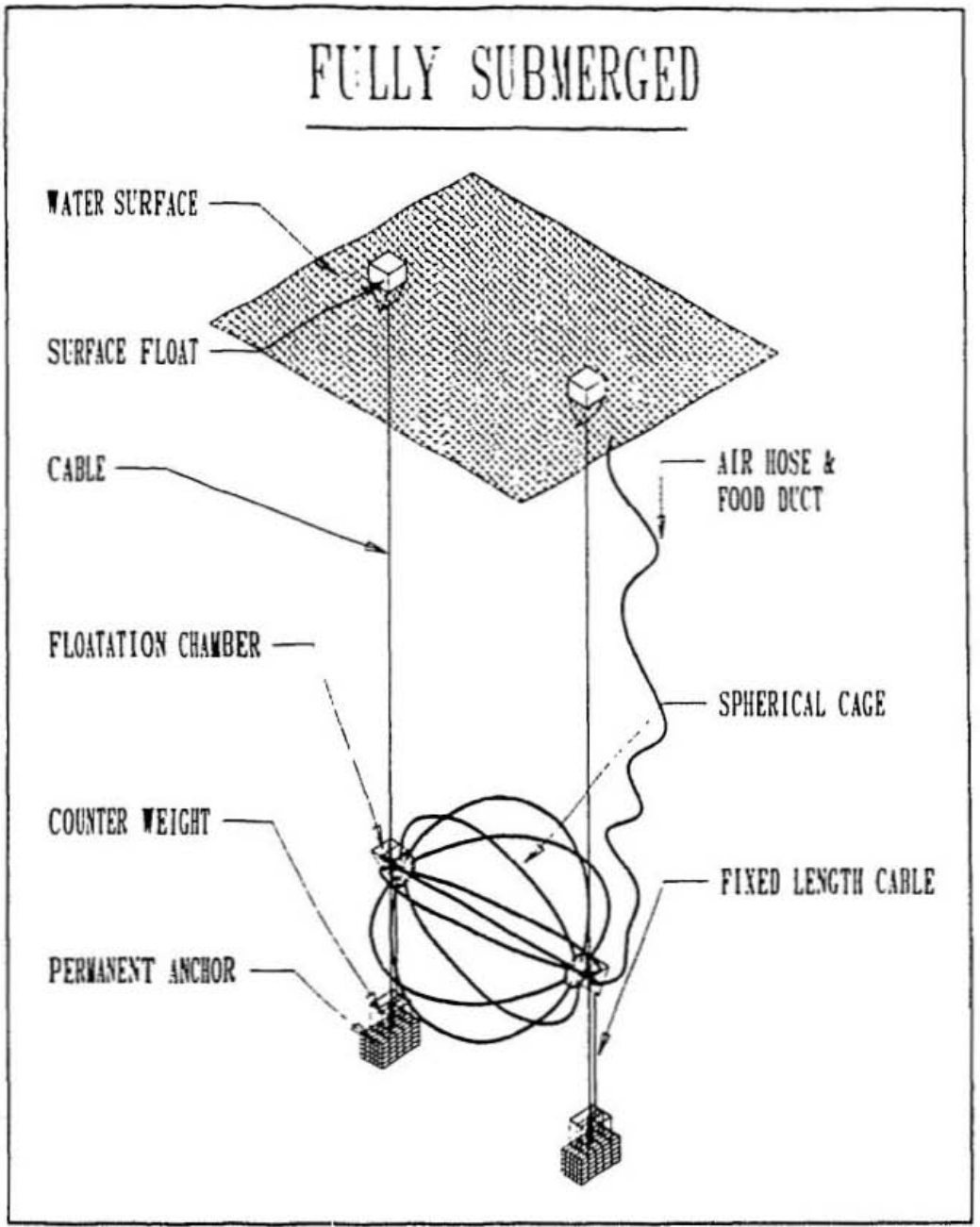

Figure 1.1 - Spherical cage in fully submerged position

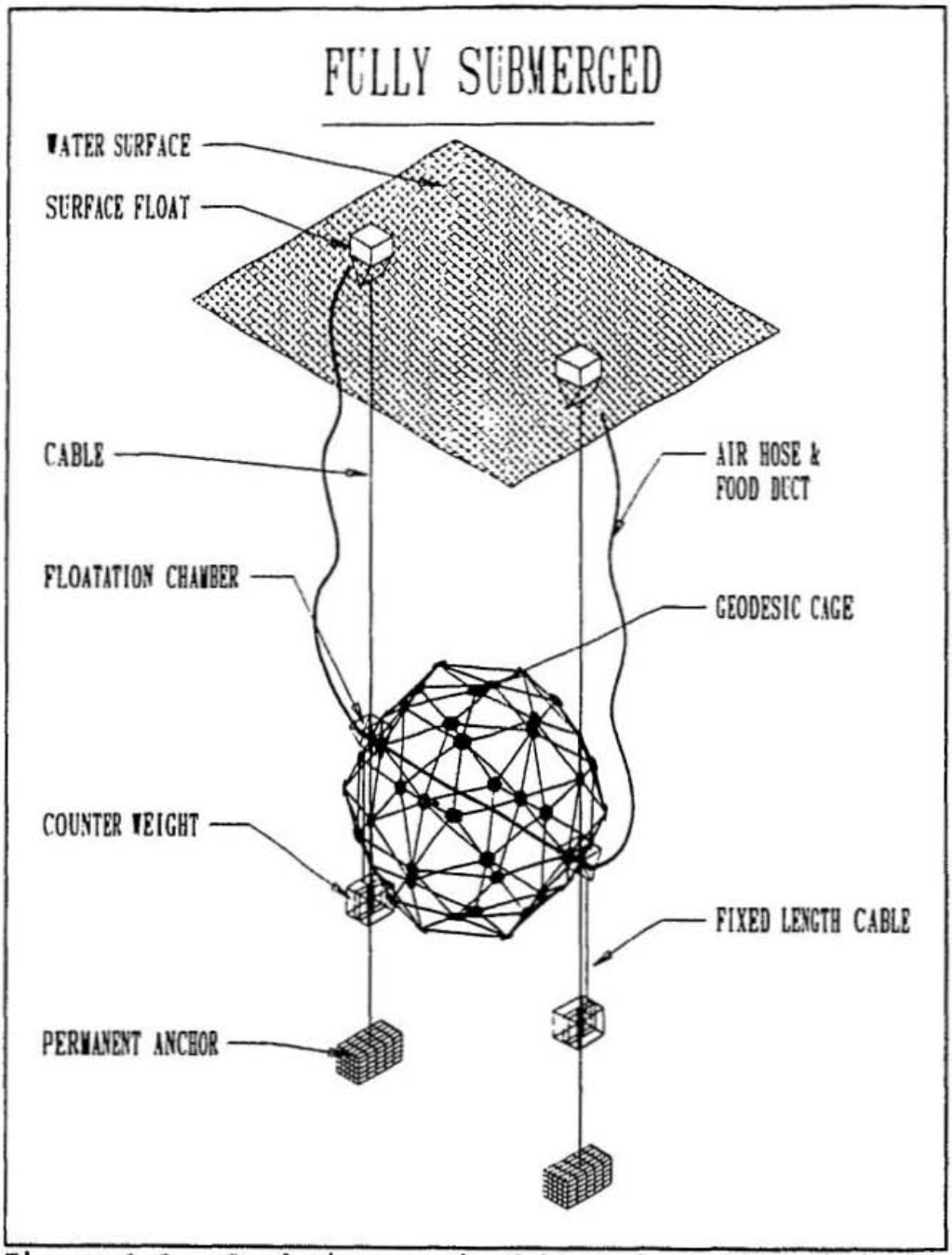

Figure 1.2 - Geodesic cage in fully submerged position

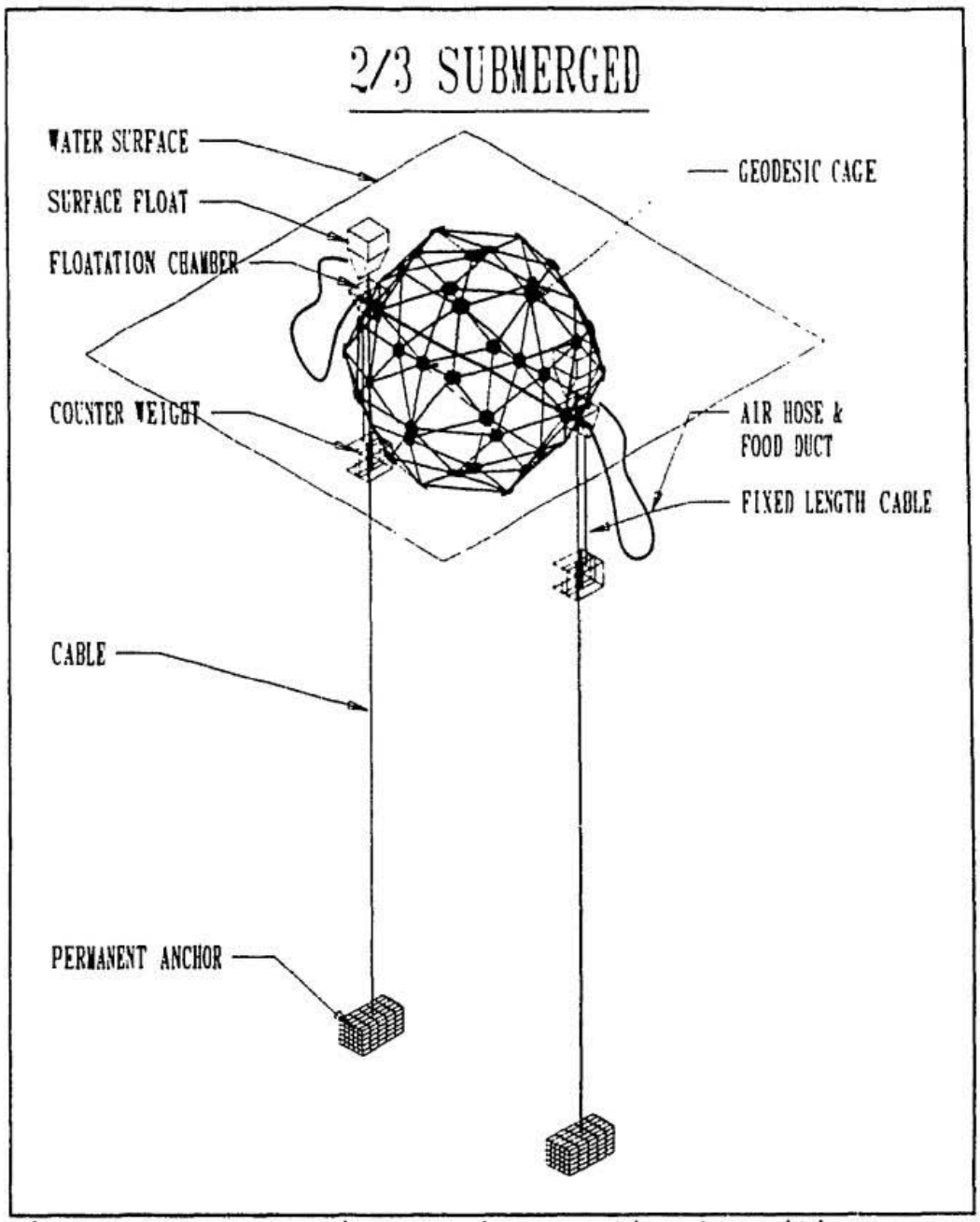

Figure 1.3 - Geodesic cage in operational position

cage can be lowered below the water surface during storm and winter conditions, and raised so that the axle is near the water surface for servicing. In the servicing position, the floatation chambers can be used as working platforms, about half of the cage is exposed to the air and the cage can be rotated about its axle. Therefore, the inspection, repair and exchange of cage net can be carried out easily during continuous operation without removing the fish from the cage. Also the problem of net-fouling by marine organisms can be greatly reduced and practically eliminated by rotating the cage regularly and exposing to the air any marine growth which has occurred. Having dried, this growth will fall off the net.

Compared to the conventional cage system, the globe-shaped fish cage also has the following advantages. The shape of the cage offers the largest volume to surface ratio and very high structural strength. Because the net is supported throughout the surface by the cage frame, net deformation in current is small and the cage volume does not change with current velocity. Also the same net will provide protection against bird predation. It has also been found that a round cage would reduce stress on the farmed fish, a leading cause of disease and mortality in aquaculture. Certain fish in a group tend to be aggressive and cause stress by forcing groups into a herd. In a round cage, aggressive fish could not easily

find a territory to dominate and the species could grow with less stress (Norman, 1991).

A cage at sea will experience the actions of winds, currents and waves. For a submersible cage, wind forces may not be so important, but current forces and wave forces are very important in designing a safe cage structure and mooring system. Under wave action the cage will have a motion of six degrees of freedom. The motion of the cage will affect the growth of the fish inside the cage and the dynamic force responses in the mooring system. Therefore, an estimation of the static and dynamic responses of the cage system to environmental forces must be known to design a safe and efficient cage system.

Since the proposed prototype cage system is a quite new concept, few theoretical and experimental results or research papers can be found to guide the prototype design. The complex structure and the multi-degree of freedom of the cage system means that the interaction between the structure, nets and moorings is not readily determined by mathematical calculation. In order to have a better understanding of the hydrodynamic performance of the proposed prototype cage system and provide some useful information for the prototype design, a series of model tests were carried out on two kinds of

globe-shaped fish cages, spherical and geodesic cages. The purposes of the tests were to study the resistance forces of the cages in currents when the cages were totally submerged below the water surface, to investigate the mooring force and motion responses of the cage system to waves in different submerged positions and orientations, and to observe the effects of pretension and axial stiffness of the mooring lines on the motion and mooring force responses.

In addition to being used as a guide for the prototype design, the model test results can also be used in further stages of research in the establishment, verification and calibration of a numerical model. The numerical model in turn may offer a general tool for a variety of purposes of the prototype design such as altering dimensions, mass, moment of inertia, net, stiffness of mooring lines, floatation chamber geometry, submerged depth of the cage and water depth of the site, as well as optimizing design parameters of the system. In view of the many assumptions and simplifications made in constructing a numerical model, feed back from model tests is extremely important in validating the results. Therefore, model tests are necessary.

In this thesis, theoretical background and qualitative analyses of the problem are presented, experimental

methodology is described, and the model test results and their application in the prototype design are presented and analyzed. When the experiments were conducted, there was no detailed prototype design, so this was only a primary experimental research aiming at having a better understanding of the responses of the proposed cage and mooring system to environmental forces and providing information for the prototype design and the establishment and verification of numerical models. All the parameters and test results presented in this thesis are referred to the models.

2 REVIEW OF LITERATURE

Because offshore cage aquaculture is a newly developed industry, not much published literature on hydrodynamics of fish cage systems was found. Most of the research is focused on the conventional square shape surface collar floating sea-cage with conventional mooring system; few, or no, published research papers are available on globe-shaped submersible cage system at the present stage.

Beveridge (1987) published a book on cage aquaculture which is a synthesis of available information on cages and cage aquaculture. This book gives us a general picture of the development of cage culture, diversity of cage types and their advantages and disadvantages, environmental forces on cages and the simple method to estimate these forces, cage construction, and the biological considerations in cage aquaculture. According to this book, there is evidence that the coefficients of drag of the netting materials are independent of current velocity over the range typically encountered at fish farm sites (0.33 - 1.87 m/s). The author also described submersible cage designs as a strategy against stormy conditions and problems with ice.

Rudi et al (1988) gave a general description of a

preliminary study of the wind force, current force, wave induced cage motions and mooring analyses of a conventional floating cage system. Prediction of current force is based on normal empirical methods with the following formulation:

$$F = \frac{1}{2}\rho C_D V^2 A = \frac{1}{2}\rho V^2 \sum_{i=1}^{n} C_{Di} A_i \qquad (2.1)$$

where F is the drag force, ρ is the density of water, V is the current velocity, C_D is the total drag coefficient, A is the projected area, C_{Di}, A_i is the local drag coefficient and projected area of element No. i and n is the total number of elements of the structure. Quasi-static method is used in mooring analysis, taking no account of the inertia or hydrodynamic loads on the mooring line. Motion amplitude is calculated by determining first the wave force acting on a fixed cage and then the forces acting on the cage when it is forced to oscillate in calm water with the same period of oscillation as the wave and with unit motion amplitude. However, for a globe-shaped cage system which has a more complicated shape, these methods can only be used to interpret the experimental results or provide some qualitative results, but it is difficult to use them to provide some quantitative results.

Aarsnes et al (1990) developed a method for calculation of current forces on cage net which was found to reproduce the

current forces from the model tests within the range 0.9-1.3 times the measured forces. The drag and lift coefficient for the current forces acting on a planar net panel were treated as a function of the heading between the current and the net plane and the solidity ratio of the net. The decrease of current velocity at downstream net panels caused by the shielding effects of the upstream net panels was taken into account in the calculations. Because this method was derived from the tests of planar net panel, it seems that it can not be used directly to calculate the current forces of the net on a globe-shaped fish cage because the interaction between net segments would be different.

Model testing of a square-shape Wavemaster cage system was carried out by Whittaker et al (1990) to determine the movements and mooring force responses of the cage system under wave action. In the tests, the Froude number was ensured to be the same in both the model and the prototype. Considerable care was taken to select a net material which could accurately reproduce the motions of the prototype. Drag tests were performed on a series of the samples of nets in a towing tank. A net with a drag force/velocity characteristic approximately 1.5 times that of a clean prototype net was chosen for the model in order to represent the presence of a heavily fouled net. This is a appropriate method to select a model net

material, but the comparison of the force/velocity characteristics of the prototype and model nets should be in different velocity ranges scaled according to the Froude law.

Instrumentation, data analysis techniques and test results of irregular wave tests on several model and prototype sea-cages were provided by Linfoot and Hall (1986). It was found that the presence of the net significantly reduced the heave and pitch motion responses of the cages at resonance frequencies. Therefore, the net used in the cage model tests should be carefully selected in order that the model tests can represent the prototype properly. Linfoot and Hall (1989) also conducted model testing of single-point mooring systems for sea-cage flotillas at a scale of 1:16. Fibrous nylon net of 5 mm knot-to-knot was used to simulate a moderately fouled twine net. Obviously, this is not a model net scaled down from the prototype net according to the model scale, but how the model net was chosen was not presented in their paper.

Most fish will suffer when kept in waters with temperatures near 0° C. To avoid the low-temperate problems and problems arising from environmental loads in the surface region, an underwater offshore sea cage has been developed to a pre-engineering level in Norway (Dahle et al, 1989). Calculations show the cage will experience less environmental

forces when it is submerged below the water surface, but no experiment has been conducted to confirm these calculations.

Oltedal et al (1988) developed a computer program for simulation of the responses to environmental loads of complex floating fish farms. The program does not comprise an exact solution of the complicated hydrodynamic problem related to floating fish cages. It represents only an engineering approach based on approximate methods to improve the computational method available for fish farms. The program output has to be verified by comparisons with known results as obtained from model testing. Therefore, model testing plays a very important role in the numerical model establishment of a fish cage system.

3 THEORETICAL BACKGROUND

3.1 Variation of Wave Motion with Depth below Water Surface and its Effect on Submersible Fish Cage

One of the major considerations of submersible fish cage design is that the cage would be submerged below the water surface during storms to reduce the wave forces and motions of the cage and hence reduce the forces in the mooring system and stress on the farmed fish. In order to study the effectiveness of this method, linear wave theory can be used to determine the variation of wave motion with distance below the water surface and its effect on a submersible fish cage.

A two-dimensional wave propagating in the x direction is defined in Figure 3.1 in which the various symbols used to characterize the wave are given. From linear wave theory it is known that the amplitudes of water particle velocities, accelerations and displacements induced by wave action in x and z directions are functions of position along the water column.

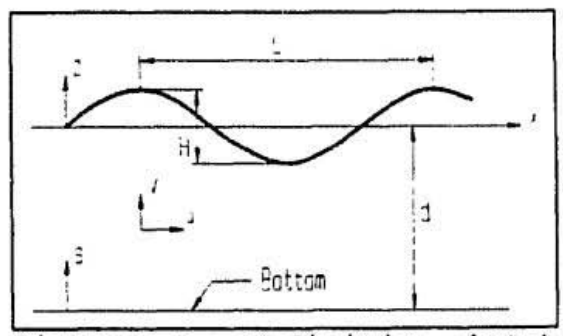

Figure 3.1 - Definition sketch for a progressive wave

The horizontal water particle velocity and acceleration are written as (Chakrabarti, 1987):

$$u = \frac{\pi H}{T} \frac{\cosh ks}{\sinh kd} \cos(kx - \omega t) \qquad (3.1)$$

$$\dot{u} = \frac{2\pi^2 H}{T^2} \frac{\cosh ks}{\sinh kd} \sin(kx - \omega t) \qquad (3.2)$$

and the vertical water particle velocity and acceleration are written as:

$$v = \frac{\pi H}{T} \frac{\sinh ks}{\sinh kd} \sin(kx - \omega t) \qquad (3.3)$$

$$\dot{v} = -\frac{2\pi^2 H}{T^2} \frac{\sinh ks}{\sinh kd} \cos(kx - \omega t) \qquad (3.4)$$

where T is the wave period, H is the wave height, $k = 2\pi/L$ is the wave number, L is the wave length, d is the water depth, $s = z+d$ is the elevation from the ocean floor, and $\omega = 2\pi/T$ is the angular frequency of the wave.

The horizontal and vertical water particle displacements, ξ and η, are given by

$$\xi = -\frac{H}{2} \frac{\cosh ks}{\sinh kd} \sin(kx - \omega t) \qquad (3.5)$$

and

$$\eta = \frac{H}{2} \frac{\sinh ks}{\sinh kd} \cos(kx - \omega t) \qquad (3.6)$$

Squaring and adding yields the water particle trajectory as

$$\frac{\xi^2}{A^2} + \frac{\eta^2}{B^2} = 1 \qquad (3.7)$$

in which

$$A = \frac{H}{2} \frac{\cosh ks}{\sinh kd} \qquad (3.8)$$

$$B = \frac{H}{2} \frac{\sinh ks}{\sinh kd} \qquad (3.9)$$

are the semiaxes in x and z directions respectively and are measures of the horizontal and vertical displacements of the water particles.

Certain simplifications of the above equations can be made depending on the ratio of the water depth d to the wave length L. For deep water waves, $d/L \geq 0.5$, the expressions may be simplified by the following approximations

$$\frac{\cosh ks}{\sinh kd} = \frac{\sinh ks}{\sinh kd} = e^{kz} \qquad (3.10)$$

and for shallow water waves, $d/L < 0.05$

$$\frac{\cosh ks}{\sinh kd} = \frac{1}{kd} \qquad (3.11)$$

$$\frac{\sinh ks}{\sinh kd} = 1 + \frac{z}{d} \qquad (3.12)$$

The variations of particle orbits and velocity amplitudes with depth below water surface for shallow, intermediate and

deep water waves are shown in Figure 3.2. For deep water waves, the water particle movements produced by waves decay exponentially with the depth below the water surface. At a depth of about L/9, the movements are approximately halved, and at L/2 the movements will decrease to about 4% of those at the surface. For shallow water waves, horizontal movements almost do not decay with depth and the vertical movements decrease approximately linearly, so the horizontal particle displacement near the bottom can still be large. Note that the maximum amplitude of vertical displacement (at water surface) of a water particle is equal to the wave amplitude, H/2, while the maximum amplitude of horizontal displacement is equal to the wave amplitude for deep water waves and is larger than the wave amplitude for intermediate and shallow water waves.

In order to obtain a clearer idea of the possible advantages in submerging the cage at a particular depth below the water surface, consider the kinetic energy distribution within a wave. Derived from linear wave theory, the ratio of the kinetic energy at any elevation "s" to that at the mean water surface where s = d is given in dimensionless form by Dean and Harleman (1966) as

$$\frac{KE(s)}{KE(d)} = \frac{\cosh ks}{\cosh kd} \qquad (7.13)$$

This relation is plotted in Figure 3.3 for d/L = 0.05 (shallow

water limit), 0.1, 0.2, 0.3, 0.5 (deep water limit), 0.7, and 0.9. This figure shows that for deep water waves ($d/L \geq 0.5$) the energy is concentrated near the surface, with the decrease of d/L in intermediate water waves ($0.05 < d/L < 0.5$) the energy begins to be distributed to lower water, and eventually for shallow water waves ($d/L \leq 0.05$) the energy concentration is nearly uniform with depth. One further relationship which may be more helpful is the percentage of kinetic energy above any elevation. This is obtained as (Dean and Harleman, 1966)

$$\frac{\int_s^d KE(s)\,ds}{\int_0^d KE(s)\,ds} \times 100\% = \left[1 - \frac{\sinh 2ks}{\sinh 2kd}\right] \times 100\% \qquad (3.14)$$

This equation is plotted in Figure 3.4. It shows that a cage in deep water waves occupying only a small relative portion of the depth (say 20%) in the surface will interact with a significant portion of the kinetic wave energy (equal to or larger than 71%), when the cage is submerged some distance below the water surface the kinetic energy encountered by the cage will be greatly reduced. It can also be found from this figure that a cage in shallow water waves will encounter almost the same portion of kinetic energy at different depths along the water column. The value of d/L is a function of wave period and water depth of the site. Table 3.1 gives some examples of the wave period ranges corresponding to deep,

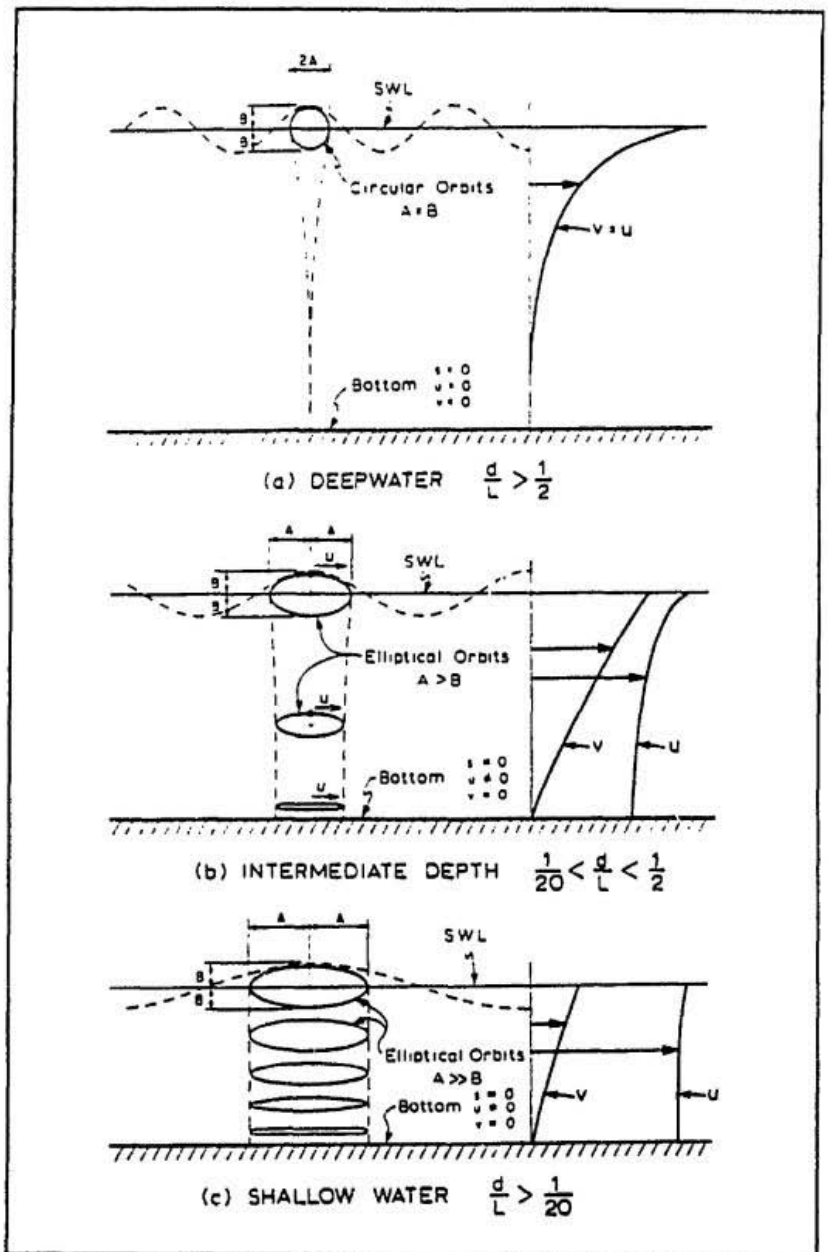

Figure 3.2 - Variation of particle orbits and kinematics with depth by linear theory (Chakrabarti, 1987)

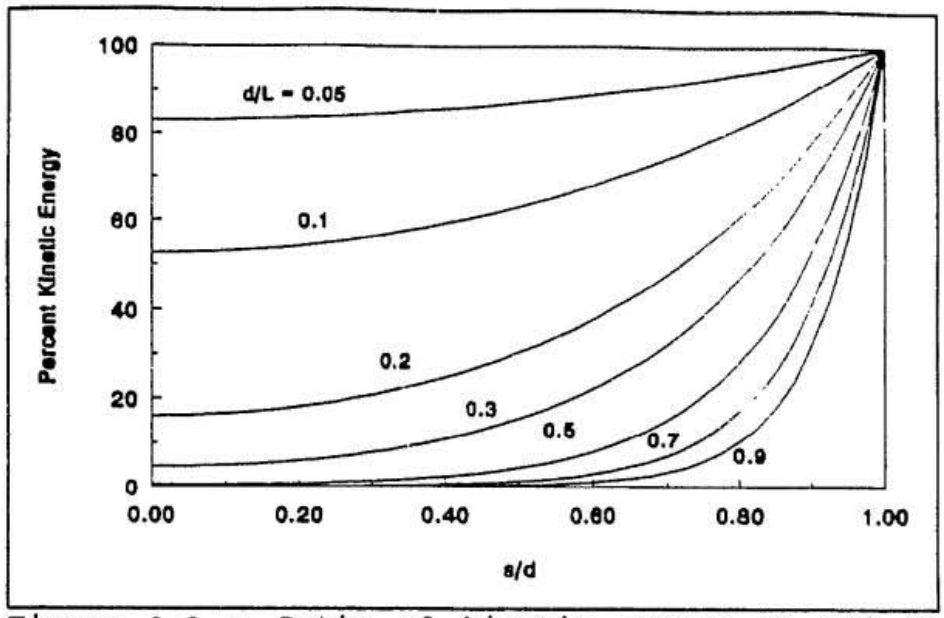

Figure 3.3 - Ratio of kinetic energy at s/d to kinetic energy at s/d = 1.0 (water surface)

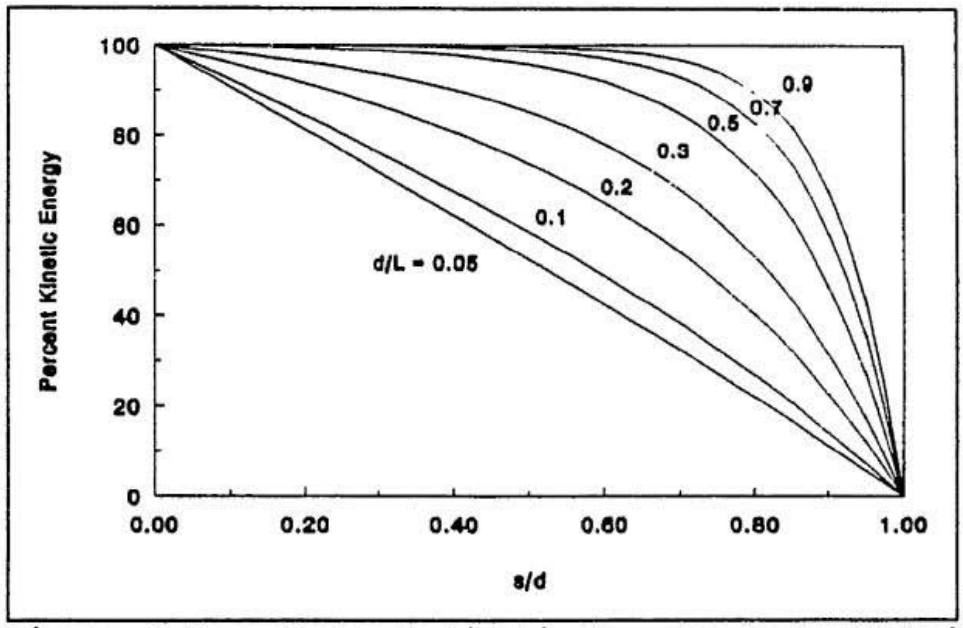

Figure 3.4 - Percent kinetic energy concentrated above elevation s/d

intermediate and shallow water waves for different water depths.

Table 3.1 - Wave period ranges corresponding to deep, intermediate and shallow water waves

Water Depth (m)	Water Wave Type		
	Deep	Intermediate	Shallow
2	$T \leq 1.6$	$1.6 < T < 9.2$	$T \geq 9.2$
20	$T \leq 5.1$	$5.1 < T < 29.0$	$T \geq 29.0$
30	$T \leq 6.2$	$6.2 < T < 33.6$	$T \geq 33.6$
40	$T \leq 7.2$	$7.2 < T < 41.1$	$T \geq 41.1$
50	$T \leq 8.0$	$8.0 < T < 45.9$	$T \geq 45.9$

Unit: second

From the discussions above it can be predicted that the method of submerging the cage some distance below the water surface to reduce the wave forces and motions of the cage and hence reduce the forces in the mooring system will be very effective in deep water waves and part of the intermediate water waves. With the decrease of d/L this method will become less and less effective in intermediate water waves and not effective in shallow water waves. Therefore, the effectiveness of this method depends on the water depth and wave period of the site. Nevertheless, submerging the cage below the water surface can still reduce the vertical wave action on the cage

to some degree in all the cases.

3.2 Motion and Mooring Force Responses of the Moored Cage to Wave Action

3.2.1 Motion response

The moored cage of the proposed cage system may experience six degrees of motion under wave action as shown in Figure 3.5. The definitions of surge, sway, heave, yaw, pitch, and roll used in this thesis are with respect to the cage. The motion along a horizontal line perpendicular to the axle of the cage is termed as surge, the motion along the direction of the axle of the cage is sway, and the vertical motion is heave. The angular motion about a vertical axis is called yaw, the angular motion about the axle of the cage is pitch, and the angular motion about a horizontal axis perpendicular to the axle of the cage is roll.

Under the assumptions of linear wave, linearized damping and no current, the motion of the moored cage in regular waves can be described by a set of coupled differential equations

$$\sum_{k=1}^{6} \left[(m_{jk}+M_{jk})\,\ddot{s}_k + C_{jk}\dot{s}_k + (K_{Rjk}+K_{Mjk})\,s_k \right] = F_j \sin(\omega t-\varepsilon_j) \qquad j = 1,2,\ldots,6 \tag{3.15}$$

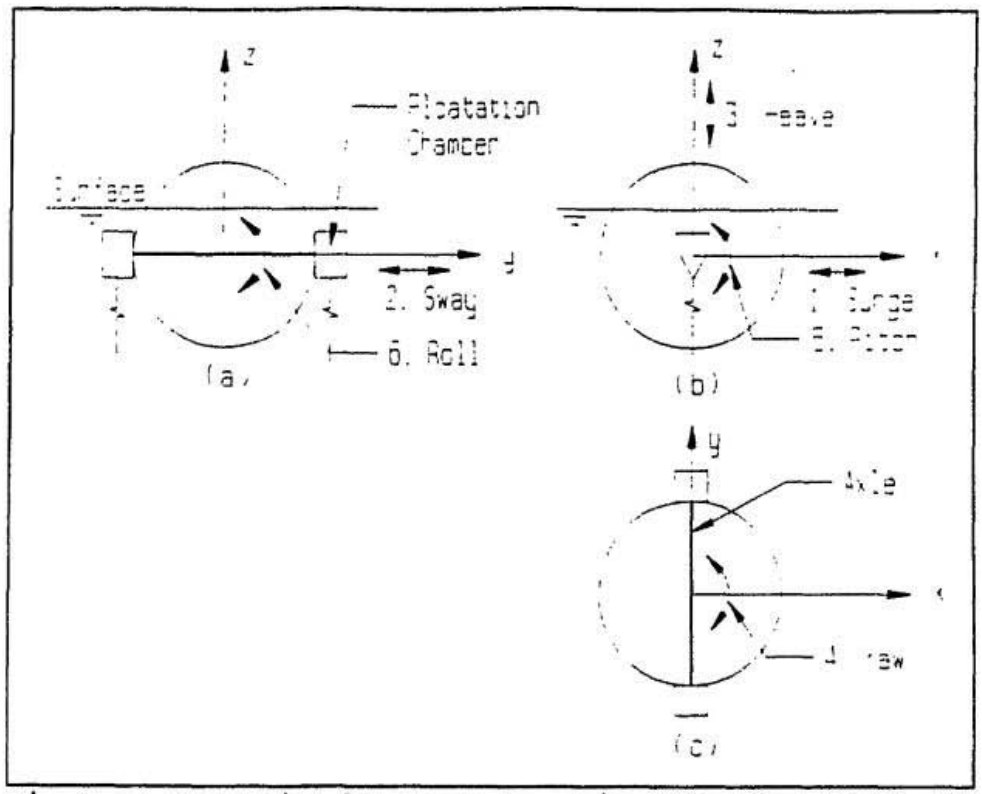

Figure 3.5 - Six degrees of motion of the cage. (a) Front view, (b) Side view, (c) Top view.

where m_{jk} is the mass matrix containing the mass and moment of inertia of the cage, M_{jk} is the added mass or moment of inertia of the cage in direction j due to acceleration in direction k, s_k is the cage motion in direction k, C_{jk} is the damping coefficient of the cage in direction j due to the cage motion in direction k, K_{Mjk} is the spring constant of the mooring system in direction j due to the cage motion in direction k, K_{Rjk} is the hydrostatic restoring force coefficient in direction j due to the cage motion in direction k, and F_j and ε_j are the amplitude of wave force or moment and the

corresponding phase angle in direction j. Unfortunately, it is difficult to obtain the exact mathematical solutions of the coupled equations of motion. In order to illustrate qualitatively how the parameters of the system would affect the motion and mooring force responses, it is assumed that the six degrees of motion of the cage are uncoupled.

The uncoupled equations of cage motion can be simplified as

$$(m_j+M_j)\ddot{s}_j+C_j\dot{s}_j+(K_{Rj}+K_{Mj})s_j = F_j\sin(\omega t-\varepsilon_{j1}) \qquad j = 1,2,\ldots,6 \tag{3.16}$$

where m_j is the mass of the cage for j = 1,2,3 and moment of inertia of the cage in direction j for j = 4,5,6, M_j is the added mass of the cage for j = 1,2,3 and added moment of inertia for j = 4,5,6 in direction j, s_j is the cage motion in direction j, C_j is the damping coefficient of the cage in direction j, K_{Rj} and K_{Mj} are the hydrostatic restoring force coefficient and spring constant of the mooring system in direction j, F_j and ε_{j1} are the amplitude of wave force or moment acting on the cage in direction j and the corresponding phase angle to incident wave. The added mass or moment of inertia M_j and the damping coefficient C_j of the cage depend on the geometry of the submerged parts of the cage and the net, the direction of motion, and the frequency of the incident wave. The hydrostatic restoring force coefficient K_{Rj} and

spring constant K_{Mj} of the mooring system depend on the submerged position of the cage, the direction of motion and the axial stiffness of the mooring lines. The wave exciting force amplitude F_j and phase angle ε_{j1} are functions of submerged position, geometry of the cage and net, direction of motion, and frequency of the incident wave.

The solutions of the equations consist of a transient part and a steady-state part. Because of the existence of damping, the transient part would disappear after a few initial oscillations following the start of the motion. The steady-state solutions are of significance and can be written as

$$s_j = S_j \sin(\omega t - \varepsilon_{j1} - \varepsilon_{j2}) \qquad (3.17)$$

where the amplitude of the motion response is

$$S_j = \frac{F_j}{\sqrt{[(K_{Rj}+K_{Mj}) - (m_j+M_j)\omega^2]^2 + (C_j\omega)^2}} = \frac{\frac{F_j}{K_{Rj}+K_{Mj}}}{\sqrt{[1-(\frac{\omega}{\omega_{nj}})^2]^2 + [2\Delta_j\frac{\omega}{\omega_{nj}}]^2}} \qquad (3.18)$$

and the phase angle between the motion response and the exciting force is

$$\varepsilon_{j2} = \tan^{-1}\frac{C_j\omega}{K_{Rj}+K_{Mj}-(m_j+M_j)\omega^2} = \tan^{-1}[\frac{2\Delta_j\frac{\omega}{\omega_{nj}}}{1-(\frac{\omega}{\omega_{nj}})^2}] \qquad (3.19)$$

The term

$$\Delta_j = \frac{C_j}{2\sqrt{(K_{Rj}+K_{Mj})(m_j+M_j)}} \qquad (3.20)$$

is the damping factor in direction j, and

$$\omega_{nj} = \sqrt{\frac{K_{Rj}+K_{Mj}}{m_j+M_j}} \qquad (3.21)$$

is the natural (angular) frequency of the motion in direction j. When the frequencies of the incident waves are near the natural frequency in direction j, resonance will happen and the cage will have the largest motion response in this direction. At this point the damping has a profound effect on the motion amplitude. Increasing the damping of the cage will reduce the motion response significantly. However, at lower or higher frequencies away from the natural frequency the response will decrease and the damping have a negligible effect.

From Equations (3.18) to (3.21) it can be found that the mass or moment of inertia, the damping coefficient, the submerged position of the cage, and the stiffness of the mooring lines may affect the motion responses of the cage system. Some of the influences of these parameters are analyzed below for the motions of surge, sway, heave and roll. The motions of pitch and yaw would be very small for the

proposed cage system and are not included here. In all the analyses, the effects of the surface floats are neglected because their sizes are much smaller compared to those of the floatation chambers of the cage and the cage structure.

3.2.1.1 Surge and sway

For the motions of surge and sway, the hydrostatic restoring force coefficient K_R is zero. When the horizontal deflection is much smaller than the length of the mooring line, the restoring force from the two mooring lines can be approximated as

$$F_M = 2T\frac{\Delta x}{l} \tag{3.22}$$

so the mooring spring constant for surge and sway is

$$K_M = 2\frac{T}{l} \tag{3.23}$$

where T is the pretension in each mooring line, Δx is the deflection of surge or sway and l is the length of the tension mooring lines. Then the natural frequency of the surge or sway motion can be calculated as

$$\omega_n = \sqrt{\frac{2T/l}{m+M}} \tag{3.24}$$

Therefore, the natural frequencies and hence the motions of surge and sway are not significantly influenced by the

stiffness of the mooring lines but, rather, they are affected mainly by the pretension and length of the mooring lines, and also the mass and added mass of the cage. Because the frequencies of the incident waves may be much larger than the natural frequencies of surge and sway, the effect of damping may be negligible.

3.2.1.2 Heave

For the motion of heave, the hydrostatic restoring force coefficient K_R is mainly caused by the buoyancy change of the two floatation chambers of the cage. When the floatation chambers are on the water surface, K_R can be approximated as

$$K_R = 2\rho g S_F \tag{3.25}$$

where ρ is the density of water, g is the acceleration of gravity and S_F is the section area of the floatation chamber in the water line. When the floatation chambers are submerged below the water surface, K_R is about zero. The spring constant of mooring system in heave motion is

$$K_M = 2K \tag{3.26}$$

where K is the axial spring constant of the individual mooring line. The natural frequency of the heave motion will be

$$\omega_n = \sqrt{\frac{2(\rho g S_F + K)}{m+M}} \tag{3.27}$$

when the floatation chambers of the cage are on the water surface, and will be

$$\omega_n = \sqrt{\frac{2K}{m+M}} \qquad (3.28)$$

when the floatation chambers are submerged below the water surface. Consequently, the natural frequency of the heave motion will become smaller and mainly depend on the stiffness of the mooring lines and the mass of the cage when the floatation chambers of the cage are submerged below the water surface. The stiffness of the mooring lines will influence the response of the heave motion significantly. With the increase of stiffness of the mooring lines, the natural frequency of the heave motion will become larger and the amplitude of the motion will become smaller. The pretension of the mooring lines has little effect on the heave motion as long as the pretension is large enough to prevent the mooring lines from slackening off, while the mass of the cage will affect the natural frequency and hence the response of the motion. Because the frequencies of the sea waves may be close to the natural frequency of heave, the damping of the cage may be important in determining the amplitude of the heave motion.

3.2.1.3 Roll

Because the distance between the centre of buoyancy and

the centre of gravity of the cage will be small in the proposed system, when the floatation chambers of the cage are on the water surface the hydrostatic restoring force coefficient K_R of roll can be approximately calculated as

$$K_R = \frac{1}{2}\rho g S_p d^2 \qquad (3.29)$$

where d is the distance between the centres of the two floatation chambers (and is also the distance between the two mooring lines in the proposed system), and when the floatation chambers are submerged below the water surface K_R is about zero. The spring constant K_M from the mooring system is

$$K_M = \frac{1}{2}Kd^2 \qquad (3.30)$$

where d is the distance between the two mooring lines. When the floatation chambers of the cage are on the water surface, the natural frequency of roll will be

$$\omega_n = \sqrt{\frac{(K+\rho g S_p)\, d^2}{2(I+I_A)}} \qquad (3.31)$$

where I is the moment of inertia and I_A is the added moment of inertia of the roll motion. When the floatation chambers are submerged, the natural frequency will become

$$\omega_n = \sqrt{\frac{Kd^2}{2(I+I_A)}} \qquad (3.32)$$

Therefore, conclusions similar to those of the heave motion

can be obtained, substituting moment of inertia for mass. Also, the distance between the two mooring lines will affect the natural frequency and the amplitude of the roll motion.

3.2.2 Mooring force response

Suppose the wave forces acting on the mooring lines are negligible, the dynamic force responses in the two mooring lines of the cage can be estimated by the quasi-static method after the motion responses of the cage are known. The motions of the connecting points of the mooring lines are used to predict the dynamic mooring force responses (Oortmerssen, 1986). The dynamic force responses in the mooring lines depend on the instantaneous changes of the cable length which are affected by the horizontal and vertical motions of the cage, and can be calculated as

$$F_M = K\Delta l \qquad (3.33)$$

where F_M is the dynamic force in the mooring line, K is the axial spring constant of the mooring line and Δl is the change of cable length caused by the cage motions.

Assuming the horizontal excursions of surge and sway are small compared to the length of the mooring lines in the equilibrium position, the extensions of mooring lines caused by surge and sway will be very small and the contribution of

surge and sway to the dynamic force responses in the mooring lines will be negligible. When the cage is oriented with its axle parallel to the wavefront, the dynamic forces in the mooring lines will be mainly caused by the heave motion of the cage and can be estimated for both lines as

$$F_M = Kz \tag{3.34}$$

where z is the instantaneous heave motion of the cage. When the cage is oriented with its axle perpendicular or oblique to the wavefront, the dynamic forces in the mooring lines will be mainly caused by the combined effect of heave and roll, the force in the sea side mooring line can be approximated as

$$F_M = K(z - \frac{d}{2}\sin\phi) \tag{3.35}$$

where ϕ is the instantaneous roll motion of the cage, and the force in the lee side mooring line can be estimated as

$$F_M = K(z + \frac{d}{2}\sin\phi) \tag{3.36}$$

In such case, the phase angle between heave and roll will be important in determining the dynamic force in each mooring line.

Because the mooring force responses are mainly determined by the heave and roll motions of the cage, the parameters which affect the heave and roll responses will also affect the mooring force responses. The responses will be different when

the cage is in different submerged positions. The stiffness of the mooring lines will influence the responses significantly. Also the mass and moment of inertia of the cage will affect the mooring force responses. Pretension in the mooring lines will have little effect on the mooring force responses as long as it is large enough to prevent the mooring lines from being slack.

3.3 Hydraulic Modelling

Small scale model tests are a convenient means of predicting full-scale performance. Their use can help to avoid disastrous mistakes in prototype design. In order to predict the performance of the prototype cage system by means of model tests, certain laws of similarity must be observed. These model laws provide relationships between variables pertaining to the model and the prototype, thus enabling measurements of the model tests to be used to predict prototype values.

In addition to geometric similarity, the model and the prototype must also achieve dynamic similarity. For the fish cage tests to be conducted, this means the Reynolds number (the ratio of viscous forces to inertial forces)

$$Re = \frac{VL}{\nu} \qquad (3.37)$$

and the Froude number (the ratio of gravitational force to inertial forces)

$$Fr = \frac{V}{\sqrt{gL}} \qquad (3.38)$$

must be the same in both the model and prototype, in which V is a particular velocity, L is a typical length of the structure and ν is the kinematic viscosity of the fluid. The Reynolds number ensures the similarity of the viscous forces, while the Froude number ensures the similarity of the gravitational forces. Unfortunately, in practice such requirements cannot be met. Therefore, special considerations must be taken into account according to the characteristics of the tests.

3.3.1 Resistance Tests

Because the resistance tests of the cage are to be conducted with the models submerged below the water surface, no significant surface waves will be created and the free surface effects are negligible. The flow around a submerged object is a totally viscous phenomenon. The drag force on such a object is caused by frictional resistance and by pressure differences across the object, neither of which are related to gravitational effects (Sharp, 1981). The effect of Froude number is then unimportant. Therefore, Reynolds number must

have the same values in the model and prototype and Reynolds law should be used to upscale the model test results to prototype values. Table 3.2 gives the scale factors for length, velocity and force based on Reynolds law (Sharp, 1981).

Table 3.2 - Scale factors based on Reynolds law

Parameter	Definition	Scale Factor
Length	L_p/L_m	λ
Velocity	V_p/V_m	$(\nu_p/\nu_m)(1/\lambda)$
Force	F_p/F_m	$(\rho_p/\rho_m)(\nu_p/\nu_m)^2$

m - model p - prototype λ - L_p/L_m

Because the models are to be tested in water ($\nu_p/\nu_m \approx 1.0$, $\rho_p/\rho_m \approx 1.0$), from Table 3.2 it can be found the model velocity should be λ times greater than the expected prototype velocity and the force acting on the model is about the same as the force acting on the prototype. This is obviously impractical because of the limitation of the test facility. In most cases, the Reynolds numbers in the prototype will be much larger than the Reynolds numbers which can be achieved in the model tests. Therefore, when the Reynolds number in the prototype is out of the range of the Reynolds number tested, some approximations have to be made to use the model test results to predict prototype values.

The cage frame and net can approximately be considered as consisting of many small cylindrical elements which are normal or inclined to the current direction. The drag forces on the inclined cylinders can be decomposed into their normal and tangential components and the tangential components can usually be neglected (Chakrabarti, 1987). Therefore, the drag force of the element i in the direction of current can be calculated as

$$dF_i = \frac{1}{2} \rho C_{Di} D_i V^2 \sin^3\theta_i \, ds_i \qquad (3.39)$$

where C_{Di} is the drag coefficient of the cylindrical element, D_i is the diameter of the element, ds_i is the length of the element and θ_i is the angle between the element and the current direction. The resistance force of the frame and net F is therefore equal to the integration of dF_i

$$F = \frac{1}{2} \rho V^2 \Sigma C_{Di} D_i \sin^3\theta_i \, ds_i \qquad (3.40)$$

The drag coefficient C_{Di} is dependent on the Reynolds number and surface roughness of the cylindrical element.

Figure 3.6 shows how the drag coefficient C_D changes with the Reynolds number. As the Reynolds number is on the left side of the subcritical flow regime, the drag coefficient is larger than that in the subcritical flow regime and decreases significantly with the Reynolds number. When the Reynolds

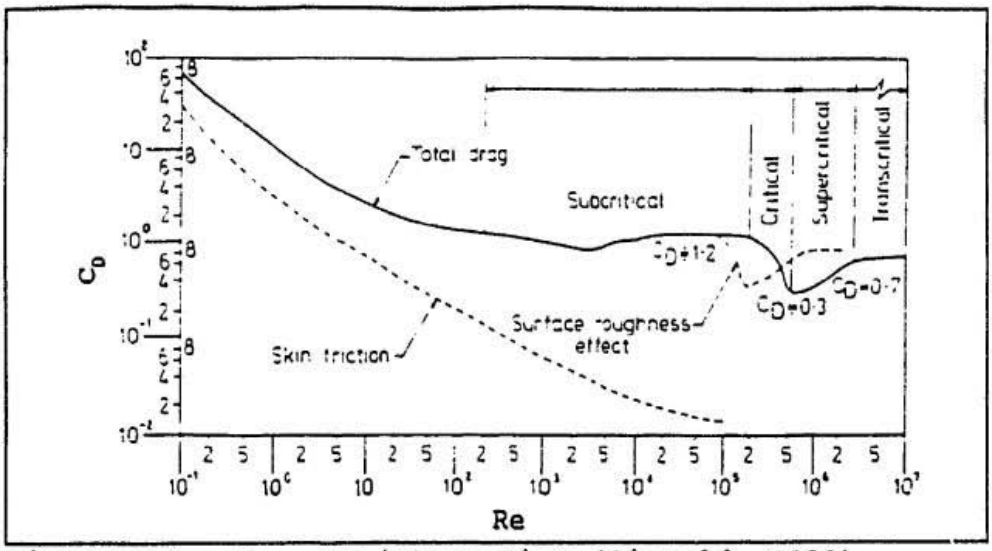

Figure 3.6 - C_D - Re interaction (Gisvold, 1980)

number is within the range of subcritical flow regime, the drag coefficient is relatively constant and can be approximately considered to be independent of Reynolds number. When the Reynolds number is within the range of critical and supercritical flow regime, the drag coefficient varies significantly with the Reynolds number and becomes smaller than that in the subcritical flow regime. Consequently, if the model tests are carried out in the subcritical flow regime and the flow regime of the prototype is still within the subcritical range, it can be assumed that the resistance force coefficients of the cage frame and net obtained from the model tests do not change because of the increase of Reynolds number in the prototype, and can still be used to estimate the resistance forces of the prototype frame and net. When the flow regime of the prototype is critical or supercritical, the

resistance force coefficients obtained from the model tests are larger than the actual values in the prototype and the resistance forces of the prototype would be overpredicted. Thus, a correction factor should be introduced according to the Reynolds number and surface roughness of the prototype if a more accurate estimation is wanted.

For the tests to be carried out, a model net which is scaled down geometrically from the prototype net cannot reproduce the resistance force of the prototype net appropriately when the Reynolds numbers of the model and the prototype are not the same, special care has to be taken to select a proper model net (see section 3.3.3 below).

As for the resistance forces of the floatation chambers of the cage, because the sharp edges of the chambers tend to cause flow separation regardless of the character of the boundary layer, the forces are insensitive to Reynolds number (White, 1986). Therefore, it is reasonable to assume that the resistance force coefficients obtained from the model tests do not change significantly with the increase of the Reynolds number in prototype and are still valid to be used to estimate the resistance forces of the prototype floatation chambers.

3.3.2 Moored tests

In order to achieve dynamic similarity between the model and the prototype, both the Froude number and the Reynolds number should be as similar as possible in the model and the prototype. Unfortunately, as both the model and the prototype operate in water, it is impossible to correctly scale the test results to prototype values in which both the Froude and Reynolds similarity criteria are satisfied simultaneously (Sharp, 1981). This means that all the forces cannot be correctly scaled.

Since the effects of gravity tend to dominate waves and wave induced motions of floating objects, Froude law should be used to upscale the model test results to prototype values. This means the Reynolds numbers in the model are a factor of $\lambda^{3/2}$ smaller than those in the prototype and the viscous forces may not be correctly scaled. Nevertheless, from the discussion in section 3.3.1 it can be found that for the floatation chambers of the cage the effect of Reynolds number on viscous forces may be negligible, and for the cage frame the effect of Reynolds number on viscous forces may also be relatively unimportant as long as the Reynolds numbers in the model frame and in the prototype frame are both within the range of subcritical flow regime. However, the viscous forces acting

on the net will influence the motions of the cage to some extent (because of the small twine diameter the forces on the net will be dominated by the drag components) and the effect of Reynolds number on the viscous forces cannot be neglected, special care has to be taken to select a model net which would reproduce the motions of the prototype as accurately as possible (see section 3.3.3 below).

In addition to Froude law, the governing equations of motions of a moored object, which include defining equations involving the relevant quantities, must also hold for both the model and the prototype and should also be used to develop appropriate relationships between the different relevant scale factors (Sarpkaya and Isaacson, 1981). Table 3.3 gives the scale factors based on Froude law and the governing equations of motions.

3.3.3 Selection of a proper model net

It is almost impossible to find a model net which is scaled down from the prototype net according to the geometric scale. Even if such a model net can be found, it is not appropriate to be used in the planned resistance tests and moored tests in which the Reynolds numbers of the model and the prototype will not be the same. For both resistance tests

Table 3.3 - Scale factors based on Froude law

Parameter	Definition	Scale Factor
Length	L_p/L_m	λ
Mass	m_p/m_m	$(\rho_p/\rho_m)\lambda^3$
Moment of inertia	I_p/I_m	$(\rho_p/\rho_m)\lambda^5$
Time	t_p/t_m	$\lambda^{1/2}$
Wave period	T_p/T_m	$\lambda^{1/2}$
Wave frequency	f_p/f_m	$1/\lambda^{1/2}$
Wave height	H_p/H_m	λ
Water depth	h_p/h_m	λ
Submerged depth	s_p/s_m	λ
Spring constant	K_p/K_m	$(\rho_p/\rho_m)\lambda^2$
Force	F_p/F_m	$(\rho_p/\rho_m)\lambda^3$
Velocity	V_p/V_m	$\lambda^{1/2}$
Linear displacement	x_p/x_m	λ
Angular displacement	α_p/α_m	1

m - model p - prototype $\lambda = L_p/L_m$

and moored tests, the twine diameter of the model net will be so small that the Reynolds number of the model net will be on the left side of the subcritical flow regime where the Reynolds number influences the viscous force significantly, while the Reynolds number of the prototype net is within the range of subcritical flow regime where the viscous force is almost independent of the Reynolds number. Therefore, the model net cannot reproduce the prototype net properly and the scale error caused by the difference of Reynolds number in the

model and the prototype will not be negligible.

The following method was proposed to select a net for the model tests of the cage system. First, the drag forces of the prototype net at different velocities were measured in a towing tank. Next, the measured drag forces and corresponding velocities were scaled down by using the scale factors based on Froude law, so the target drag force-velocity relationship for the selection of model net was obtained. Then, a number of net materials, whose areas were $1/\lambda^2$ of the area of the tested prototype net and whose twine diameters were just large enough to ensure the Reynolds numbers in the model tests would be within the range of subcritical flow regime, were tested in the towing tank and the one which had approximately the same drag force-velocity relationship as the target relationship was chosen as the model net. This meaned if the **unit area** of the prototype net had a drag force-velocity relationship

$$F_p = kV_p^2 \tag{3.41}$$

the **unit area** of the model net would also have the same drag force-velocity relationship

$$F_m = kV_m^2 \tag{3.42}$$

in which the constant k was the same as in Equation (3.41). The differences were that the relation for the model net was

obtained in a smaller velocity range ($V_m = V_p/\lambda^{1/2}$) and the twine diameter of the model net was smaller than that of the prototype net.

Because the moored tests have to be carried out according to Froude law while the forces on the net are dominated by the drag components, a model net selected with the method above is appropriate for the moored tests. It can ensure that the forces on the prototype net can be properly reproduced in the moored tests. Also, such a model net is appropriate for the resistance tests. Within the range of subcritical flow regime the resistance force can be approximately considered to be independent of the Reynolds number. In such case, "Reynolds number models" may be designed and operated according to Froudian scaling requirements (Sharp, 1981). A similar method was used by Whittaker et al (1990) in a model testing of a cage system.

4 EXPERIMENTAL STUDY

When the experiments were conducted, there was no detailed prototype design. The purposes of the experiments were to understand how the proposed cage and mooring system would respond to the environmental forces; to investigate how the parameters of the system, such as stiffness and pretension of the mooring lines as well as submerged depth and orientation of the cage, would affect the responses of the cage system, and to provide some useful information for the prototype design and numerical model establishment.

The model tests were designed by assuming the model scale was 13.5 (Estimating that the diameter of the prototype cage would be 12.0 m). All parameters and test results presented in this thesis are referred to the model tests and should be upscaled to prototype values according to the model scale and appropriate model laws.

4.1 Test Facility and Models

4.1.1 Wave/tow tank facility

The model tests were carried out in the wave/tow tank at Memorial University of Newfoundland, St. John's, Canada as

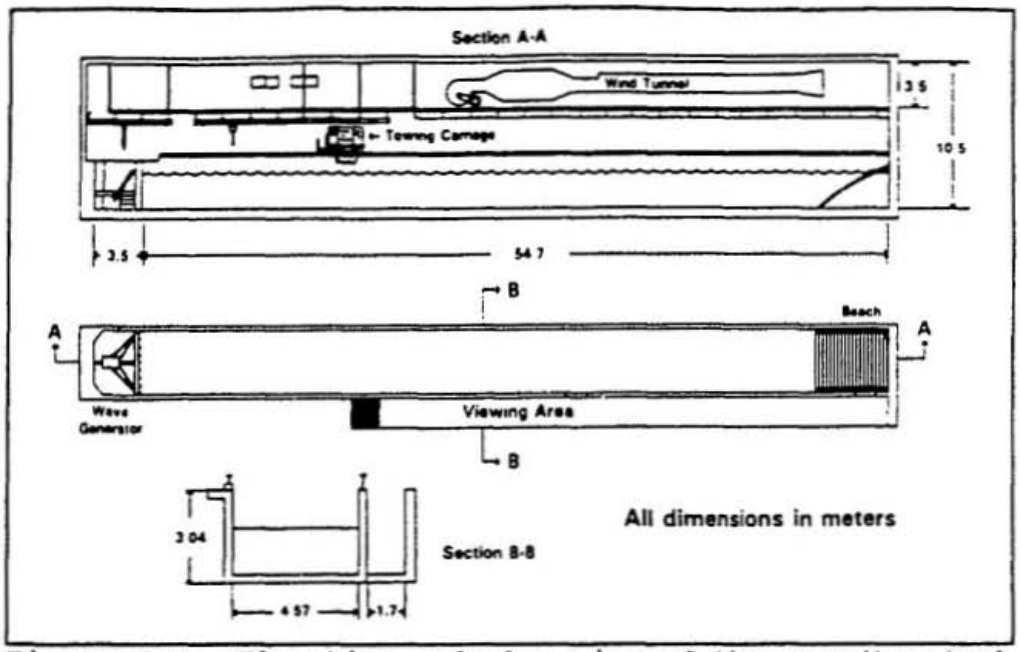

Figure 4.1 - Elevation and plan view of the wave/tow tank (OERC, 1990)

shown in Figure 4.1.

The wave tank has inside dimensions of 58.27 m in length, 4.57 m in width, and 3.04 m in depth, with a maximum operational water depth of 2.13 m. At one end is an MTS closed-loop, servo-controlled piston type wave generator, which reduces the operating length of the tank to 54.74 m. The wave generator can generate regular waves and irregular waves of any theoretical spectrum. Several large viewing windows are conveniently located in one of the tank's walls, enabling visual and photographic analysis of a model's motion at both surface and subsurface elevations.

A towing carriage runs on parallel rails 4.88 m apart on top of the tank wall, for use in towing tests and resistance tests. The carriage has a net weight of 3.9 tonnes and can obtain a maximum speed of 5.0 m/s.

4.1.2 Spherical and geodesic models

The spherical model, as shown in Figure 4.2, was made of aluminum alloy. It consisted of eight half bows and two bow reinforcements, with diameter of 9 mm, and an axle with

Figure 4.2 - Spherical model

diameter of 13 mm. The bows were fastened to two round plates fixed at two ends of the axle. The diameter of the model was 900 mm. Two floats made of styrofoam which simulated the floatation chambers of the prototype cage were attached at two far ends of the axle, with a distance of 1050 mm between the centres of the two floats. Figure 4.3 gives the dimensions of the float.

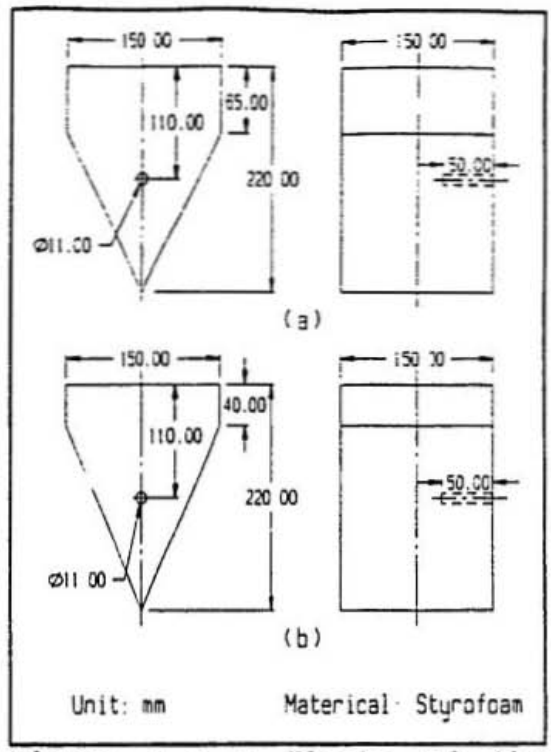

Figure 4.3 - Floats of the models. (a) For spherical model, (b) For geodesic model

The geodesic model, with a diameter of 850 mm, consisted of wood bar elements, copper joints and an axle (see Figure 4.10 below). The diameter of the bar elements was 6 mm and the diameter of the axle was 13 mm. Similar to the spherical model, two floats which simulated the floatation chambers of the prototype were attached at two ends of the axle, with the centres of the two floats 990 mm apart. The size of the float was a little smaller than that of the spherical model and the dimensions are also shown in Figure 4.3.

In order to measure the six degrees of motion of the cage with the Selspot system (see section 4.3.2 below), a frame with Selspot LEDs was fixed at the top of the model during the moored tests. Some weights were added at the bottom of the model to balance the measurement frame and keep the model floating straight upward. When the model was submerged from the surface to middle, and from the middle to bottom position, some more weights were added on the axle near the two floats to reduce the buoyancy of the cage and keep the pretension of the mooring lines about the same.

Table 4.1 and 4.2 summarize the general parameters of the spherical and geodesic models. The mass and moment of inertia of the roll motion in the tables include the measurement frame and the weights added.

4.1.3 Model Net

If a net material which was scaled down geometrically from the prototype net was used as a model net, such a model net couldn't reproduce the force acting on the prototype net appropriately in the present resistance tests and moored tests in which the Reynolds numbers of the model and the prototype were not the same (see section 3.3.3 above). Therefore, a series of tests were conducted and a model net was selected

Table 4.1 - Parameters of the spherical cage model

.meter of the model		900 mm
Diameter of bow elements		9 mm
Diameter of axle		13 mm
Distance between floats		1050 mm
Mass	Surface position	6.00 kg
	Middle position	6.23 kg
	Bottom position	6.33 kg
Moment of inertia of roll	Surface position	1.98 kgm^2
	Middle position	2.12 kgm^2
	Bottom position	2.33 kgm^2

Table 4.2 - Parameters of the geodesic model

Diameter of the model		850 mm
Diameter of the bar elements		6 mm
Diameter of the axle		13 mm
Distance between floats		990 mm
Mass	Surface position	4.90 kg
	Middle position	5.30 kg
	Bottom position	5.44 kg
Moment of inertia of roll	Surface position	1.88 kgm^2
	Middle position	1.95 kgm^2
	Bottom position	2.11 kgm^2

by using the method described in section 3.3.3 before the present tests were carried out. Such a model net ensured that the forces acting on the prototype net were reproduced properly in the resistance tests and moored tests.

4.1.4 Mooring system

The prototype mooring system, as shown in Figure 1.1, was modelled by two 0.8 mm steel cables in combination with two springs. Because the steel cable had very high stiffness, it was the spring that provided the required axial stiffness to simulate the prototype mooring line. Because the effect of the surface float was negligible due to its small size compared to the cage and the floatation chambers of the cage, no surface float was used in the model moored tests.

The axial spring constant of the prototype mooring line is a function of material, length and mean (equilibrium) tension of the mooring line (Wilson, 1969). Because there was no detailed design of the prototype mooring system, it was supposed that nylon rope with a diameter of 40 mm would be used, the length of the mooring line would be about 25 m, and the mean tension in each mooring line would be about 2000 kg. Using the formulas and figures provided by Wilson (1969) the axial spring constant of the prototype mooring line was

estimated as about K_p = 1500 kg/m.

Using the scale factor in Table 3.3, the axial spring constant of the model mooring line was then calculated as about K_m = 8 kg/m. In different submerged positions, the length of the mooring line would be changed, so the spring constant of the mooring line would be different. In the model tests, K_m = 10 kg/m was used in all positions for the reason of simplification and easy comparison.

4.2 Resistance Tests

4.2.1 Experimental arrangement

The resistance tests were performed by using the towing carriage of the wave/tow tank, a model holding frame, a pivoting pole, a holding assembly and a force transducer. Figure 4.4 shows a schematic of this arrangement.

The cage model was held rigidly below the water surface by the model holding frame which was suspended from the towing carriage through the pivoting pole. The model holding frame was constructed with steel pipe and steel rectangular bar.

The pivoting pole was used to hold the model holding

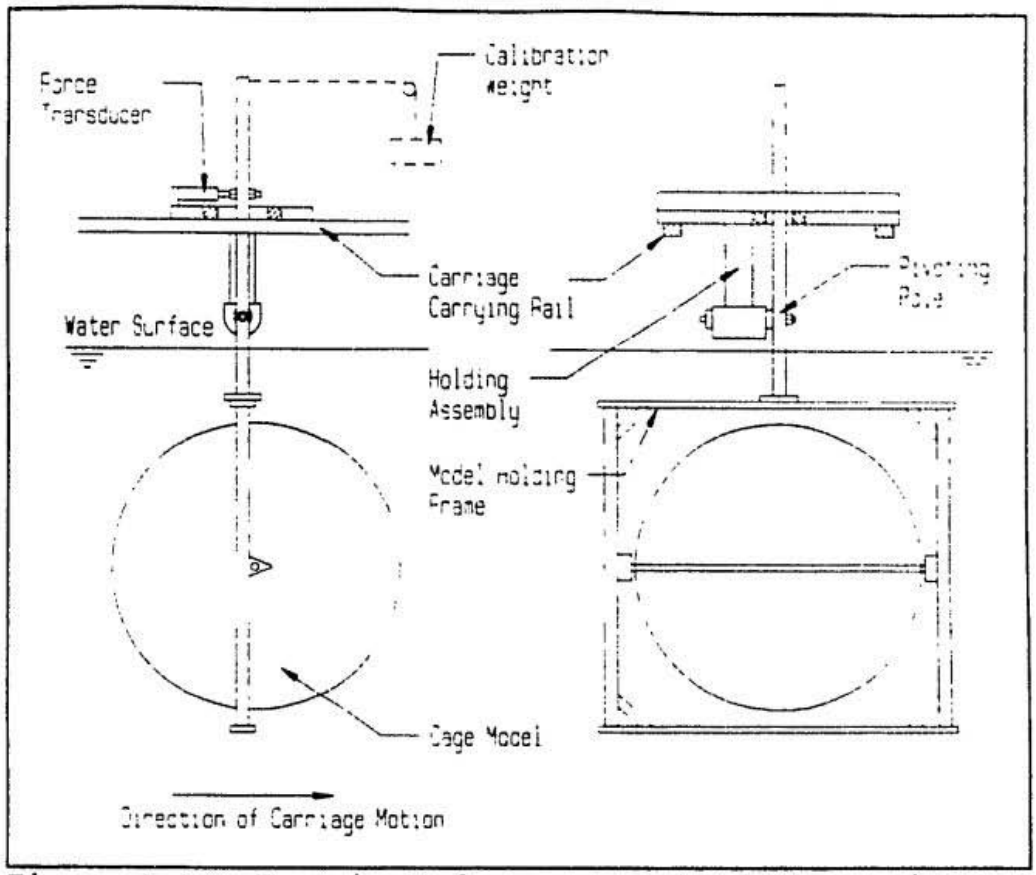

Figure 4.4 - Experimental arrangement of the resistance tests

frame in the water. It had a circular disk welded to its submerged end. Matching the holes drilled in the disk and the frame enabled the frame to be bolted to the pivoting pole. The bolt hole positions were preset so that the frame and the models could form specific angles with the direction of motion when it was attached to the carriage. This disk allowed precise changes of angle between tests.

The holding assembly consisted of a rectangular plate

which was fixed with the two carrying rails of the towing carriage, and a shaft and bearing arrangement which was attached to a length of pipe extending down from the rectangular plate and was used to support the pivoting pole. When the carriage was in motion, the resistance forces of the model holding frame and the model tended to rotate the pivoting pole and shaft clockwise. A force transducer was attached between the rectangular plate and the upper end of the pivoting pole. This force transducer provided a reaction force which prevented the rotation of the pivoting pole and generated an electric signal output which was a linear function of the applied force. The total resistance force of the model holding frame and the model was then measured.

The models were submerged about 30 cm below the water surface in all the tests, so the free surface effects should be negligible.

4.2.2 Instrumentation and data acquisition

Data acquired during the resistance tests were the resistance forces acting on the model holding frame and the model. A block diagram of the instrumentation and data recording system is provided in Figure 4.5.

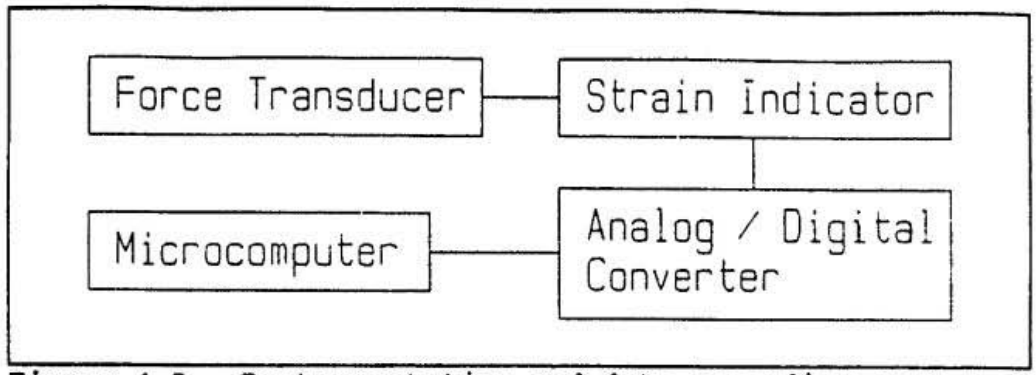

Figure 4.5 - Instrumentation and data recording system of the resistance tests

The outputs of the force transducer (Model: 1363-1K-20P1) were amplified and monitored by a Type 1526 Strain Indicator before they were digitized and recorded by a Keithley System 570 analog to digital converter and a HP-86 microcomputer with a S570 data acquisition program and a calibration file. The digitized results of each run of test were then displayed on the computer screen for instant examination, and stored on a floppy disk for future processing.

From time to time the force transducer was calibrated with the S570 data acquisition program and the calibration file was updated. When in calibration, calibrated weights were attached through a pulley horizontally to an eye bolt installed at the upper end of the pivoting pole (see Figure 4.4). The distance between the eye bolt and the shaft centre of the holding assembly was chosen to be equal to the distance between the centre of the model holding frame and the shaft

centre of the holding assembly. Therefore, the digitized outputs of the computer were the actual values of resistance forces acting on the model frame and the model and no further conversion was needed.

For each run of tests, data were acquired during a 30 second time period. Data recording was initiated about 4 seconds before the carriage was set in motion so that the first 4 seconds' data could provide an averaged zero for the data analyses. The carriage reached the constant desired velocity from rest within less than 4 seconds, so the resistance force was measured for more than 20 seconds.

4.2.3 Experimental procedure

All the tests were carried out with the axle of the cage models parallel (90°), perpendicular (0°) and oblique (45°) to the direction of carriage motion, at velocities of 0.2, 0.4, 0.6, 0.8, 1.0, 1.2, 1.4 and 1.6 m/s. Due to the measuring range of the force transducer, tests at higher velocities were not conducted.

First, the resistance forces of the empty model holding frame were tested. Then, the net which was to be used on the cage models was put on the model holding frame and the tests

were repeated. Next, the spherical model and geodesic model were placed in the model holding frame and tested. Finally, the model net was added to the spherical model and geodesic model and the tests were repeated again. Because it was impossible to fix the floats and the model in the holding frame at the same time, one of the floats for the geodesic model was tested separately. Using this procedure, it was possible to determine the resistance forces of all the individual components. It should be noted that the interaction between components was assumed to be small.

4.2.4 Method of data analysis

The data files obtained from the tests were analyzed by a PLTKLY PC plotting program (WT, 1990) with a PC computer and the averaged resistance forces were obtained over about 20 seconds' records. The averaged values were then used in the resistance force calculations. The resistance force of the tested model was obtained by subtracting the resistance force of the empty model holding frame from the total resistance force of the frame and model. The resistance force of the net on the model was calculated by subtracting the resistance force of the model without net from the resistance force of model with net.

After the resistance forces of each series of tests were obtained at different velocities, the coefficients

$$C_r = \frac{F_r}{V^2} \tag{4.1}$$

were calculated to examine the relationship between the current velocity and the resultant resistance force, where F_r is the resistance force obtained from the test and V is the corresponding velocity. Also, the least square method was used to fit the test results by assuming that the resistance force and the current velocity have a relationship of

$$F = kV^2 \tag{4.2}$$

and the constant k was obtained.

The errors of test results at a velocity of 0.2 m/s may be relatively large because of the low values of the resistance forces. Also, the errors of the test results of the float and the planar net at 90° may also be relatively large because of the low values of the resistance forces compared to those of the model holding frame. Any errors in the measurements of resistance forces of the model holding frame may cause large relative errors in these results.

4.3 Moored Tests

4.3.1 Experimental arrangement

The moored tests were conducted in the wave tank described in section 4.1.1 above. Figure 4.6 shows a schematic of the experimental arrangement.

The model was held in position by its mooring system. Two O-ring load cells were connected between the bottom of the floats and the upper ends of the springs by means of quick-rings. Two 0.8 mm steel cables consisted of the remaining portions of the mooring lines. The cables ran from the lower ends of the springs vertically downwards to the eye bolts which were bolted to a heavy steel frame on the bottom of the tank, passed through the eye bolts and then went up to the cable clampers fixed on the cat walk.

The O-ring load cells were used to measure the force responses in the mooring lines and the springs to provide the required axial stiffness of the mooring lines. By rotating the steel frame on the bottom of the tank, the orientation of the cage model to the incident wave was changed. The cage model was kept in different submerged positions by adjusting the lengths of cables passing through the cable clampers.

4.3.2 Instrumentation and data acquisition

Data acquired during the moored tests were incident wave data, mooring force data and cage motion data. Figure 4.7 provides a block diagram of the instrumentation and data recording system.

The time histories of the wave profiles were measured by standard twin wire linear resistance type wave probes at two locations (see Figure 4.6). One probe (front probe) was placed about 1.5 m upstream of the model on the tank's centre line. Another probe (side probe) was placed by the side of the model at a distance of about 1.5 m from the centre line of the tank. The outputs of the probes were amplified by an amplifier.

The time history of mooring force in each mooring line was measured by the fully waterproofed strain gauge of the O-ring load cell in that line. The strain gauge outputs were amplified by a Vishay Instruments 2120 Strain Gauge Conditioner System, and then sent to a Model 3323 low-pass filter of 3 Hz upper cutoff.

The amplified outputs of the wave probes and strain gauges were then digitized simultaneously by a 32 channel Keithley System 570 analog to digital converter and a HP-86

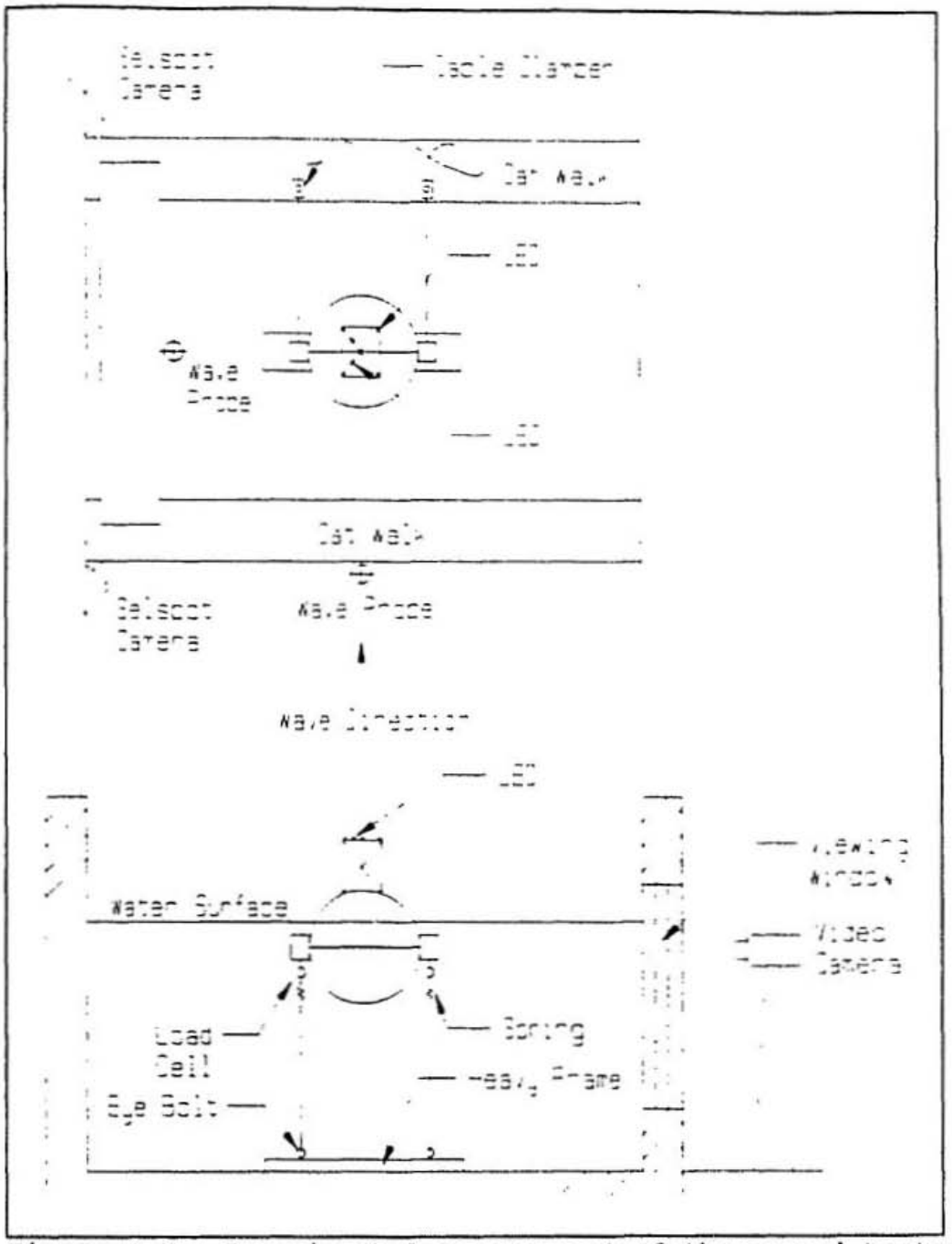

Figure 4.6 - Experimental arrangement of the moored tests

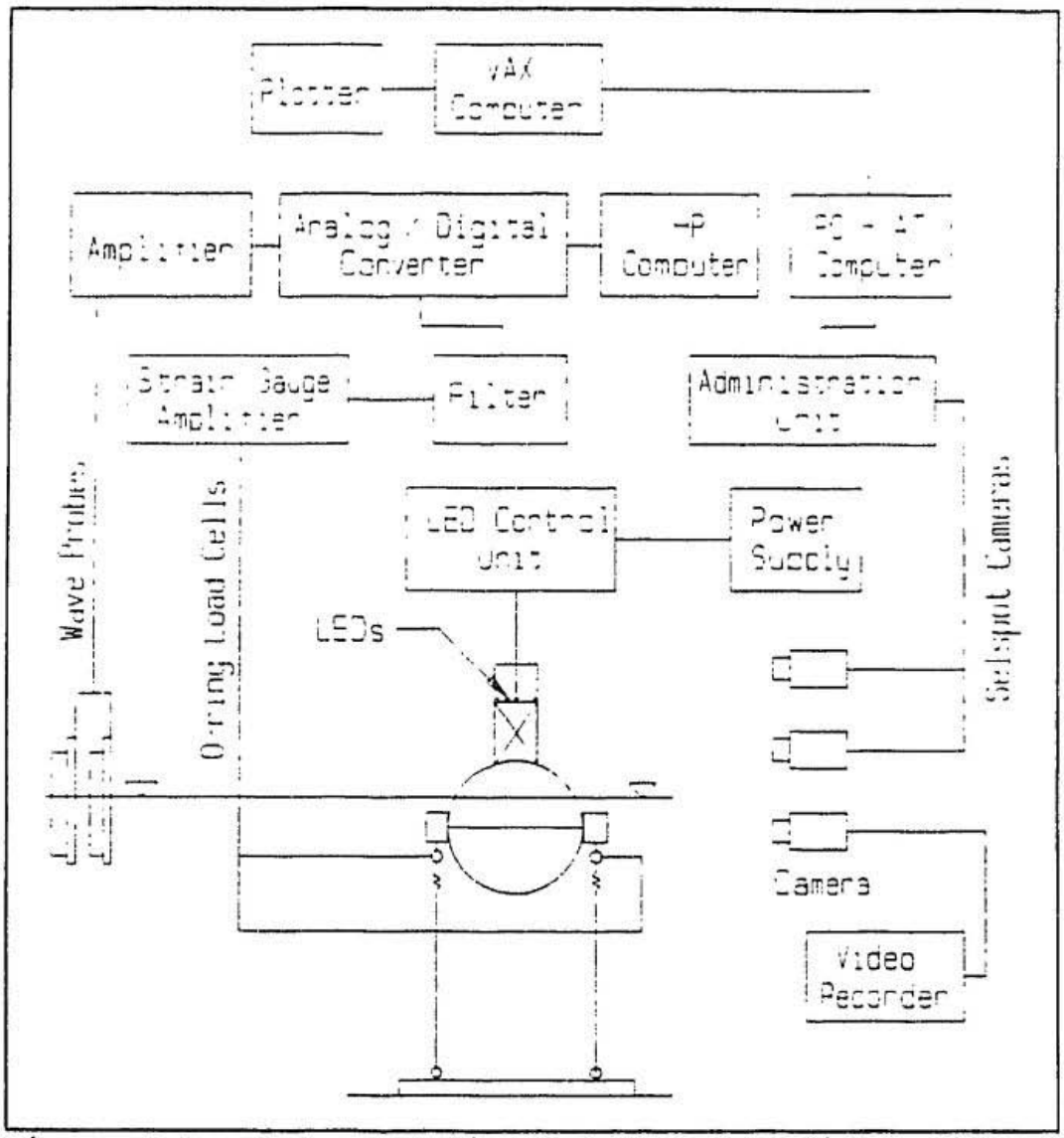

Figure 4.7 - Instrumentation and data recording system of the moored tests

microcomputer with a S570 data acquisition program and a calibration file. The digitized incident wave and mooring force results of each run of test were displayed on the computer screen for instant monitoring, recorded in a floppy disk and then transferred to a Digital VAX 8530 computer through the PC-AT computer mentioned below. Prior to the start of tests each day the wave probes and the load cells were calibrated with the S570 data acquisition program and the calibration file was updated.

The six degrees of motion of the cage were measured simultaneously by the Selspot (selective spot) System manufactured by Selective Electronic Co. (SELCOM) of Sweden. This optical-electronic device provides accurate measurement of the three dimensional position of a rigid body with respect to a fixed coordinate system (OERC, 1990). Seven infrared light emitting diodes (LEDs) were strategically located on a frame which was fixed at the top of the model. In order to prevent any measurement error caused by the reflection of the infrared light rays by the water surface, a thin black cardboard was fixed right below the LEDs. Two infrared sensitive cameras placed approximately 90° from each other monitored the movement of the LEDs, and supplied this information to the administration unit that digitized the data and fed them to a PC-AT microcomputer at the rate of 312.5

frames per second. The microcomputer collected the data at the rate of 19.5 frames per second by averaging the successive frames, and displayed a real time view of the LEDs on the screen for monitoring. After each test run was finished, the raw data file was transferred over a high speed Ethernet link from the PC-AT to the VAX 8530 computer where it was processed. The system software installed in the VAX 8530 was then used to calculate the time series records of the six degrees of motion of the cage model and the results were plotted approximately 10 minutes later on an HP plotter for examination. The processed data files, which provided displacement versus time for the six degrees of motion, were used for further analyses.

During the entire test program a video camera was also used to record the motion of the cage through the viewing window in the side wall of the tank. These video records were used in visual analysis later.

For regular wave tests incident wave, mooring force and motion data were collected simultaneously for 60 seconds, while for irregular wave tests data were collected for 120 seconds. The data collecting program in the PC-AT computer was initiated by the S570 data acquisition program in the HP-86 computer so that the incident wave and mooring force data

could be related to the motion data. Also, a digital timer initiated at the same time was displayed on the video records. In all the tests, data recording was initiated after several waves had passed the model and steady state had been reached.

4.3.3 Experimental procedure

The moored tests of both the spherical and geodesic models were carried out in regular waves and irregular waves. The regular wave tests were run at frequencies of 0.36, 0.44, 0.58, 0.72, 0.86 and 1.0 Hz at two different wave heights, 5 cm and 10 cm. Table 4.3 gives the corresponding wave periods for the model and the prototype (λ = 13.5). Irregular waves were generated by using the Bretscheider spectrum which had a significant wave height of 10 cm and a peak frequency of 0.6 Hz as a target spectrum. The water depth of the wave tank was set to be 2.0 m in all the tests.

Table 4.3 - Wave frequencies used in regular wave tests and corresponding wave periods for model and prototype

Frequency (Hz)	0.36	0.44	0.58	0.72	0.86	1.00
Model Period (s)	2.78	2.27	1.72	1.39	1.16	1.00
Prototype Period (s) (λ = 13.5)	10.21	8.35	6.33	5.10	4.27	3.67

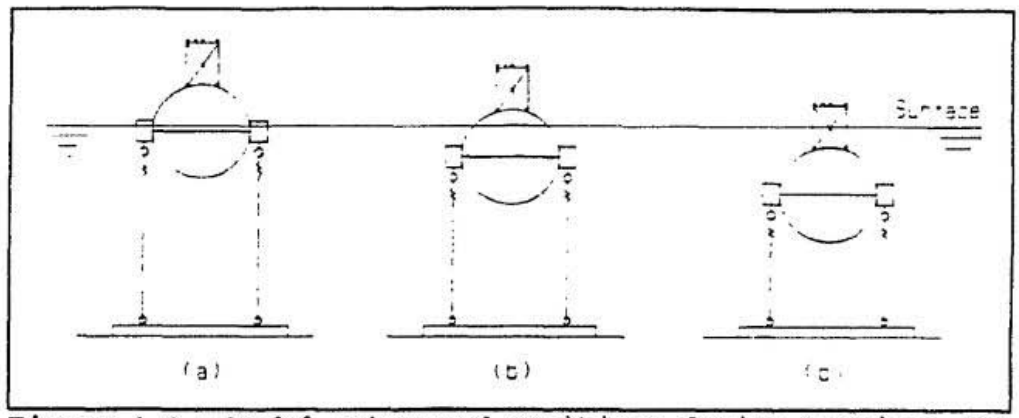

Figure 4.8 - Model submerged positions during testing. (a) Surface position, (b) Middle position, (c) Bottom position

Both models were tested in three submerged positions as shown in Figure 4.8, surface position (axle 10 cm below water surface), middle position (axle 30 cm below water surface) and bottom position (axle 65 cm below water surface); and in two orientations as shown in Figure 4.9, parallel orientation (axle parallel to wavefront) and perpendicular orientation (axle perpendicular to wave front). In the middle submerged position, orientation with axle 45° to the wavefront was also tested. The surface position simulated the servicing position, the middle position the operational position and the bottom position the fully submerged position of the prototype cage system. Because of the limitation of the frame on which the LEDs of the Selspot system were fixed, the present bottom position was the deepest the cage model could go. Figure 4.10 shows the geodesic model in the middle position and parallel orientation.

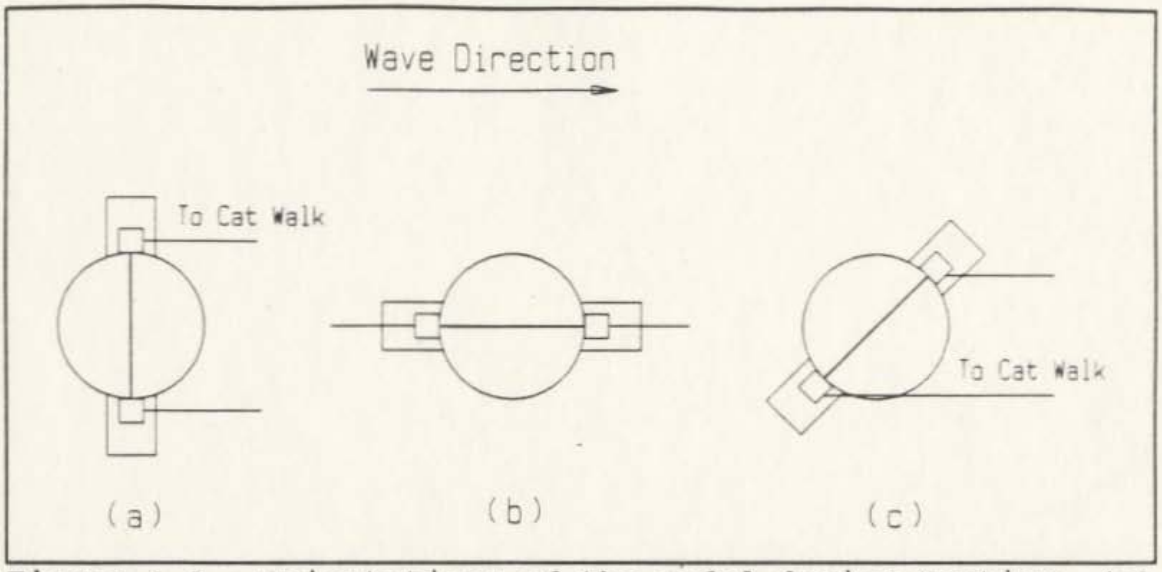

Figure 4.9 - Orientations of the model during testing. (a) Parallel orientation, (b) Perpendicular orientation, (c) 45° orientation

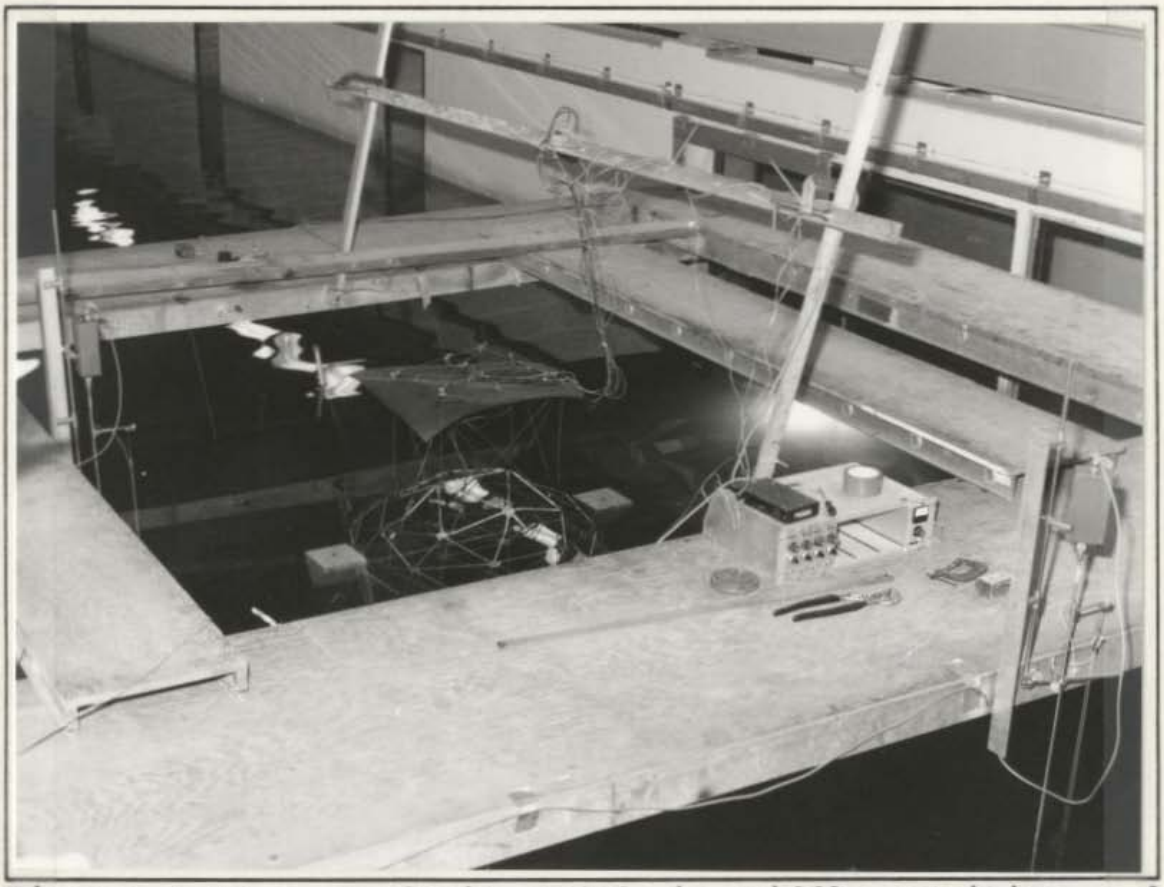

Figure 4.10 - Geodesic model in middle position and parallel orientation

In most tests springs with constant K = 10 kg/m were used in the mooring lines, and in the tests of the geodesic model in the middle and bottom positions springs with constant K = 30 kg/m were also used to investigate the effect of stiffness of the mooring lines on the responses of motions and mooring forces. The pretension in each mooring line was about 700 g in most tests. Pretension of 900 g was also used in the tests of the geodesic model in the middle and bottom positions with parallel orientation to see the effect of the pretension. When the model was submerged from the surface position to the middle position and then to the bottom position, the buoyancy of the model would increase because of the increase of the submerged volume. Therefore, some weights were added to the axle near the floats of the model to reduce the buoyancy and keep the pretension in the mooring lines about the same.

4.3.4 Method of data analysis

When the wave maker moved from its rest position to its position ready to work in the beginning of series of tests every morning and afternoon, it pushed the water slowly and created a very low frequency standing wave in the wave tank. This standing wave has a period of the fundamental mode and sometimes second mode free oscillation of the tank. The natural free oscillating period of the tank can be calculated

as (Dean and Dalrymple, 1984)

$$T_n = \frac{2l}{n\sqrt{gd}} \tag{4.3}$$

where l = 54 m is the length of the tank, d = 2.0 m is the water depth of the tank and n is the number of nodes in the tank. The fundamental mode natural free oscillating period of the tank is

$$T = \frac{2\times 54}{\sqrt{9.8\times 2.0}} = 24.4 \ (s)$$

and the second mode natural free oscillating period is

$$T = \frac{2\times 54}{2\sqrt{9.8\times 2.0}} = 12.2 \ (s)$$

This standing wave decreased very slowly with time, so it was impossible to wait for it to completely calm down before the tests were carried out. Consequently, most tests were conducted with the existence of this standing wave in the tank and test records contained the effects of the standing wave. The influence can be seen obviously from the plots of the test records. Therefore, when data of regular wave tests were analyzed with a PC-AT computer to obtain the averaged amplitudes of the incident wave, dynamic mooring forces, motions of the cage, fast Fourier transforms were used to filter the effects of the low frequency standing wave in the tank, and only the components of the frequencies close to the frequencies of the incident waves were used to calculate the

averaged amplitudes.

Because of the relatively high reflection rates of the low frequency waves in the tank, the wave records of the front probe were significantly different from the wave records of the side probe and the averaged wave amplitudes from the front probe records were significantly smaller than those from the side probe records at frequencies of 0.33 and 0.44 Hz. These differences were not caused by the phase differences of waves between the two locations, but by the different incident wave and reflected wave interactions at different parts along the length of the tank. At higher frequencies of 0.58, 0.72, 0.86 and 1.0 Hz, there were almost no such differences between the wave records of the front probe and the side probe. Therefore, it was concluded that the motion of the model did not affect the wave records of the side probe, and the wave records from the side probe, which represent better the waves acting on the model, were used to calculate the amplitudes of the incident waves.

After the amplitudes of the incident wave, mooring forces and motions of the cage were obtained, the Response Amplitude Operators (RAOs) of the mooring forces and cage motions at each frequency point were obtained as

$$RAO(f) = \frac{Response\ Amplitude\ (f)}{Wave\ Amplitude\ (f)} \qquad (4.4)$$

For irregular wave tests, fast Fourier transforms were conducted on the test data to calculate the energy spectra of incident waves, mooring force and motion responses. Then the frequency transfer functions (i.e. the RAOs) were obtained as

$$H(f) = \sqrt{\frac{S_{yy}(f)}{S_w(f)}} \qquad (4.5)$$

where $S_{yy}(f)$ is the spectral density estimate of mooring force or motion response and $S_w(f)$ is the spectral density estimate of the incident wave. Again, wave records from the side probe were used as input to calculate the spectra of the incident waves.

5 EXPERIMENTAL RESULTS AND DISCUSSIONS

All the test results presented in this chapter are referred to the model tests and should be upscaled to prototype values according to the actual model scale and appropriate scale factors and approximations discussed in sections 5.1.2 and 5.2.3 below.

5.1 Resistance Tests

5.1.1 Resistance forces of the models

The resistance forces of the spherical frame with net, spherical frame without net, net on the spherical frame for three orientations, axle of the cage parallel (90°), oblique (45°) and perpendicular (0°) to the current direction, are given in Figures 5.1, 5.2 and 5.3 respectively. The corresponding resistance forces for the geodesic model are given in Figures 5.4, 5.5 and 5.6. Figure 5.7 gives the resistance forces of the planar model net tested on the 1.0 m × 1.0 m model holding frame. Figure 5.8 provides the resistance forces of one of the two floats used on the geodesic model. In these figures, the scattered points show the actual test results and the smooth curves show the equations regressed from the results of each test series with

the least square method. Numerical test results can be found in Appendix A and the originally measured results (containing the resistance forces of the model holding frame) from which the above results are derived (see section 4.2.4 above) can be found in Appendix B.

In the velocity range of testing the relationships between the current velocity and the resultant resistance force for the both models, net and float can be fitted very well with the quadratic function

$$F = kV^2 \qquad (5.1)$$

in which k is a constant obtained by using the least square method to fit the results of each test series with velocities from 0.2 m/s to 1.6 m/s. The resistance coefficients at different velocities,

$$C_r = \frac{F_r}{V^2} \qquad (5.2)$$

in which F_r is the resistance force obtained from the test and V is the corresponding velocity, change only a little randomly about the values of k (see Appendix A) and seem to be independent of the current velocity and hence the Reynolds number in the velocity range of testing. The variation may be partly caused by the random errors in the measurements. Therefore, the quadratic equations regressed from the test results can be used to interpolate the resistance forces very

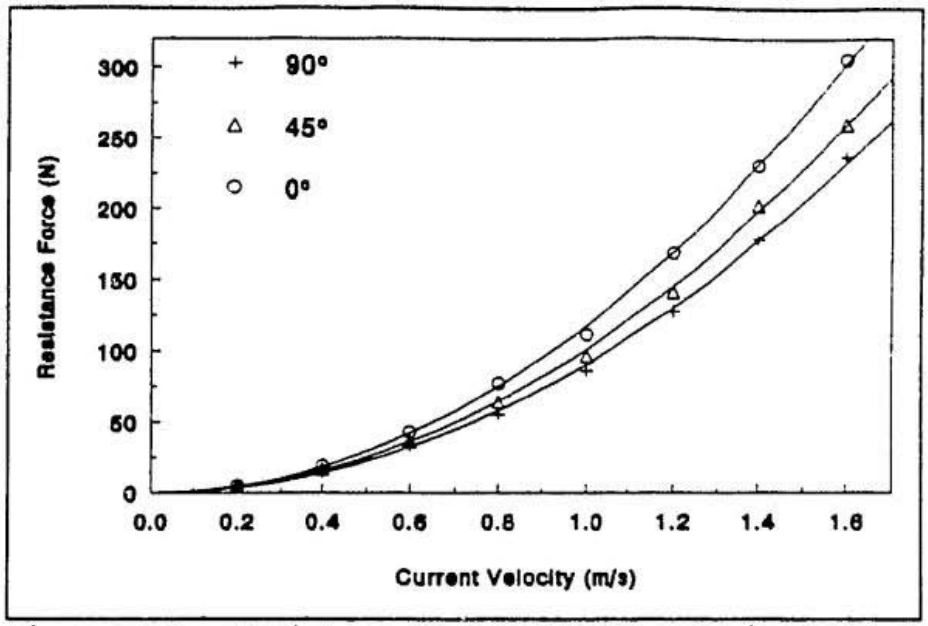

Figure 5.1 - Resistance force of the spherical frame with net

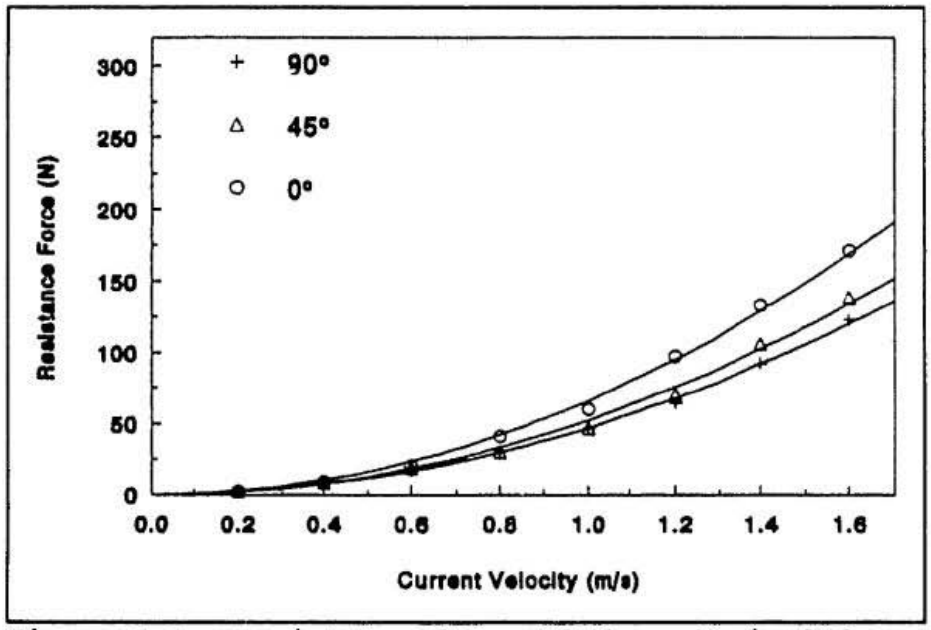

Figure 5.2 - Resistance force of the spherical frame without net

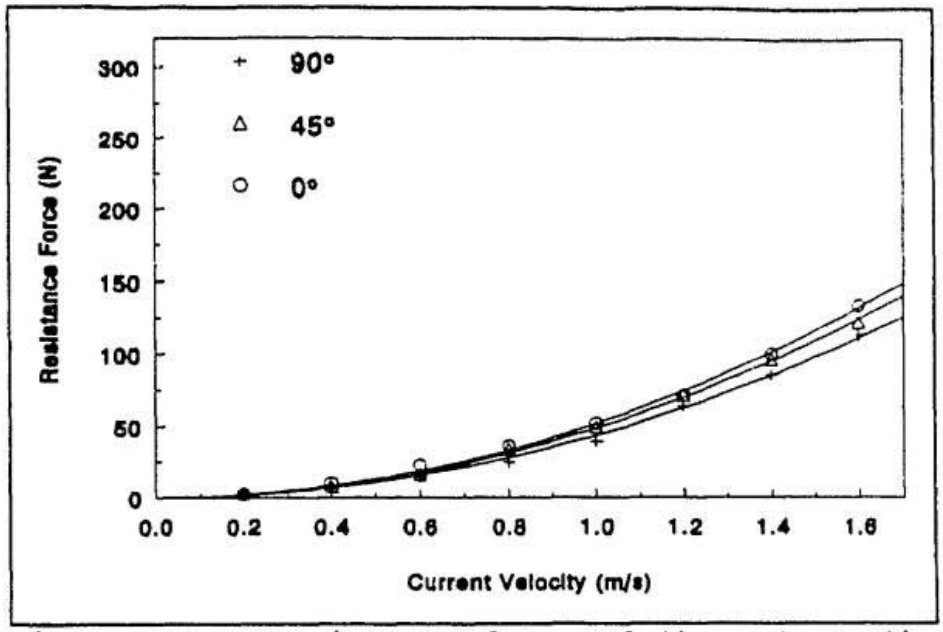

Figure 5.3 - Resistance force of the net on the spherical frame

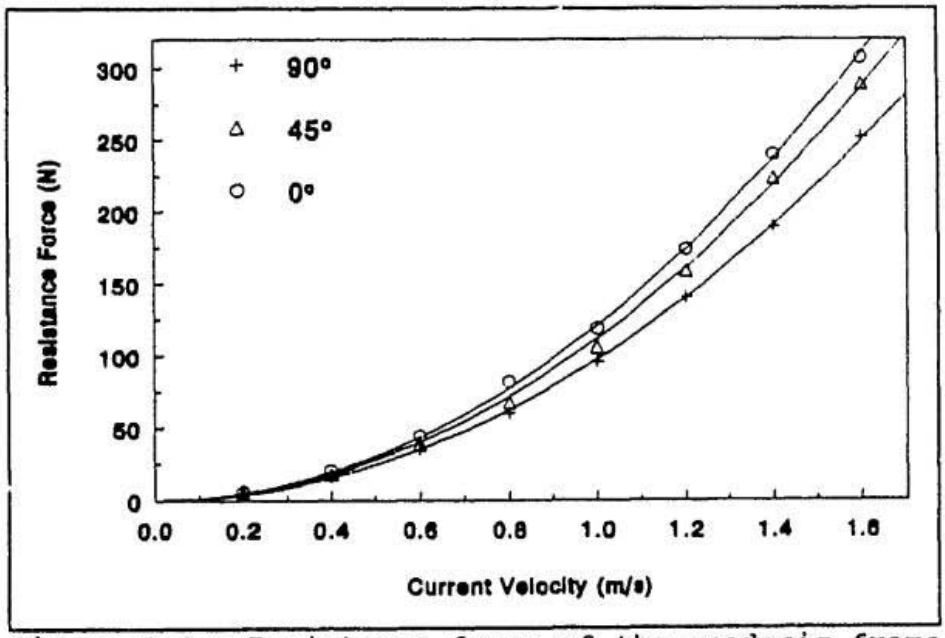

Figure 5.4 - Resistance force of the geodesic frame with net

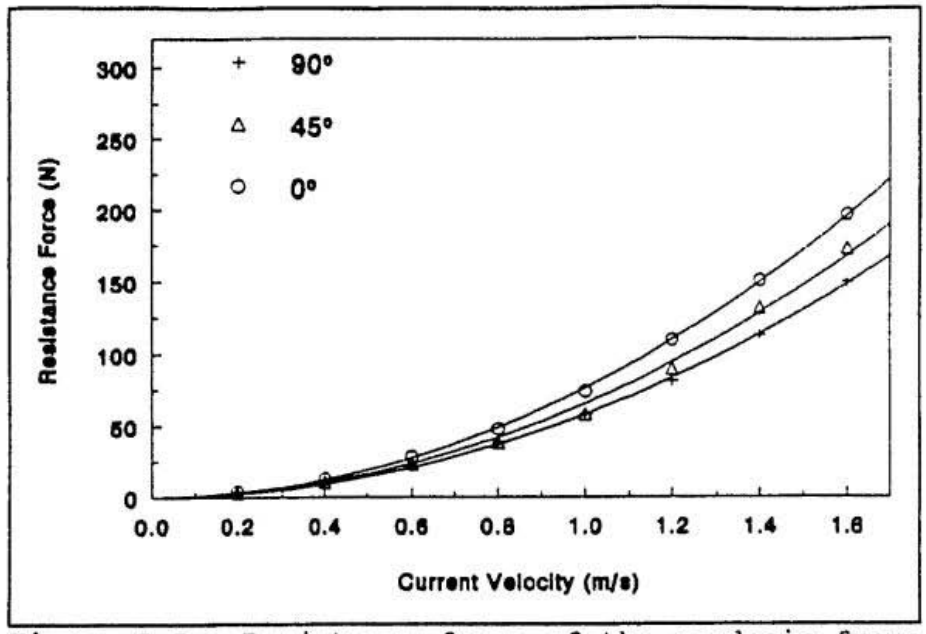

Figure 5.5 - Resistance force of the geodesic frame without net

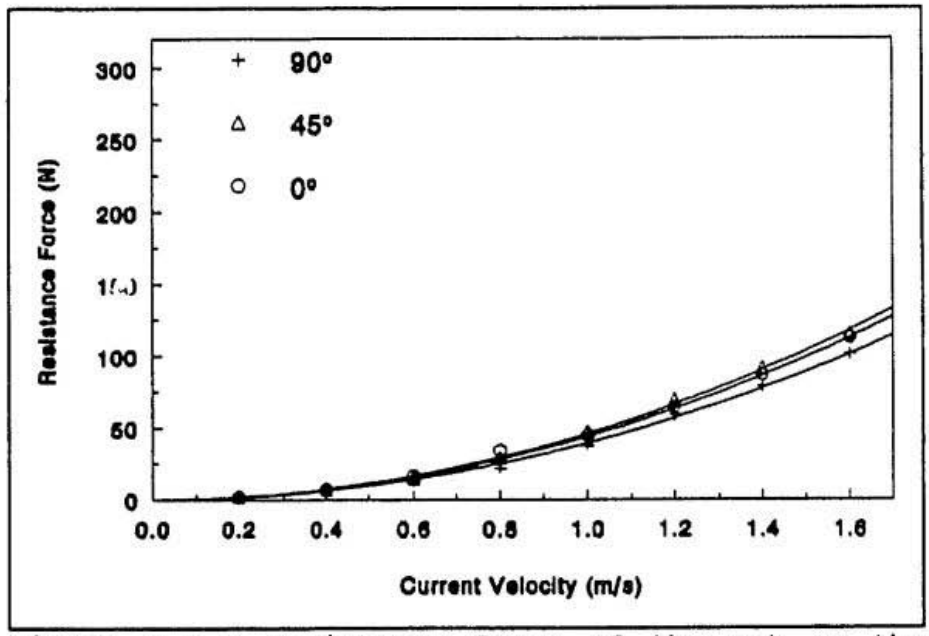

Figure 5.6 - Resistance force of the net on the geodesic frame

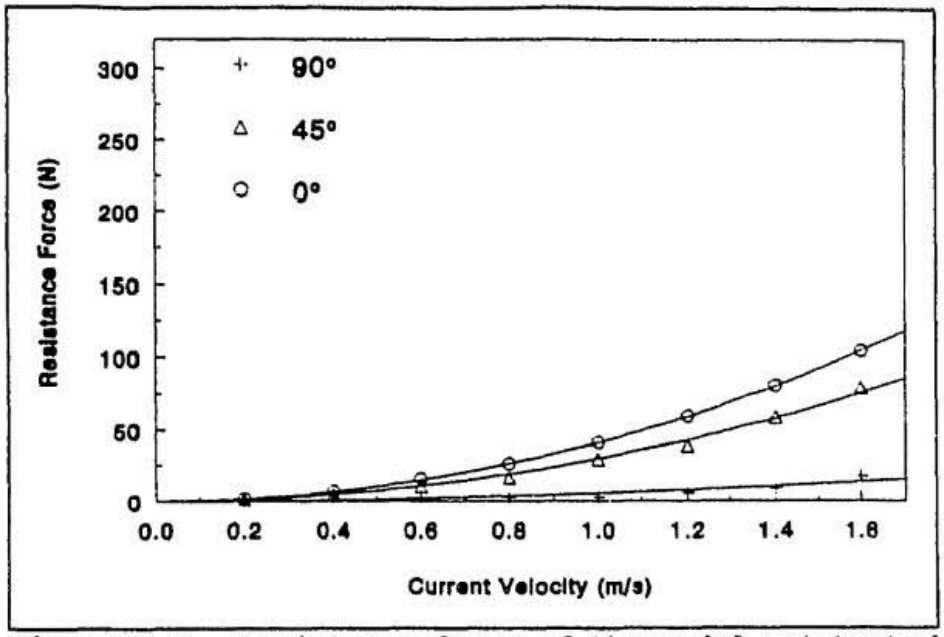

Figure 5.7 - Resistance force of the model net tested on the 1.0 m × 1.0 m model holding frame

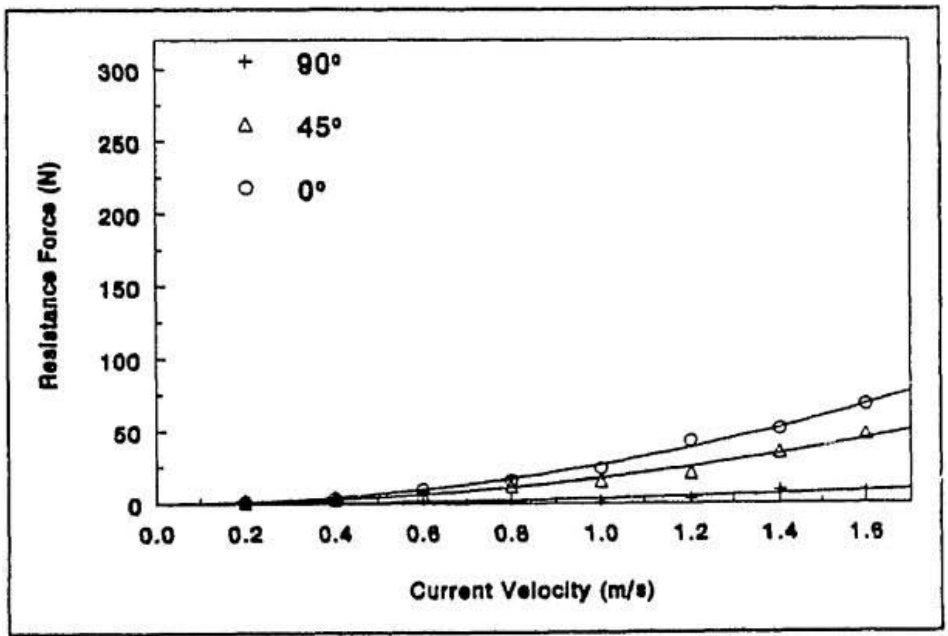

Figure 5.8 - Resistance force of the float

well. The only exceptions are the tests of the float and the planar model net at 90° orientation; because, in these two cases, the errors of the test results are relatively large (see section 4.2.4 above).

From section 3.3.1 it is known that the cage frame and net can be approximately considered as consisting of many small cylindrical elements which are normal or inclined to the current direction, and the total resistance force can be approximated as

$$F = \frac{1}{2}\rho V^2 \Sigma C_{Di} D_i \sin^3\theta_i \, ds_i \qquad (5.3)$$

in which the drag coefficient C_{Di} of the cylindrical element is a function of the Reynolds number and surface roughness as shown in Figure 3.6. Because the elements which have a small angle to the current direction make little contribution to the total resistance force, the Reynolds numbers of the elements of both model frames, elements of the model net and the axles of both models are approximately calculated as in Table 5.1.

From Table 5.1 it can be found that in the velocity range of testing the Reynolds numbers of all the elements are within the range of subcritical flow regime where the drag coefficients of the cylindrical elements are relatively constant and can be approximately considered to be independent

Table 5.1 - Reynolds number ranges of model testing

	Diameter (mm)	Re Number (V = 0.2 m/s)	Re Number (V = 1.6 m/s)
Net	1.5	285	2277
Spherical Frame	3.0	1708	13662
Geodesic Frame	6.0	1139	9108
Axles	13.0	2467	19734

$Re = VD/\nu$ $\quad \nu = 1.054\ m^2/s$

of the Reynolds number. Therefore, the coefficient C_t of the total resistance force almost does not change with the current velocity and the quadratic equation $F = kV^2$ can be used to fit the test results very well in the present tests. Provided the Reynolds numbers of the elements are still within the range of subcritical flow regime, it can be predicted that the regressed equation can also be used to extrapolate the resistance forces outside the tested velocity range. If the Reynolds numbers are within the range of critical or supercritical flow regime, the drag coefficients of the elements will vary significantly with the Reynolds number, the coefficient C_t will change with the velocity and the equation $F = kV^2$ can no longer be used to fit the results of each series of tests.

The resistance force of the float is also insensitive to Reynolds number because the sharp edges of the float tend to cause flow separation regardless of the character of the

boundary layer. Therefore, the quadratic function $F = kV^2$ can also be used to fit the test results of the float well.

For the both cage models, the resistance force is minimum when the axle of the cage is parallel (90°) to the current direction and maximum when the axle of the cage is perpendicular (0°) to the current direction. This is partly caused by the axle of the cage and partly caused by the fact that the cage frame is not perfectly symmetrical about the cage centre. The resistance force of the float is also minimum at 90° and maximum at 0°. Therefore, it can be concluded that the cage system will have maximum resistance force when its axle is perpendicular to the current direction and minimum resistance force when its axle is parallel to the current direction. The differences of the least square fitted constants k among different orientations are compared in Table 5.2.

From table 5.2 it can also be found that, for the net on the models, there are also a few differences among the resistance forces in different orientations. This is because both cage frames are not uniform spheres. The differences for the net on the geodesic frame are smaller because the geodesic frame is more uniform than the spherical frame.

Table 5.2 - Comparison of resistance forces at different orientations

	90°	45°	0°
Spherical Frame	47.19	52.61	66.25
Spherical frame with net	90.84	101.34	118.05
Net on Spherical Frame	43.59	48.68	51.79
Geodesic Frame	58.23	65.87	76.75
Geodesic Frame with Net	97.47	111.97	120.97
Net on Geodesic Frame	39.49	46.00	43.96
Float	3.29	17.38	26.60

Unit: Ns^2/m^2

The resistance force of the geodesic cage frame is about 20 percent larger than the resistance force of the spherical cage frame, although the diameter of the spherical model is 90 cm while the diameter of the geodesic model is 85 cm. Comparing based on the same cage diameter, the resistance force of the geodesic frame will be about 35 percent larger than that of the spherical frame. This is because the geodesic frame has more bar components and joints than the spherical frame.

5.1.2 Application of the model test results to prototype

When the cage model is submerged well below the water surface, the resistance force is mainly caused by the

viscosity of the fluid; therefore, scale factors (Table 3.2) based on Reynolds law should be used to upscale the model test results to prototype values (see section 3.3.1 above). From section 5.1.1 it is known that the quadratic equations regressed from the test results can be used to interpolate the resistance forces of the model frames, net and float very well, so, according to the scale factors in table 3.2, the resistance forces of the prototype can be calculated as

$$F_p = \frac{\rho_p}{\rho_m} k\lambda^2 V_p^2 \qquad (5.4)$$

in which F_p is the prototype resistance force, k is the constant regressed from the model test results, λ is the model scale and V_p is the current velocity of the prototype.

Theoretically, Equation (5.4) is valid only in a small current velocity range of the prototype where the Reynolds number of the prototype is within the Reynolds number range of the model tests. For example, if the model scale is λ = 13.5, the equation is only valid in the prototype velocity range from about 0.2/13.5 = 0.0015 m/s to 1.6/13.5 = 0.119 m/s (assume ν_p/ν_m = 1). In practice, the current velocity of the prototype may be as large as 1.5 m/s, so the Reynolds number of the prototype will be much larger than that of the model testing. Because of the limitation of the test facility, it

is impossible to conduct tests at higher model velocities. In such case, some approximations have to be made to use the test results to predict the resistance forces of the prototype and these are discussed below.

5.1.2.1 Resistance force of the cage frame

The cage frames can be approximately considered as consisting of many small cylindrical elements. From section 3.3.1 it is known that as long as the Reynolds numbers of the prototype frame elements are still within the range of subcritical flow regime ($200 < Re < 2\times10^5$ for smooth cylinder and about $200 < Re < 8\times10^4$ for a roughened cylinder, depending on the surface roughness of the prototype frame elements) where the drag coefficients of the cylinder elements can be approximately considered to be independent of the Reynolds numbers, it is appropriate to assume that the resistance force coefficient of the cage frame does not change significantly with the increase of the Reynolds number and Equation (5.4) can also be used to extrapolate the resistance force of the prototype frame when the prototype current velocity is higher than 0.119 m/s (for $\lambda = 13.5$). Therefore, the resistance force of the prototype frame can be estimated as

$$F_{frame} = \frac{\rho_p}{\rho_m} k_{frame} \lambda^2 V^2 \qquad (5.5)$$

in which k_{frame} is the constant of the cage frame regressed from the model test results. For model scale $\lambda = 13.5$, assuming the cylindrical elements of the prototype frames are smooth and the resistance forces are mainly caused by the bows and bow reinforcements of the spherical cage or the bar components of the geodesic cage, Equation (5.5) can be used in prototype calculations with current velocity up to 1.7 m/s for the spherical frame and 3.1 m/s for the geodesic frame, which are high enough for many applications.

In practice the cylinder elements of the prototype frames may not be smooth, so the flow regime of the prototype will become critical at a smaller Reynolds number which depends on the surface roughness and Equation (5.5) be appropriate in a smaller velocity range. For example, for a prototype frame whose cylindrical elements have such a surface roughness that the flow regimes will begin to become critical when Re = 8×10^4, Equation (5.5) can only be used in prototype calculations when the current velocity is lower than about 0.69 m/s for the spherical frame and 1.25 m/s for the geodesic frame. When the flow regime of the prototype frame is critical or supercritical, the results would be overpredicted and a

correction factor K_c should be introduced if a more accurate estimation is wanted (see section 3.3.1). Thus the resistance force of the prototype frame should be estimated as

$$F_{frame} = \frac{\rho_p}{\rho_m} k_{frame} K_c \lambda^2 V^2 \qquad (5.6)$$

where K_c should be determined according to the Reynolds number and surface roughness. Table 5.3 shows the K_c derived from Figure 3.6 for the case above and can be used as an example. If no correction is made, a conservative estimation may be obtained.

5.1.2.2 Resistance force of the net on the cage

Because special consideration has been taken to select the model net, the resistance force of the net on the prototype cage frame can be approximated as

$$F_{net} = \frac{\rho_p}{\rho_b} k_{net} \lambda^2 V^2 \qquad (5.7)$$

where k_{net} is the constant obtained from the model tests.

Also, from the tests of both models it is found that the resistance force of the net on the model frame is about two times (Spherical model: 2.0 for 0°, 1.9 for 45° and 1.7 for 90°; Geodesic model: 2.0 for 0°, 2.0 for 45° and 1.8 for 90°)

Table 5.3 - Example of correction factors K_c for resistance force calculations of spherical and geodesic frames

Reynolds Number		Flow Regime		Velocity Range (m/s)		K_c
Model	Prototype	Model	Prototype	Spherical	Geodesic	
3×10^2-2×10^4	$<8\times10^4$	Subcritical	Subcritical	<0.69	<1.25	1.0
3×10^2-2×10^4	8×10^5-1×10^5	Subcritical	Critical	0.69-0.86	1.25-1.56	0.95
3×10^2-2×10^4	1×10^5-1.2×10^5	Subcritical	Critical	0.86-1.04	1.56-1.87	0.90
3×10^2-2×10^4	1.2×10^5-1.4×10^5	Subcritical	Critical	1.04-1.21	1.87-2.19	0.75
3×10^2-2×10^4	1.4×10^5-1.6×10^5	Subcritical	Critical	1.21-1.39	2.19-2.50	0.50
3×10^2-2×10^4	1.6×10^5-1.8×10^5	Subcritical	Critical	1.39-1.56	2.50-2.81	0.32

the resistance force of a planar net of the same material which is normal to the current direction and has an area equal to the area of the cross section of the cage frame. Applying this relationship to the prototype, a second method of estimating the resistance force of the net on the prototype frame can be developed. If the resistance force coefficient of the **unit area** of the planar prototype net is known as C(V), then the resistance force of the net on the prototype frame can be estimated as

$$F_{net} = 2\,C(V)\,V^2 S \qquad (5.8)$$

where S is the area of the cross section of the prototype frame. Coefficient C(V) can be obtained by testing the prototype net on a planar frame in a towing tank, so the difficulty of reproducing the prototype net in the model testing can be avoided. C(V) may also be obtained directly from the manufacturer. Therefore, without conducting more tests, it is still possible to predict the resistance forces of different nets used on the prototype frame.

5.1.2.3 Resistance force of the floatation chamber

Because the sharp edges of the float tend to cause flow separation regardless of the character of the boundary layer, the resistance force of the float is insensitive to the Reynolds number. Therefore, it can be assumed that the

resistance force coefficient of the float does not change significantly with the increase of the Reynolds number and the resistance force constant regressed from the model test results is also valid for extrapolating the resistance forces of the prototype floatation chambers. Consequently, the total resistance force of the prototype floatation chambers can be estimated as

$$F_{float} = 2\frac{\rho_p}{\rho_m} k_{float} \lambda^2 V^2 \qquad (5.9)$$

where k_{float} is the constant obtained from the model tests.

5.1.2.4 Total resistance force of the cage system

The total resistance force of the cage system can be obtained by adding the resistance forces of the cage frame, the net on the frame and the floatation chambers together. It should be noted that, because the cage and the float are tested separately, the test results do not reflect the interaction between the cage and the floatation chambers.

5.2 Moored Tests

Detailed motion and mooring force responses obtained from each series of regular wave tests with incident wave heights of 5 cm and 10 cm and irregular wave test are given in

appendix C for the spherical cage model and in appendix D for the geodesic cage model in the form of figures. In all these figures the lines are the results from the irregular wave tests and the scattered points are the results from the regular wave tests.

Comparing the results in appendix C and D, it can be found that there are no significant differences between the motion and mooring force responses of the spherical cage and the geodesic cage. The resonant frequencies of the spherical model are a little lower than those of the geodesic model because the mass of the spherical model is larger, but the trends of the responses of both models are almost the same. Unless mentioned specially, the discussions hereafter apply to both models.

In general, the irregular wave tests and the regular wave tests give essentially the same information on the frequency responses of the system. The motion and mooring force responses obtained from the irregular wave tests agree with the results from the regular wave tests very well, especially in the high frequency range. In the low frequency range, the results from the irregular wave tests tend to be larger then those from the regular wave tests. The discrepancies in the low frequency range are partly attributed to the inaccuracies

in the measurement of incident waves because of the higher reflection rate of the low frequency waves from the absorbed beach of the tank, and partly caused by the second-order forces (slowly-varying forces) due to the differences in the frequencies of wave components in the irregular wave tests.

To produce reasonable approximations to the continuous frequency responses of the system, a large number of regular wave tests are required. On the other hand, irregular wave tests can provide estimates of the complete frequency responses of the system, for the frequency range of interest, in a single test. Therefore, irregular wave tests are recommended in any future tests of the cage system.

For the regular wave tests, the time histories of the motion and mooring force responses are almost harmonic. Test results with incident wave height H = 5 cm tend to be larger then those with incident wave height H = 10 cm. The differences are significant near the resonant frequencies and insignificant away from the resonant frequencies. The nonlinear damping forces of the cages, which increase quadratically instead of linearly with relative flow velocity, cause the differences. Near the resonant frequency the damping has a profound effect on motion response. Increasing the damping will reduce the motion response significantly. At

lower or higher frequencies away from the resonant frequency the damping has a negligible effect (see section 3.2.1 above).

5.2.1 Motion responses

5.2.1.1 Responses in different orientations

In parallel orientation, the major degrees of motion are surge and heave. In perpendicular orientation, the major degrees of motion are sway, heave and roll. Other degrees of motion are small, so they are not presented in this thesis.

Figures 5.9 - 5.11 give the comparisons between heave responses in parallel orientation and in perpendicular orientation, and Figures 5.12 - 5.14 the comparisons between surge responses in parallel orientation and sway responses in perpendicular orientation (both are the motion along the wave direction) for the spherical model. Figures 5.15 - 5.20 give the corresponding comparisons for the geodesic model. In these figures and the figures hereafter, the lines present the results from the irregular wave tests and the scatter points the results from the regular wave tests with incident wave height H = 10 cm. In order to simplify the figures, results from the regular wave tests with incident wave height H = 5 cm are not shown.

From Figures 5.9 - 5.20 it can be found that the heave responses in perpendicular orientation are significantly smaller than those in parallel orientation and the sway responses in perpendicular orientation are significantly smaller than the surge responses in parallel orientation, especially at the high frequencies. In perpendicular orientation, because the floats at two ends of the axle of the cage ride along the wave direction, a phase difference exists between the wave exciting forces on the two floats when the wave length of the incident wave is not equal to the distance between the two floats. In such case, the total wave exciting forces of heave and sway in perpendicular orientation are smaller than the total wave exciting forces of heave and surge in parallel orientation, so the motions in perpendicular orientation are smaller. But a significant roll motion is induced in perpendicular orientation because of the floats riding along the wave direction. The phase difference between heave and roll will significantly affect the amplitudes of the vertical displacements of the lee side and sea side ends of the cage and the force responses in the lee side and sea side mooring lines (see section 5.2.2.1 below).

For 45° orientation, the major degrees of motion are sway, surge, heave, yaw and roll. The responses of heave and roll are similar to those in perpendicular orientation. The

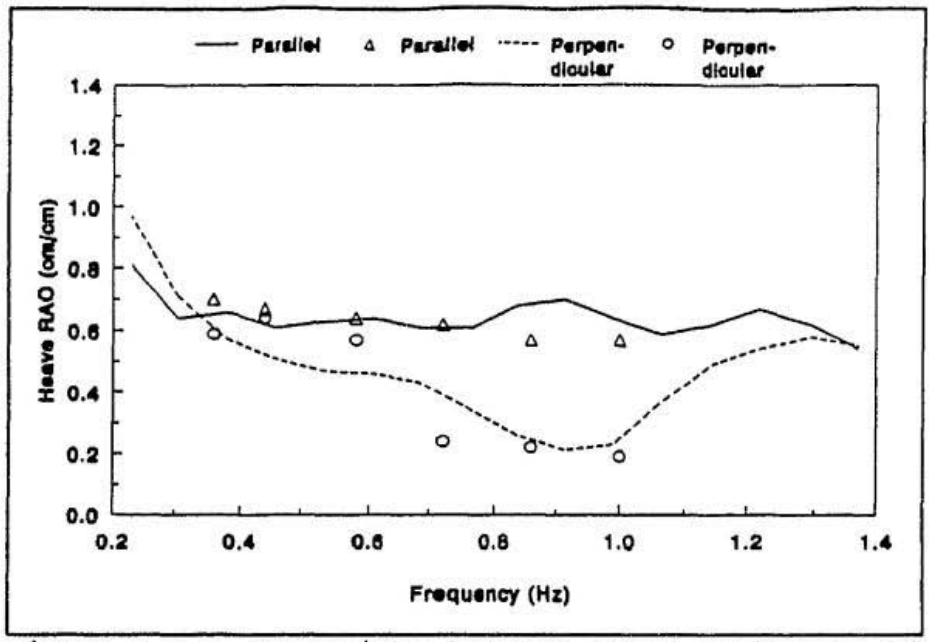

Figure 5.9 - Comparison between heave responses of two orientations: spherical model, surface position

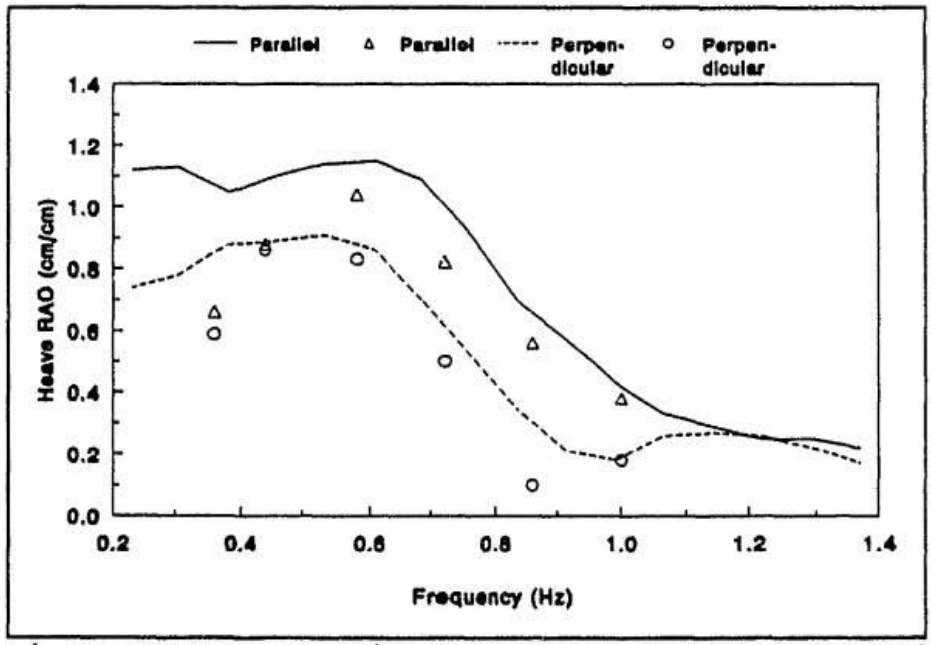

Figure 5.10 - Comparison between heave responses of two orientations: spherical model, middle position

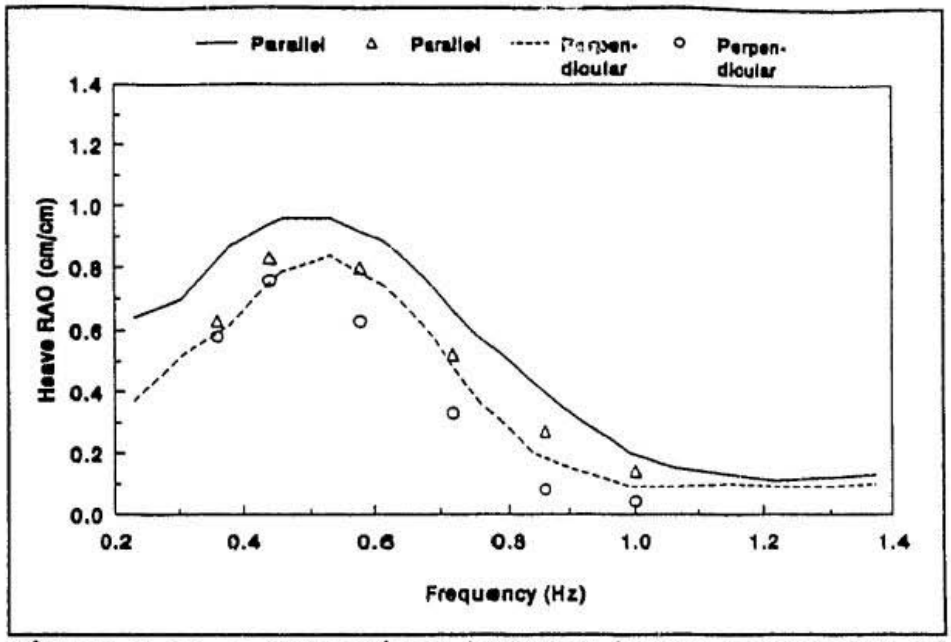

Figure 5.11 - Comparison between heave responses of two orientations: spherical model, bottom position

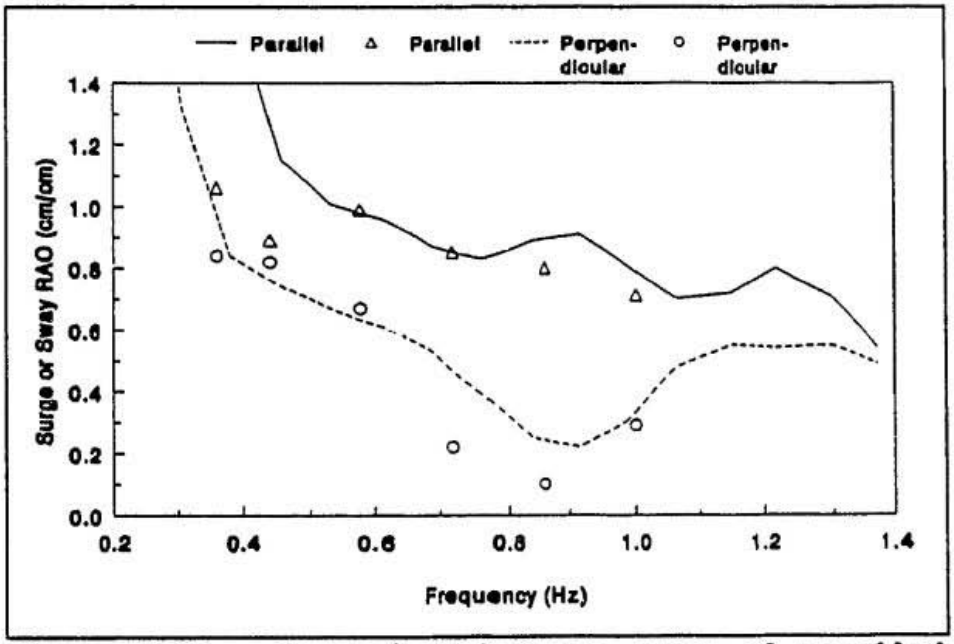

Figure 5.12 - Comparison between surge of parallel orientation and sway of perpendicular orientation: spherical model, surface position

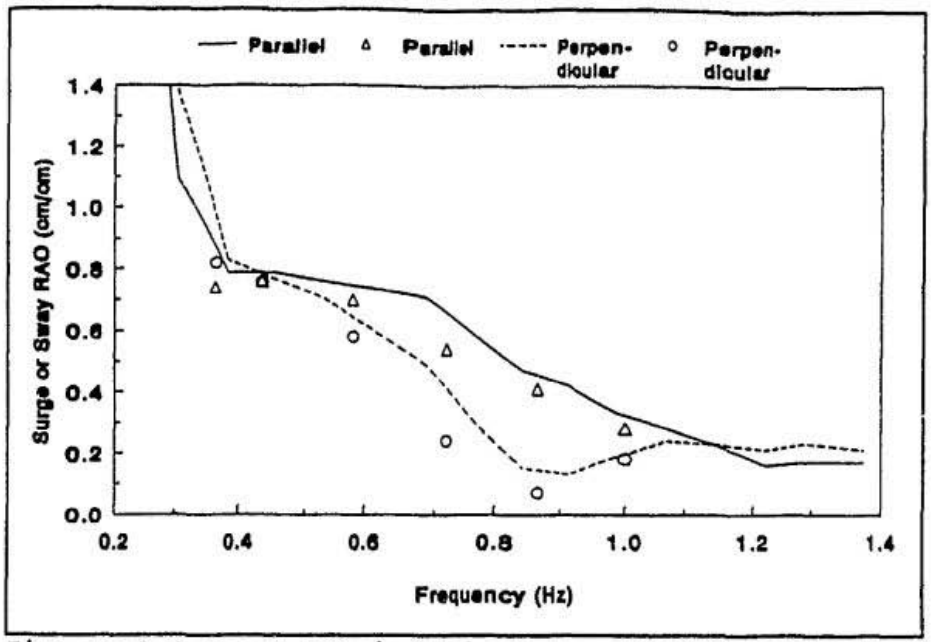

Figure 5.13 - Comparison between surge of parallel orientation and sway of perpendicular orientation: spherical model, middle position

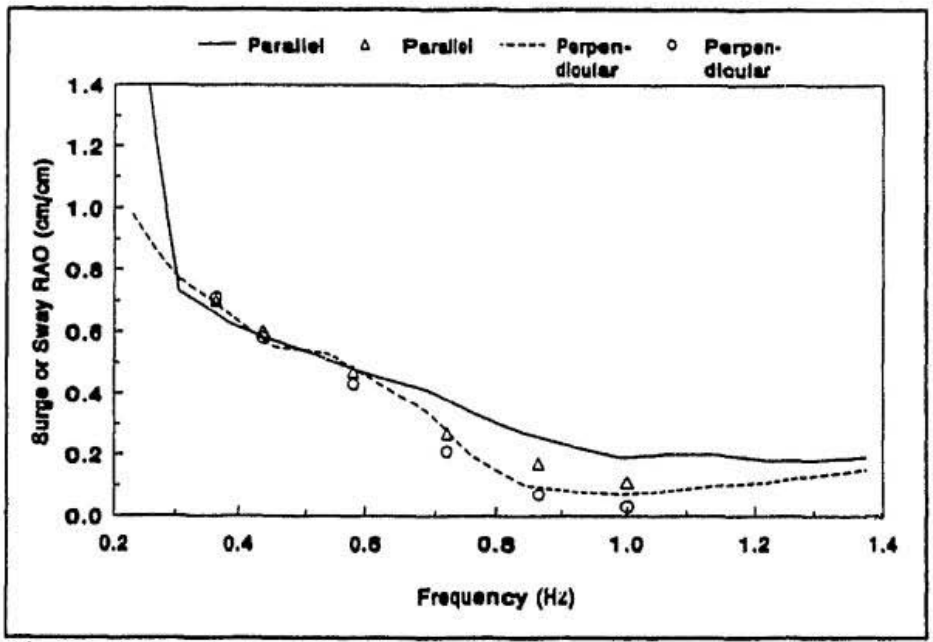

Figure 5.14 - Comparison between surge of parallel orientation and sway of perpendicular orientation: spherical model, bottom position

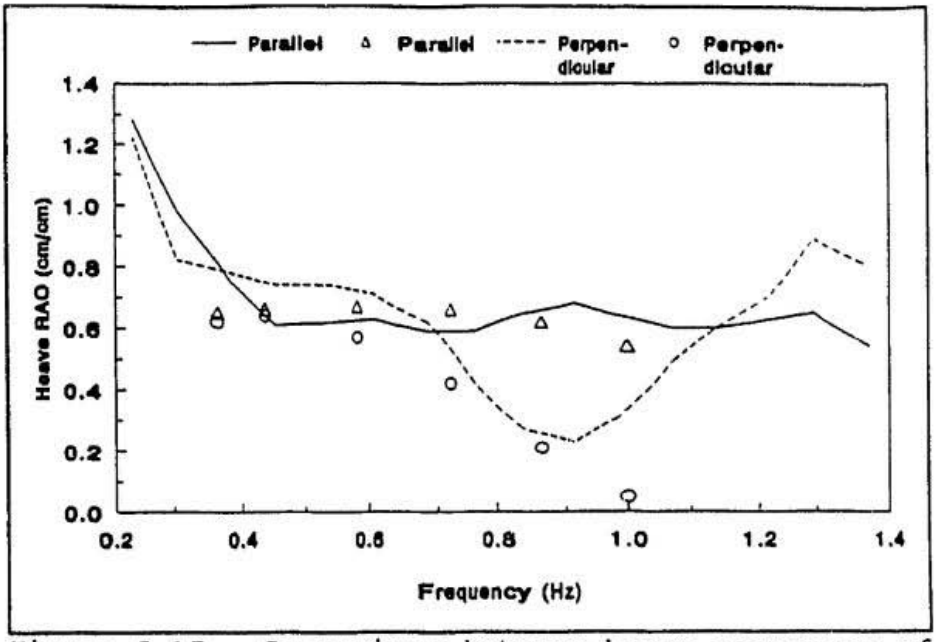

Figure 5.15 - Comparison between heave responses of two orientations: geodesic model, surface position

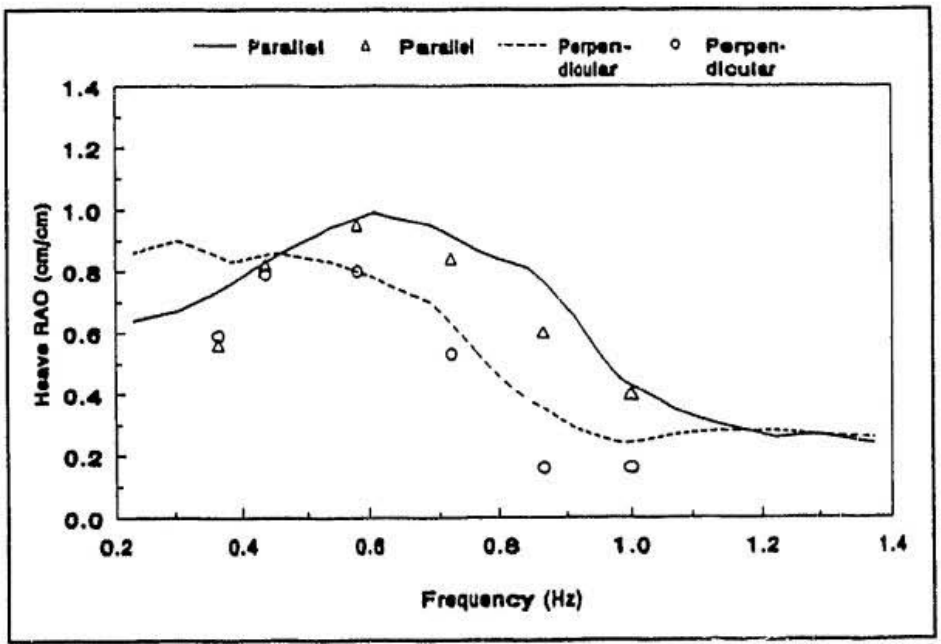

Figure 5.16 - Comparison between heave responses of two orientations: geodesic model, middle position

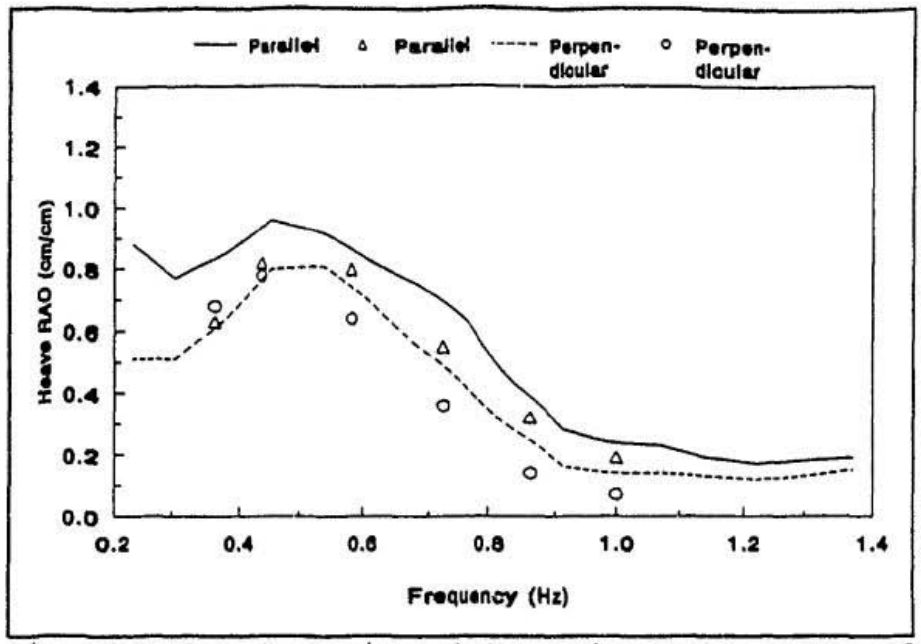

Figure 5.17 - Comparison between heave responses of two orientations: geodesic model, bottom position

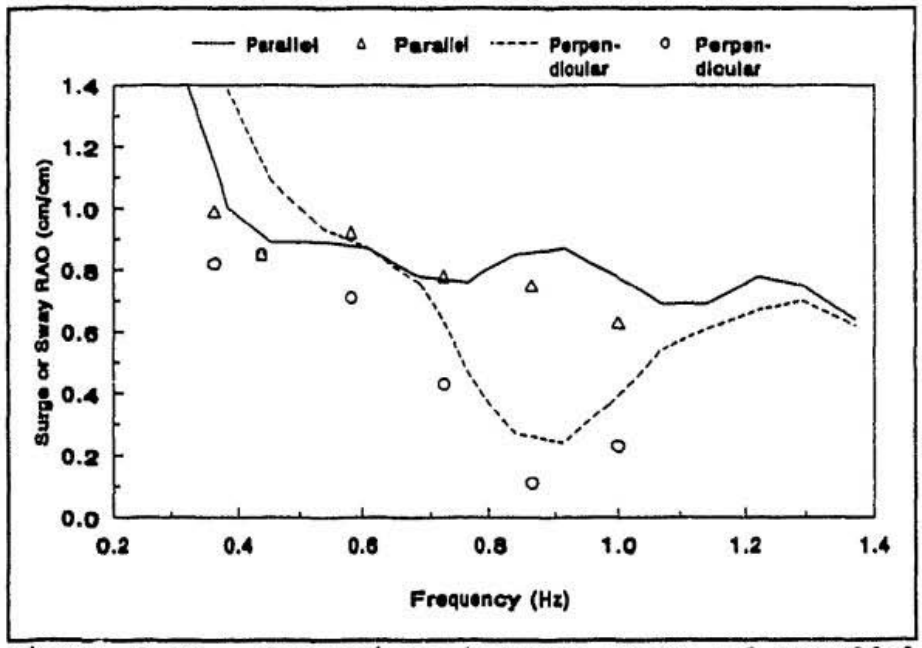

Figure 5.18 - Comparison between surge of parallel orientation and sway of perpendicular orientation: geodesic model, surface position

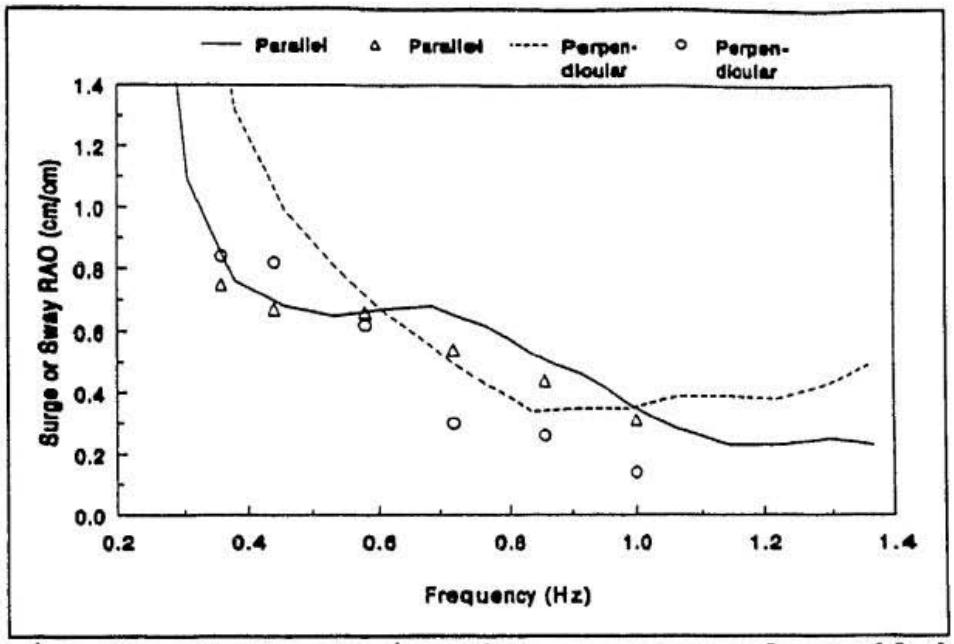

Figure 5.19 - Comparison between surge of parallel orientation and sway of perpendicular orientation: geodesic model, middle position

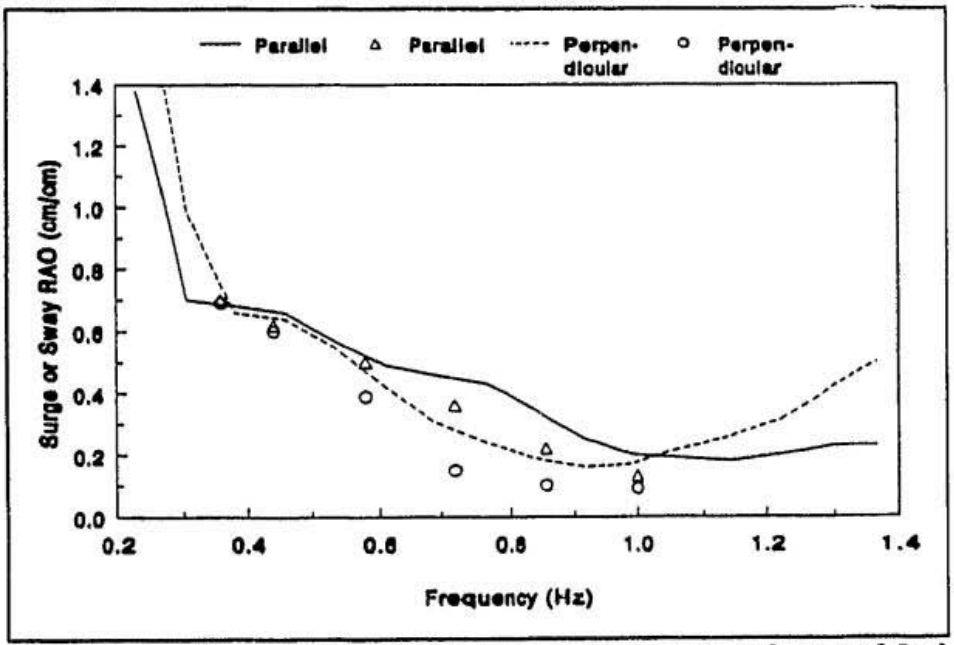

Figure 5.20 - Comparison between surge of parallel orientation and sway of perpendicular orientation: geodesic model, bottom position

maximum yaw amplitude is only about 4°, so it seems impossible for the two mooring lines to be tangled up when the cage is oblique to the wave direction.

5.2.1.2 Responses in different submerged positions

5.2.1.2.1 Parallel orientation

The comparisons of surge and heave responses in different submerged positions in parallel orientation are given in Figures 5.21 and 5.22 for the spherical model, in Figures 5.23 and 5.24 for the geodesic model and in Figures 5.25 and 5.26 for the geodesic model with stiffer mooring lines (K = 30 kg/m instead of K = 10 kg/m).

The surge responses decrease with the submerged depth. The responses are largest in the surface position and smallest in the bottom position. The differences are relatively small in the low frequency range and large in the high frequency range.

The heave responses change only a little with frequency in the surface position, but increase with frequency until reaching their maximum and then decrease with frequency in the middle and bottom positions. In the low frequency range, the

heave responses in the middle and bottom positions are larger than those in the surface position. With the increase of frequency, the heave responses in the middle and bottom positions begin to decrease and become significantly smaller than the responses in the surface position in the high frequency range.

Comparing the heave responses in the middle and bottom positions, there are few differences at the low frequencies. As the frequency increases, the responses in the bottom position become significantly smaller than those in the middle position and the differences increase with the increase of frequency.

When the frequency is higher than 0.625 Hz, the incident wave in the tank is a deep water wave. In a deep water wave, the wave energy is concentrated near the water surface and the wave motion decreases exponentially with the depth below the water surface, so that the wave force acting on the cage and hence the motions of the cage decrease significantly when the cage is submerged some distance below the water surface (see section 3.1 above). When the frequency becomes lower than 0.625 Hz, the incident wave begins to become an intermediate water wave. The decrease of wave motion with the depth below the water surface becomes smaller and smaller with the

decrease of wave frequency, so do the decreases of the wave force acting on the cage and the motions of the cage. Therefore, in the low frequency range the differences between the motion responses in the middle and bottom positions are small, while in the higher frequency range the motion responses in the bottom position are significantly smaller than those in the middle position. The test results confirm the qualitative prediction that the method of submerging the cage some distance below the water surface to reduce the wave forces and motions of the cage and the forces in the mooring system is very effective in deep water waves, but becomes less and less effective in intermediate water waves.

The differences between the heave responses in the surface position and middle position are caused by the combined effects of the increase of submerged volume of the cage (which may increase the total wave force acting on the cage, especially at the low frequencies), the decrease of wave motion with depth (which may reduce the wave force acting on the cage, especially at the high frequencies), and the decrease of the heave restoring force caused by the submergence of the two floats of the cage (which changes the natural frequency of the heave motion) in the middle position.

5.2.1.2.2 Perpendicular orientation

Figures 5.27, 5.28 and 5.29 show the comparisons of sway, heave and roll responses in different submerged positions in perpendicular orientation for the spherical model, Figures 5.30, 5.31 and 5.32 show the comparisons for the geodesic model and Figures 5.33 and 5.34 show the comparisons for the geodesic model with stiffer mooring lines.

For the sway motion, the responses decrease with the submerged depth of the cages. The cages have the largest responses in the surface position and the smallest responses in the bottom position.

For the heave motion, the responses in the middle and bottom positions tend to be larger at the low frequencies and smaller at the high frequencies than those in the surface position. Also, the responses in the bottom position are smaller than those in the middle position and the differences tend to be small at the low frequencies and large at the high frequencies.

As for the roll motion, the responses in the middle position are larger than those in the surface position at almost all but the higher frequencies and the responses in the

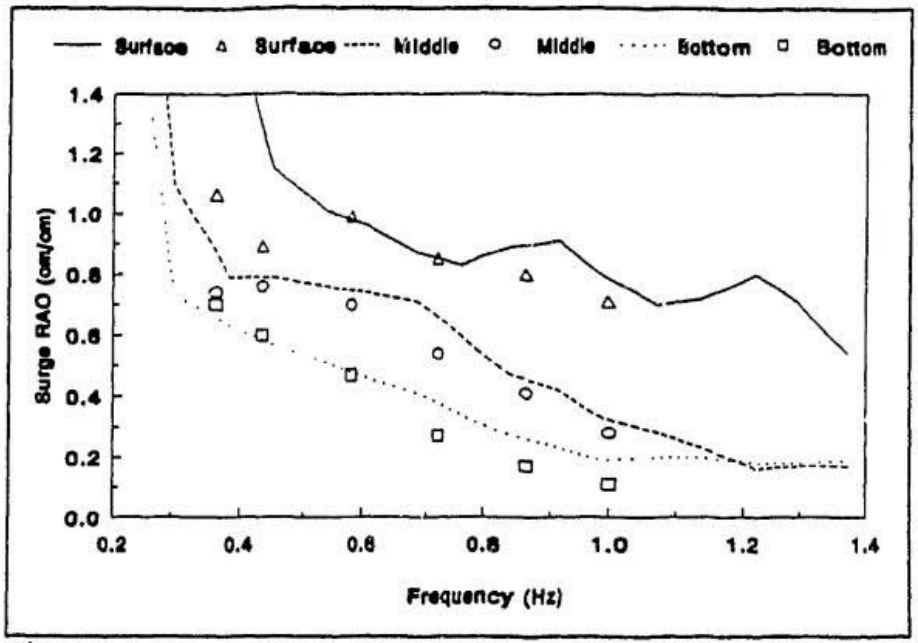

Figure 5.21 - Surge responses in different submerged positions: spherical model, parallel orientation

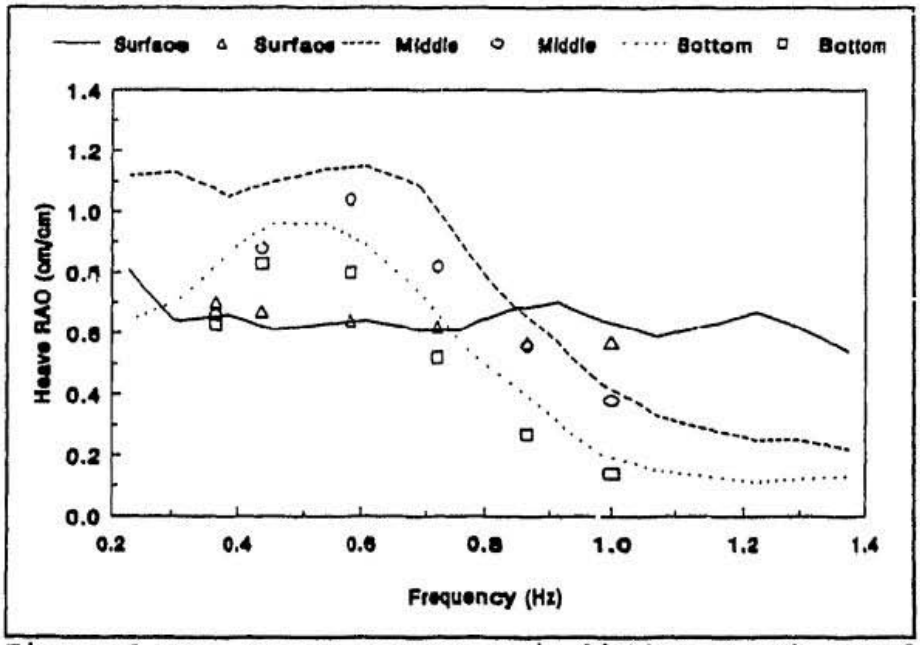

Figure 5.22 - Heave responses in different submerged positions: spherical model, parallel orientation

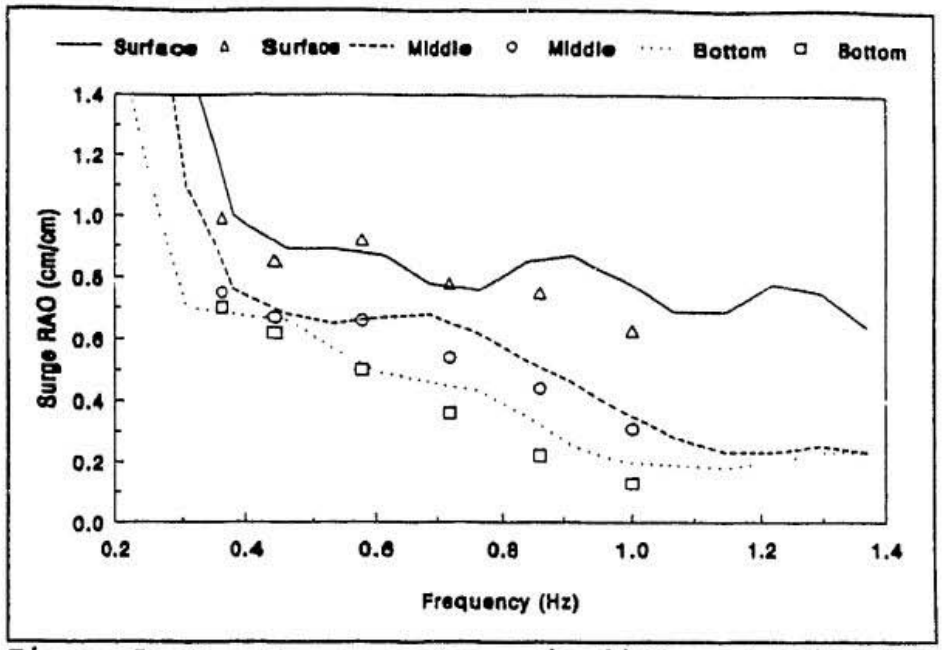

Figure 5.23 - Surge responses in different submerged positions: geodesic model, parallel orientation

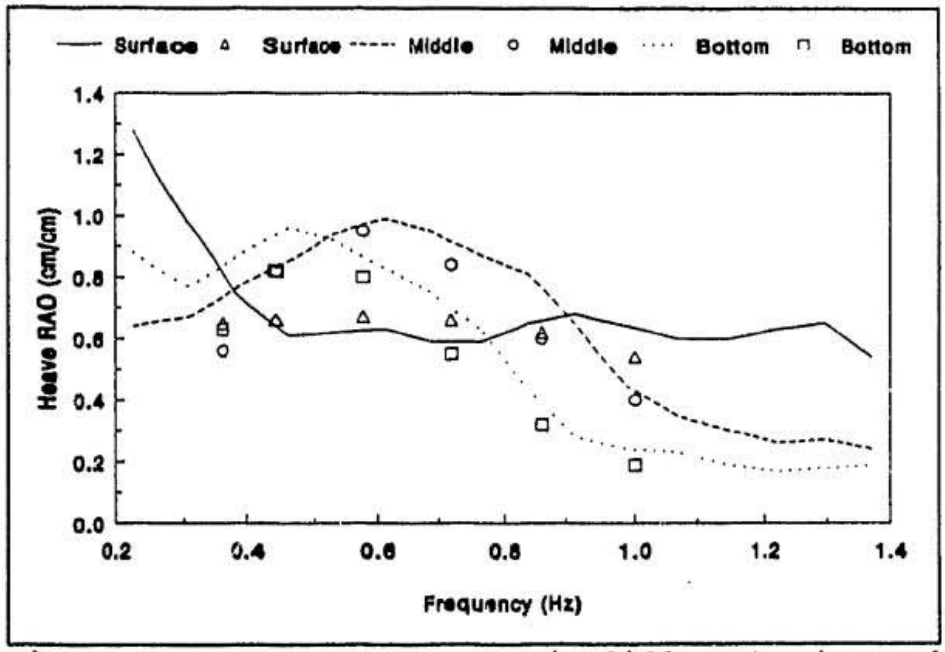

Figure 5.24 - Heave responses in different submerged positions: geodesic model, parallel orientation

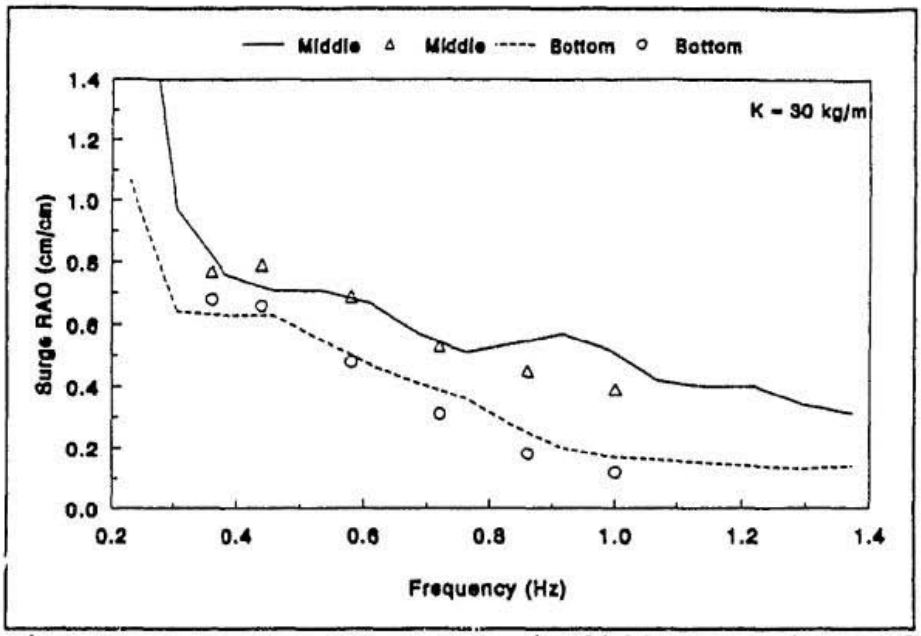

Figure 5.25 - Surge responses in different submerged positions: geodesic model, parallel orientation, with stiffer mooring lines

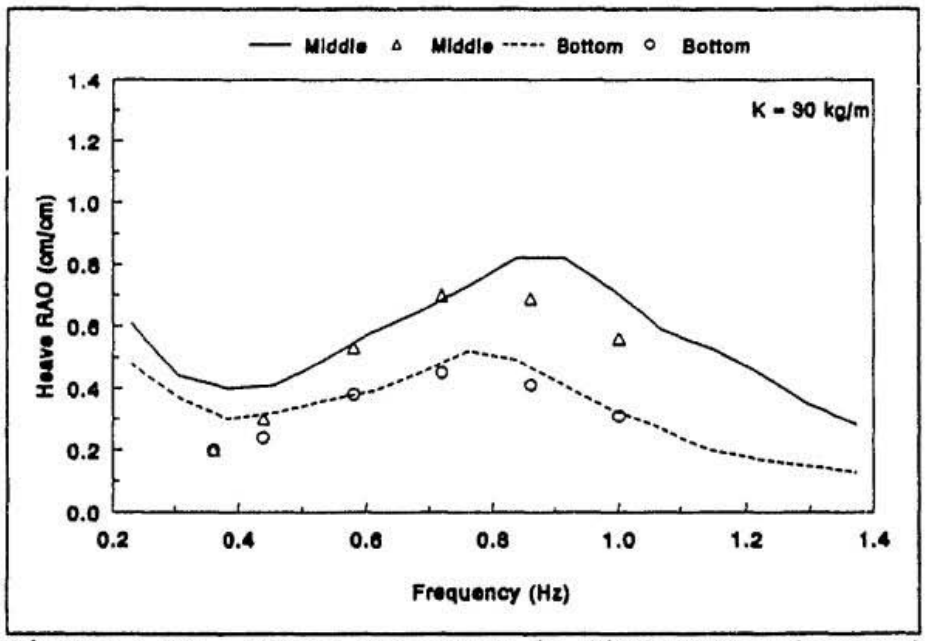

Figure 5.26 - Heave responses in different submerged positions: geodesic model, parallel orientation, with stiffer mooring lines

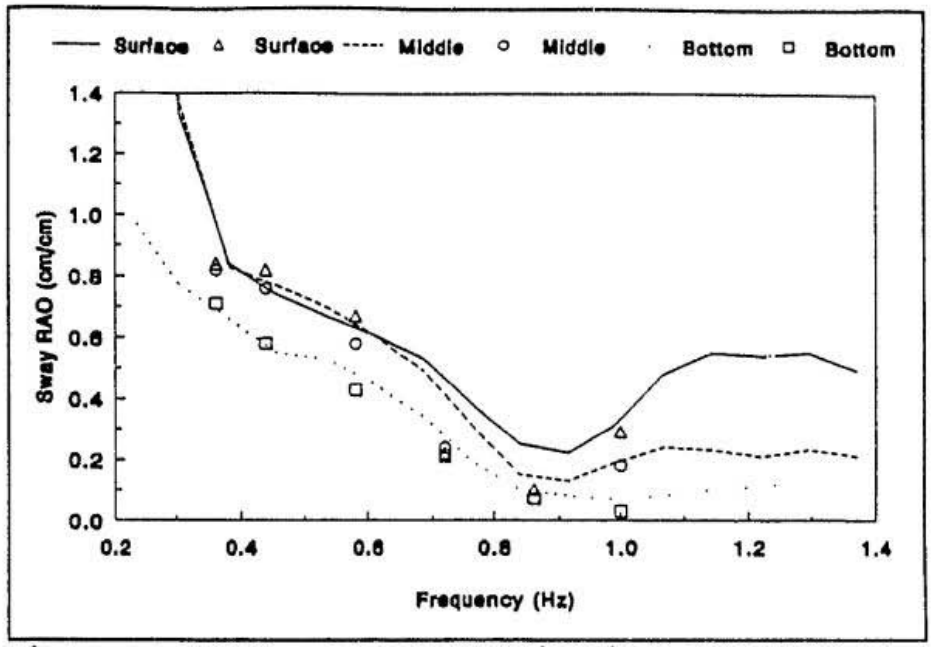

Figure 5.27 - Sway responses in different submerged positions: spherical model, perpendicular orientation

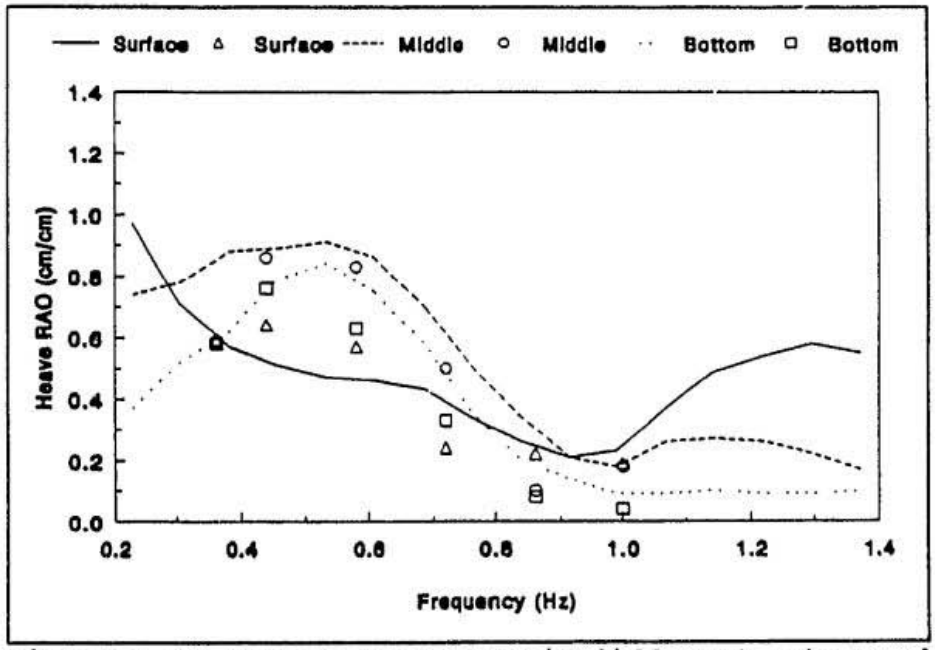

Figure 5.28 - Heave responses in different submerged positions: spherical model, perpendicular orientation

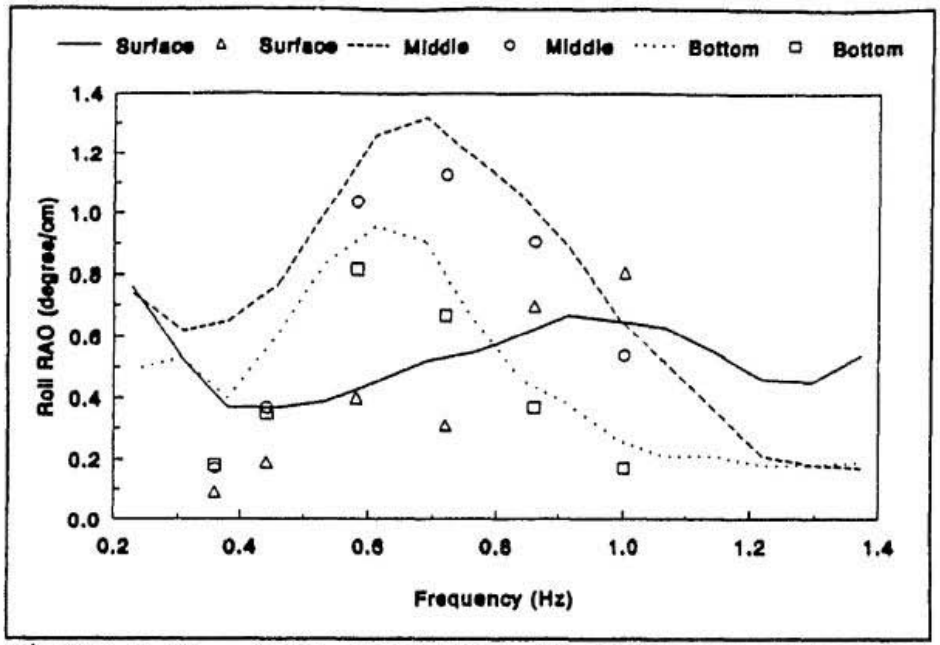

Figure 5.29 - Roll responses in different submerged positions: spherical model, perpendicular orientation

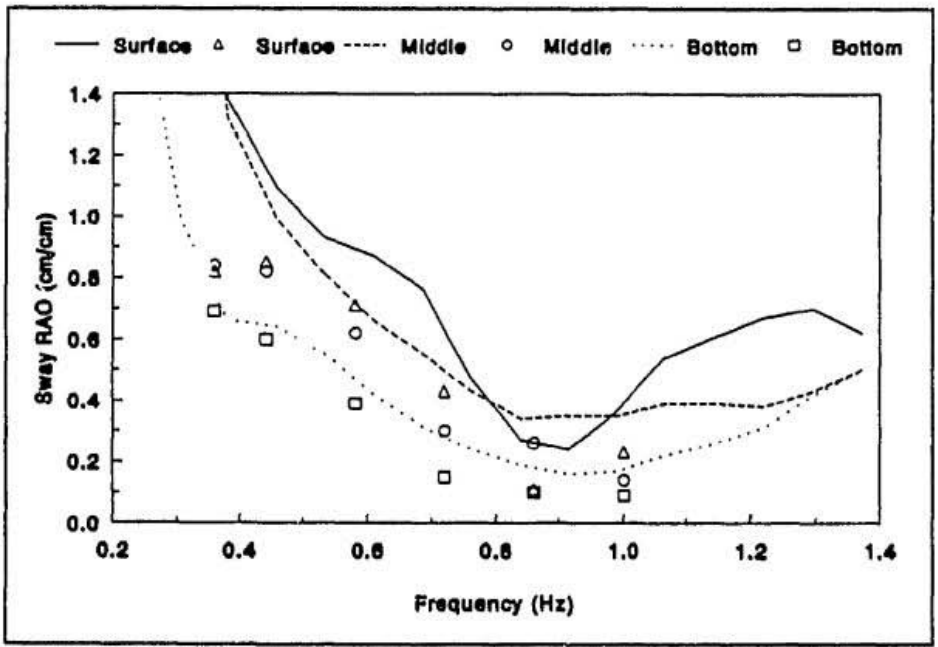

Figure 5.30 - Sway responses in different submerged positions: geodesic model, perpendicular orientation

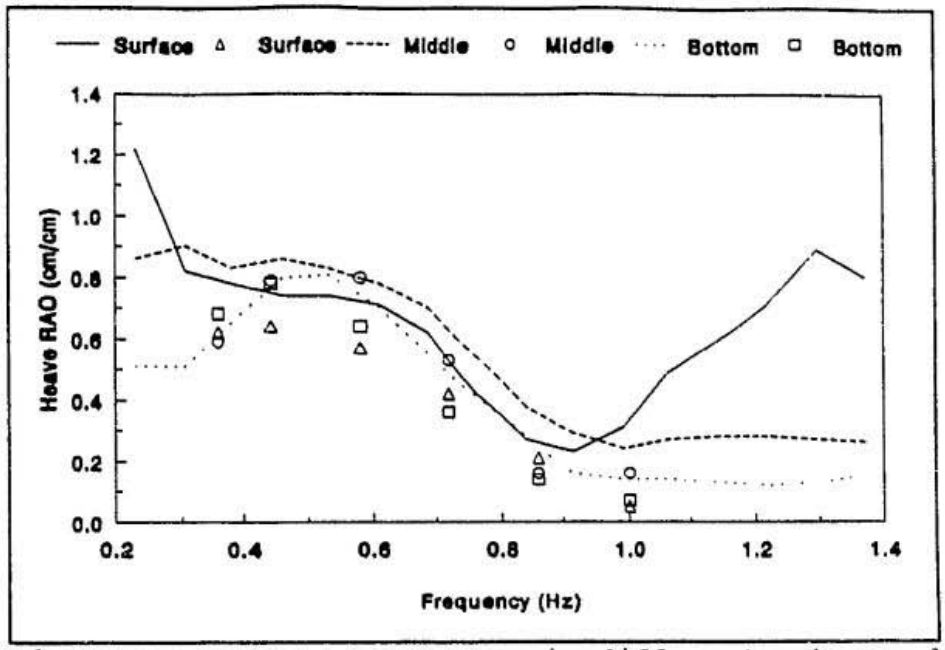

Figure 5.31 - Heave responses in different submerged positions: geodesic model, perpendicular orientation

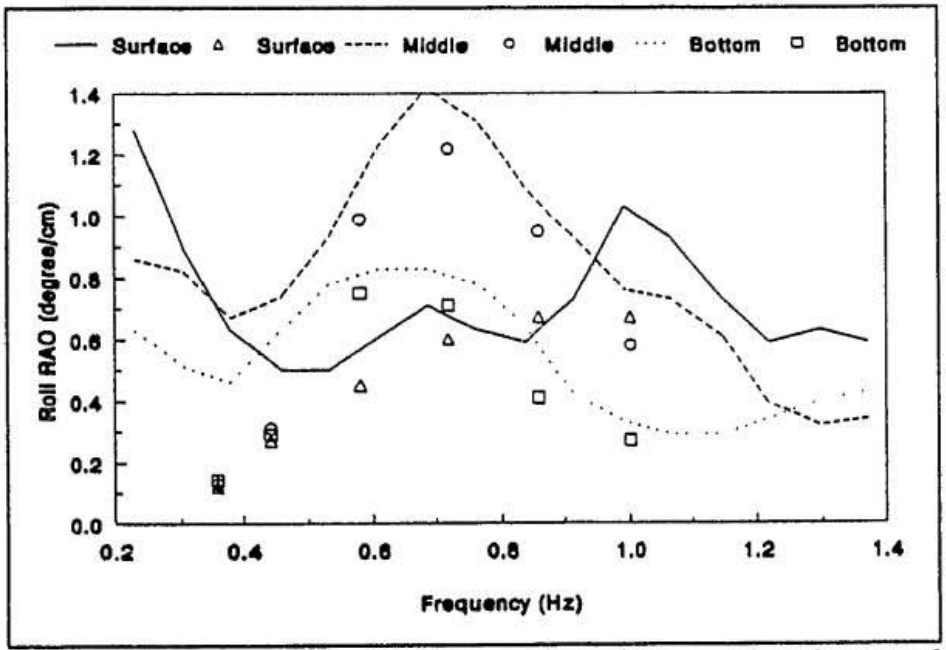

Figure 5.32 - Roll responses in different submerged positions: geodesic model, perpendicular orientation

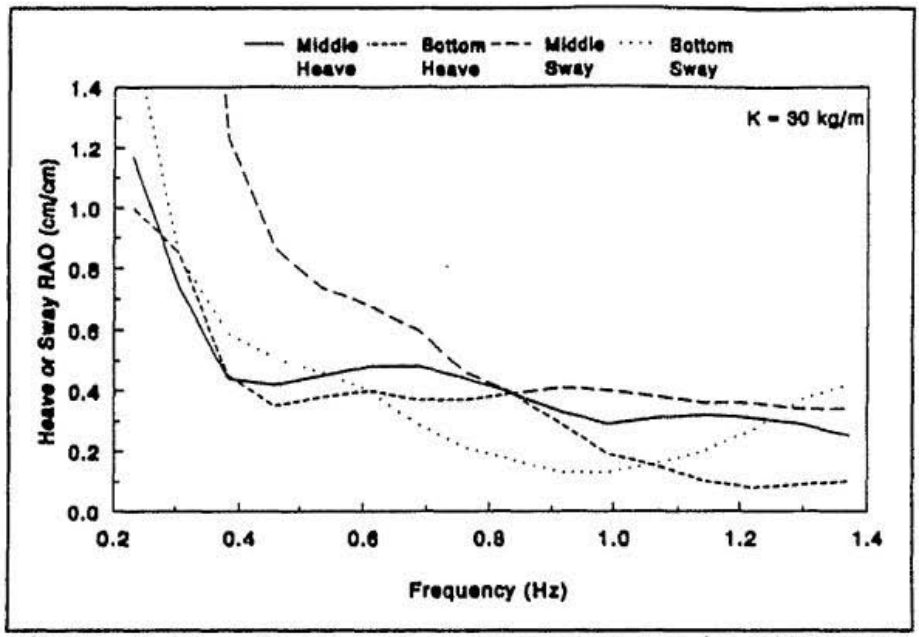

Figure 5.33 - Heave and sway responses in different submerged positions: geodesic model, perpendicular orientation, with stiffer mooring lines

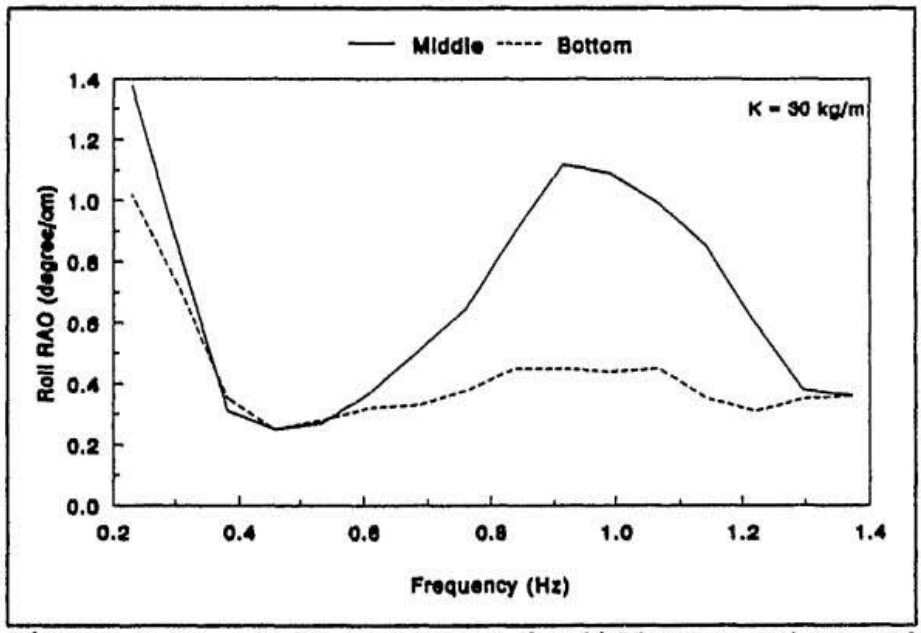

Figure 5.34 - Roll responses in different submerged positions: geodesic model, perpendicular orientation, with stiffer mooring lines

bottom position are larger at the low frequencies and smaller at the high frequencies than those in the surface position. The responses in the bottom position are smaller than the responses in the middle position. Again, the differences are small at the low frequencies and large at the high frequencies.

In the surface position the cage has the largest roll response when half of the wave length is equal to the distance between the two floats, because the roll exciting force is maximum at this point. In the middle and bottom positions the peak frequencies of the roll responses move toward lower frequencies, partly because the restoring forces and hence the natural frequencies of the roll motion are reduced by the submergence of the floats, and partly because the high frequency waves decrease with the depth below the water surface more than the low frequency waves.

5.2.1.3 Effects of pretension and stiffness of mooring lines

Figures 5.35 - 5.38 show the effect of pretension of the mooring lines on the heave and surge responses of the geodesic model in the middle and bottom positions of parallel orientation. It can be found that the increases of pretensions in the two mooring lines have only a small effect on the

motion responses. In the middle position, the responses of heave and surge with pretension of 900 g in each mooring line are a little larger than those with pretension of 700 g. In the bottom position, the responses are almost the same. It should be noted that the change of pretension was achieved by reducing the mass of the model, so it can also be concluded that a small change of mass has little effect on the motion responses of the cage.

Figures 5.39 - 5.46 show the effect of stiffness of the mooring lines on the motion responses of the geodesic model in the middle and bottom positions. As predicted in section 3.2.1, the stiffness of the mooring lines has little effect on the surge response of parallel orientation and the sway response of perpendicular orientation, but has a significant effect on the heave response of parallel orientation and the heave and roll responses of perpendicular orientation. For those responses affected by the mooring line stiffness, with the increase of spring constant in each mooring line from 10 kg/m to 30 kg/m the peak frequencies of the responses move to higher frequencies, and the amplitudes of the responses decrease except near the resonant frequencies. At the low frequencies, responses with K = 30 kg/m are much smaller than those with K = 10 kg/m, while at the high frequencies, responses with K = 30 kg/m are a little larger. From section

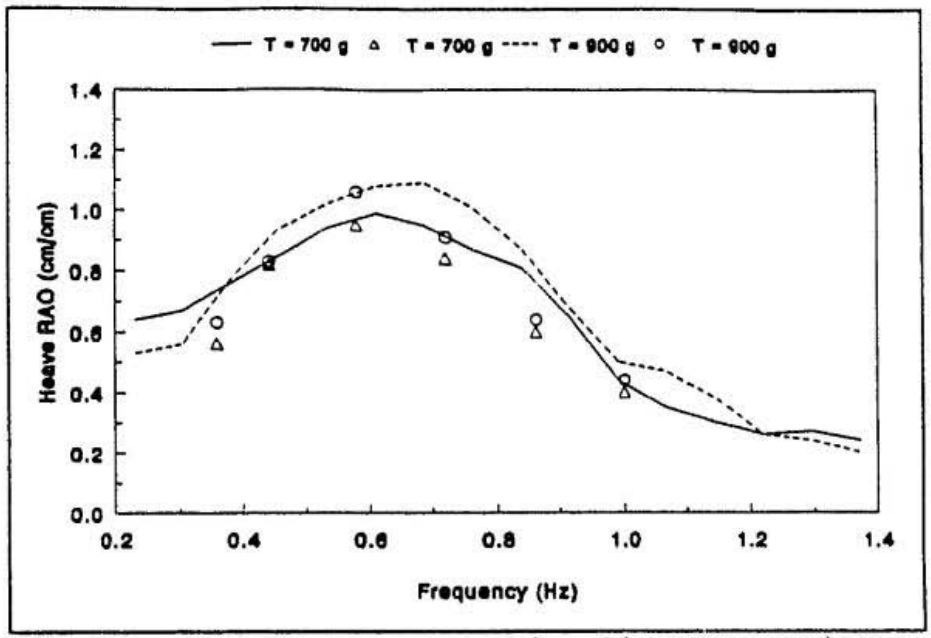

Figure 5.35 - Effect of mooring line pretension on heave response: middle position, parallel orientation

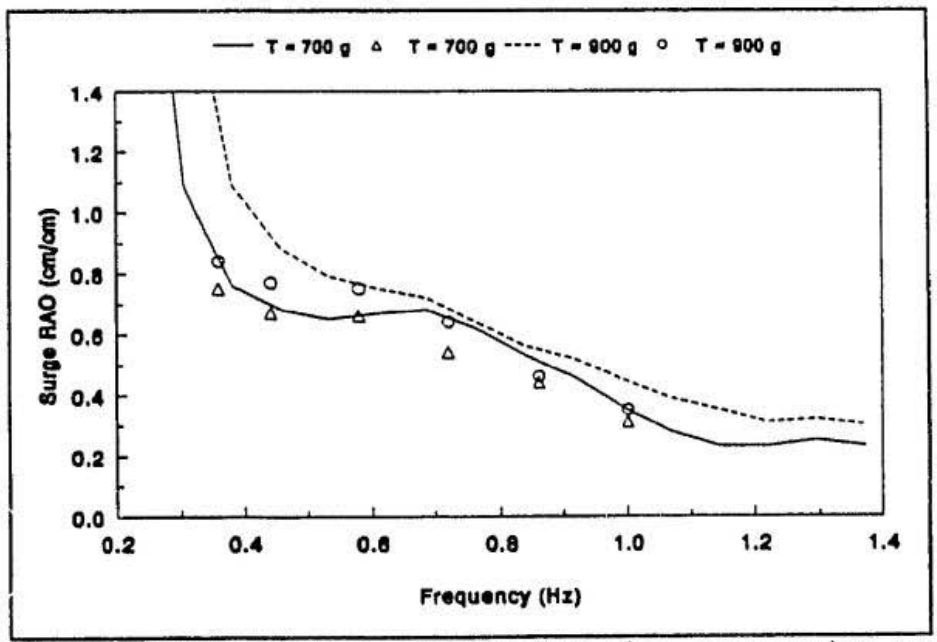

Figure 5.36 - Effect of mooring line pretension on surge response: middle position, parallel orientation

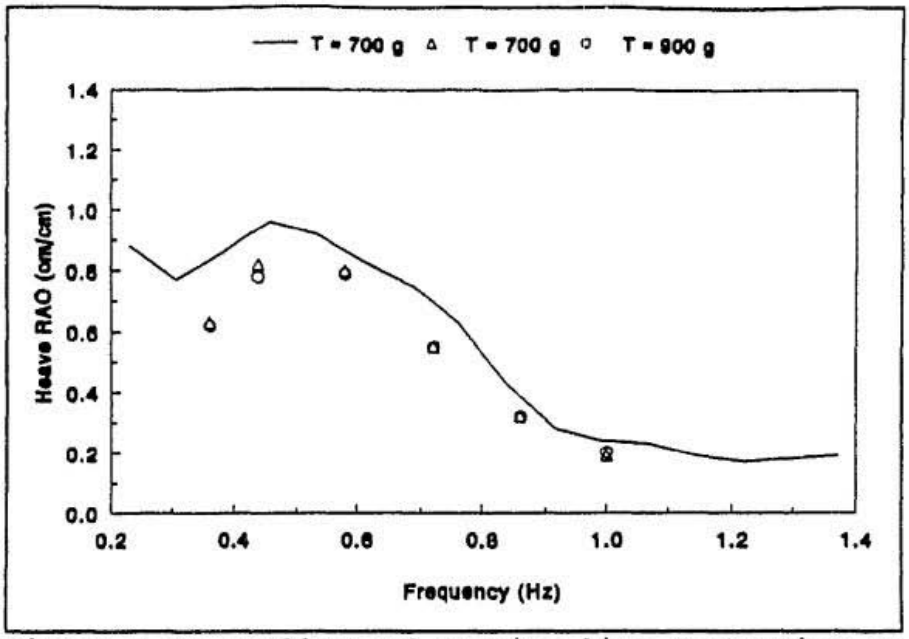

Figure 5.37 - Effect of mooring line pretension on heave response: bottom position, parallel orientation

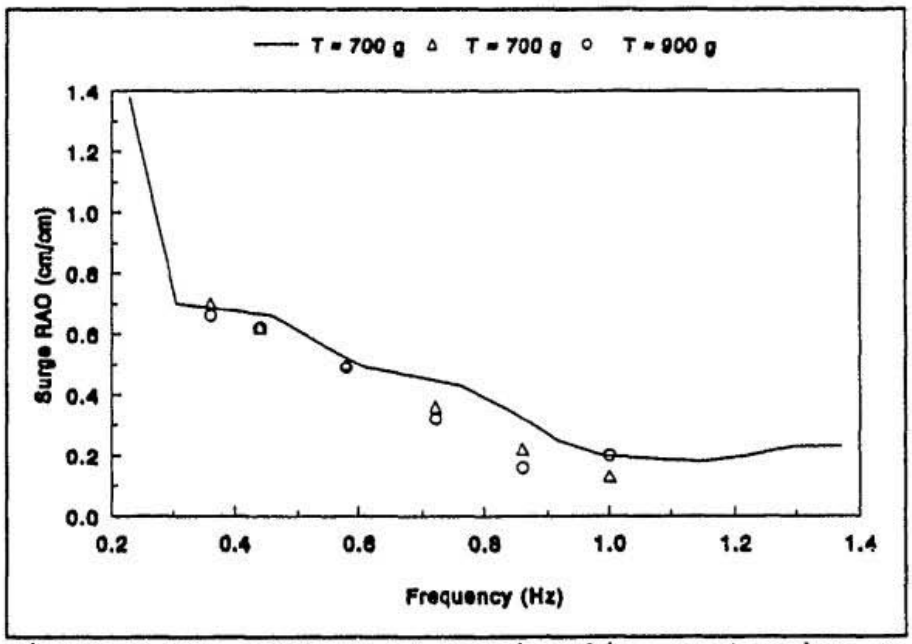

Figure 5.38 - Effect of mooring line pretension on surge response: bottom position, parallel orientation

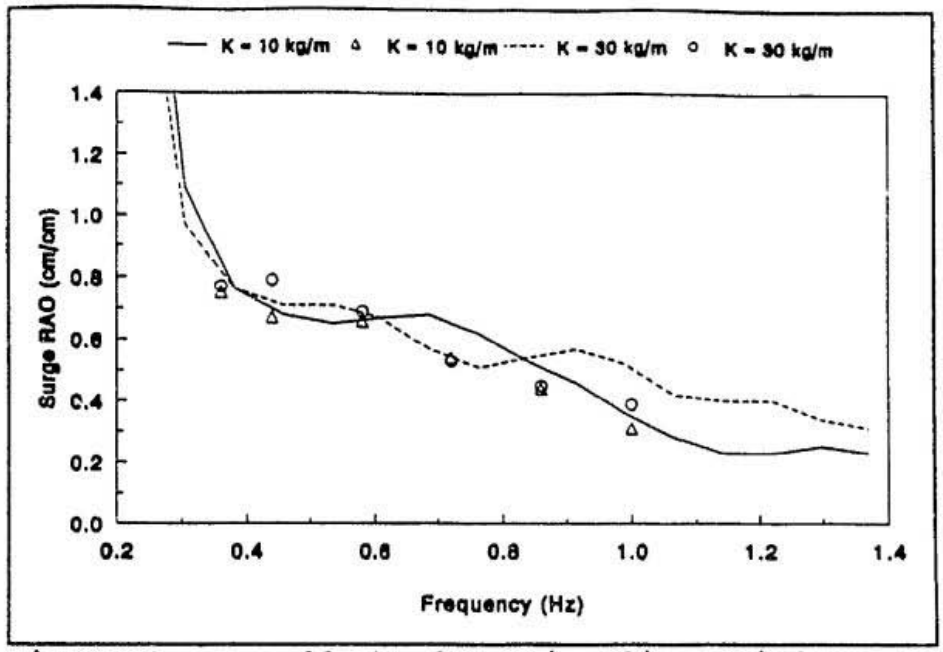

Figure 5.39 - Effect of mooring line stiffness on surge response: middle position, parallel orientation

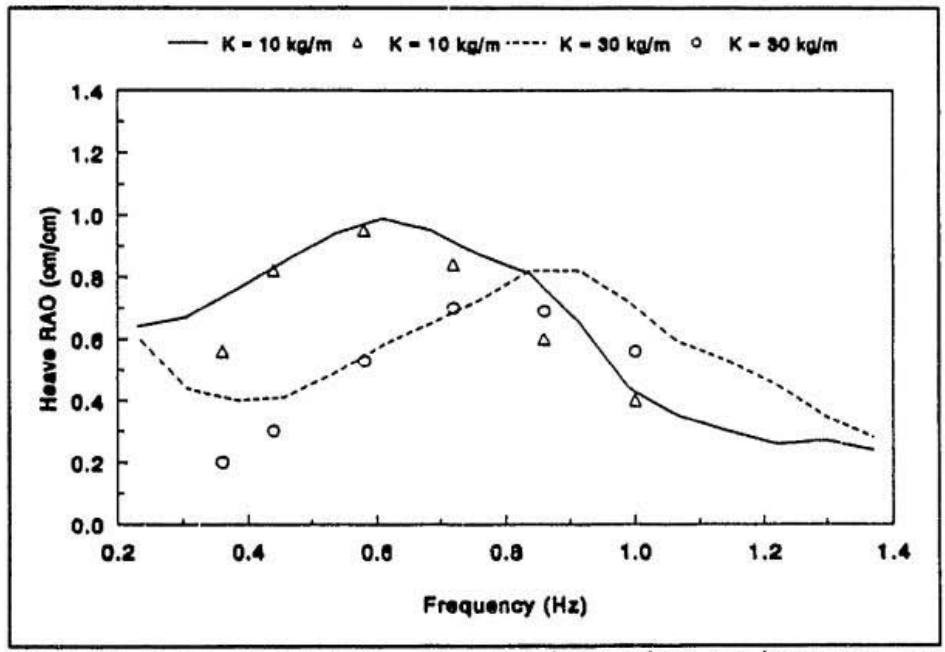

Figure 5.40 - Effect of mooring line stiffness on heave response: middle position, parallel orientation

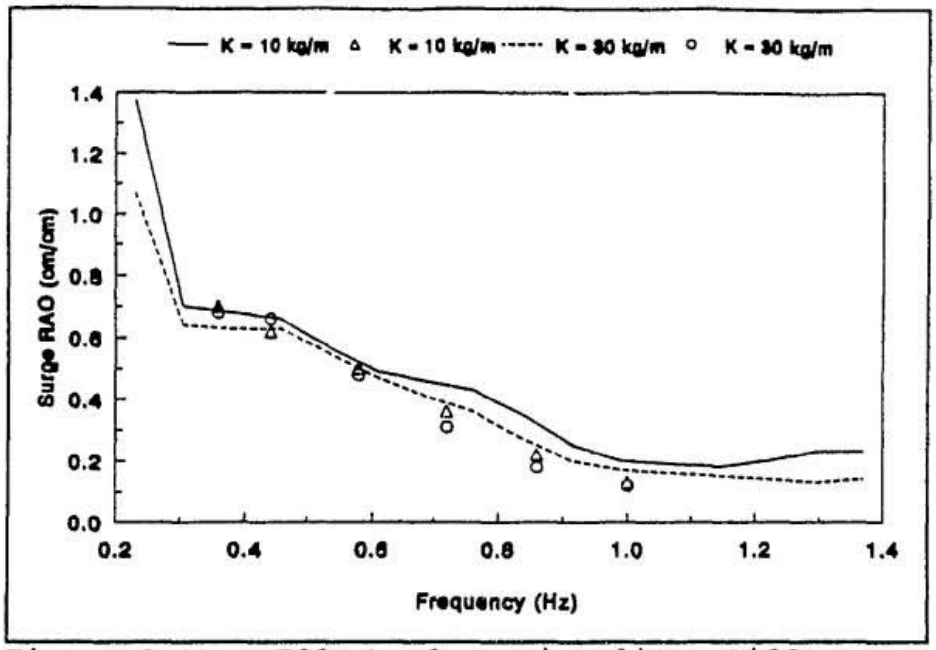

Figure 5.41 - Effect of mooring line stiffness on surge response: bottom position, parallel orientation

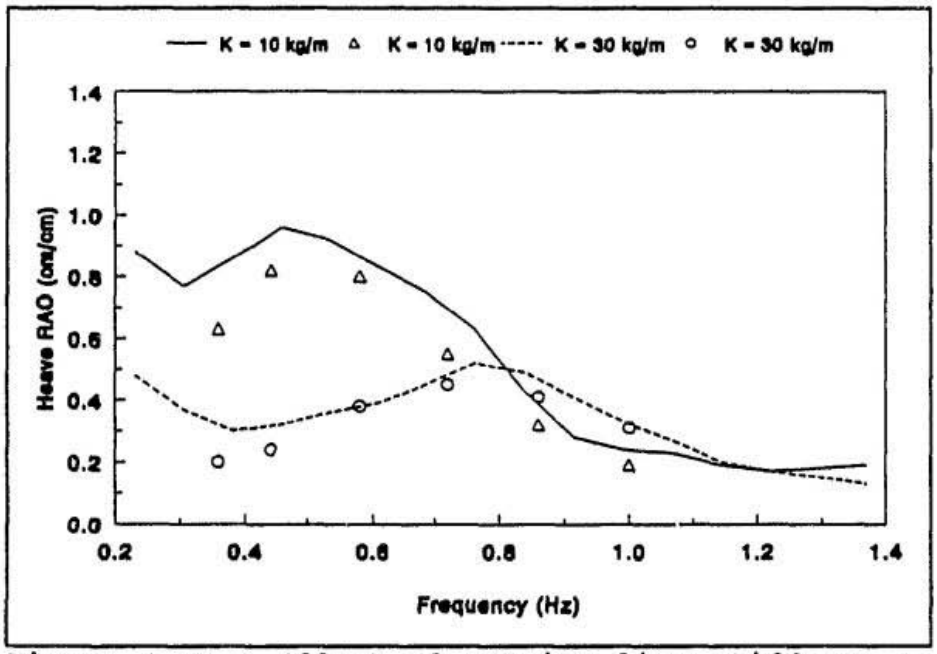

Figure 5.42 - Effect of mooring line stiffness on heave response: bottom position, parallel orientation

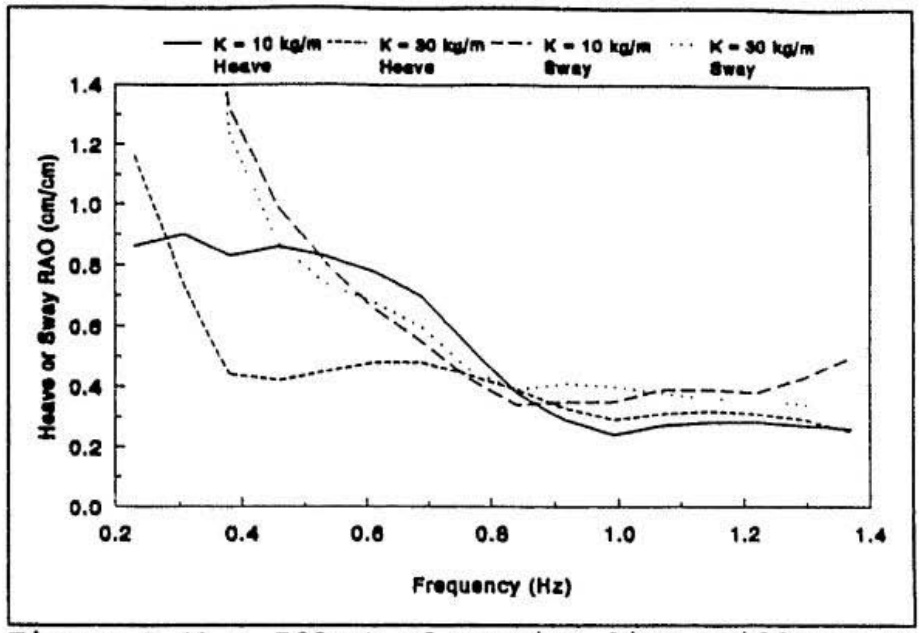

Figure 5.43 - Effect of mooring line stiffness on heave and sway responses: middle position, perpendicular orientation

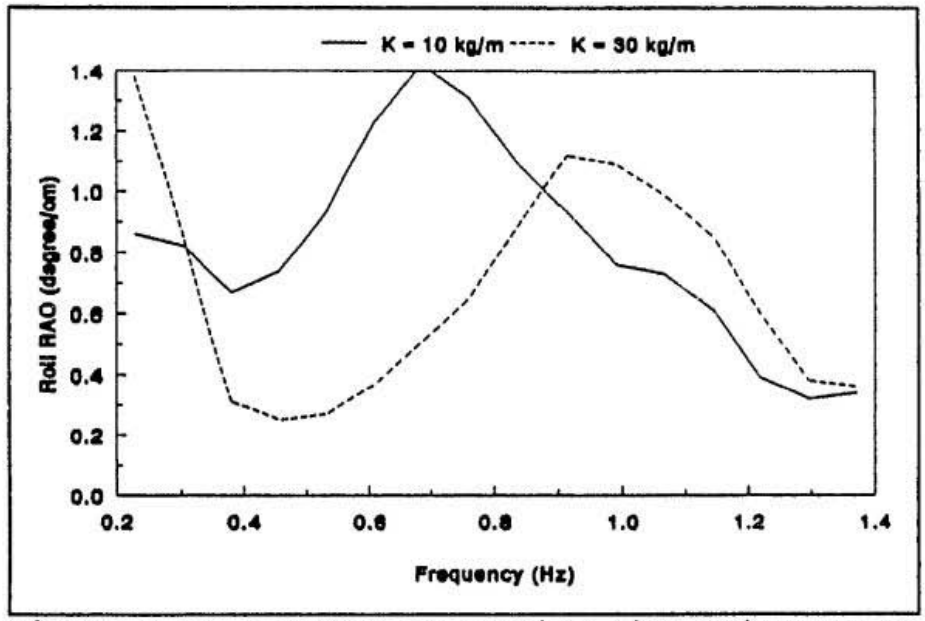

Figure 5.44 - Effect of mooring line stiffness on roll response: middle position, perpendicular orientation

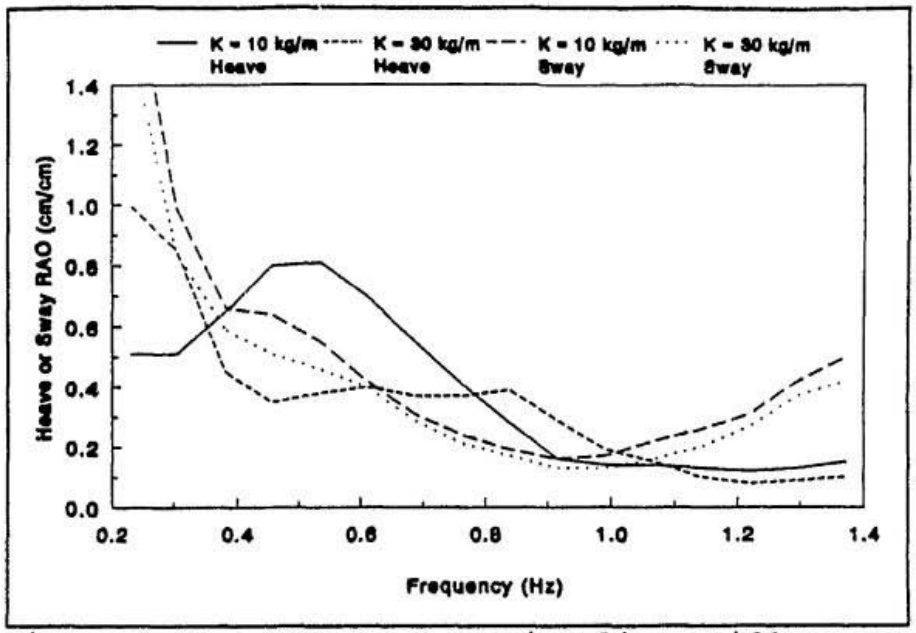

Figure 5.45 - Effect of mooring line stiffness on heave and sway responses: bottom position, perpendicular orientation

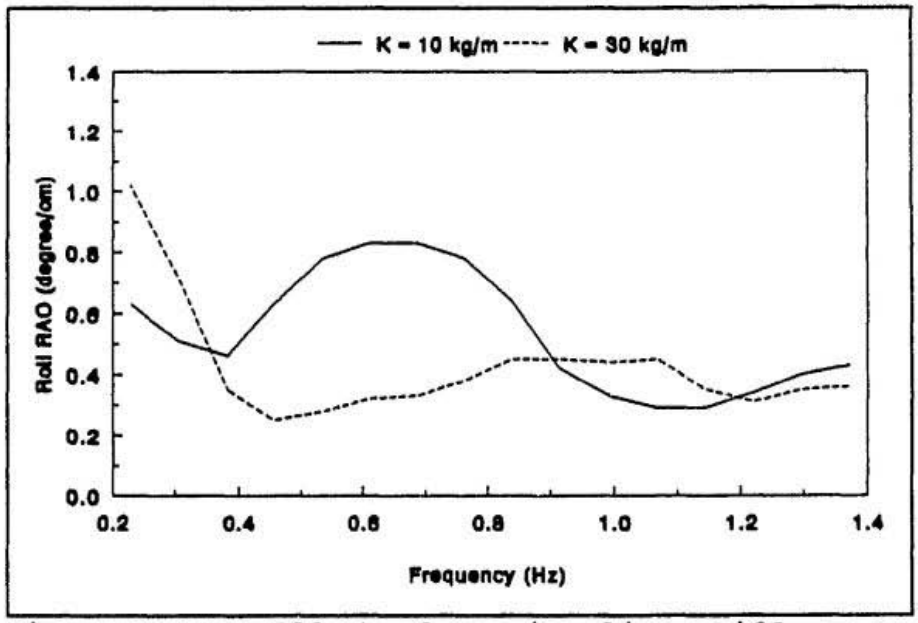

Figure 5.46 - Effect of mooring line stiffness on roll response: bottom position, perpendicular orientation

3.2.1 it has been known that the natural frequencies of the heave and roll motions will become higher with the increase of spring constant of the mooring lines.

5.2.2 Mooring force responses

5.2.2.1 Responses in different orientations

The comparisons among the responses of both mooring lines in parallel orientation, sea side and lee side mooring lines in perpendicular orientation for the three submerged positions are given respectively in Figures 5.47 - 5.49 for the spherical model and in Figures 5.50 - 5.52 for the geodesic model. In parallel orientation, the dynamic force responses in the two mooring lines are about the same. Therefore, the average values of the two mooring lines were used to present the responses of both mooring lines in these figures and the figures hereafter.

In perpendicular orientation, two different phenomena can be observed. When the model is in the surface position, the force responses in the sea side mooring line are a little larger than the force responses in the lee side mooring line. When the model is in the middle and bottom positions, the responses in the lee side mooring line are much larger than

the responses in the sea side mooring line in the low frequency range and the differences decrease as the frequency increases.

In the surface position, the differences between the mooring force responses in parallel orientation and perpendicular orientation are small. In the middle and bottom positions, the force responses in the lee side mooring line in perpendicular orientation are significantly larger than the force responses in the both mooring lines in parallel orientation; while the force responses in the sea side mooring line in perpendicular orientation are smaller in the low frequency range and a little larger in the high frequency range than the force responses in parallel orientation.

The major motions of the cage in parallel orientation are surge and heave. By comparing the frequency responses of mooring forces, surge and heave motions, it can be found that the mooring force and heave responses have almost the same trend. Therefore, it can be concluded that in parallel orientation the mooring forces are mainly caused by the heave motion of the cage. The amplitudes of the surge motion are not large enough to cause any significant forces in the mooring lines. For the maximum surge amplitude of about 5 cm in the surface position, the corresponding extension of either

mooring line is only about 0.03 percent.

On the other hand, the major motions of the cage in perpendicular orientation are sway, heave and roll. Again, the amplitudes of sway are not large enough to cause any significant forces in the mooring lines. The mooring force responses are mainly caused by the combined effect of the heave and roll motions of the cage, and the phase difference between heave and roll will significantly affect the force responses in the sea side and lee side mooring lines.

The differences between the force responses in the sea side and lee side mooring lines in perpendicular orientation are mainly caused by the phase difference between the heave and roll motions of the cage. Figure 5.53 gives the effect of the phase difference on the vertical displacements at the ends of the sea side and lee side mooring lines. The larger the displacement is, the larger the force responses in the mooring line will be. When the phase difference is 0°, the amplitude of the vertical displacement at the end of the lee side mooring line is

$$A_{lee} = A_{heave} + \frac{d}{2}\sin(A_{roll}) \qquad (5.10)$$

where A_{heave} is the amplitude of heave, A_{roll} is the amplitude of roll and d is the distance between the sea side and lee side

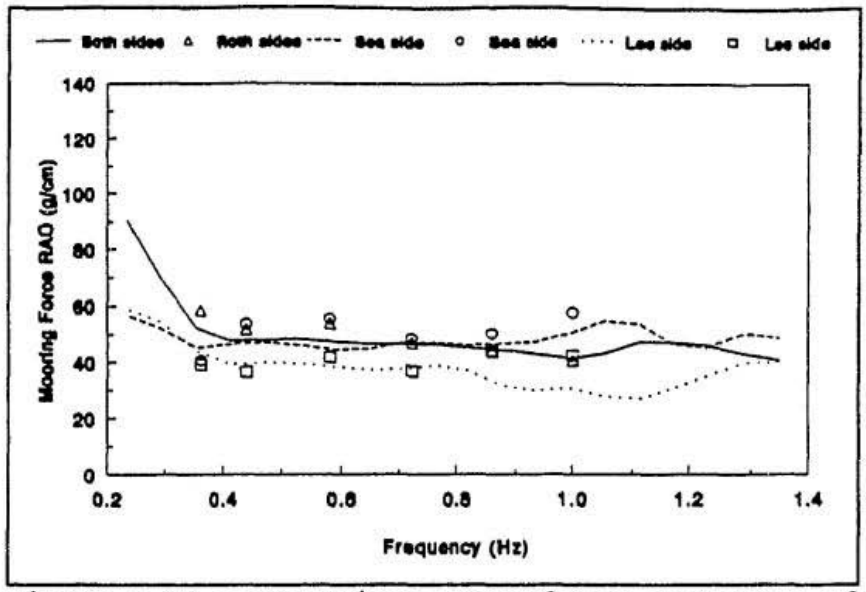

Figure 5.47 - Comparison among force responses of both mooring lines in parallel orientation, sea side and lee side mooring lines in perpendicular orientation: spherical model, surface position

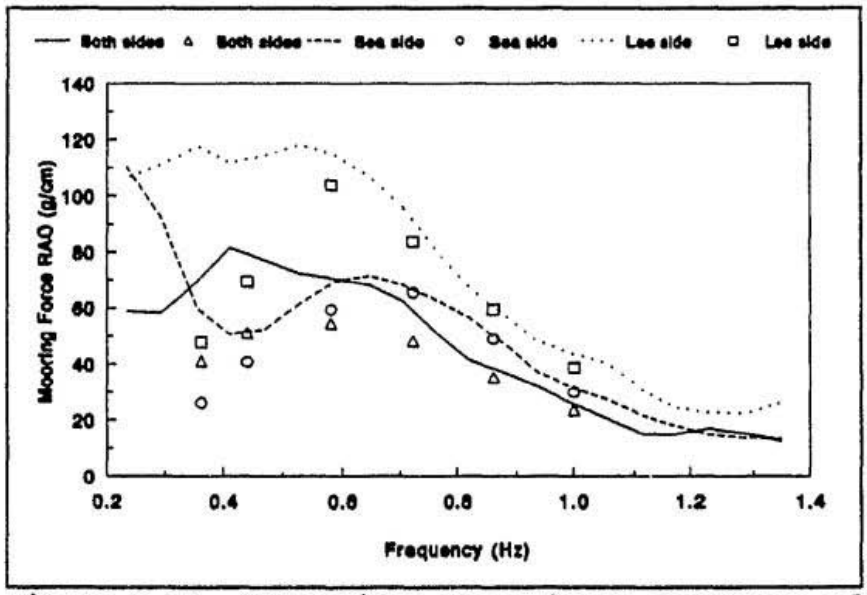

Figure 5.48 - Comparison among force responses of both mooring lines in parallel orientation, sea side and lee side mooring lines in perpendicular orientation: spherical model, middle position

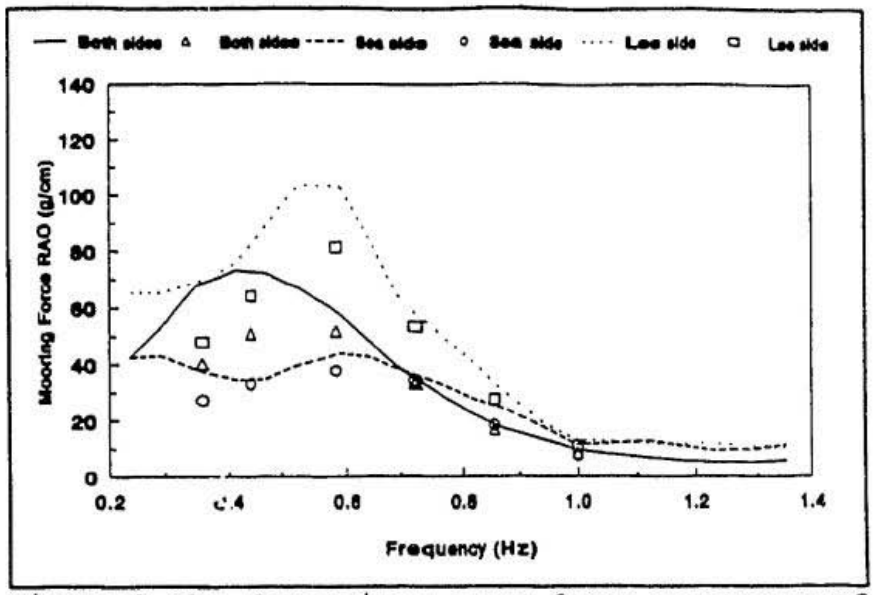

Figure 5.49 - Comparison among force responses of both mooring lines in parallel orientation, sea side and lee side mooring lines in perpendicular orientation: spherical model, bottom position

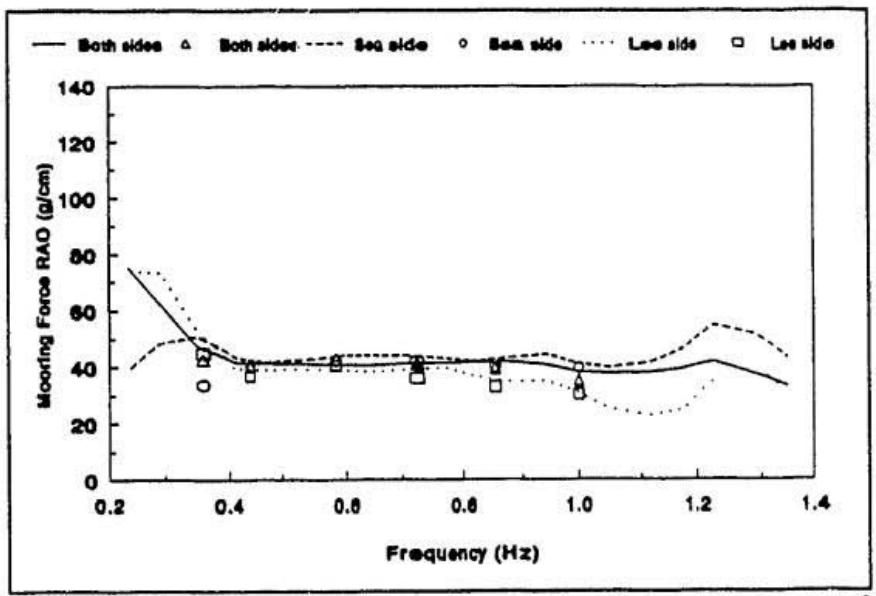

Figure 5.50 - Comparison among force responses of both mooring lines in parallel orientation, sea side and lee side mooring lines in perpendicular orientation: geodesic model, surface position

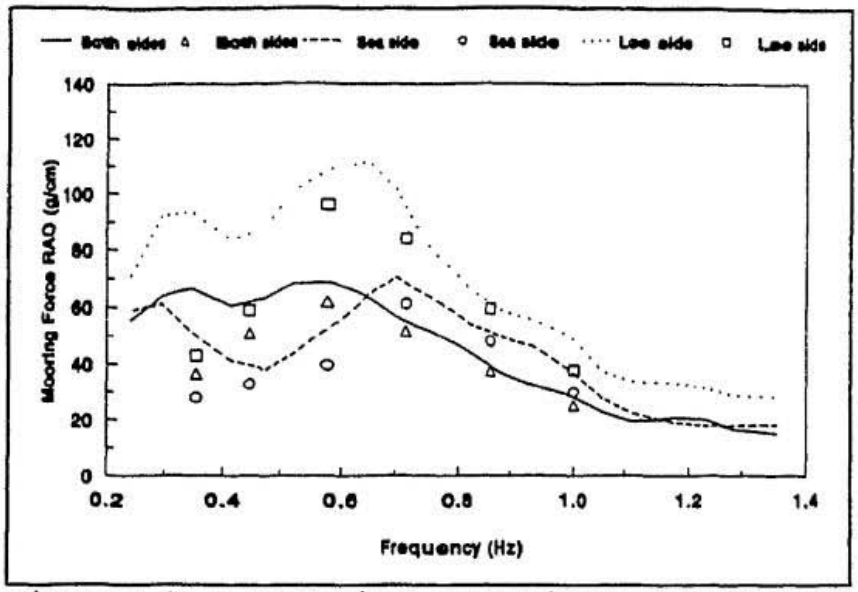

Figure 5.51 - Comparison among force responses of both mooring lines in parallel orientation, sea side and lee side mooring lines in perpendicular orientation: geodesic model, middle position

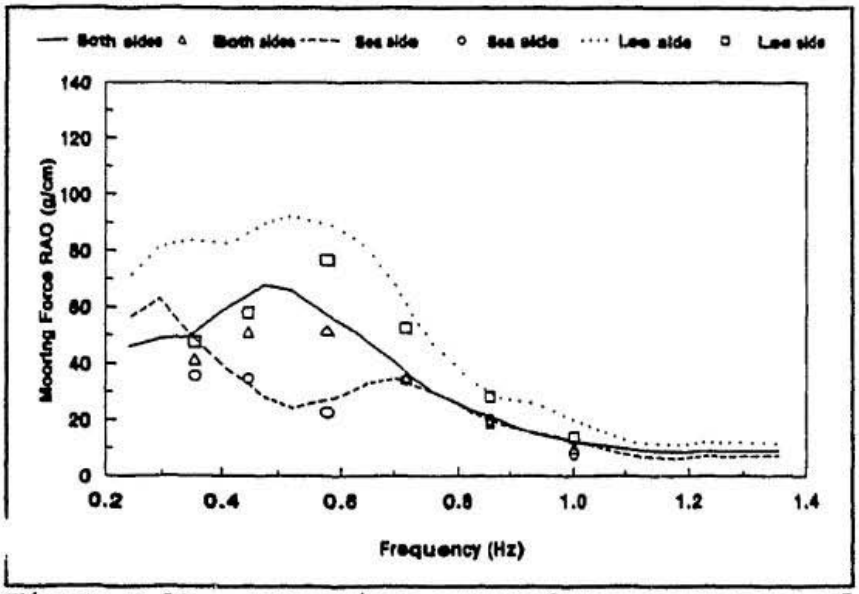

Figure 5.52 - Comparison among force responses of both mooring lines in parallel orientation, sea side and lee side mooring lines in perpendicular orientation: geodesic model, bottom position

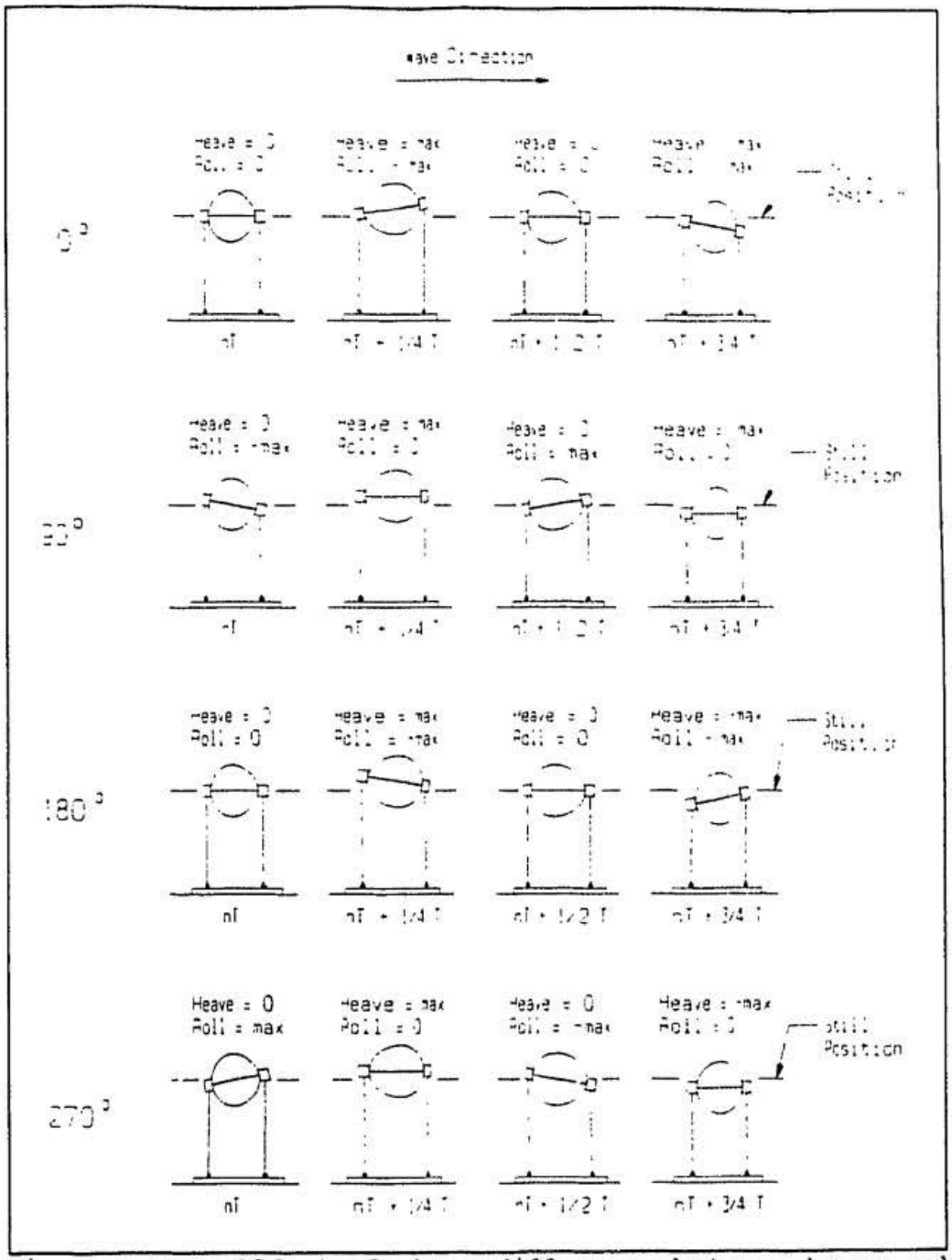

Figure 5.53 - Effect of phase difference between heave and roll on the extensions of sea side and lee side mooring lines

mooring lines; while the amplitude of the vertical displacement at the end of the sea side mooring line is

$$A_{sea} = \left| A_{heave} - \frac{d}{2}\sin(A_{roll}) \right| \qquad (5.11)$$

The amplitude of the vertical displacement at the end of the lee side mooring line will be much larger than that at the end of the sea side mooring line if both the heave and roll motions of the cage are significant. Consequently, the force response in the lee side mooring line will be significantly larger than that in the sea side mooring line. When the phase difference is 180°, the situation is just reversed. The amplitude of the vertical displacement at the end of the sea side mooring line will be much larger than that at the end of the lee side mooring line, hence the force response in the sea side mooring line will be significantly larger than that in the lee side mooring line. When the phase difference is 90° or 270°, the amplitude of the vertical displacements at the ends of both the lee side and sea side mooring lines are

$$A_{lee,\ sea} = \max\left[A_{heave},\ \frac{d}{2}\sin(A_{roll})\right] \qquad (5.12)$$

The amplitudes of the force responses in the both mooring lines will be about the same, and will be much smaller than the response in the lee side mooring line in the case of 0° phase difference or the response in the sea side mooring line in the case of 180° phase difference. Therefore, when the

phase difference between the heave and roll motions of the cage is close to 0° or 180°, there will be a significant difference between the responses in the sea side and lee side mooring lines and the amplitude of the vertical displacement on one side of the cage will be significantly larger than that on the other side of the cage; when the phase difference is close to 90° or 270°, the difference between the force responses in the two mooring lines will be small and the amplitudes of the vertical displacements on two sides of the cage will be about the same.

The phases of heave and roll of the cage are determined by the frequency of the incident wave, the mass and added mass or inertia and added inertia of the cage, the damping of the cage for heave or roll, and the restoring and restraining coefficients of the heave or roll motion. In order to reduce the mooring force responses, special care should be made in the design of the prototype cage system so that the phase difference between heave and roll will be about 90° or 270° in the mainly concerned wave frequency range of the cage site. In such case, the mooring forces in the lee side and sea side mooring line will be about the same and the mooring system will be safer. The adjustment of the phase difference can be made by changing some of the parameters mentioned above.

From the plotting outputs of heave and roll motions of the regular wave tests, it is found, for the geodesic model at the frequency of 0.58 Hz where the differences between the force responses in the lee side and sea side mooring lines are maximum in the middle and bottom positions, that the phase difference between the heave and roll motions of the cage is about 100° in the surface position, 30° in the middle position and 15° in the bottom position. From the video record it can also be found that, in the middle and bottom positions, the vertical displacements of the lee side end of the cage are significantly larger than those of the sea side end. These observations confirm the analysis above. The differences among the surface, middle and bottom positions are caused by the change of restoring forces due to the submergence of the two floats and the change of damping and added mass due to the change of submerged volume in different positions. In the middle and bottom positions, the difference between the force responses in the lee side and sea side mooring lines decreases with frequency because the heave motion of the cage becomes insignificant at the high frequencies.

According to the test results in the middle position, the lee side and sea side mooring force responses of 45° orientation are similar to those of perpendicular orientation.

5.2.2.2 Responses in different submerged positions

5.2.2.2.1 Parallel orientation

Comparisons of mooring force responses in different submerged positions are shown in Figure 5.54 for the spherical model, Figure 5.55 for the geodesic model and Figure 5.56 for the geodesic model with stiffer mooring lines (K = 30 kg/m instead of K = 10 kg/g).

Similar to the heave responses, the force responses change little with frequency in the surface position, but first increase and then decrease with frequency in the middle and bottom positions. In the low frequency range the mooring force responses in the middle and bottom positions tend to be larger than those in the surface position. With the increase of frequency, the responses in the middle and bottom position begin to decrease and become significantly smaller than those in the surface position in the high frequency range.

Comparing the responses in the middle and bottom positions, it can be found that the differences are very small at the low frequencies. With the increase of frequency, the responses in the bottom position become significantly smaller than the responses in the middle position at the high

frequencies and the differences increase with the increase of frequency.

5.2.2.2.2 Perpendicular orientation

Figures 5.57 and 5.58 present the comparisons of the force responses of the sea side and lee side mooring lines in different submerged positions for the spherical model, Figures 5.59 and 5.60 for the geodesic model and Figure 5.61 for the geodesic model with stiffer mooring lines.

For the sea side mooring line, the responses in the bottom position are smaller than the responses in the surface position; the responses in the middle position tend to be larger at the low frequencies and smaller at the high frequencies than the responses in the surface position. For the lee side mooring line, the force responses in both the middle and bottom positions are significantly larger than the responses in the surface position in a wide frequency range, and at the high frequencies the responses in the bottom position begin to become smaller than those in the surface position.

Comparing the force responses in the middle and bottom positions for both the sea side and lee side mooring lines,

the differences are very small in the low frequency range, but the force responses in the bottom position are reduced significantly in the high frequency range.

5.2.2.3 Effects of pretension and stiffness of mooring lines

From the test results shown in Figures 5.62 and 5.63 for the geodesic model in the middle and bottom positions and parallel orientation, it can be found that, when the pretension in each mooring line is changed from 700 g to 900 g, the mooring force responses change little. This confirms the prediction in section 3.2.2 that pretension of the mooring lines has little effect on the mooring force response as long as it is large enough to prevent the mooring lines from being slack. It should be noted that the change of the pretension was achieved by reducing the mass of the cage model, so it can also be concluded that a small change of mass has little effect on the mooring force responses.

The effect of stiffness of the mooring lines on the mooring force responses are shown in Figures 5.64 - 5.69 for the geodesic model in the middle and bottom positions. It can be noted that the stiffness of the mooring lines has a significant effect on the mooring force responses. With the increase of the spring constant of the mooring lines, the peak

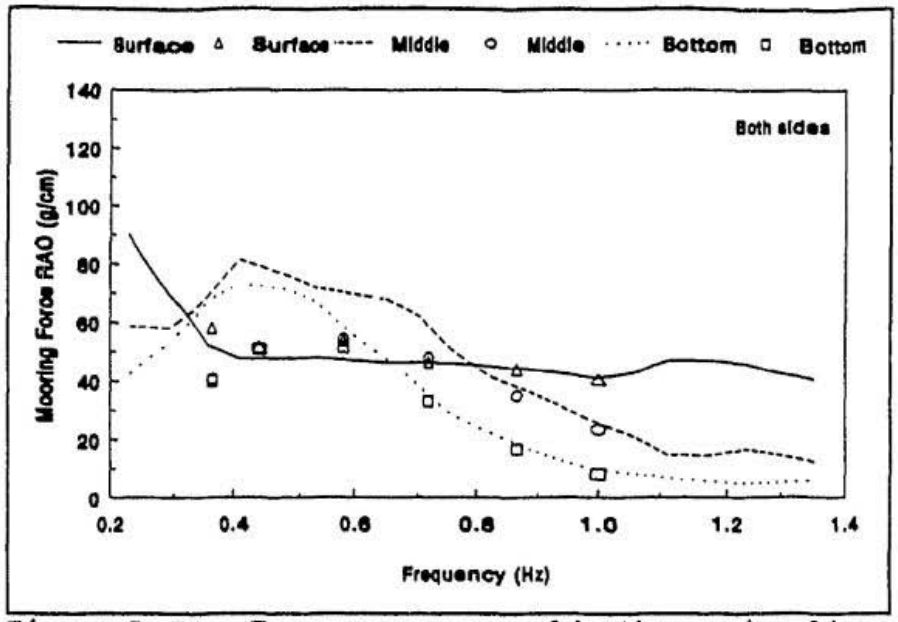

Figure 5.54 - Force responses of both mooring lines in different submerged positions: spherical model, parallel orientation

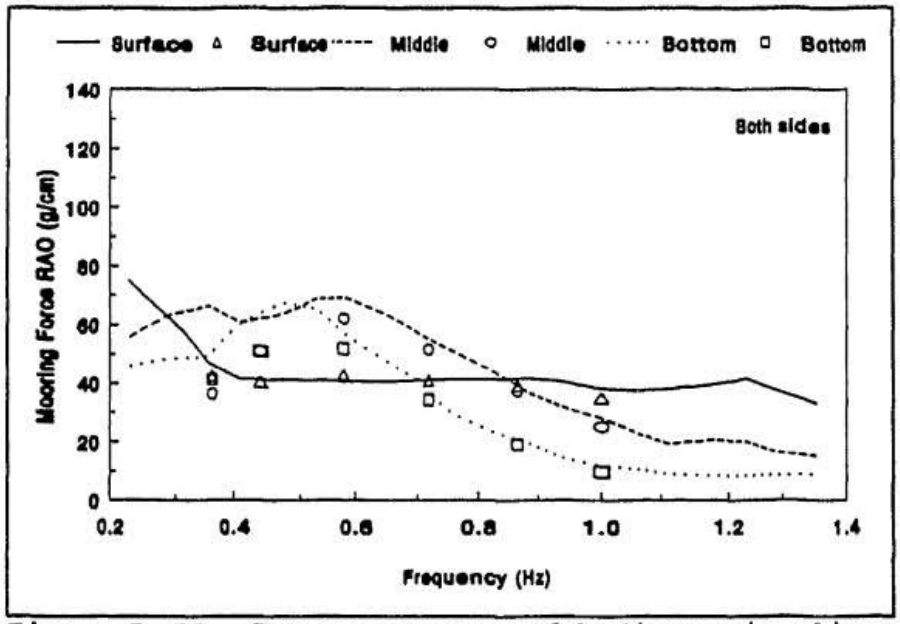

Figure 5.55 - Force responses of both mooring lines in different submerged positions: geodesic model, parallel orientation

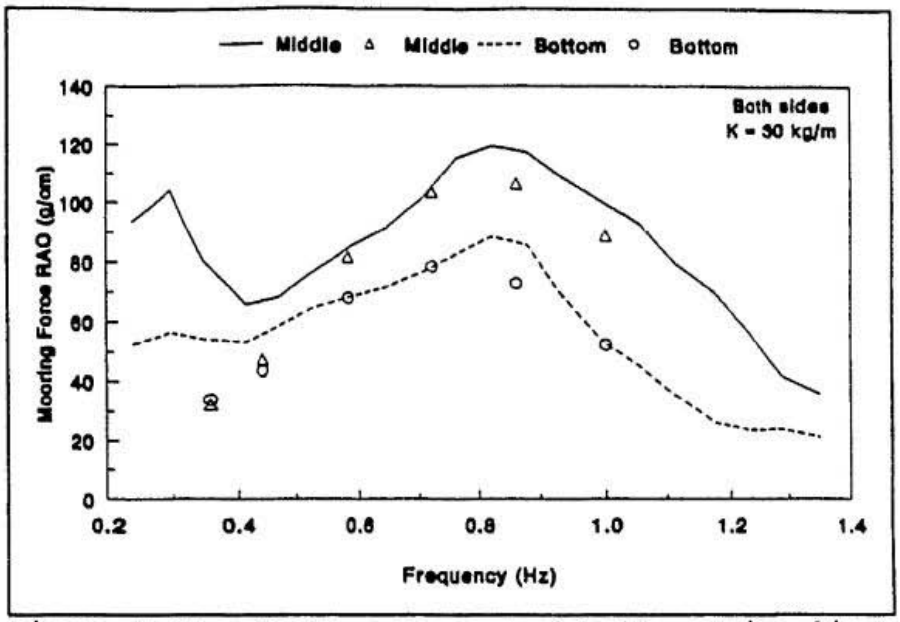

Figure 5.56 - Force responses of both mooring lines in different submerged positions: geodesic model, parallel orientation, with stiffer mooring lines

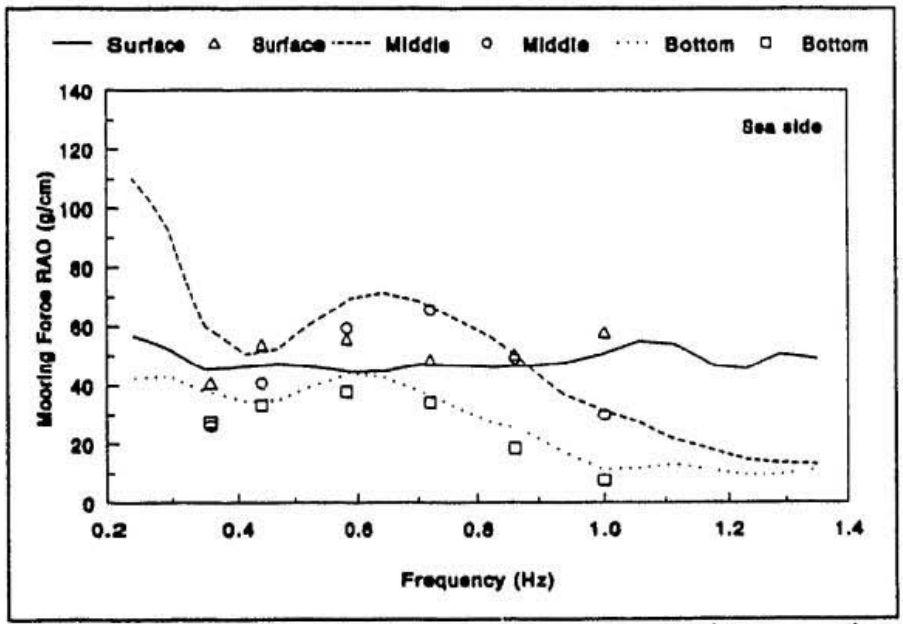

Figure 5.57 - Force responses of sea side mooring line in different submerged position: spherical model, perpendicular orientation

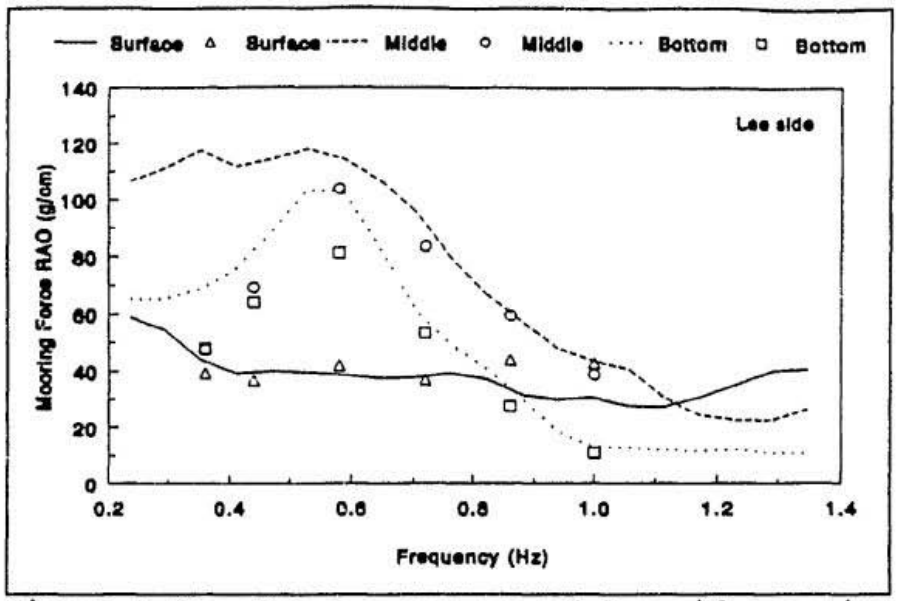

Figure 5.58 - Force responses of lee side mooring line in different submerged positions: spherical model, perpendicular orientation

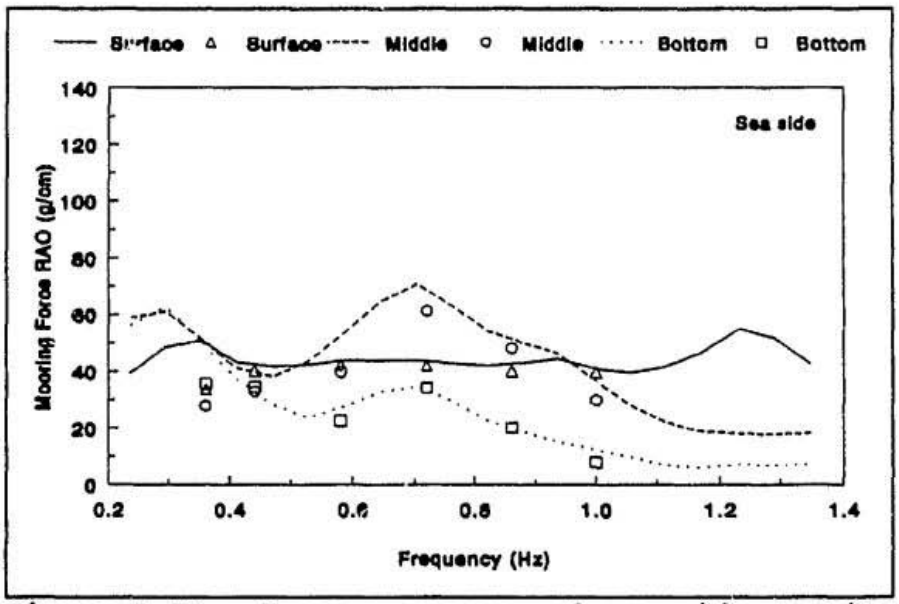

Figure 5.59 - Force responses of sea side mooring line in different submerged positions: geodesic model, perpendicular orientation

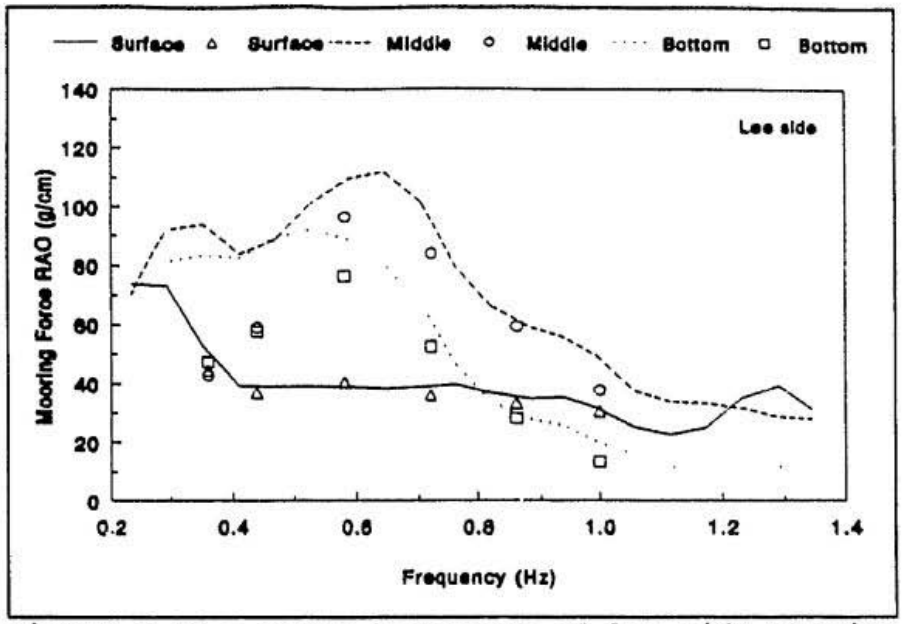

Figure 5.60 - Force responses of lee side mooring line in different submerged positions: geodesic model, perpendicular orientation

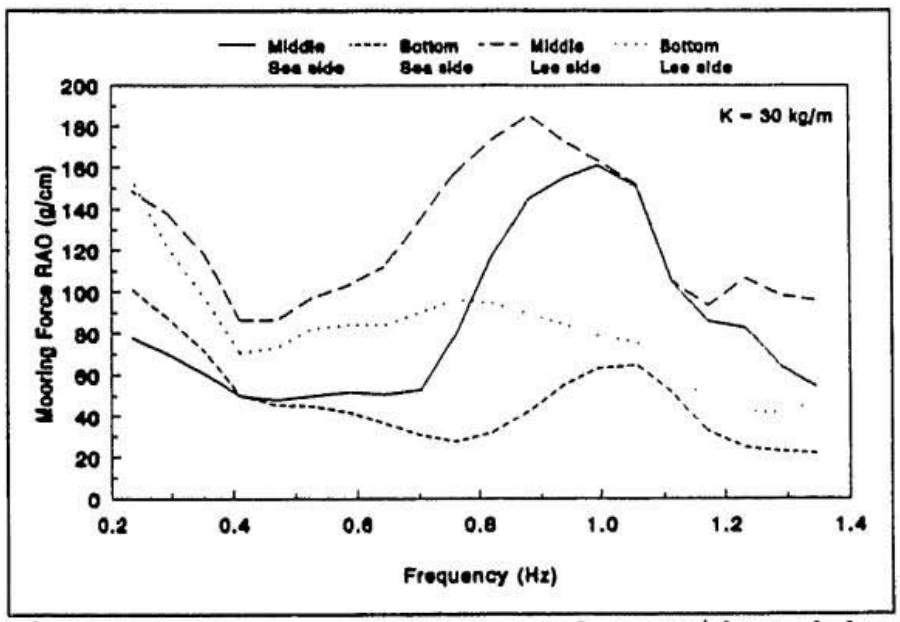

Figure 5.61 - Force responses of sea side and lee side mooring lines in different submerged positions: geodesic model, perpendicular orientation, with stiffer mooring lines

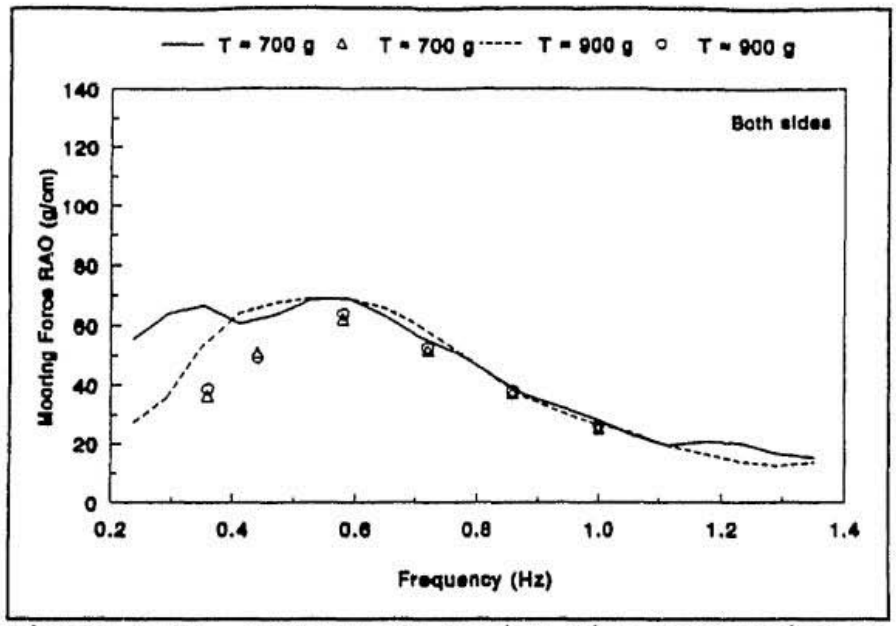

Figure 5.62 - Effect of mooring line pretension on force responses of both mooring lines: middle position, parallel orientation

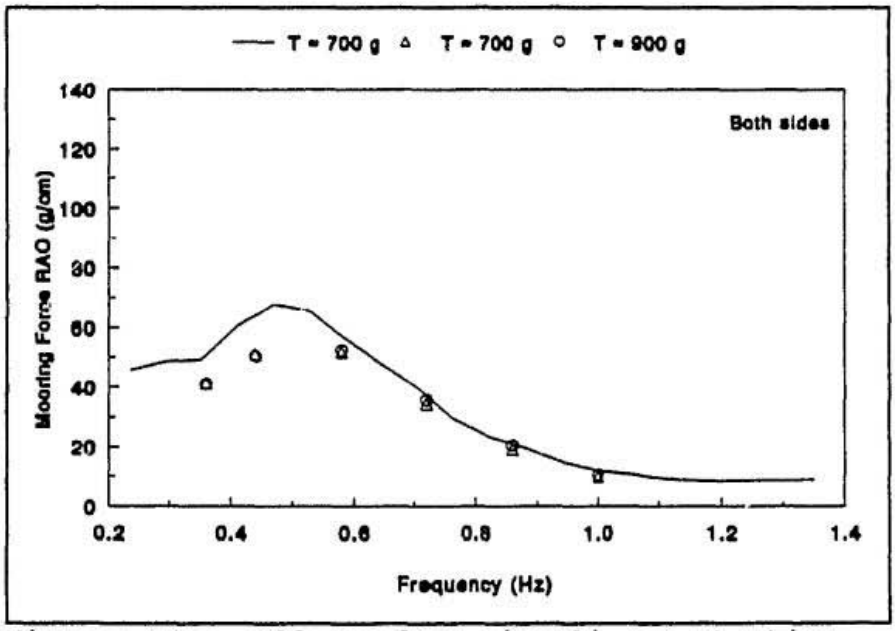

Figure 5.63 - Effect of mooring line pretention on force responses of both mooring lines: bottom position, parallel orientation

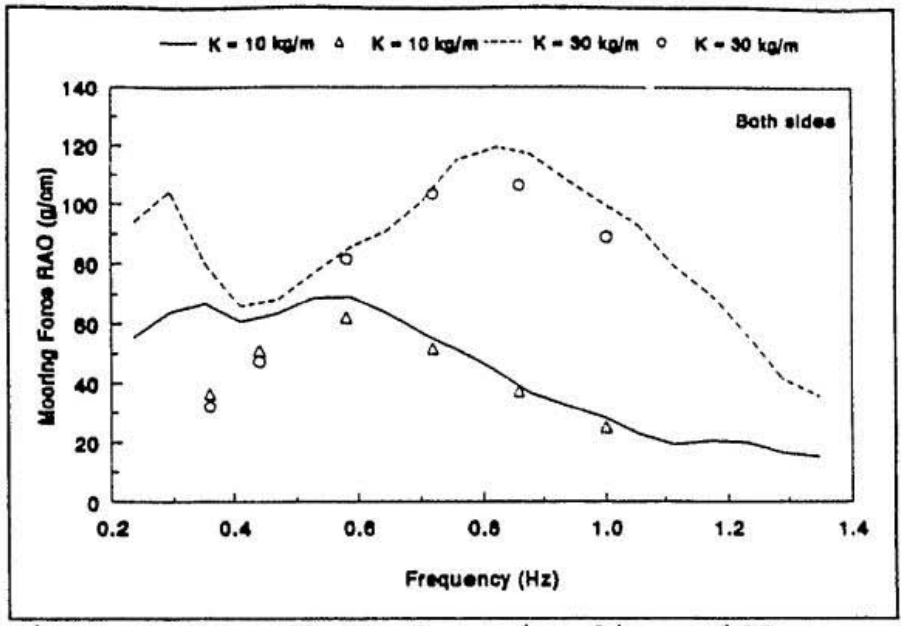

Figure 5.64 - Effect of mooring line stiffness on force responses of both mooring lines: middle position, parallel orientation

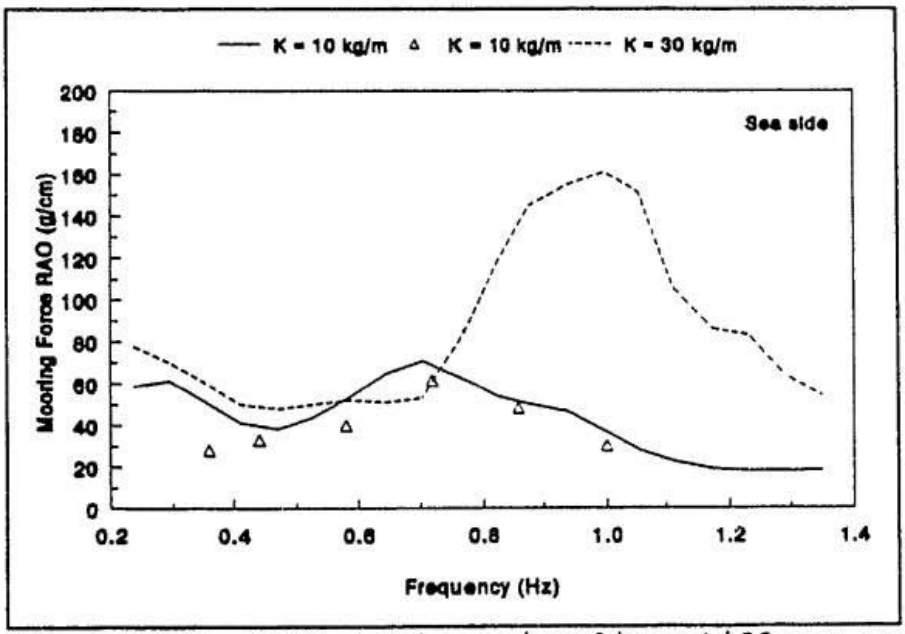

Figure 5.65 - Effect of mooring line stiffness on force response of sea side mooring line: middle position, perpendicular orientation

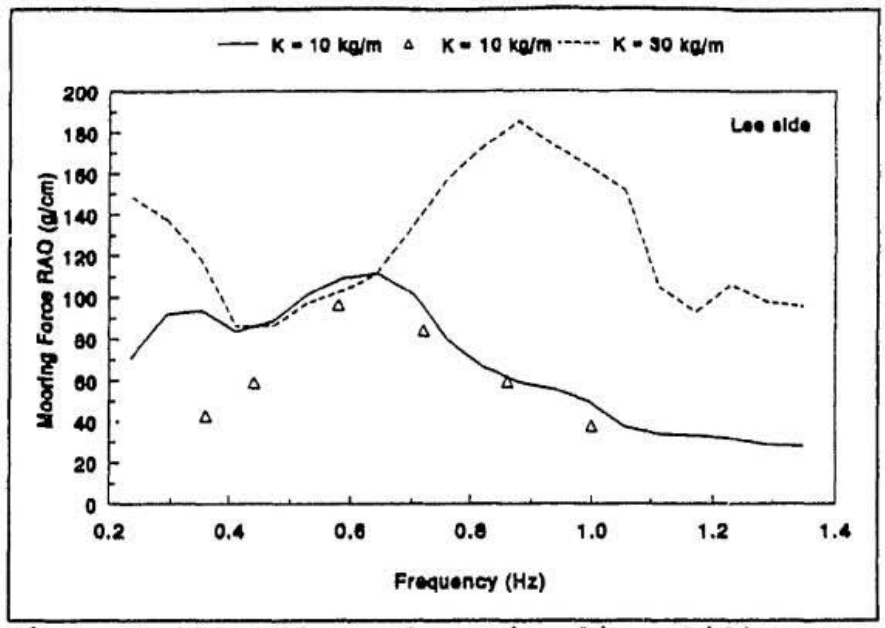

Figure 5.66 - Effect of mooring line stiffness on force response of lee side mooring line: middle position, perpendicular orientation

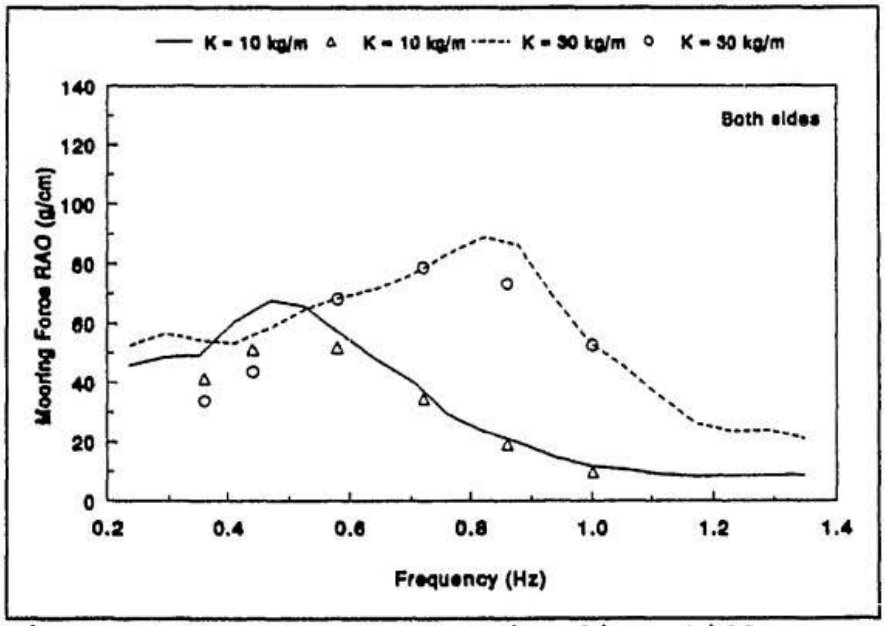

Figure 5.67 - Effect of mooring line stiffness on force responses of both mooring lines: bottom position, parallel orientation

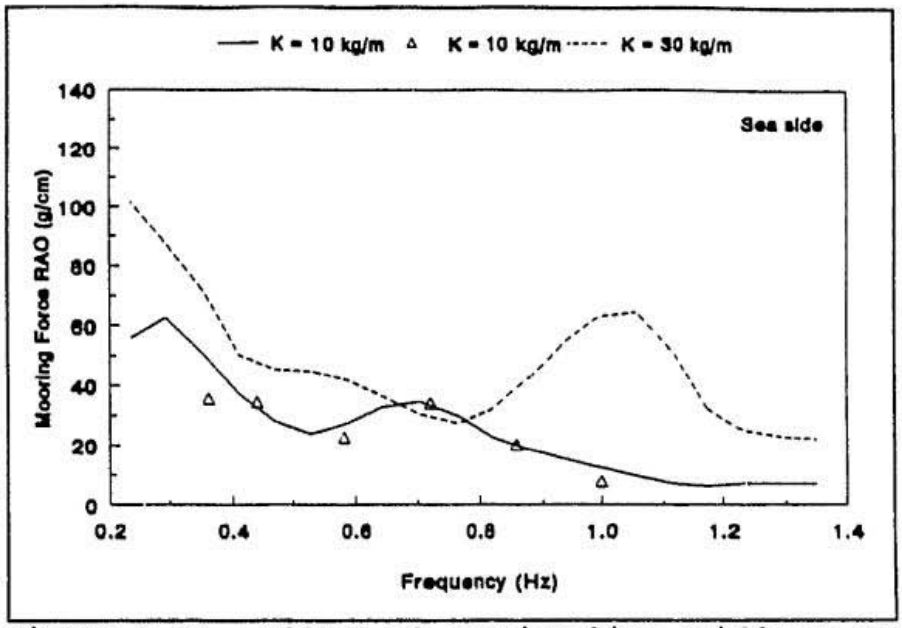

Figure 5.68 - Effect of mooring line stiffness on force response of sea side mooring line: bottom position, perpendicular orientation

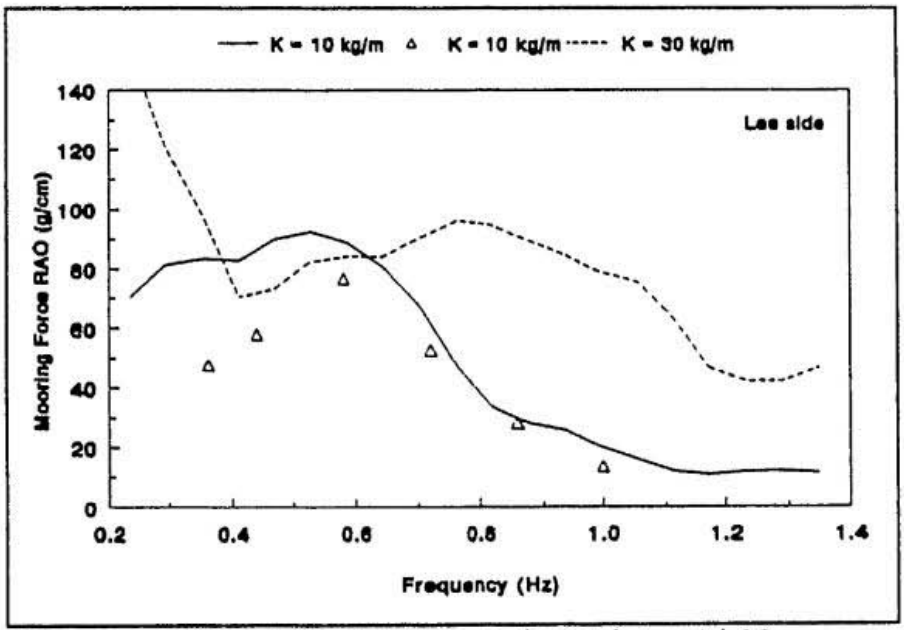

Figure 5.69 - Effect of mooring line stiffness on force response of lee side mooring line: bottom position, perpendicular orientation

frequencies of the responses move to higher frequencies and the amplitudes become larger. In almost the whole frequency range, the force responses with K = 30 kg/m are significantly larger than those with K = 10 kg/m, especially at the high frequencies. Therefore, the stiffness of the mooring lines is an important parameter in the design of the cage mooring system.

5.2.3 Application of the model test results to prototype

Since the effects of gravity tend to dominate waves and wave induced motion of a floating object, scale factors shown in Table 3.3 which are based on the Froude law should be used to upscale the model test results to prototype values (see section 3.3.2 above).

Theoretically, the model test results can only be used to predict the responses of the prototypes whose parameters are similar to those used in the model tests according to the scale factors in Table 3.3. When the model tests were conducted, there was no detailed prototype design. The parameters of the final design may be different from those used in the model tests. Therefore, considerable care and necessary correction should be taken when using the model test results in the prototype design if the parameters of the

prototype are not similar to those used in the model tests, especially if the water depth of the site and the stiffness of the mooring lines are different. According to the test results, a small changes in mass and moment of inertia do not change the responses of the cage significantly.

An effective way of applying the model test results to the prototype design is establishing a numerical model, guided by the observations from the model tests, and then using the data obtained from the model tests to verify and calibrate the numerical model. The numerical model in turn may offer a general tool for a variety of purposes for the prototype design such as predicting the responses of the cage systems which have different dimensions, mass, moment of inertia, net, stiffness of mooring lines, submerged depth and water depth of the sites as well as optimizing the design parameters of the cage system. This method can even overcome the difficulty of reproducing the prototype responses in model tests caused by the conflict of Froude and Reynolds' similarity criteria.

Although the results presented apply only to the particular cage, mooring, net, submerged depth and water depth configurations tested, the observations of the general behaviour of the cage system and the effects of orientation and submerged position of the cage and stiffness and

pretension of the mooring lines on the responses of the cage system should be able to apply to similar cage system designs.

For the prototype cage system, currents and waves occur at the same time. The existence of currents may affect the responses of the cage system to waves, but such influence is not contained in the moored test results presented. Further study is required to determine the influence of currents.

6 CONCLUSIONS

Qualitative analyses have been conducted and resistance tests in three orientations and moored tests in three submerged positions and three orientations have been carried out on two globe-shaped cage models (spherical cage and geodesic cage) to investigate the resistance forces of all the individual components of the cage system in currents and the motion and mooring force responses of the cage system to waves. In the resistance tests and the moored tests, a model net which is scaled down geometrically from the prototype net cannot reproduce the forces acting on the prototype net appropriately. Before the model tests were carried out, a series of tests were conducted to select a model net so that it could reproduce the prototype net properly.

The results of the resistance tests show that in the velocity range tested the relationships between the current velocity and the resulted resistance force for the both model frames, net and float can be interpolated very well with the quadratic equations regressed from the test results. For the both cage models, the resistance forces are minimum when the axles of the cages are parallel to the current direction and are maximum when the axles of the cages are perpendicular to the current direction. The resistance force of the geodesic

frame is about 35 percent larger than that of the spherical frame.

When the test results are used to predict the resistance force of the prototype, scale factors based on Reynolds law should be used and the Reynolds numbers of the prototype should be within the range of Reynolds number tested. In practice the Reynolds numbers of the prototype will be much larger than the Reynolds numbers of the model, so some approximations have to be made. For the prototype frame, the equations regressed from the test results can also be used to extrapolate the resistance force outside the range of Reynolds number tested as long as the Reynolds numbers of the prototype frame elements are still within the range of subcritical flow regime. For the prototype net and floats, the resistance forces can also be estimated with the equations regressed from the test results.

The results of the moored tests show that there are no significant differences between the motion and mooring force responses of the spherical cage and the geodesic cage. For the regular wave tests, the time histories of the dynamic mooring force and motion responses are almost harmonic. In general the motion and mooring force responses obtained from the irregular wave tests agree with those from the regular wave tests very

well, except at the low frequencies where the results from the irregular wave tests tend to be larger than those from the regular wave tests.

In parallel orientation, the major motions of the cage are surge and heave. The mooring forces are mainly caused by the heave motion and the amplitudes of surge are not large enough to cause any significant forces in the mooring lines, and the force responses in the two mooring lines are about the same. In perpendicular orientation, the major motions of the cage are sway, heave and roll. The mooring forces are mainly caused by the combined effect of the heave and roll motions. Because of the phase difference between the heave and roll motions of the cage, the vertical displacement and mooring force on one side of the cage may be significantly larger than those on the other side of the cage if both heave and roll are significant. In the present tests, in the surface position the force responses in the sea side mooring line are a little larger than those in the lee side mooring line; while in the middle and bottom positions, the force responses in the lee side mooring line are significantly larger than those in the sea side mooring line.

The heave responses in perpendicular orientation are significantly smaller than those in parallel orientation and

the sway responses in perpendicular orientation are significantly smaller than the surge responses in parallel orientation. In the surface position, the differences between the mooring force responses in parallel orientation and perpendicular orientation are small. In the middle and bottom positions, the force responses in the lee side mooring line in perpendicular orientation are significantly larger then the force responses in both mooring lines in parallel orientation. In 45° orientation, the responses of mooring force, heave and roll are similar to those in perpendicular orientation. The maximum yaw amplitude is only about 4°, so it seems impossible for the two mooring lines to be tangled up when the cage is oblique to the wave direction.

Both qualitative analysis and test results show that the method of submerging the cage below the water surface to reduce the motions of the cage and the force in the mooring system is very effective in deep water waves, but becomes less and less effective in intermediate water waves. For the mooring forces and heave motion in both orientations and the roll motion in perpendicular orientation, the responses in the middle position tend to be larger at the low frequencies and smaller at the high frequencies than those in the surface position; the differences between the responses in the middle position and bottom position are very small at the low

frequencies, but the responses in the bottom position become significantly smaller than those in the middle position at the high frequencies and the differences increase with the increase of frequency. For the surge motion in parallel orientation and the sway motion in perpendicular orientation, the responses are largest in the surface position and smallest in the bottom position; also, the differences are small at the low frequencies and significant at the high frequencies.

The change of pretension in the mooring lines has little effect on the responses of mooring forces and motions as long as the mooring lines do not go slack. Because the change of the pretension was achieved by reducing the mass of the cage model, it can also be concluded that a small change of mass does not affect the responses of the cage system significantly.

On the other hand, the stiffness of the mooring lines has a significant effect on the responses of mooring forces, heave in parallel orientation and heave and roll in perpendicular orientation, but has little effect on the responses of surge in parallel orientation and sway in perpendicular orientation. With the increase of the spring constant of the mooring lines, the peak frequencies of the response curves move to higher frequencies, the mooring force responses are increased

significantly, and except near the resonant frequencies the heave and roll responses are decreased significantly. Therefore, the stiffness of the mooring lines is an important parameter in the design of prototype cage system.

The moored test results can only be used to predict the responses of the prototypes whose parameters are similar to those used in the model tests according to the scale factors based on the Froude law. If the similarity requirements are not met, considerable care and necessary correction should be taken. However, the observations of the general behaviour of the cage system and the effects of orientation and submerged position of the cage and stiffness and pretension of the mooring lines on the responses of the cage system should be able to apply to similar cage system designs.

7 REFERENCES

- Aarsnes, J.V., Rudi, H. and Loland, G. (1990). "Current Forces on Cage, Net Deflection," in *Engineering for Offshore Fish Farming*, The Institution of Civil Engineers, Thomas Telford, London, pp. 137-152.

- Beveridge, M. (1987). *Cage Aquaculture*, Fishing News Books Ltd, Farnham.

- Chakrabarti, S.K. (1987). *Hydrodynamics of Offshore Structures*, Computational Mechanics Publications, Southampton and Boston.

- Dahle, L.A., Jorgensen, Vangen, K. and Aarsnes, J.V. (1989). "An Underwater Offshore Sea Cage," in *Aquaculture - a Biotechnology in Progress*, eds. N.D. Pauw, E. Jaspers, H. Ackefors and N. Wilkins, European Aquaculture Society, Bredene, Belgium, pp. 1001-1007.

- Dean, R.G. and Dalrymple, R.A. (1984). *Water Wave Mechanics for Engineers and Scientists*, Prentice-Hall, Inc., Englewood Cliffs, New Jersey

- Dean, R.G. and Harleman, D.R.F. (1966). "Interaction of Structures and Waves," in *Estuary and Coastline Hydrodynamics*, ed. A.T. Ippen, McGraw-Hill Book Company, INC., pp. 341-403.

- Gisvold, K.M. (1980). "Model testing of Offshore Structures," in *Underwater Technology, Offshore Petroleum Conf. Proc.*, pp. 395-415.

- Linfoot, B.T. and Hall, M.S. (1986). "Analysis of the Motions of Scale-model Sea-cage System," in IFAC Proc. Ser. No. 9, *Automation and Data Processing in Aquaculture*, ed. J.G. Balchen, Pergamon Press, Oxford, pp. 31-46.

- Linfoot, B.T. and Hall, M.S. (1989). "Model Testing of Single-point Mooring Systems for Sea-cage Flotillas," in *Aquaculture - a Biotechnology in Progress*, eds. N.D. Pauw, E. Jaspers, H. Ackefors and N. Wilkins, European Aquaculture Society, Bredene, Belgium, pp. 1029-1036.

- Norman, S. (1991). "Globe-shaped Cage May Be Good News for Aquaculturalists with Promises to Lessen Mortality,

Stress for Farmed Fish", *The Sunday Express*, St. John's, Newfoundland, Vol. 5, No. 14, 6p.

- OERC. (1990). *Wave/Tow Tank Facility*, Ocean Engineering Research Centre, Faculty of Engineering and Applied Science, Memorial University of Newfoundland, St. John's, Newfoundland.

- Oltedal, G., Lien, E. and Aarsnes, J.V. (1988). "Simulation of Fish Cage Response to Waves and Current," in *Aquaculture Engineering Technologies for the Future*, The Institution of Chemical Engineers, Symposium series No. 111, pp. 123-132.

- Oortmerssen, G.V. (1986). "Numerical Modelling of the Behaviour of Maritime Structures: An Aid for Designers and Operators," in *International Conference CADMO 86*, pp. 509-518.

- Rudi, H., Aarsnes, J.V. and Dahle, L.A. (1988). "Environmental Forces on a Floating Cage System, Mooring Considerations," in *Aquaculture Engineering Technologies for the Future*, The Institution of Chemical Engineers, Symposium series No. 111, pp. 97-122.

- Sarpkaya, T. and Isaacson, M. (1981). *Mechanics of Wave Force on Offshore Structures*, Van Nostrand Reinhold Company, New York.

- Sharp, J.J. (1981). *Hydraulic Modelling*, Butterworths, London.

- White, F.M. (1986). *Fluid Mechanics*, Second Edition, McGraw-Hill Book Company, New York.

- Whittaker, T.J.T., Bell, A.K. and Shaw, M.R. (1990). "Model Testing of a Cage System for the Offshore Environment," in *Engineering for Offshore Fish Farming*, The Institution of Civil Engineers, Thoms Telford, London, pp. 79-92.

- Wilson, W. (1969). "Elastic Characteristics of Moorings," in *Topics in Ocean Engineering*, ed. C.I. Bretscheider, Gulf Publishing Company, Houston, Texas, pp 45-81.

- WT. (1990). "S575 Data Acquisition Program and PLTKLY PC Plotting Program Commands," Wave Tank, Ocean Engineering Research Centre, Faculty of Engineering and Applied Science, Memorial University of Newfoundland, St. John's, Newfoundland.

APPENDIX A

RESISTANCE FORCES OF THE MODELS

Table A.1 - Spherical Frame with Net: 90°

Velocity (m/s)	Force (N)	Least Square Fit	$C_r = F/V^2$
0.2	3.574	3.633	89.35
0.4	14.211	14.533	88.82
0.6	33.121	32.700	92.00
0.8	55.130	58.135	86.14
1.0	86.112	90.840	86.11
1.2	128.162	130.804	89.00
1.4	178.076	178.038	90.86
1.6	236.556	232.540	92.40
Regressed Constant k = 90.84			

Table A.2 - Spherical Frame with Net: 45°

Velocity (m/s)	Force (N)	Least Square Fit	$C_r = F/V^2$
0.2	5.256	4.053	131.40
0.4	16.990	16.214	106.19
0.6	36.168	36.481	100.47
0.8	63.972	64.855	99.96
1.0	96.229	101.337	96.23
1.2	141.795	145.925	98.47
1.4	202.167	198.620	103.15
1.6	261.221	259.421	102.04
Regressed Constant k = 101.34			

Table A.3 - Spherical Frame with Net: 0°

Velocity (m/s)	Force (N)	Least Square Fit	$C_r = F/V^2$
0.2	5.236	4.722	130.90
0.4	19.312	18.888	120.70
0.6	42.797	42.498	118.88
0.8	77.374	75.552	120.90
1.0	111.748	118.051	111.75
1.2	169.025	169.994	117.38
1.4	230.348	231.380	117.52
1.6	305.477	302.211	119.33
Regressed Constant k = 118.05			

Table A.4 - Spherical Frame without Net: 90°

Velocity (m/s)	Force (N)	Least Square Fit	$C_r = F/V^2$
0.2	2.303	1.888	57.58
0.4	7.484	7.551	46.78
0.6	16.865	16.990	46.84
0.8	30.663	30.203	47.91
1.0	46.984	47.193	46.98
1.2	64.293	67.958	44.65
1.4	92.398	92.499	47.14
1.6	122.936	120.815	48.02
Regressed Constant k = 47.19			

Table A.5 - Spherical Frame without Net: 45°

Velocity (m/s)	Force (N)	Lest Square Fit	$C_r = F/V^2$
0.2	2.107	2.104	52.68
0.4	8.224	8.417	51.40
0.6	19.012	18.938	52.81
0.8	30.135	33.667	47.09
1.0	46.913	52.605	46.91
1.2	70.189	75.751	48.74
1.4	105.977	103.106	54.07
1.6	138.708	134.669	54.18
Regressed Constant k = 52.61			

Table A.6 - Spherical Frame without Net: 0°

Velocity (m/s)	Force (N)	Least Square Fit	$C_r = F/V^2$
0.2	2.242	2.650	56.05
0.4	9.370	10.601	58.56
0.6	20.351	23.852	56.53
0.8	41.155	42.403	64.30
1.0	60.093	66.256	60.09
1.2	97.527	95.408	67.73
1.4	133.322	129.861	66.49
1.6	171.365	169.615	66.94
Regressed Constant k = 66.26			

Table A.7 - Net on Spherical Frame: 90°

Velocity (m/s)	Force (N)	Least Square Fit	$C_r = F/V^2$
0.2	1.271	1.743	31.78
0.4	6.727	6.975	42.04
0.6	14.256	15.693	39.60
0.8	24.467	27.898	38.23
1.0	39.128	43.591	39.13
1.2	63.869	62.772	44.35
1.4	85.678	85.439	43.71
1.6	113.620	111.594	44.38
Regressed Constant k = 43.59			

Table A.8 - Net on Spherical Frame: 45°

Velocity (m/s)	Force (N)	Least Square Fit	$C_r = F/V^2$
0.2	3.014	1.947	75.35
0.4	7.620	7.789	47.63
0.6	15.817	17.526	43.94
0.8	33.807	31.157	52.87
1.0	49.316	48.684	49.32
1.2	71.606	70.104	49.73
1.4	96.190	95.420	49.08
1.6	122.513	124.630	47.86
Regressed Constant k = 48.68			

Table A.9 - Net on Spherical Frame: 0°

Velocity (m/s)	Force (N)	Least Square Fit	$C_r = F/V^2$
0.2	2.294	2.072	57.35
0.4	9.942	8.287	62.14
0.6	22.446	18.646	62.35
0.8	36.219	33.148	56.59
1.0	51.655	51.794	51.66
1.2	71.498	74.583	49.65
1.4	100.026	101.515	51.03
1.6	134.112	132.592	52.39
Regressed Constant k = 51.79			

Table A.10 - Geodesic Frame with Net: 90°

Velocity (m/s)	Force (N)	Least Square Fit	$C_r = F/V^2$
0.2	3.946	3.899	98.65
0.4	15.349	15.596	95.93
0.6	34.139	35.090	94.83
0.8	60.183	62.382	94.04
1.0	95.543	97.472	95.54
1.2	140.472	140.360	97.55
1.4	189.776	191.046	96.82
1.6	251.891	249.529	98.39
Regressed Constant k = 97.47			

Table A.11 - Geodesic Frame with Net: 45°

Velocity (m/s)	Force (N)	Least Square Fit	$C_r = F/V^2$
0.2	4.992	4.475	124.80
0.4	17.534	17.900	109.59
0.6	38.063	40.274	105.73
0.8	67.121	71.599	104.88
1.0	105.453	111.873	105.45
1.2	158.770	161.098	110.26
1.4	223.310	219.272	113.93
1.6	288.567	286.396	112.72
Regressed Constant k = 111.87			

Table A.12 - Geodesic Frame with net: 0°

Velocity (m/s)	Force (N)	Least Square Fit	$C_r = F/V^2$
0.2	5.721	4.839	143.03
0.4	20.030	19.354	125.19
0.6	44.373	43.547	123.26
0.8	81.819	77.418	127.84
1.0	118.638	120.965	118.64
1.2	173.908	174.190	120.77
1.4	239.887	237.092	122.39
1.6	307.326	309.671	120.05
Regressed Constant k = 120.97			

Table A.13 - Geodesic Frame without Net: 90°

Velocity (m/s)	Force (N)	Least Square Fit	$C_r = F/V^2$
0.2	3.243	2.329	81.08
0.4	9.713	9.317	60.71
0.6	21.441	20.963	59.56
0.8	38.437	37.267	60.06
1.0	58.017	58.229	58.02
1.2	81.581	83.850	56.65
1.4	113.326	114.130	57.82
1.6	150.643	149.067	58.84
Regressed Constant k = 58.23			

Table A.14 - Geodesic Frame without Net: 45°

Velocity (m/s)	Force (N)	Least Square Fit	$C_r = F/V^2$
0.2	2.852	2.635	71.30
0.4	10.520	10.540	65.75
0.6	23.264	23.715	64.62
0.8	38.059	42.159	59.47
1.0	58.106	65.874	58.11
1.2	89.678	94.858	62.28
1.4	132.128	129.112	67.41
1.6	173.362	168.637	67.72
Regressed Constant k = 65.87			

Table A.15 - Geodesic Frame without Net: 0°

Velocity (m/s)	Force (N)	Least Square Fit	$C_r = F/V^2$
0.2	3.981	3.070	99.52
0.4	12.942	12.280	80.89
0.6	28.142	27.631	78.17
0.8	47.863	49.121	74.79
1.0	74.201	76.752	74.20
1.2	110.023	110.523	76.40
1.4	151.340	150.434	77.21
1.6	197.257	196.486	77.05
Regressed Constant k = 76.75			

Table A.16 - Net on Geodesic Frame: 90°

Velocity (m/s)	Force (N)	Least Square Fit	$C_r = F/V^2$
0.2	0.703	1.580	17.58
0.4	5.636	6.319	38.23
0.6	12.692	14.218	35.26
0.8	21.746	25.276	33.98
1.0	37.526	39.494	37.53
1.2	58.621	56.872	40.71
1.4	78.449	77.409	40.03
1.6	101.248	101.106	39.55
Regressed Constant k = 39.49			

Table A.17 - Net on Geodesic Frame: 45°

Velocity (m/s)	Force (N)	Least Square Fit	$C_r = F/V^2$
0.2	2.140	1.840	53.50
0.4	7.014	7.360	43.84
0.6	14.799	16.560	41.11
0.8	29.062	29.440	45.41
1.0	47.347	46.000	47.35
1.2	69.092	66.240	47.98
1.4	91.182	90.160	46.52
1.6	115.205	117.759	45.00
Regressed Constant k = 46.00			

Table A.18 - Net on Geodesic Frame: 0°

Velocity (m/s)	Force (N)	Least Square Fit	$C_r = F/V^2$
0.2	1.740	1.758	43.50
0.4	7.088	7.033	44.30
0.6	16.231	15.824	45.09
0.8	33.956	28.132	53.06
1.0	44.467	43.960	44.47
1.2	63.885	63.298	44.36
1.4	86.696	86.155	44.23
1.6	110.069	112.529	43.00
Regressed Constant k = 43.96			

Table A.19 - Net on Model Holding Frame: 90°

Velocity (m/s)	Force (N)	Least Square Fit	$C_r = F/V^2$
0.2	0.570	0.211	14.25
0.4	1.252	0.842	7.20
0.6	2.092	1.895	5.81
0.8	2.279	3.368	3.56
1.0	2.283	5.263	2.86
1.2	5.274	7.579	3.66
1.4	9.013	10.315	4.60
1.6	16.924	13.473	6.61
Regressed Constant k = 5.26			

Table A.20 - Net on Model Holding Frame: 45°

Velocity (m/s)	Force (N)	Least Square Fit	$C_r = F/V^2$
0.2	0.912	1.180	22.80
0.4	4.419	4.720	27.62
0.6	10.104	10.619	28.07
0.8	15.846	18.879	24.76
1.0	28.978	29.498	28.98
1.2	38.183	42.477	26.52
1.4	58.352	57.816	29.77
1.6	78.247	75.515	30.69
Regressed Constant k = 29.50			

Table A.21 - Net on Model Holding Frame: 0°

Velocity (m/s)	Force (N)	Least Square Fit	$C_f = F/V^2$
0.2	1.753	1.633	43.83
0.4	6.828	6.532	42.68
0.6	15.312	14.697	42.53
0.8	25.930	26.127	40.52
1.0	40.902	40.824	40.90
1.2	59.066	58.787	41.02
1.4	80.528	80.015	41.09
1.6	103.872	104.510	40.58
Regressed Constant k = 40.82			

Table A.22 - Float: 90°

Velocity (m/s)	Force (N)	Least Square Fit	$C_f = F/V^2$
0.2	0.531	0.132	13.28
0.4	1.104	0.526	6.90
0.6	1.455	1.184	4.04
0.8	1.206	2.105	1.88
1.0	0.851	3.288	0.85
1.2	2.915	4.735	2.02
1.4	8.997	6.445	4.59
1.6	8.584	8.418	3.35
Regressed Constant k = 3.29			

Table A.23 - Float: 45°

Velocity (m/s)	Force (N)	Least Square Fit	$C_r = F/V^2$
0.2	0.486	0.695	12.15
0.4	2.670	2.781	16.69
0.6	5.794	6.257	16.09
0.8	11.483	11.124	17.94
1.0	15.167	17.381	15.17
1.2	20.679	25.029	14.36
1.4	34.950	34.068	17.83
1.6	47.119	44.497	18.41
Regressed Constant k = 17.38			

Table A.24 - Float: 0°

Velocity (m/s)	Force (N)	Least Square Fit	$C_r = F/V^2$
0.2	0.902	1.064	22.55
0.4	3.563	4.256	22.27
0.6	9.384	9.575	26.07
0.8	15.608	17.023	24.39
1.0	23.850	26.598	23.85
1.2	42.848	38.301	29.76
1.4	51.218	52.132	26.13
1.6	67.734	68.091	26.46
Regressed Constant k = 26.60			

APPENDIX B

MEASURED RESULTS OF THE RESISTANCE TESTS

Table B.1 - Empty Model Holding Frame: 90°

Velocity (m/s)	Force (N)	Least Square Fit	$C_r = F/V^2$
0.2	1.335	1.382	33.37
0.4	5.335	5.530	33.34
0.6	12.163	12.442	33.79
0.8	22.467	22.120	35.10
1.0	35.517	34.562	35.52
1.2	52.537	49.770	36.48
1.4	68.905	67.742	35.16
1.6	85.626	88.480	33.45
Regressed Constant k = 34.56			

Table B.2 - Empty Model Holding Frame: 45°

Velocity (m/s)	Force (N)	Least Square Fit	$C_r = F/V^2$
0.2	2.270	2.014	56.74
0.4	8.221	8.058	51.38
0.6	18.416	18.130	51.16
0.8	35.519	32.230	55.50
1.0	57.293	50.360	57.29
1.2	77.946	72.518	54.13
1.4	96.781	98.706	49.38
1.6	123.757	128.922	48.34
Regressed Constant k = 50.36			

Table B.3 - Empty Model Holding Frame: 0°

Velocity (m/s)	Force (N)	Least Square Fit	$C_r = F/V^2$
0.2	2.630	2.014	65.76
0.4	10.479	10.060	65.49
0.6	23.059	22.634	64.05
0.8	41.021	40.238	64.10
1.0	64.599	62.872	64.60
1.2	91.240	90.536	63.36
1.4	122.838	123.230	62.67
1.6	159.899	160.953	62.46
Regressed Constant k = 62.87			

Table B.4 - Model Holding Frame and Net: 90°

Velocity (m/s)	Force (N)	Least Square Fit	$C_r = F/V^2$
0.2	1.905	1.593	47.63
0.4	6.486	6.372	40.54
0.6	14.255	14.337	39.60
0.8	24.746	25.488	38.67
1.0	38.380	39.825	38.38
1.2	57.811	57.349	40.15
1.4	77.918	78.058	39.75
1.6	102.550	101.953	40.06
Regressed Constant k = 39.83			

Table B.5 - Model Holding and Net: 45°

Velocity (m/s)	Force (N)	Lest Square Fit	$C_r = F/V^2$
0.2	3.182	3.205	79.55
0.4	12.640	12.820	79.00
0.6	28.520	28.845	79.22
0.8	51.365	51.279	80.26
1.0	86.271	80.124	86.27
1.2	116.129	115.379	80.65
1.4	157.039	157.043	80.12
1.6	202.334	205.118	79.04
Regressed Constant k = 80.12			

Table B.6 - Model Holding Frame and Net: 0°

Velocity (m/s)	Force (N)	Least Square Fit	$C_r = F/V^2$
0.2	4.383	4.148	109.56
0.4	17.307	16.591	108.17
0.6	38.371	37.331	106.59
0.8	66.951	66.366	104.61
1.0	105.501	103.696	105.50
1.2	150.306	149.323	104.38
1.4	203.366	203,245	103.76
1.6	263.771	265.462	103.04
Regressed Constant k = 103.70			

Table B.7 - Model Holding Frame and Spherical Frame without Net: 90°

Velocity (m/s)	Force (N)	Least Square Fit	$C_r = F/V^2$
0.2	3.638	3.270	90.94
0.4	12.818	13.081	80.12
0.6	29.028	29.432	80.63
0.8	53.130	52.324	83.02
1.0	82.501	81.756	82.50
1.2	116.830	117.728	81.13
1.4	161.830	160.241	82.30
1.6	208.562	209.295	81.47
Regressed Constant k = 81.76			

Table B.8 - Model Holding Frame and Spherical Frame without Net: 45°

Velocity (m/s)	Force (N)	Least Square Fit	$C_r = F/V^2$
0.2	4.377	4.119	109.42
0.4	16.445	16.474	102.78
0.6	37.428	37.067	103.97
0.8	65.654	65.898	102.58
1.0	104.206	102.965	104.21
1.2	148.135	148.270	102.87
1.4	202.758	201.811	103.45
1.6	262.465	263.591	102.53
Regressed Constant k = 102.97			

Table B.9 - Model Holding Frame and Spherical Frame without Net: 0°

Velocity (m/s)	Force (N)	Least Square Fit	$C_r = F/V^2$
0.2	4.872	5.165	121.79
0.4	19.849	20.660	124.06
0.6	43.410	46.486	120.58
0.8	82.176	82.642	128.40
1.0	124.692	129.128	124.69
1.2	188.767	185.944	131.09
1.4	253.160	253.090	129.16
1.6	331.264	330.567	129.40
Regressed Constant k = 129.13			

Table B.10 - Model Holding Frame and Spherical Frame with Net: 90°

Velocity (m/s)	Force (N)	Least Square Fit	$C_r = F/V^2$
0.2	4.909	5.014	122.72
0.4	19.545	20.056	122.16
0.6	43.284	45.125	120.23
0.8	77.597	80.222	121.25
1.0	121.629	125.347	121.63
1.2	180.699	180.500	125.49
1.4	246.981	245.680	126.01
1.6	322.182	320.889	125.85
Regressed Constant k = 125.35			

Table B.11 - Model Holding Frame and Spherical Frame with Net: 45°

Velocity (m/s)	Force (N)	Least Square Fit	$C_r = F/V^2$
0.2	7.526	6.068	188.16
0.4	25.211	24.271	157.57
0.6	54.584	54.610	151.62
0.8	99.491	97.086	155.45
1.0	153.522	151.696	153.52
1.2	219.741	218.443	152.60
1.4	298.948	297.325	152.52
1.6	388.342	388.343	150.38
Regressed Constant k = 151.70			

Table B.12 - Model Holding Frame and Spherical Frame with Net: 0°

Velocity (m/s)	Force (N)	Least Square Fit	$C_r = F/V^2$
0.2	7.866	7.237	196.66
0.4	29.791	28.948	186.19
0.6	65.856	65.132	182.93
0.8	118.395	115.791	184.99
1.0	176.347	180.923	176.35
1.2	260.265	260.530	180.74
1.4	353.186	354.610	180.20
1.6	465.376	463.164	181.79
Regressed Constant k = 180.92			

Table B.13 - Model Holding Frame and Geodesic Frame without Net: 90°

Velocity (m/s)	Force (N)	Least Square Fit	$C_r = F/V^2$
0.2	4.578	3.702	114.44
0.4	15.047	14.806	94.04
0.6	33.604	33.315	93.35
0.8	60.904	59.226	95.16
1.0	93.534	92.540	93.53
1.2	134.388	133.258	93.33
1.4	180.231	181.379	91.95
1.6	236.269	236.903	92.29
Regressed Constant k = 92.54			

Table B.14 - Model Holding Frame and Geodesic Frame without Net: 45°

Velocity (m/s)	Force (N)	Least Square Fit	$C_r = F/V^2$
0.2	5.122	4.649	128.06
0.4	18.740	18.597	117.13
0.6	41.680	41.844	115.78
0.8	73.578	74.390	114.97
1.0	115.399	116.234	115.40
1.2	167.624	167.377	116.41
1.4	228.909	227.818	116.79
1.6	297.119	297.558	116.06
Regressed Constant k = 116.23			

Table B.15 - Model Holding and Geodesic Frame without Net: 0°

Velocity (m/s)	Force (N)	Least Square Fit	$C_r = F/V^2$
0.2	6.611	5.585	165.28
0.4	23.421	22.340	146.38
0.6	51.201	50.265	142.23
0.8	88.884	89.360	138.88
1.0	138.800	139.624	138.80
1.2	201.263	201.059	139.77
1.4	274.178	273.664	139.89
1.6	357.156	357.438	139.51
Regressed Constant k = 139.62			

Table B.16 - Model Holding Frame and Geodesic Frame with Net: 90°

Velocity (m/s)	Force (N)	Least Square Fit	$C_r = F/V^2$
0.2	5.281	5.281	132.03
0.4	20.683	21.126	129.27
0.6	46.301	47.532	128.61
0.8	82.650	84.502	129.14
1.0	131.060	132.034	131.06
1.2	193.009	190.130	134.03
1.4	258.680	258.788	131.98
1.6	337.517	338.009	131.84
Regressed Constant k = 132.03			

Table B.17 - Model Holding Frame and Geodesic Frame with Net: 45°

Velocity (m/s)	Force (N)	Least Square Fit	$C_r = F/V^2$
0.2	7.262	6.489	181.55
0.4	25.755	25.957	160.97
0.6	56.479	58.404	156.89
0.8	102.640	103.829	160.38
1.0	162.745	162.233	162.75
1.2	236.716	233.616	164.39
1.4	320.091	317.977	163.31
1.6	412.324	415.317	161.06
Regressed Constant k = 162.23			

Table B.18 - Model Holding Frame and Geodesic Frame with Net: 0°

Velocity (m/s)	Force (N)	Least Square Fit	$C_r = F/V^2$
0.2	8.351	7.343	208.76
0.4	30.509	29.373	190.68
0.6	67.432	66.089	187.31
0.8	122.840	117.492	191.94
1.0	183.267	183.581	183.27
1.2	265.148	264.357	184.13
1.4	360.874	359.819	184.12
1.6	467.225	469.968	182.51
Regressed Constant k = 183.58			

Table B.19 - Model Holding Frame and Float: 90°

Velocity (m/s)	Force (N)	Least Square Fit	$C_r = F/V^2$
0.2	1.866	1.514	46.65
0.4	6.438	6.056	40.24
0.6	13.618	13.626	37.83
0.8	23.673	24.224	36.99
1.0	36.368	37.851	36.37
1.2	55.452	54.505	38.51
1.4	77.902	74.188	39.75
1.6	94.210	96.898	36.80
Regressed Constant k = 37.85			

Table B.20 - Model Holding Frame and Float: 45°

Velocity (m/s)	Force (N)	Least Square Fit	$C_r = F/V^2$
0.2	2.756	2.710	68.89
0.4	10.891	10.839	68.07
0.6	24.210	24.387	67.25
0.8	47.002	43.354	73.44
1.0	72.460	67.741	72.46
1.2	98.625	97.548	68.49
1.4	131.731	132.773	67.21
1.6	170.876	173.418	66.75
Regressed Constant k = 67.74			

Table B.21 - Model Holding Frame and Float: 0°

Velocity (m/s)	Force (N)	Least Square Fit	$C_r = F/V^2$
0.2	3.532	3.555	88.30
0.4	14.042	14.219	87.77
0.6	32.443	31.992	90.12
0.8	56.629	56.875	88.48
1.0	88.449	88.867	88.45
1.2	128.208	127.969	89.03
1.4	174.056	174.180	88.80
1.6	227.633	227.500	88.92
Regressed Constant k = 88.87			

APPENDIX C

MOTION AND MOORING FORCE RESPONSES OF THE SPHERICAL CAGE MODEL

C.1 Surface Position, Perpendicular Orientation

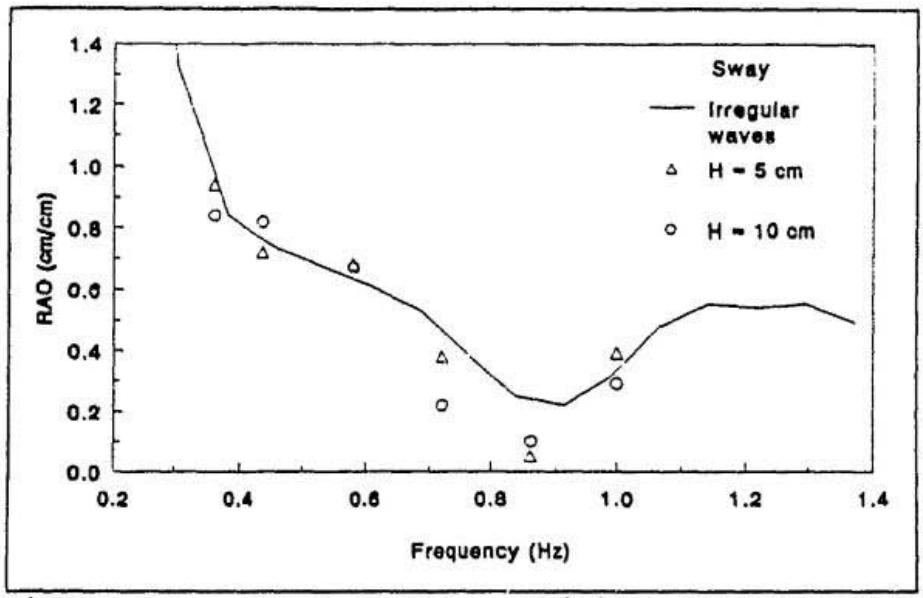

Figure C.1 - Sway: surface position, perpendicular orientation

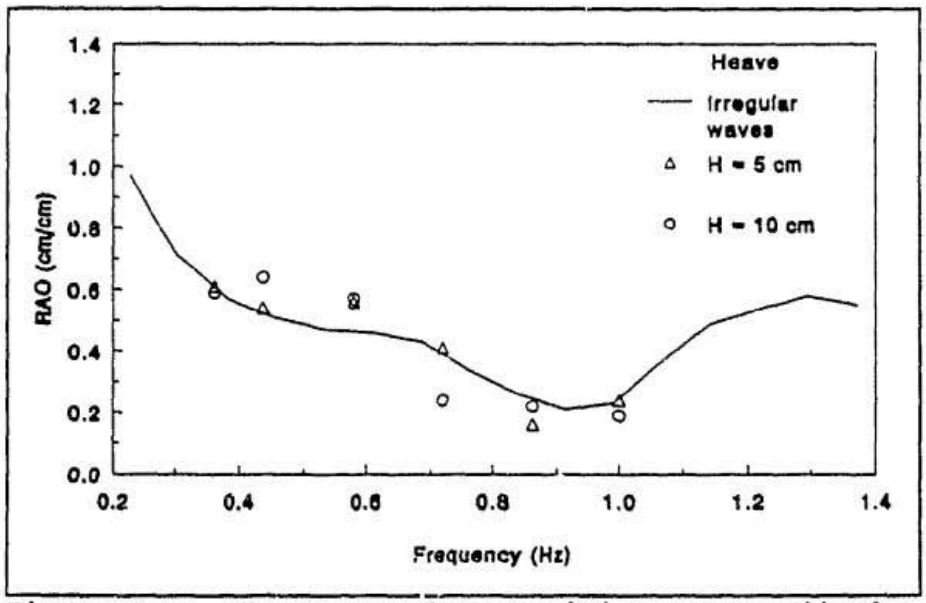

Figure C.2 - Heave: surface position, perpendicular orientation

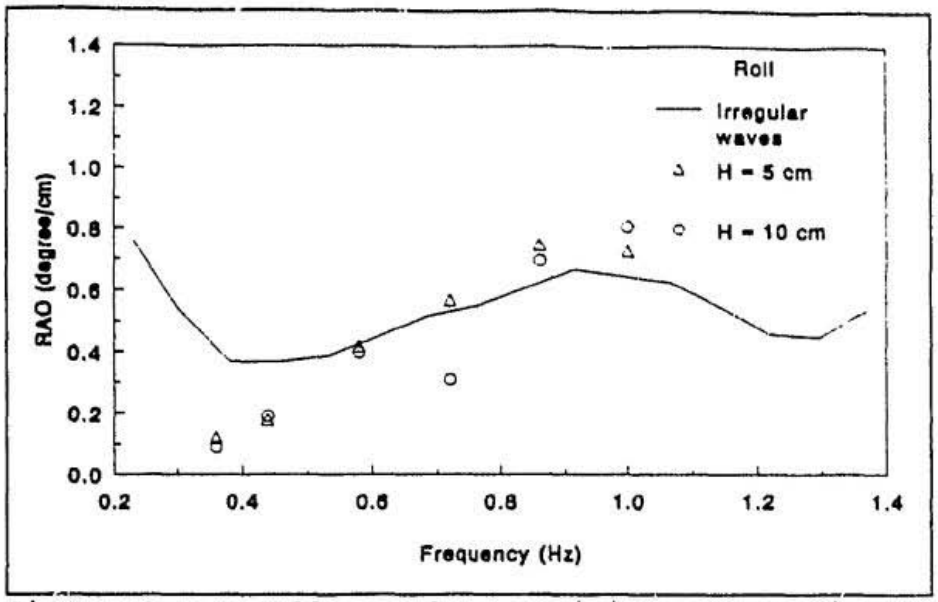

Figure C.3 - Roll: surface position, perpendicular orientation

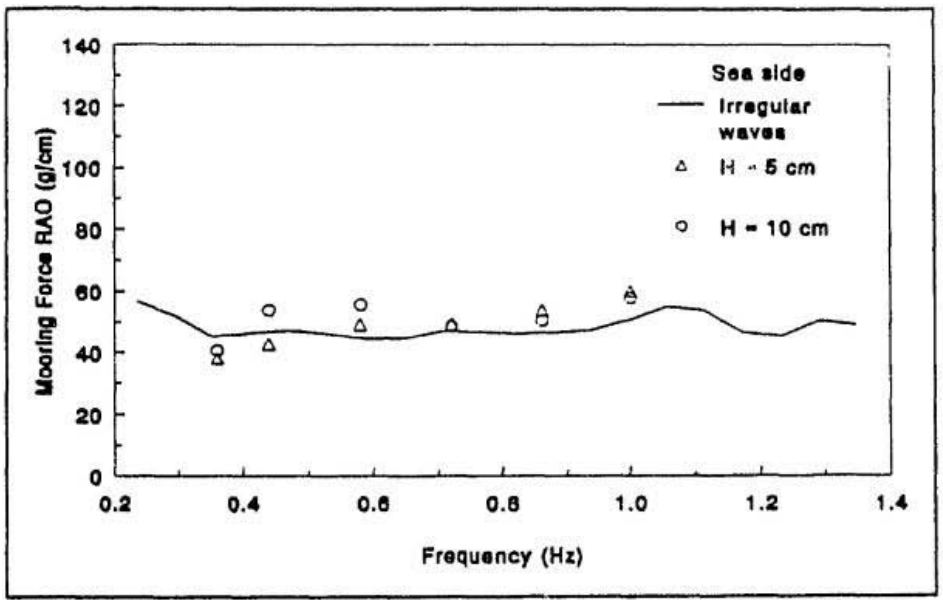

Figure C.4 - Sea side mooring line: surface position, perpendicular orientation

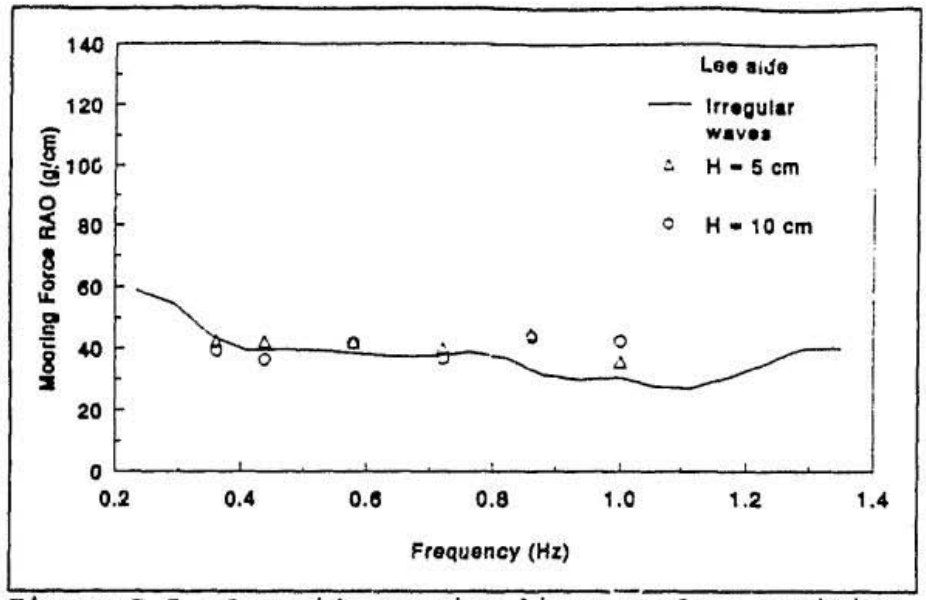

Figure C.5 - Lee side mooring line: surface position, perpendicular orientation

C.2 Middle Position, Perpendicular Orientation

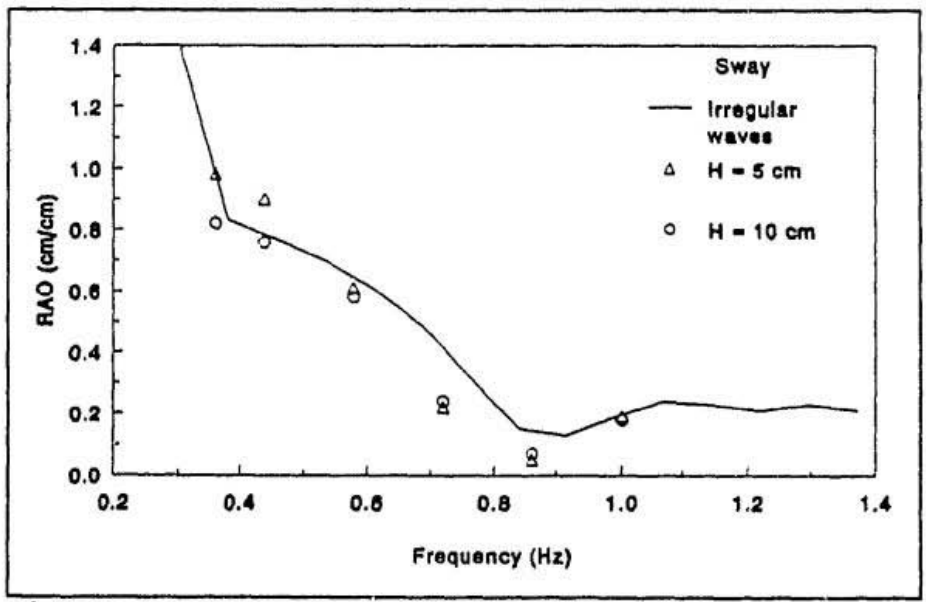

Figure C.6 - Sway: middle position, perpendicular orientation

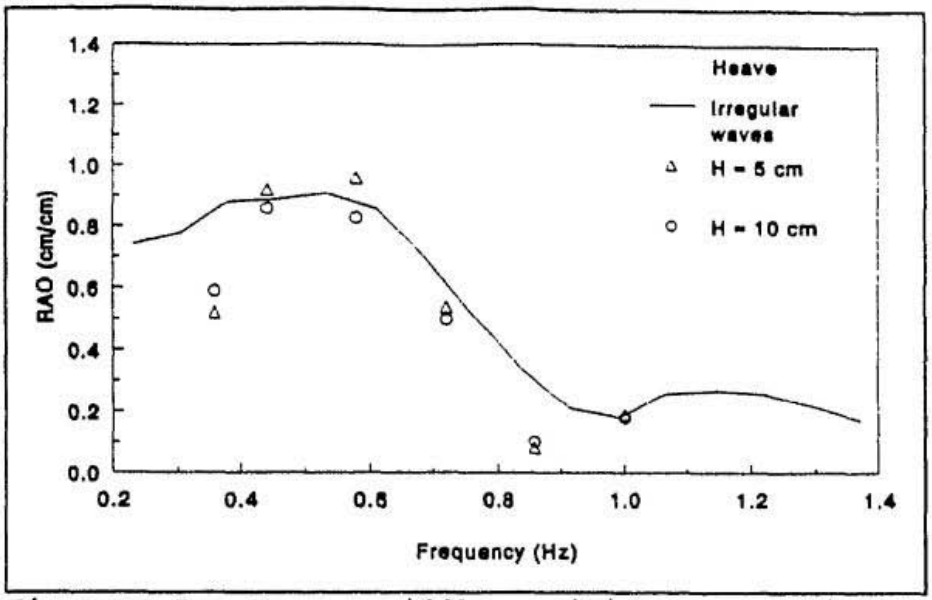

Figure C.7 - Heave: middle position, perpendicular orientation

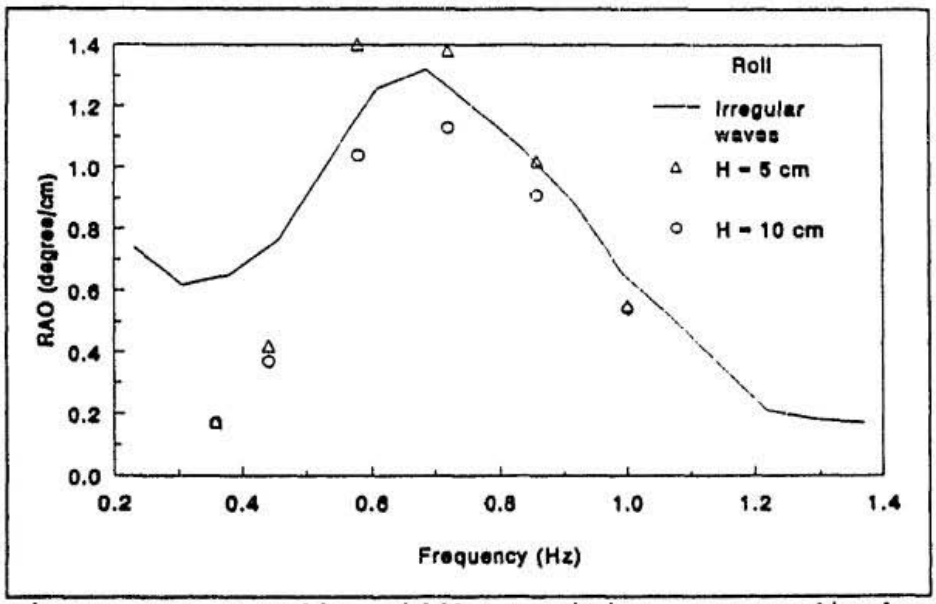

Figure C.8 - Roll: middle position, perpendicular orientation

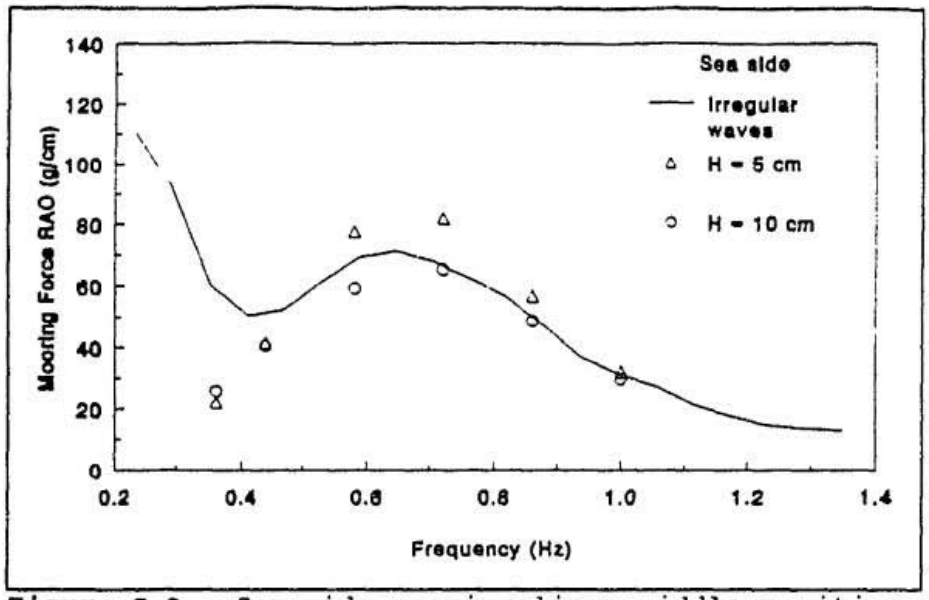

Figure C.9 - Sea side mooring line: middle position, perpendicular orientation

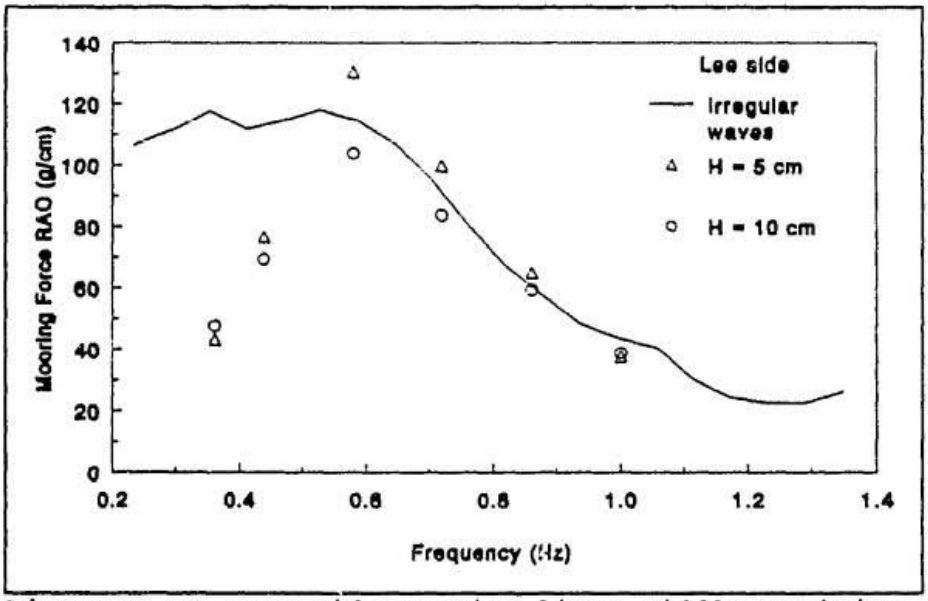

Figure C.10 - Lee side mooring line: middle position, perpendicular orientation

C.3 Bottom Position, Perpendicular Orientation

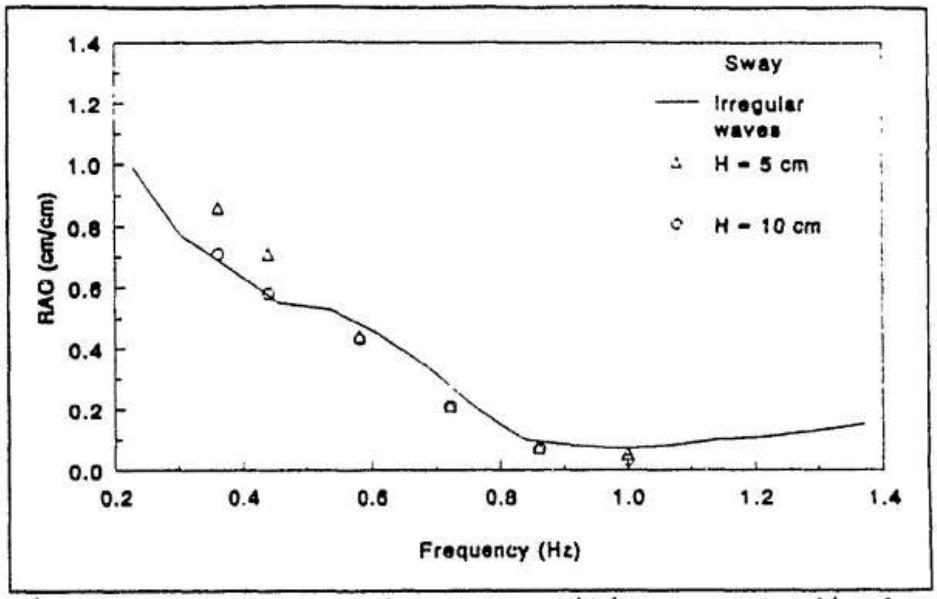

Figure C.11 - Sway: bottom position, perpendicular orientation

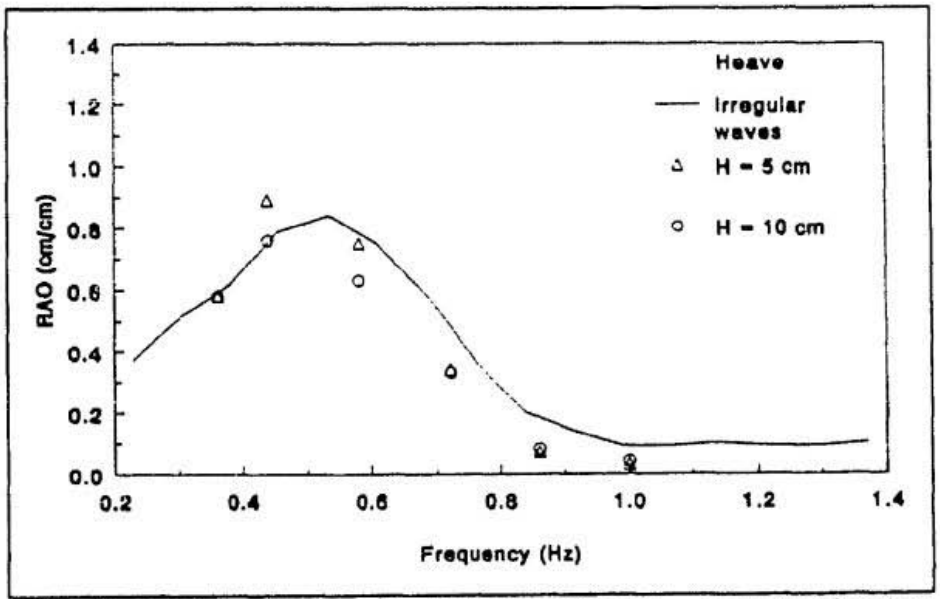

Figure C.12 - Heave: bottom position, perpendicular orientation

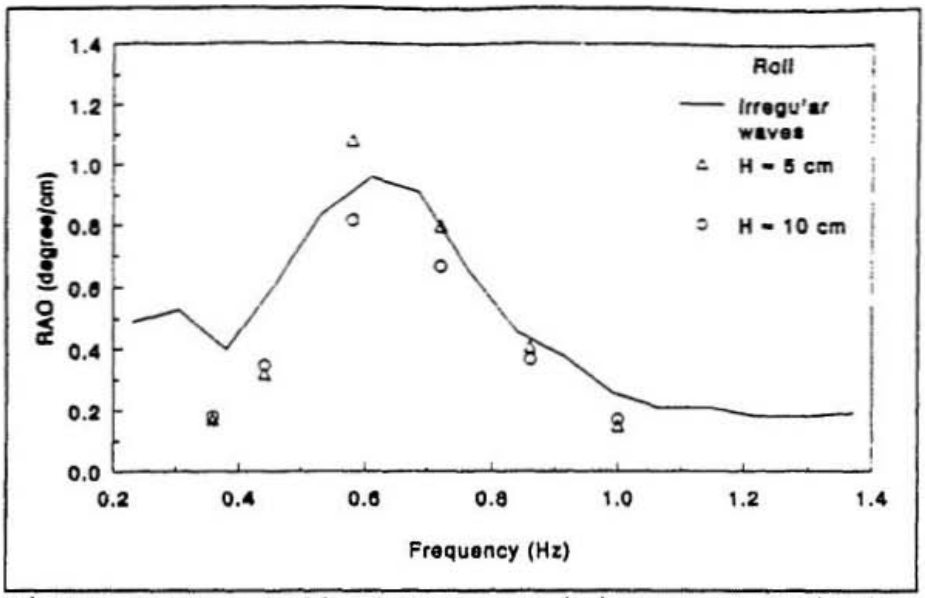

Figure C.13 - Roll: bottom position, perpendicular orientation

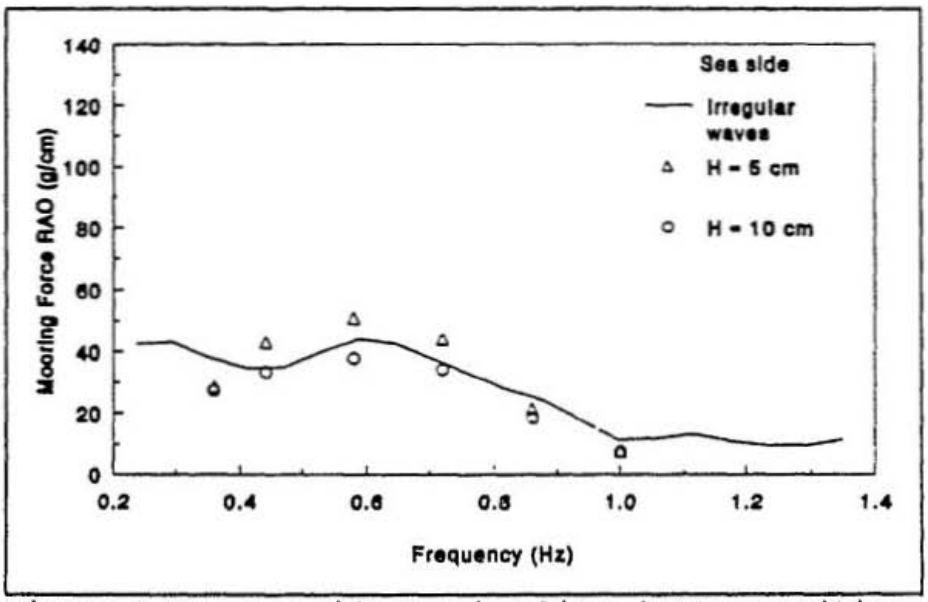

Figure C.14 - Sea side mooring line: bottom position, perpendicular orientation

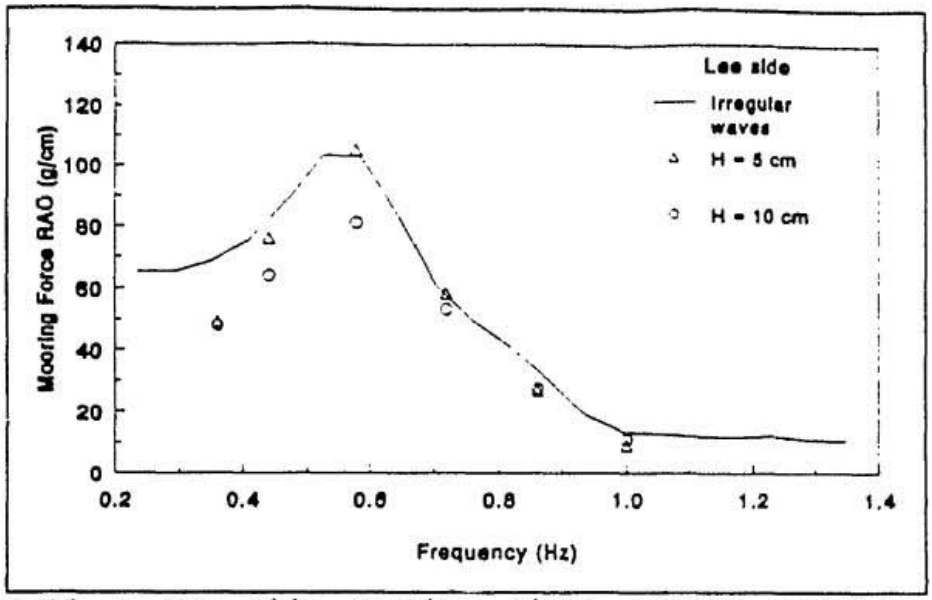

C.15 - Lee side mooring line: bottom position, perpendicular orientation

C.4 Surface Position, Parallel Orientation

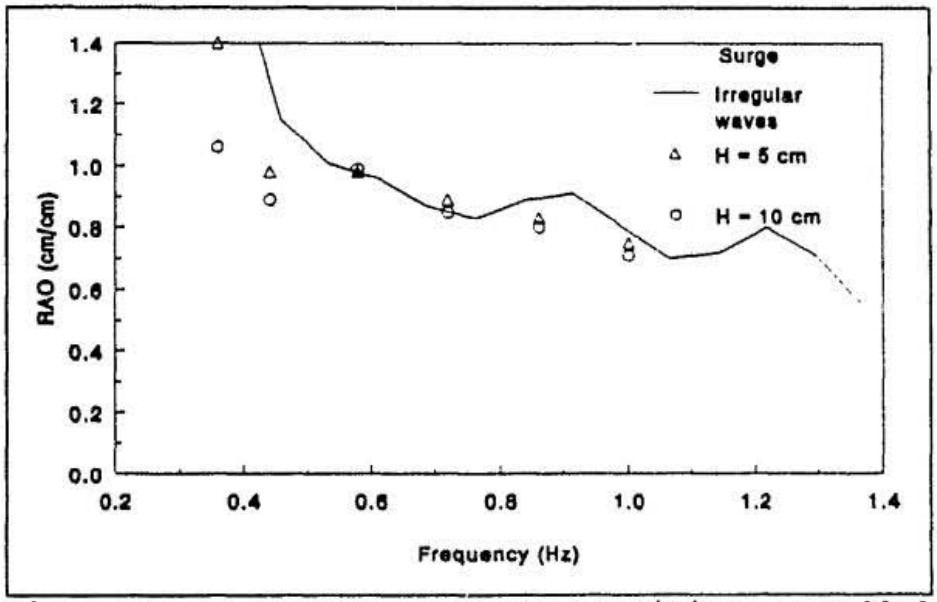

Figure C.16 - Surge: surface position, parallel orientation

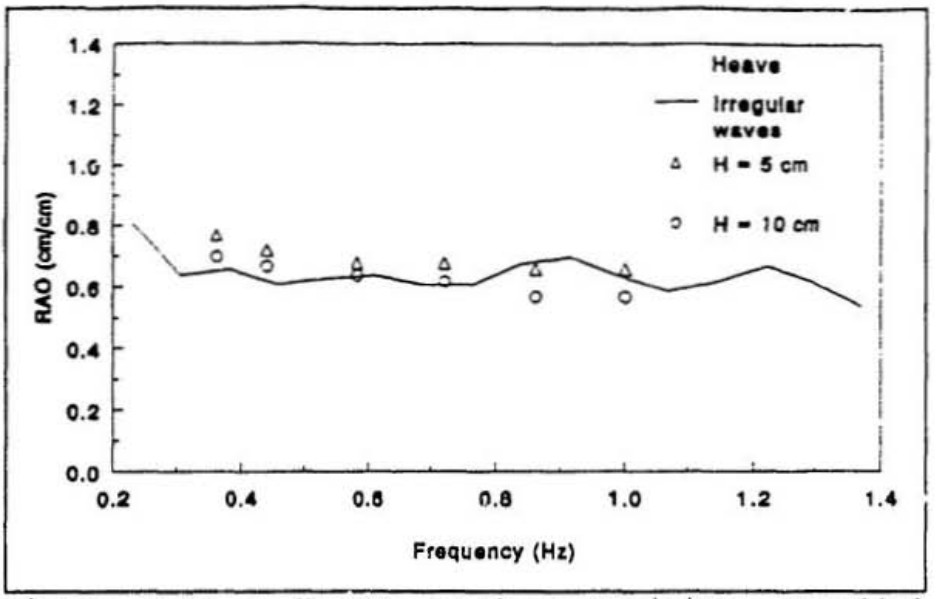

Figure C.17 - Heave: surface position, parallel orientation

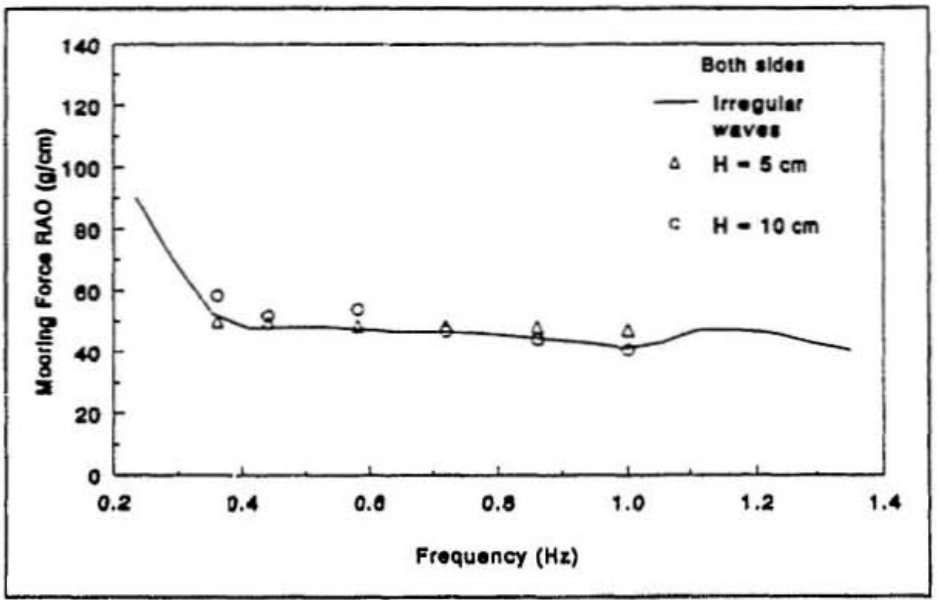

Figure C.18 - Mooring lines of both sides: surface position, parallel orientation

C.5 Middle Position, Parallel Orientation

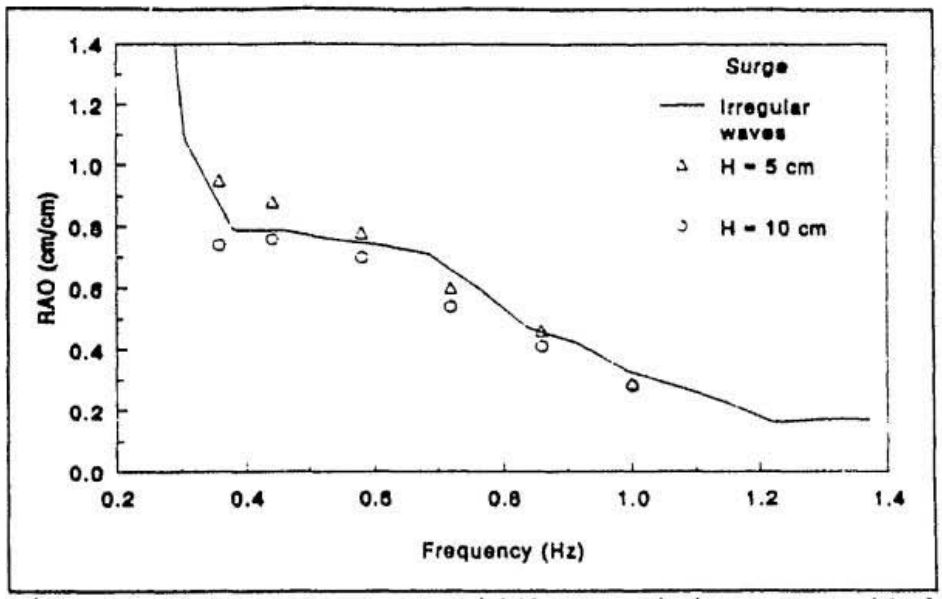

Figure C.19 - Surge: middle position, parallel orientation

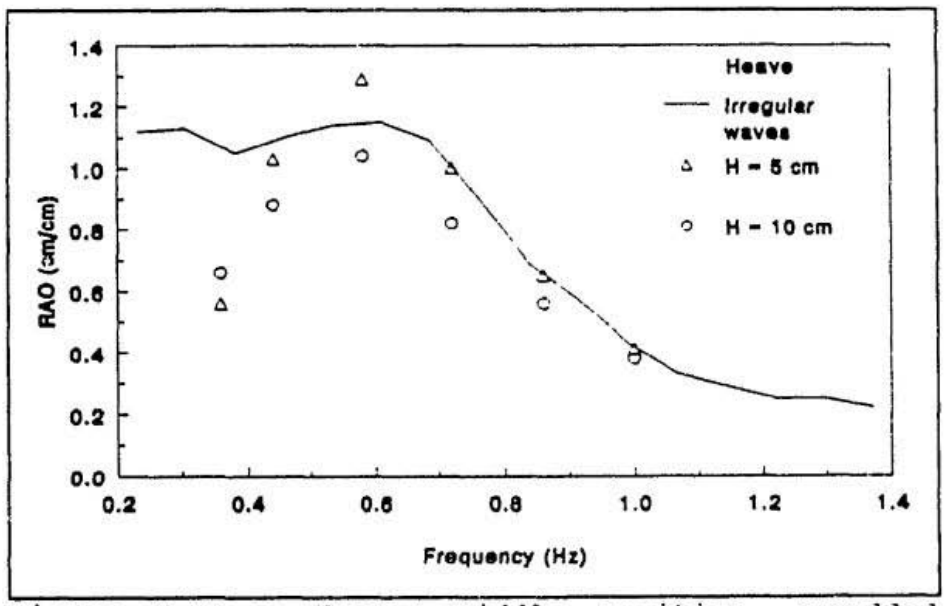

Figure C.20 - Heave: middle position, parallel orientation

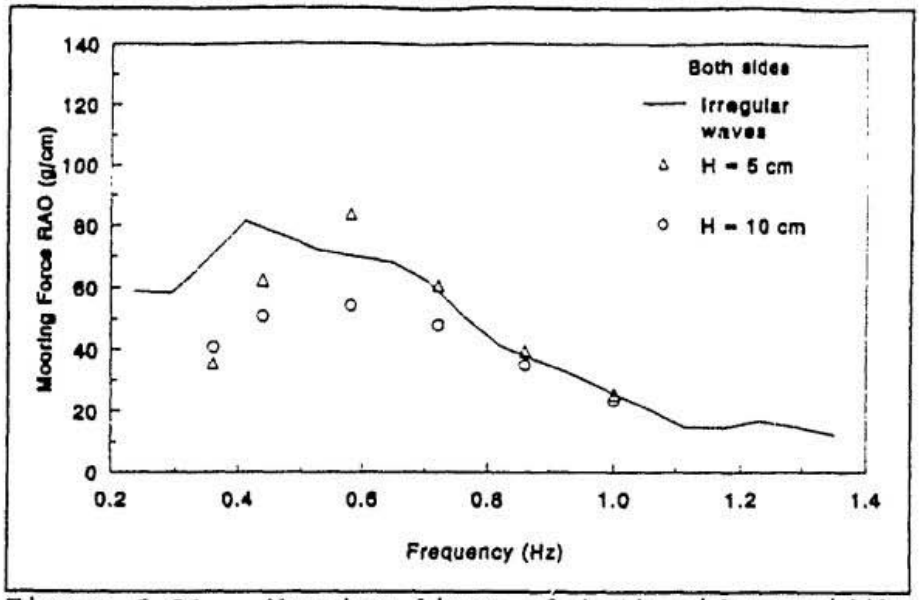

Figure C.21 - Mooring lines of both sides: middle position, parallel orientation

C.6 Bottom Position, Parallel Orientation

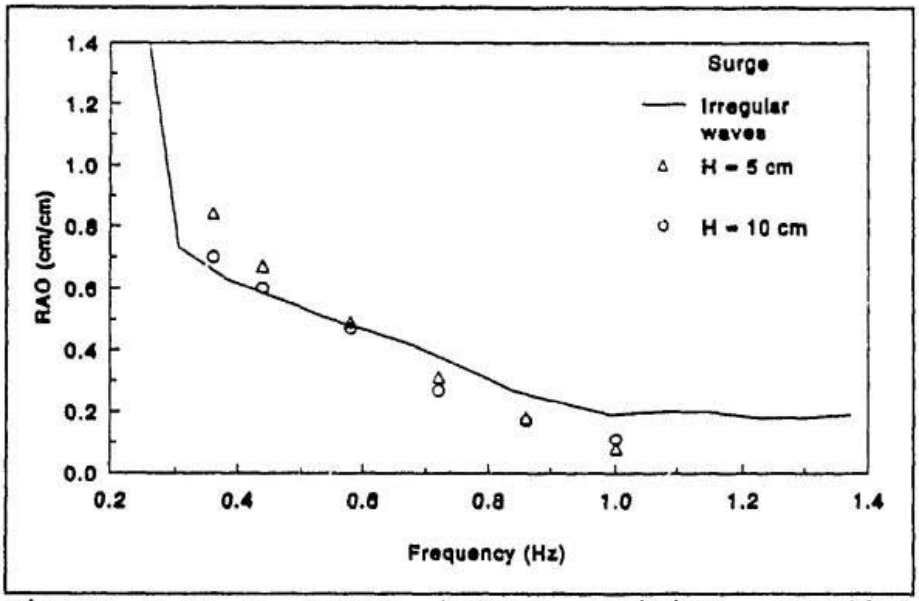

Figure C.22 - Surge: bottom position, parallel orientation

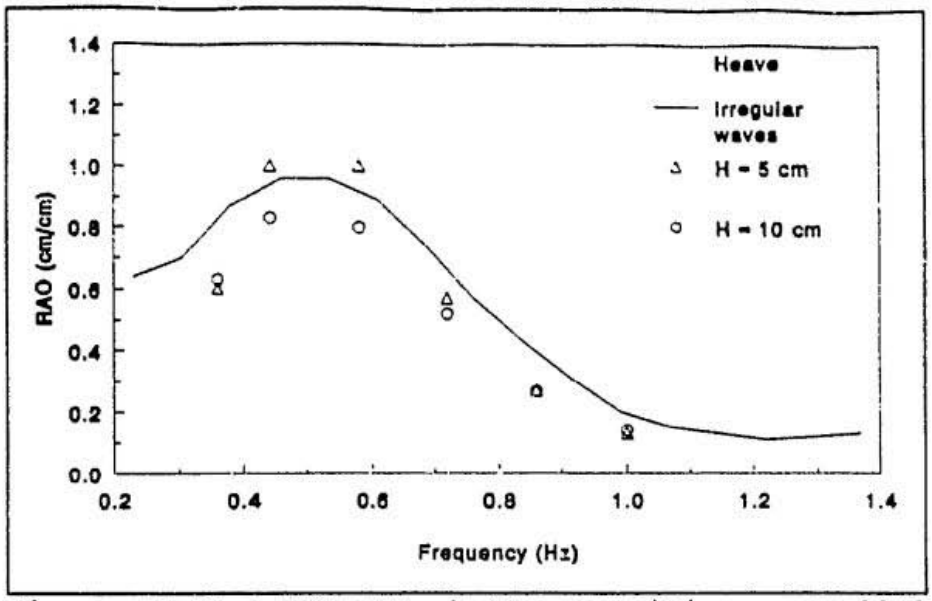

Figure C.23 - Heave: bottom position, parallel orientation

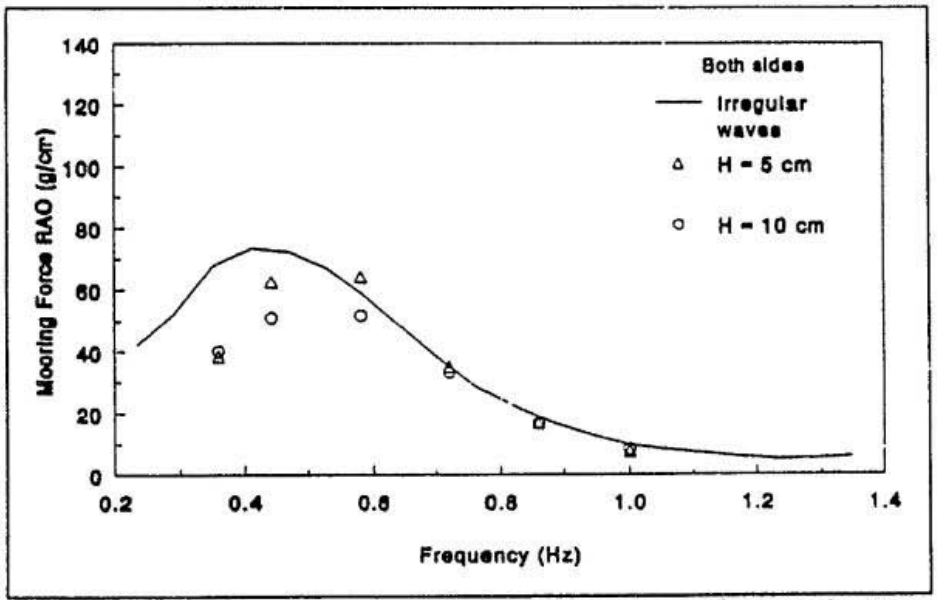

Figure C.24 - Mooring lines of both sides: bottom position, parallel orientation

C.7 Middle Position, 45° Orientation

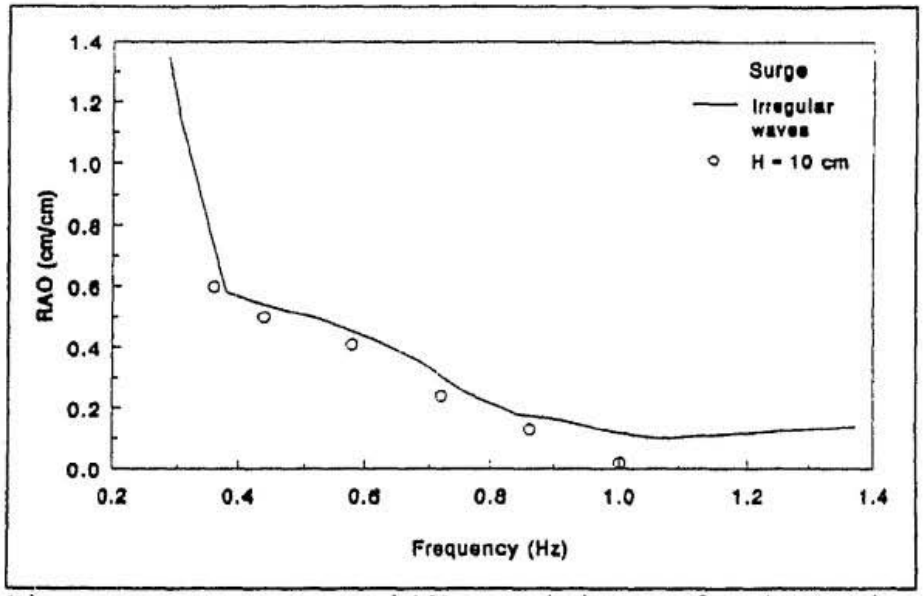

Figure C.25 - Surge: middle position, 45° orientation

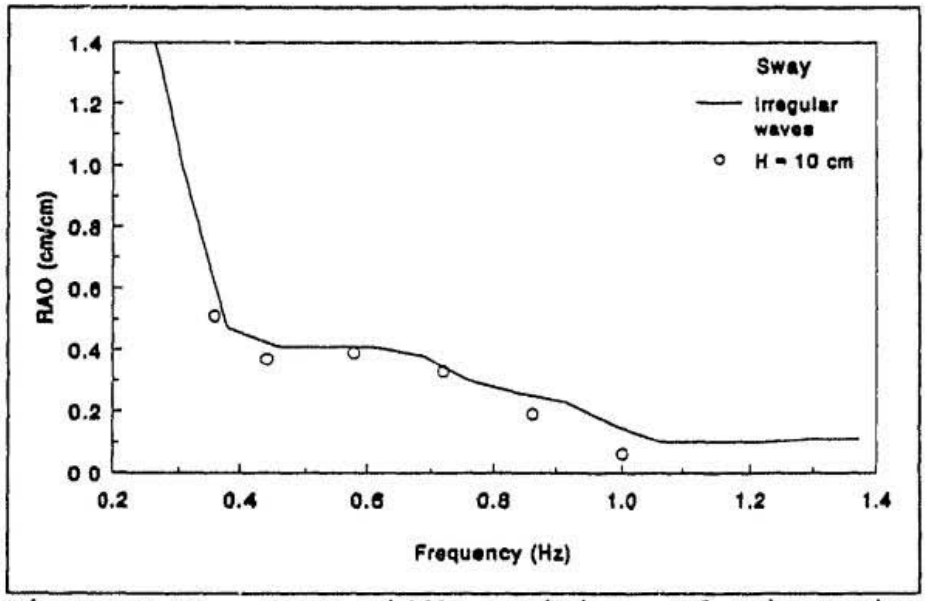

Figure C.26 - Sway: middle position, 45° orientation

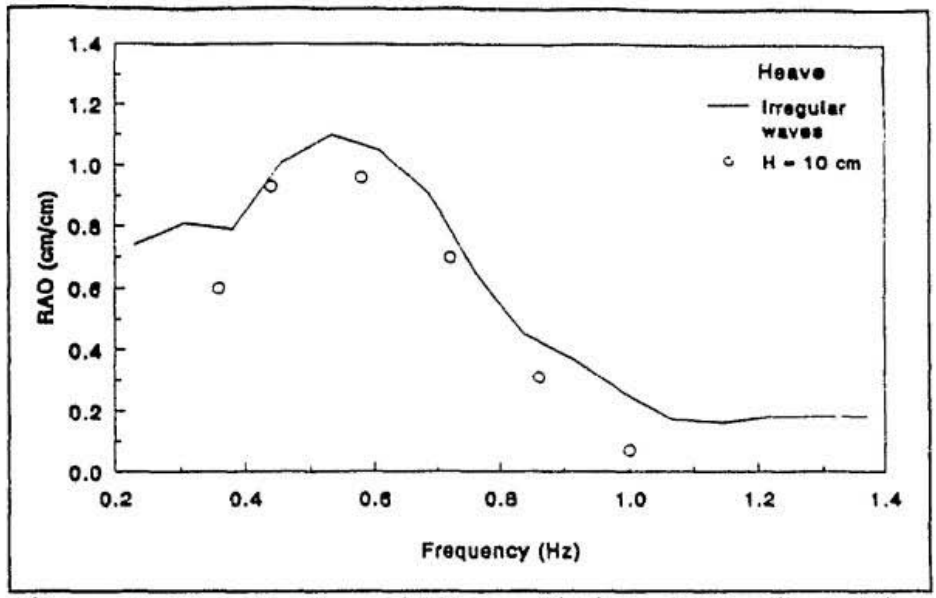

Figure C.27 - Heave: middle position, 45° orientation

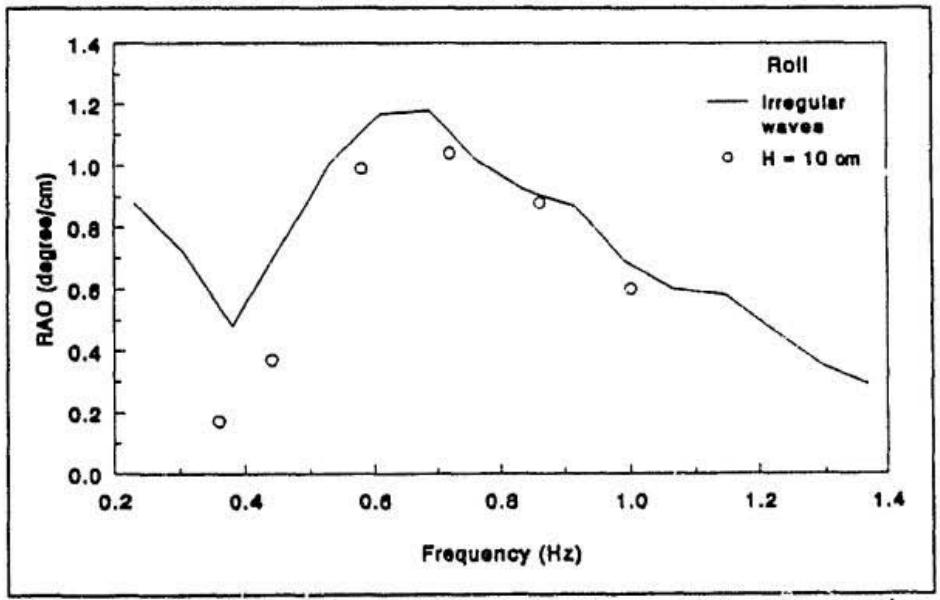

Figure C.28 - Roll: middle position, 45° orientation

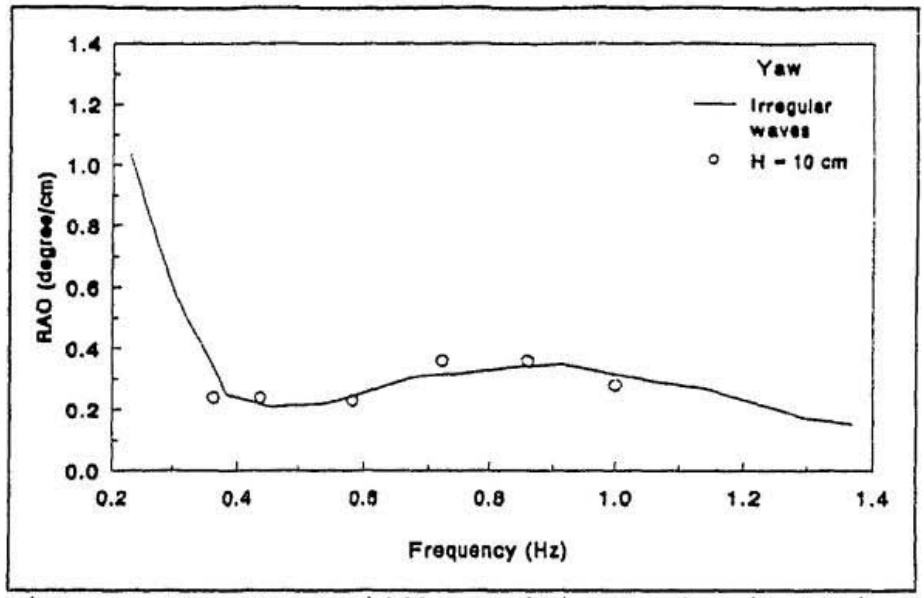

Figure C.29 - Yaw: middle position, 45° orientation

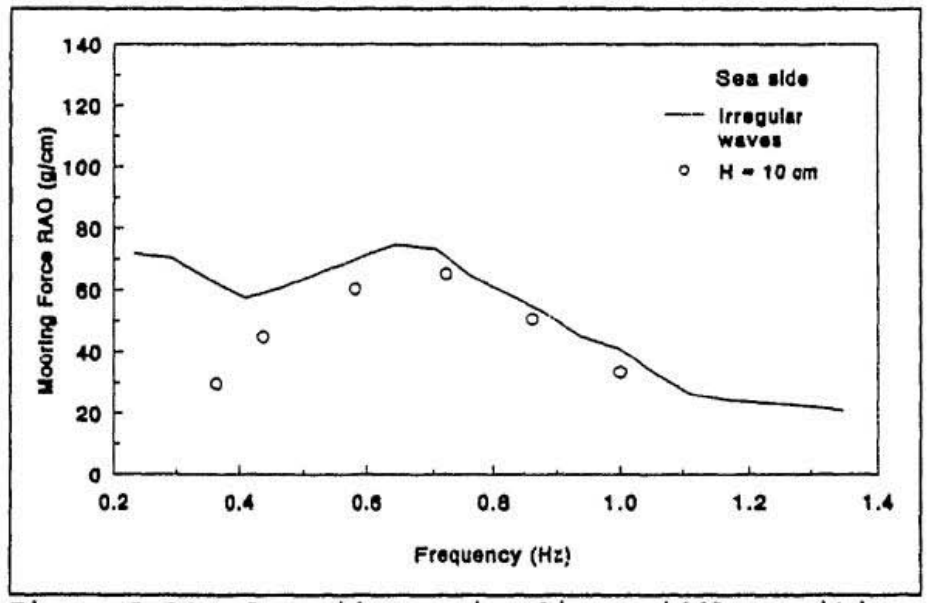

Figure C.30 - Sea side mooring line: middle position, 45° orientation

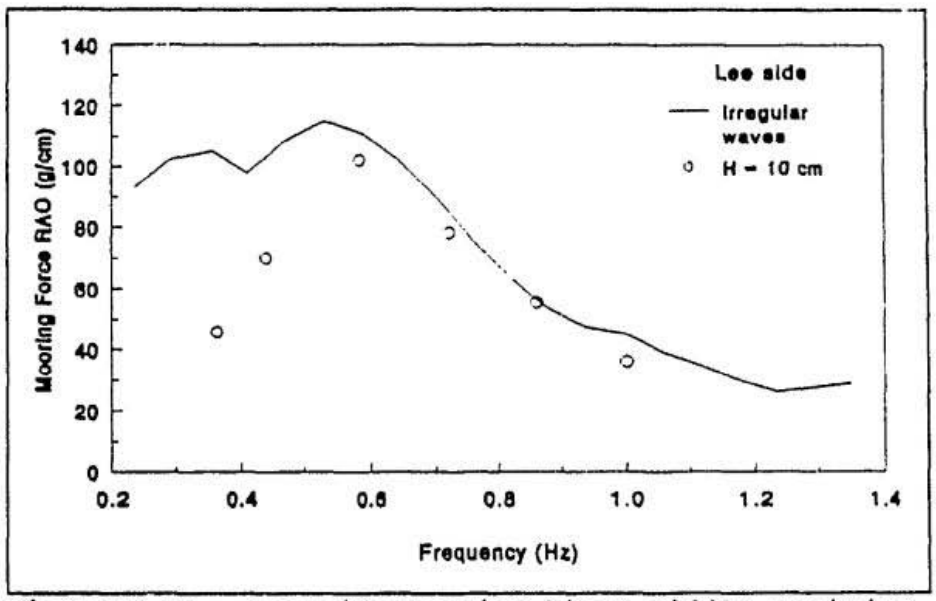

Figure C.31 - Lee side mooring line: middle position, 45° orientation

APPENDIX D

MOTION AND MOORING FORCE RESPONSES OF THE GEODESIC CAGE MODEL

D.1 Surface Position, Perpendicular Orientation

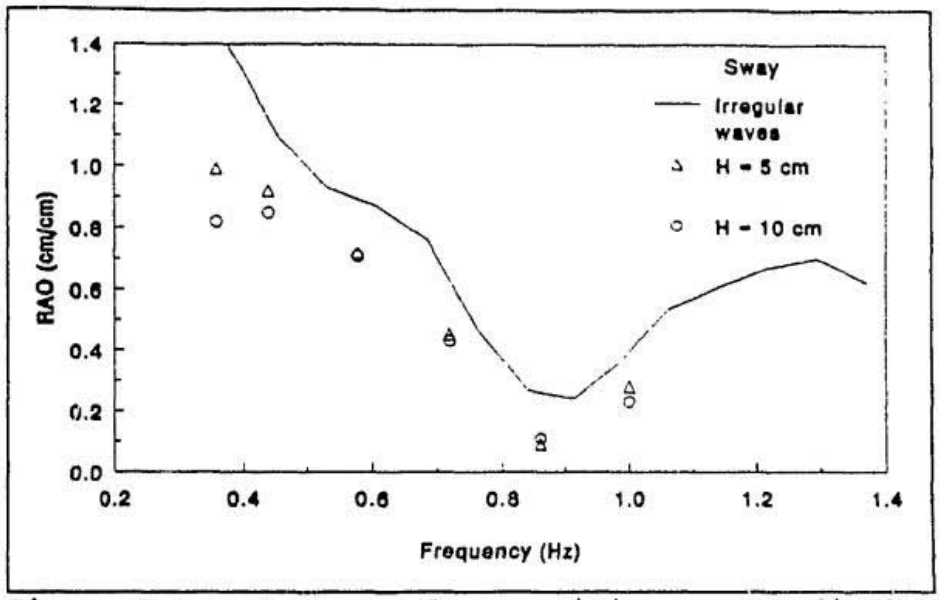

Figure D.1 - Sway: surface position, perpendicular orientation

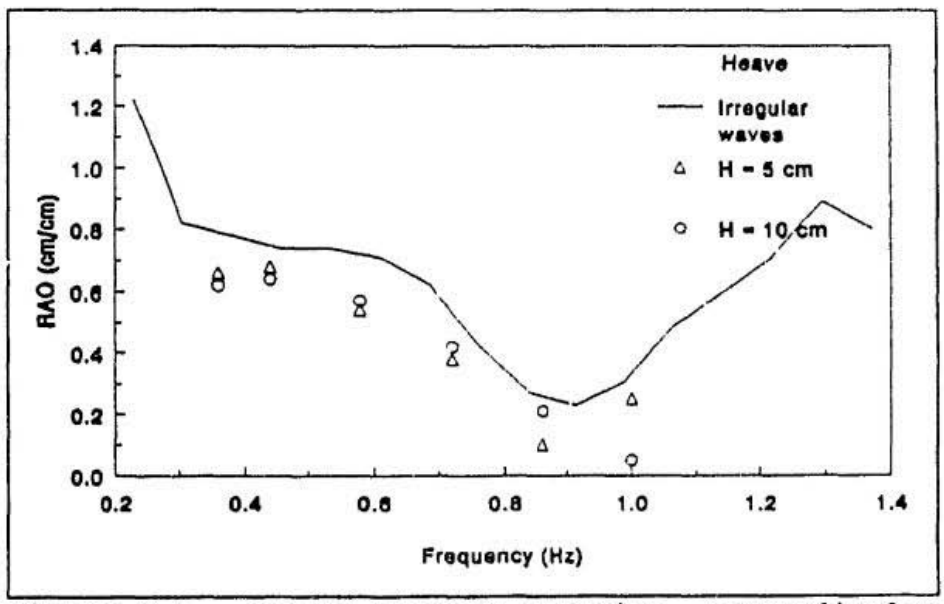

Figure D.2 - Heave: surface posotion, perpendicular orientation

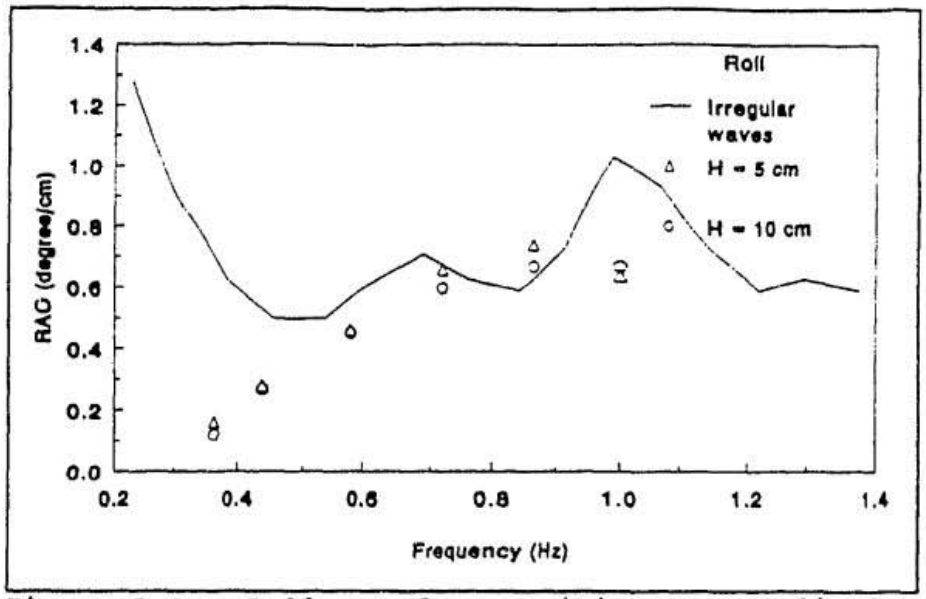

Figure D.3 - Roll: surface position, perpendicular orientation

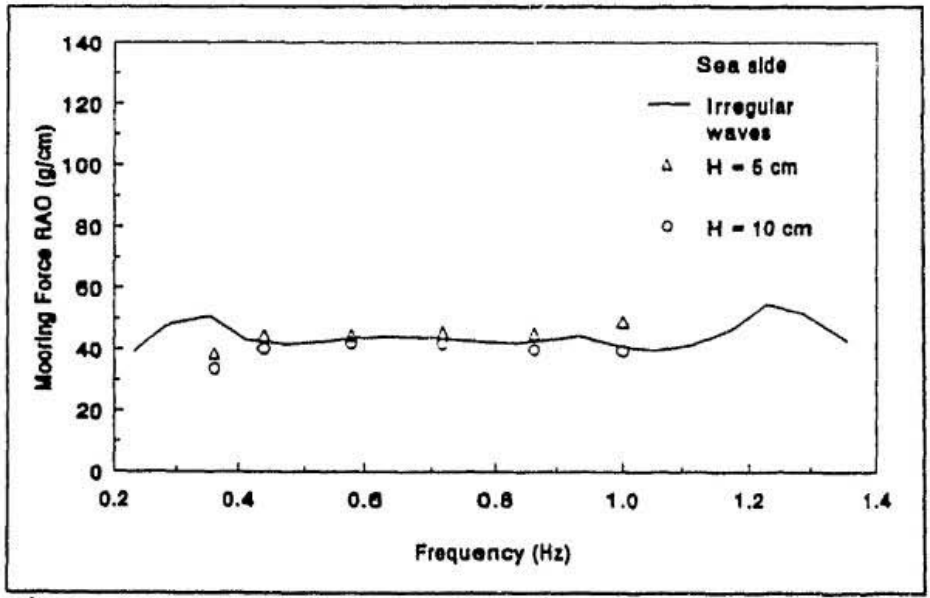

Figure D.4 - Sea side mooring line: surface position, perpendicular orientation

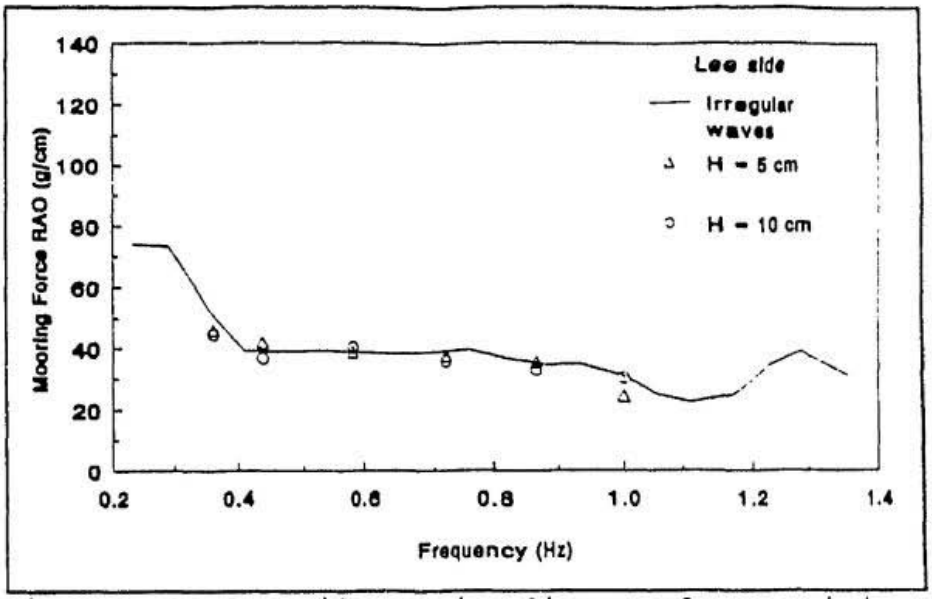

Figure D.5 - Lee side mooring line: surface position, perpendicular orientation

D.2 Middle Position, Perpendicular Orientation

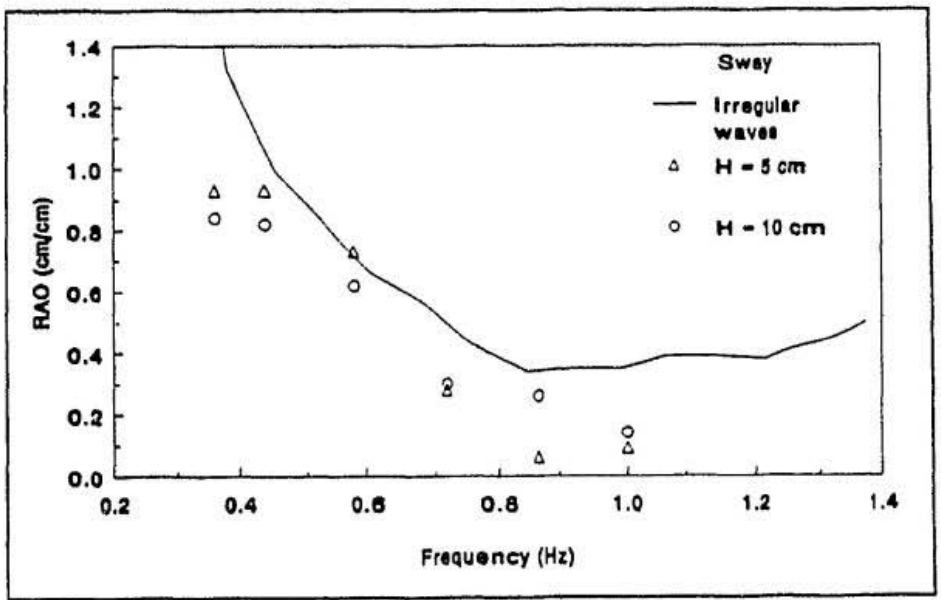

Figure D.6 - Sway: middle position, perpendicular orientation

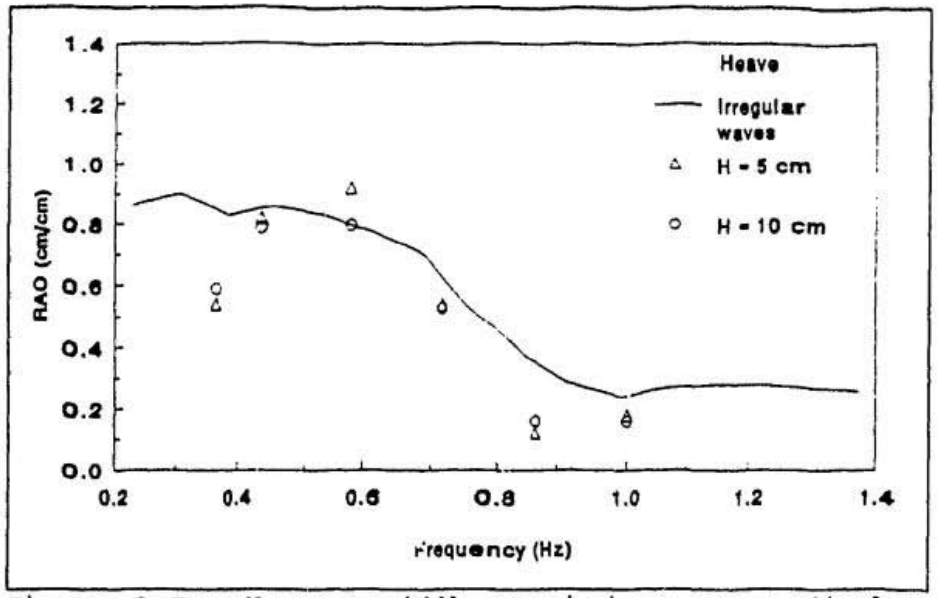

Figure D.7 - Heave: middle position, perpendicular orientation

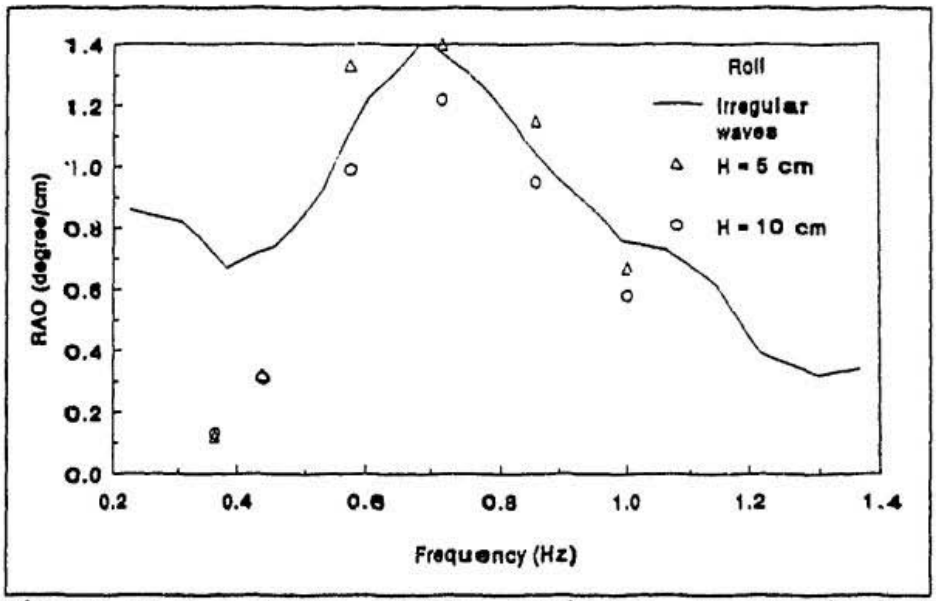

Figure D.8 - Roll: middle position, perpendicular orientation

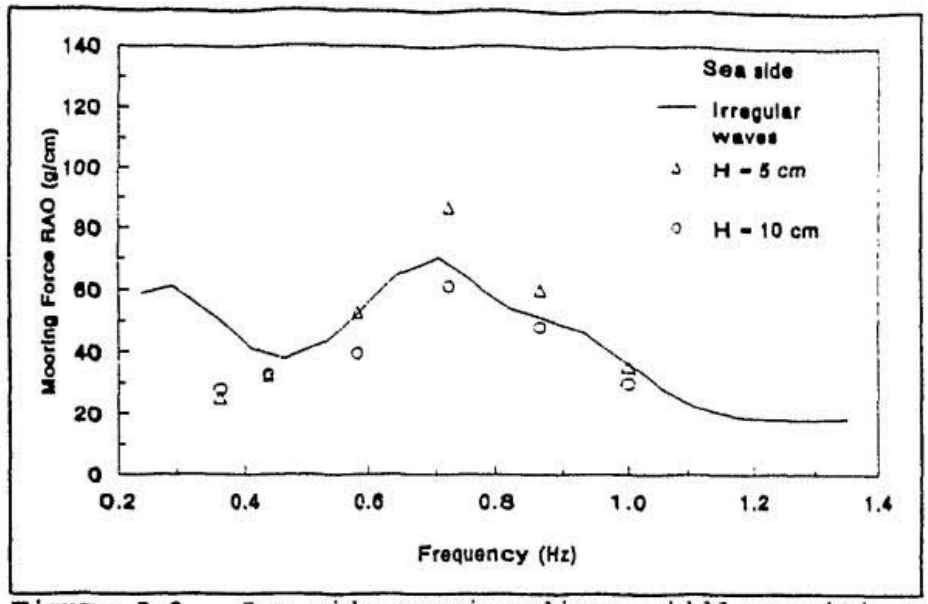

Figure D.9 - Sea side mooring line: middle position, perpendicular orientation

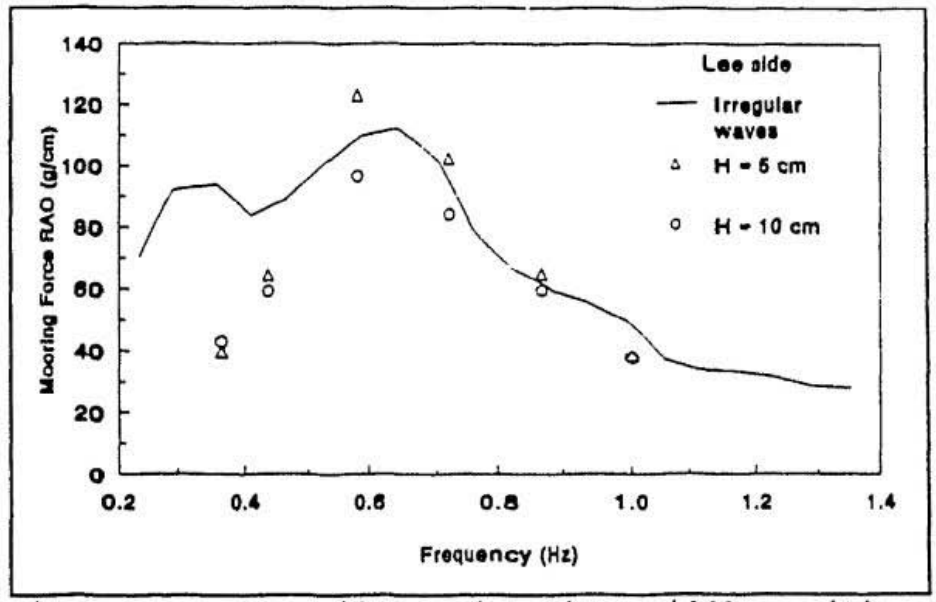

Figure D.10 - Lee side mooring line: middle position, perpendicular orientation

D.3 Bottom Position, Perpendicular Orientation

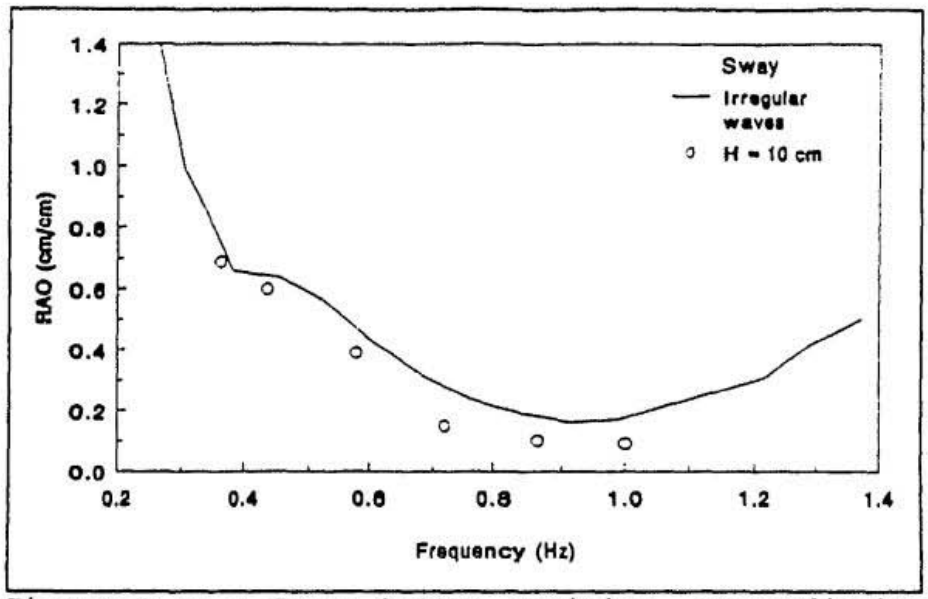

Figure D.11 - Sway: bottom position, perpendicular orientation

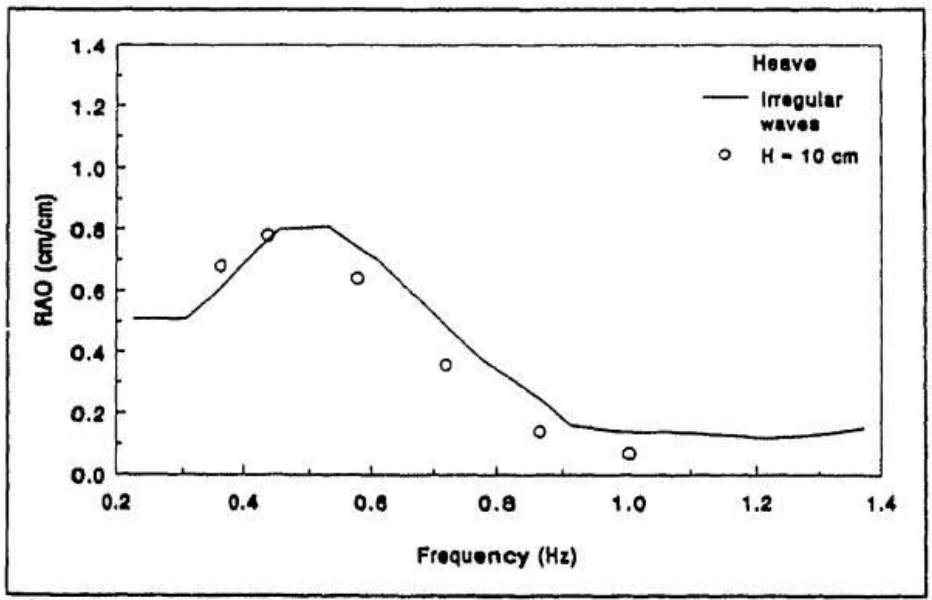

Figure D.12 - Heave: bottom position, perpendicular orientation

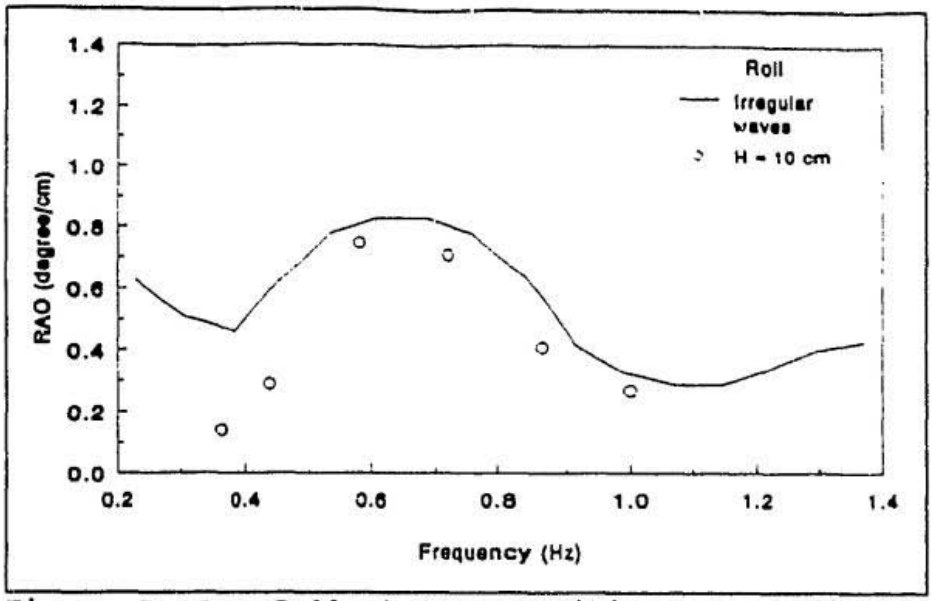

Figure D.13 - Roll: bottom position, perpendicular orientation

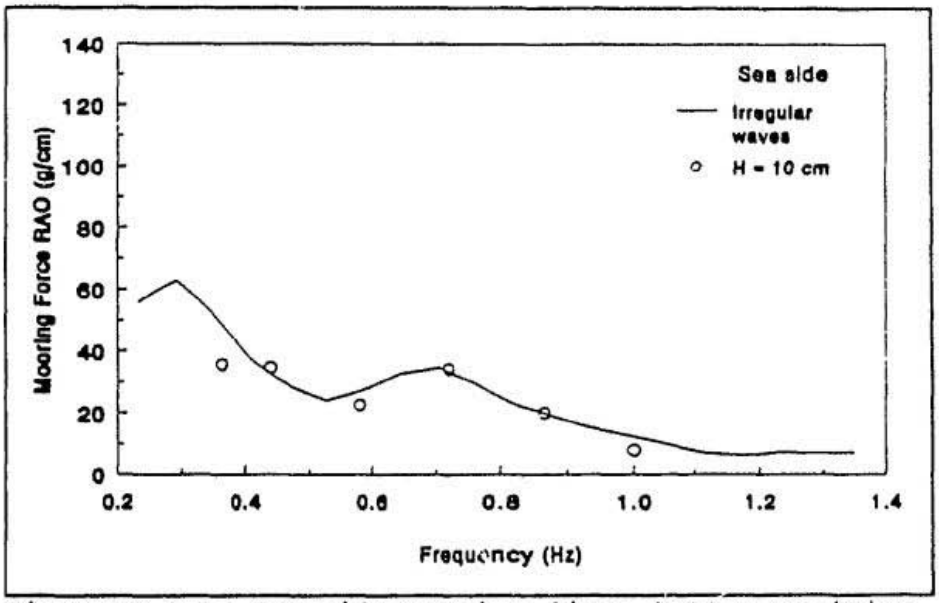

Figure D.14 - Sea side mooring line: bottom position, perpendicular orientation

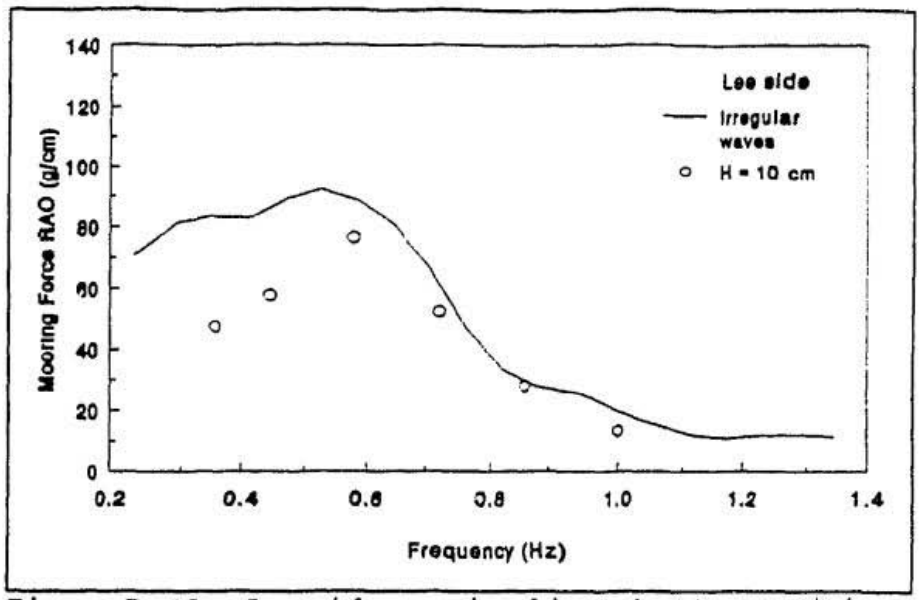

Figure D.15 - Lee side mooring line: bottom position, perpendicular orientation

D.4 Surface Position, Parallel Orientation

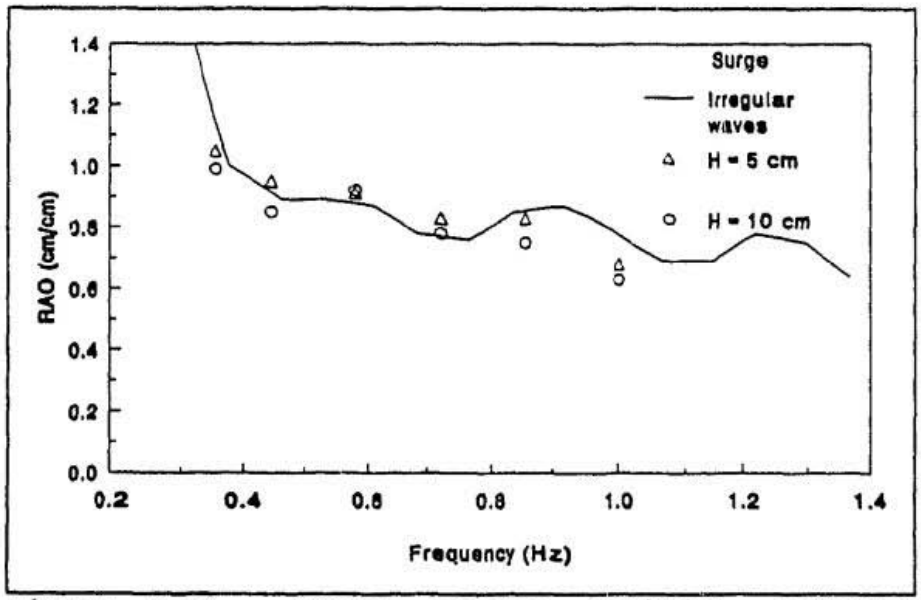

Figure D.16 - Surge: surface position, parallel orientation

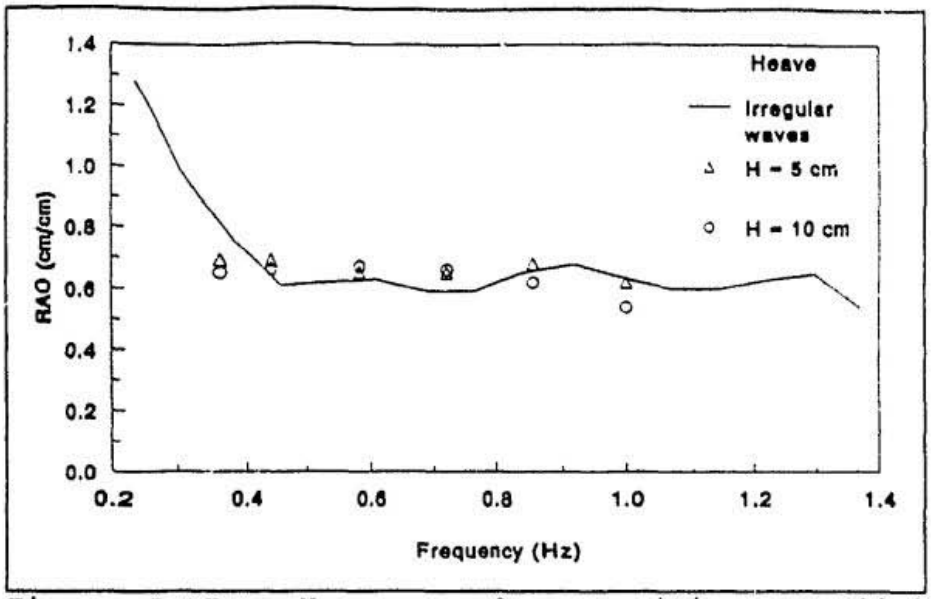

Figure D.17 - Heave: surface position, parallel orientation

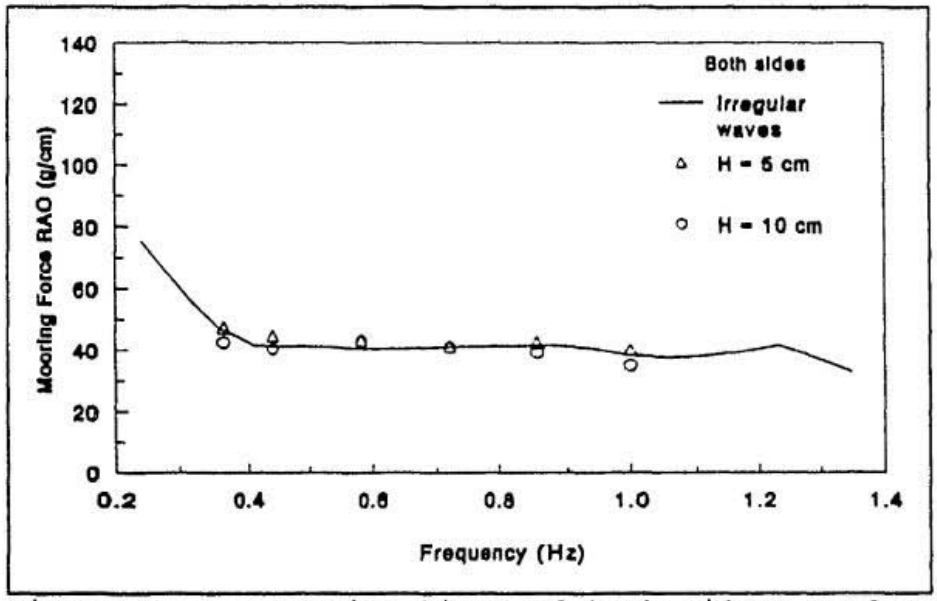

Figure D.18 - Mooring lines of both sides: surface position, parallel orientation

D.5 Middle Position, Parallel Orientation

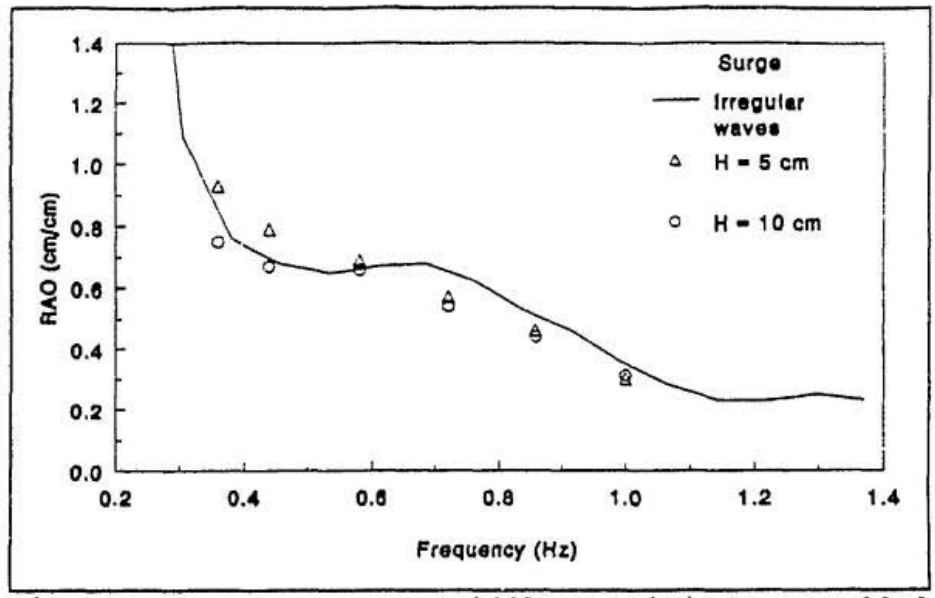

Figure D.19 - Surge: middle position, parallel orientation

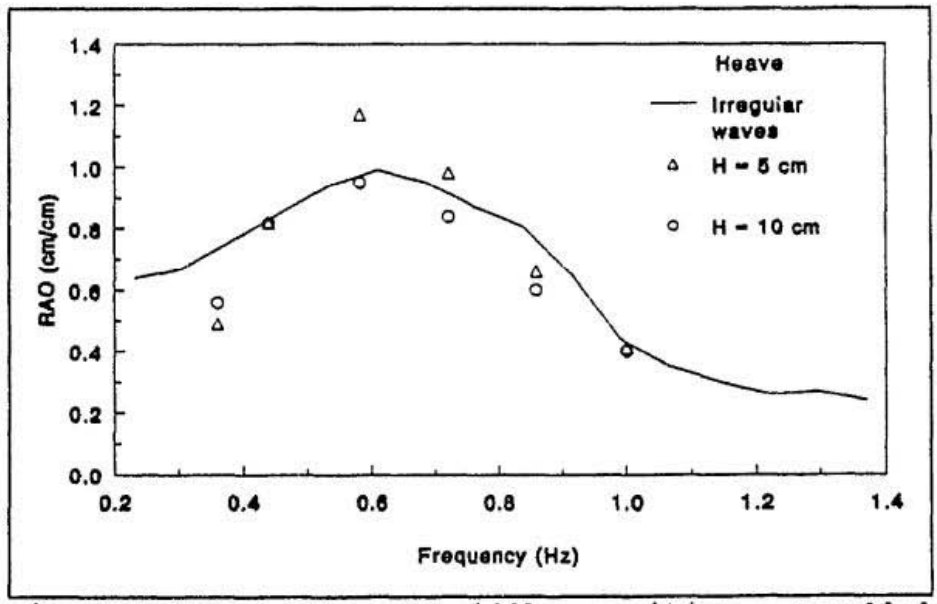

Figure D.20 - Heave: middle position, parallel orientation

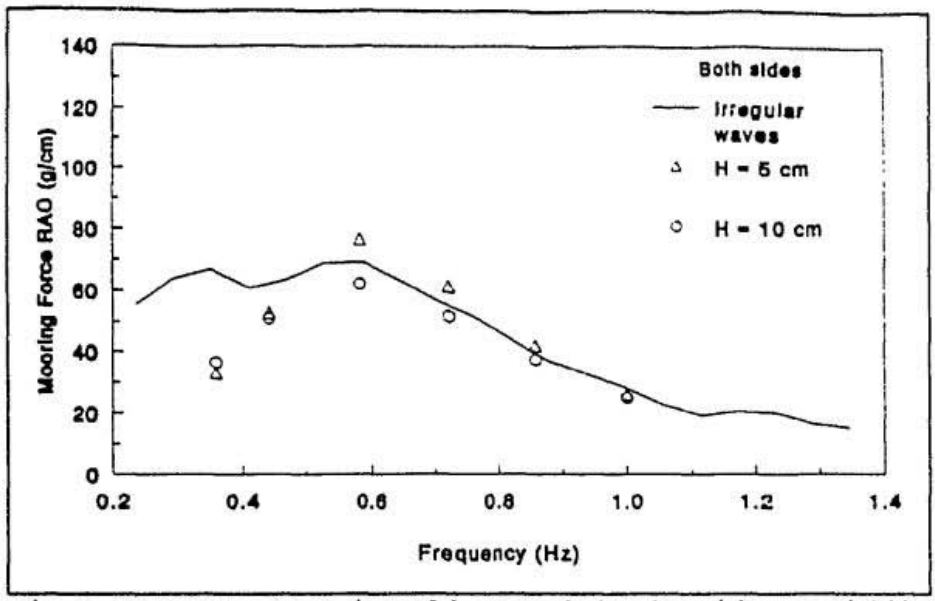

Figure D.21 - Mooring lines of both sides: middle position, parallel orientation

D.6 Bottom Position, Parallel Orientation

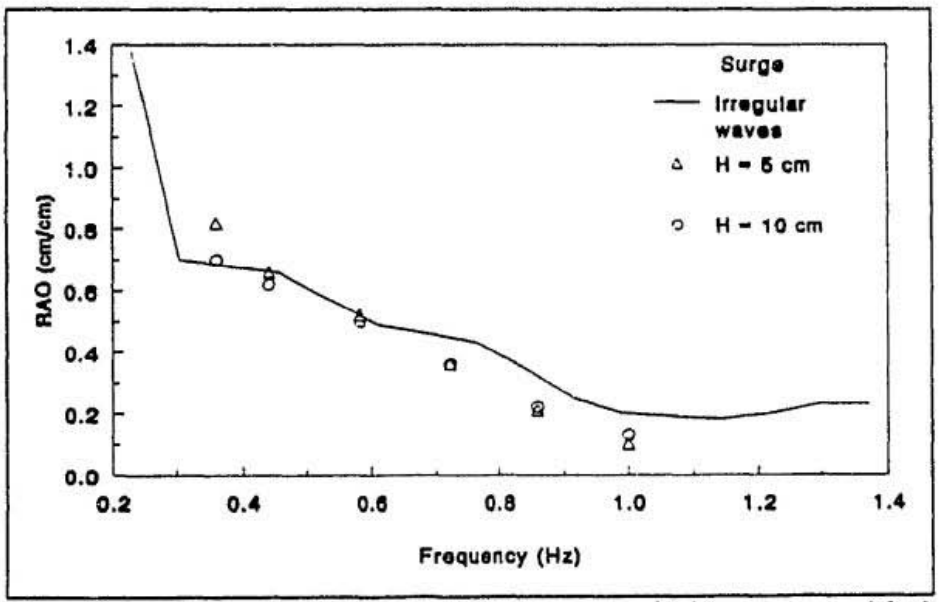

Figure D.22 - Surge: bottom position, parallel orientation

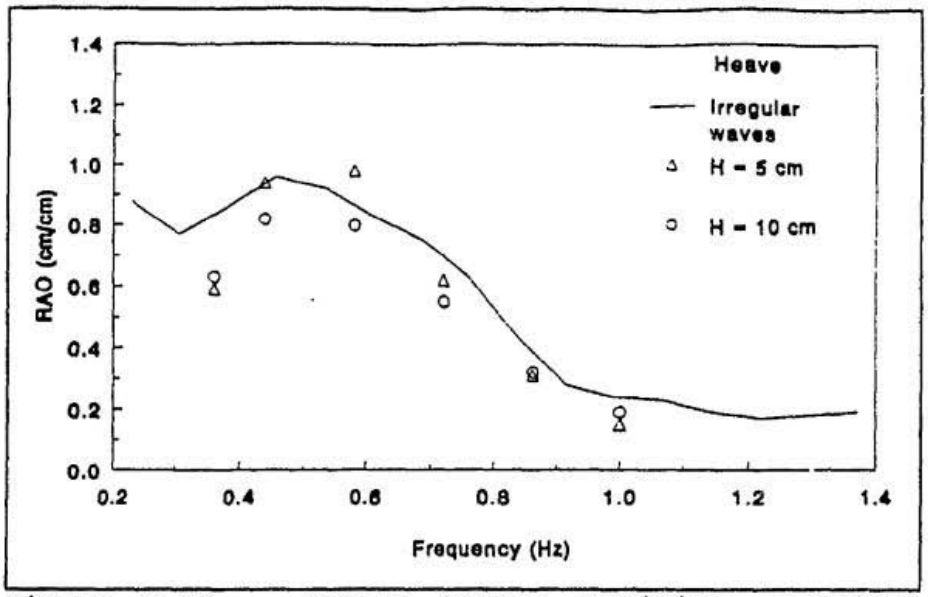

Figure D.23 - Heave: bottom position, parallel orientation

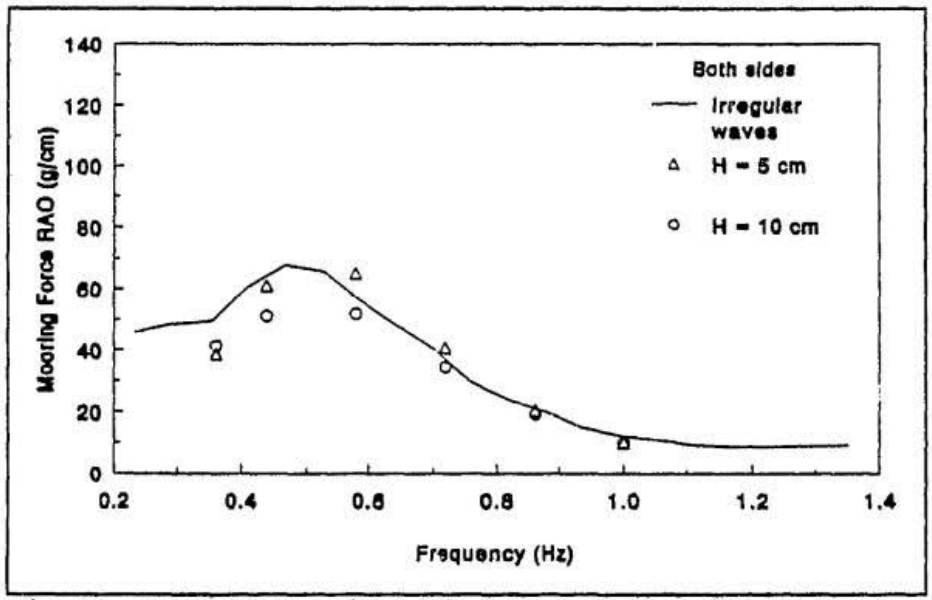

Figure D.24 - Mooring lines of both sides: bottom position, parallel orientation

D.7 Middle Position, 45° Orientation

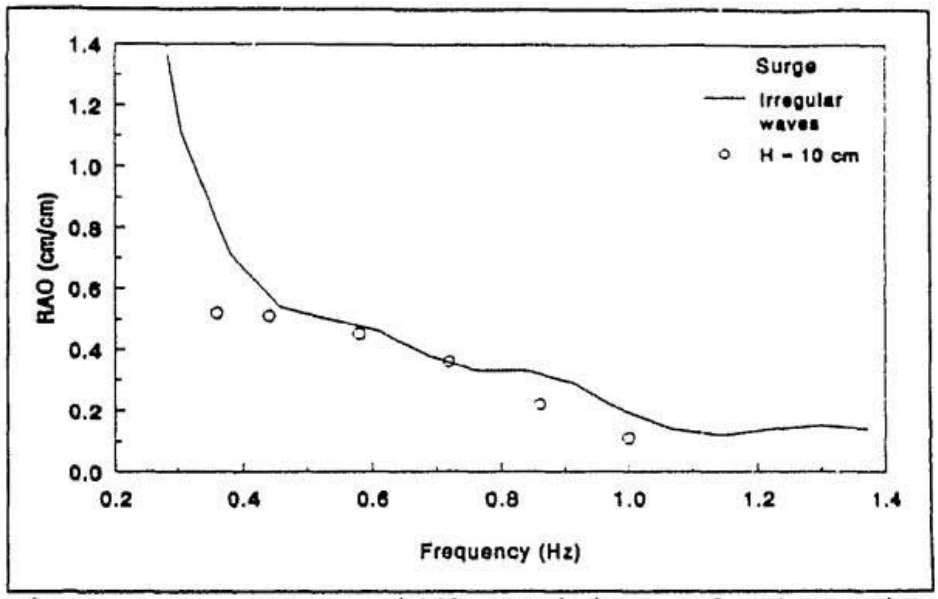

Figure D.25 - Surge: middle position, 45° orientation

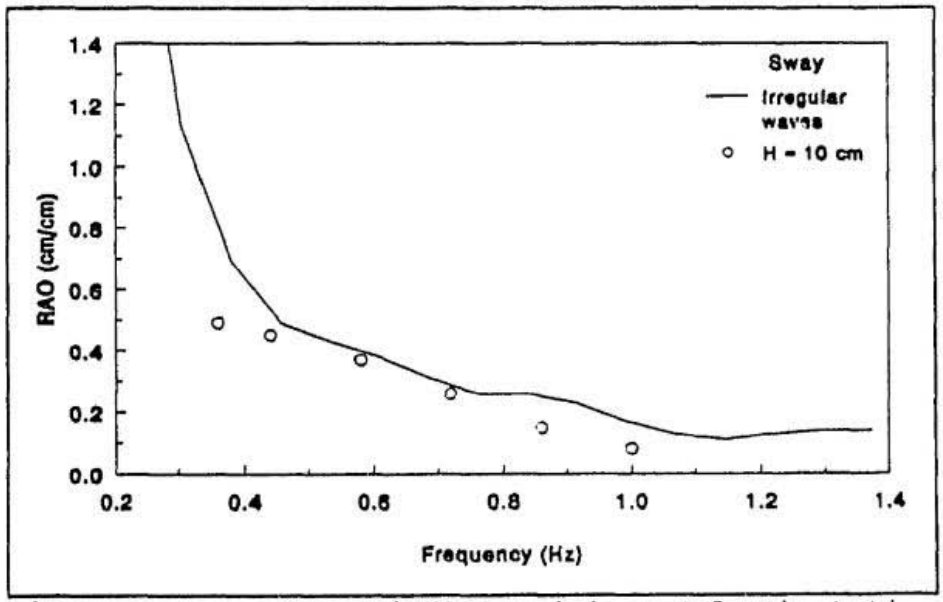

Figure D.26 - Sway: middle position, 45° orientation

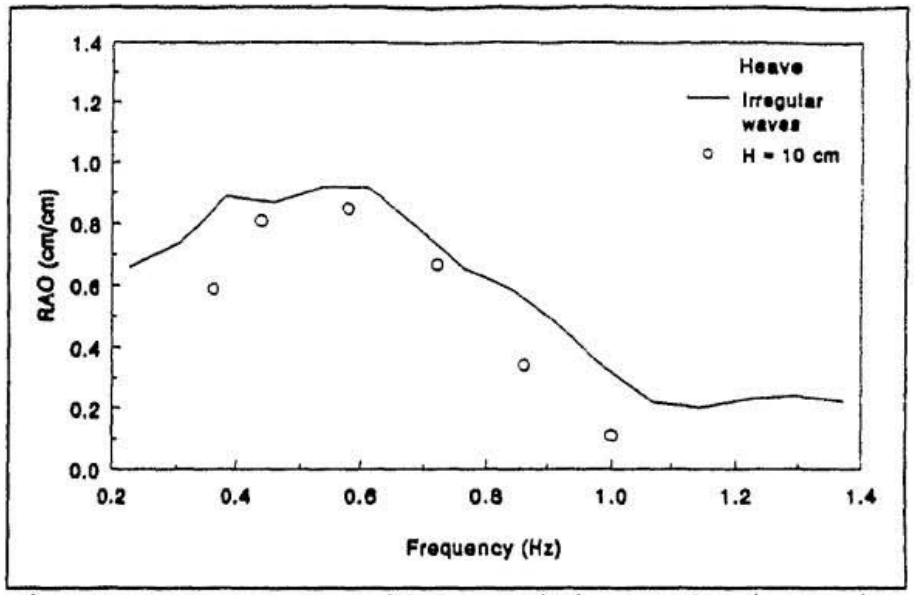

Figure D.27 - Heave: middle position, 45° orientation

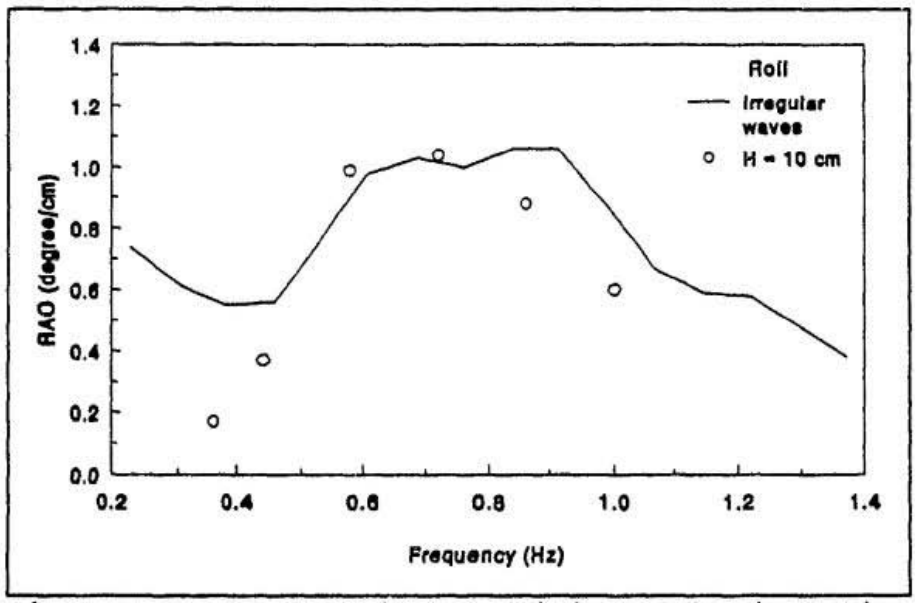

Figure D.28 - Roll: middle position, 45° orientation

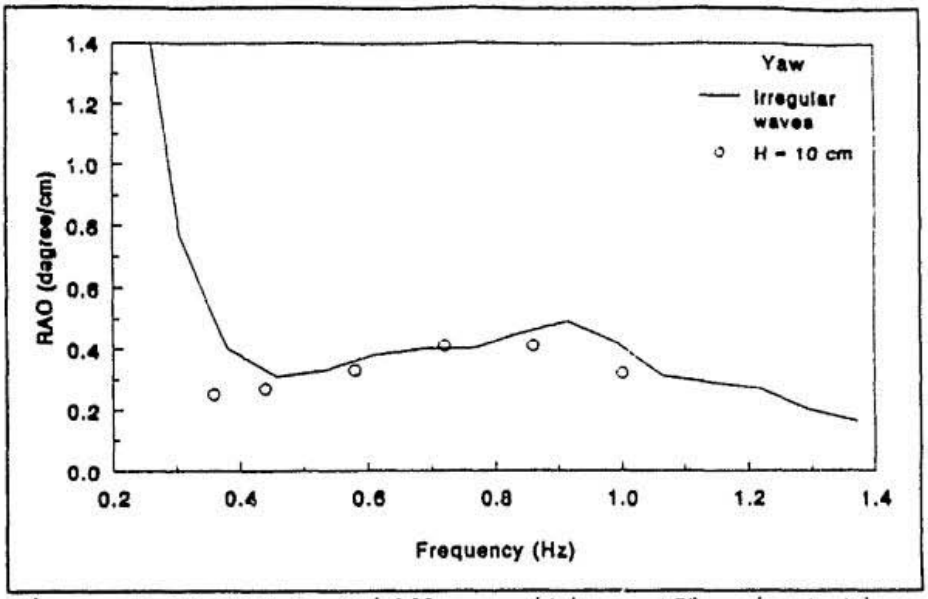

Figure D.29 - Yaw: middle position, 45° orientation

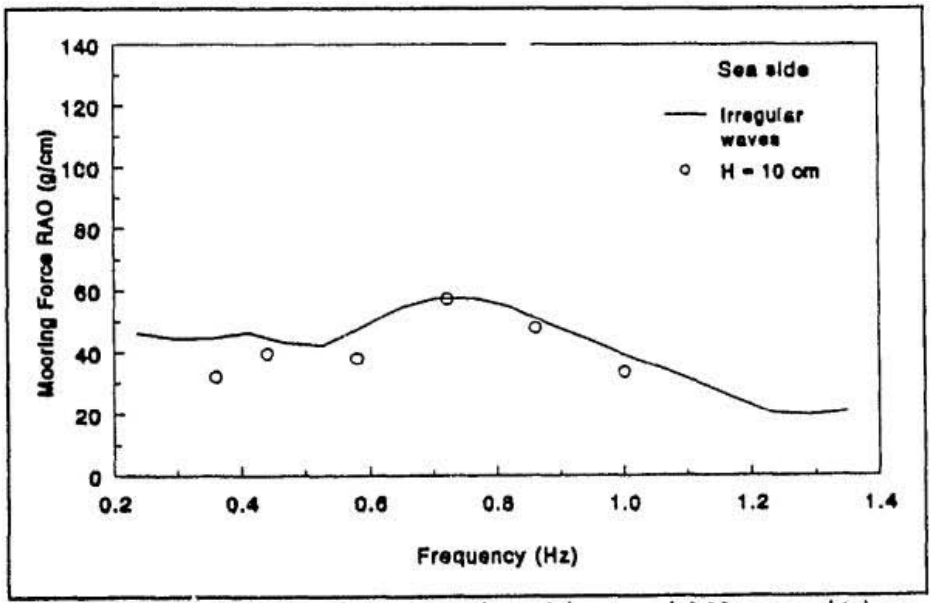

Figure D.30 - Sea side mooring line: middle position, 45° orientation

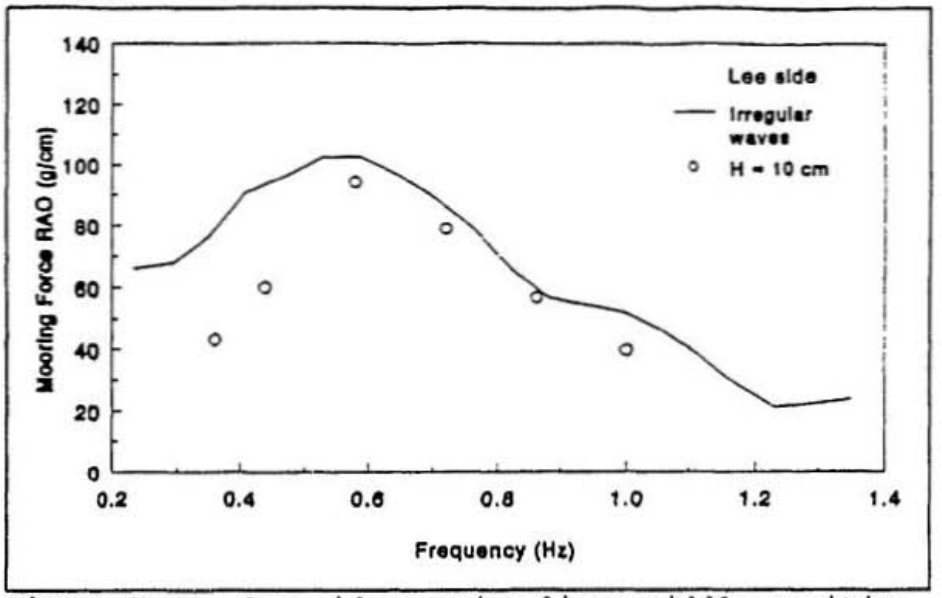

Figure D.31 - Lee side mooring line: middle position, 45° orientation

D.8 Middle Position, Parallel Orientation, with Stiffer Mooring lines (K = 30 kg/m instead of K = 10 kg/m)

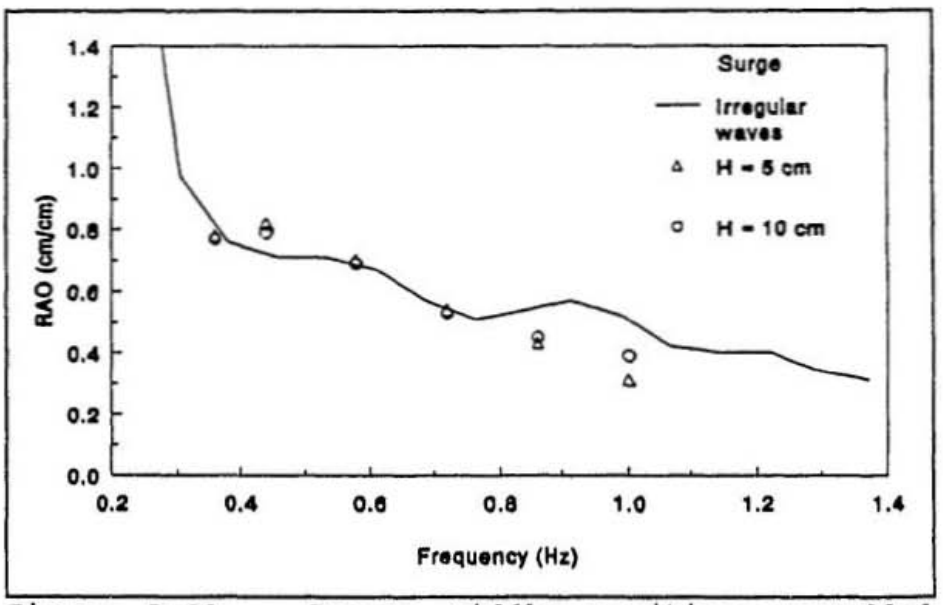

Figure D.32 - Surge: middle position, parallel oerientation, with stiffer mooring lines

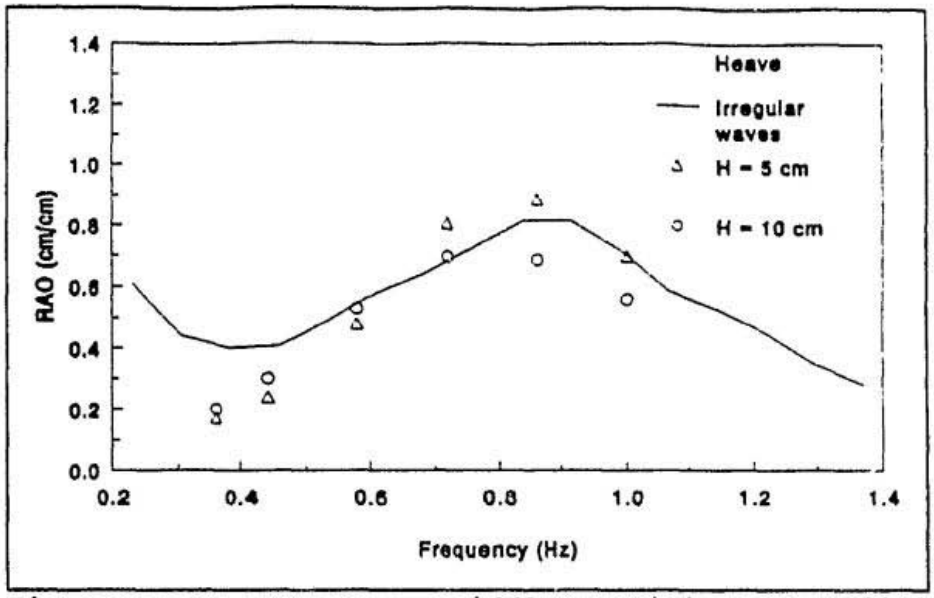

Figure D.33 - Heave: middle position, parallel orientation, with stiffer mooring lines

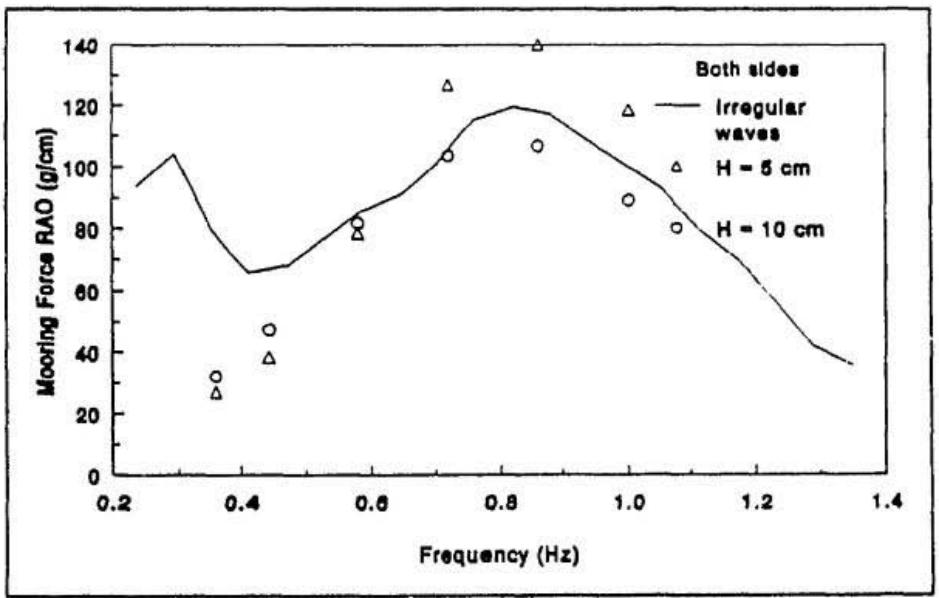

Figure D.34 - Mooring lines of both sides: middle position, parallel orientation, with stiffer mooring lines

D.9 Bottom Position, Parallel Orientation, with Stiffer Mooring lines (K = 30 kg/m instead of K = 10 kg/m)

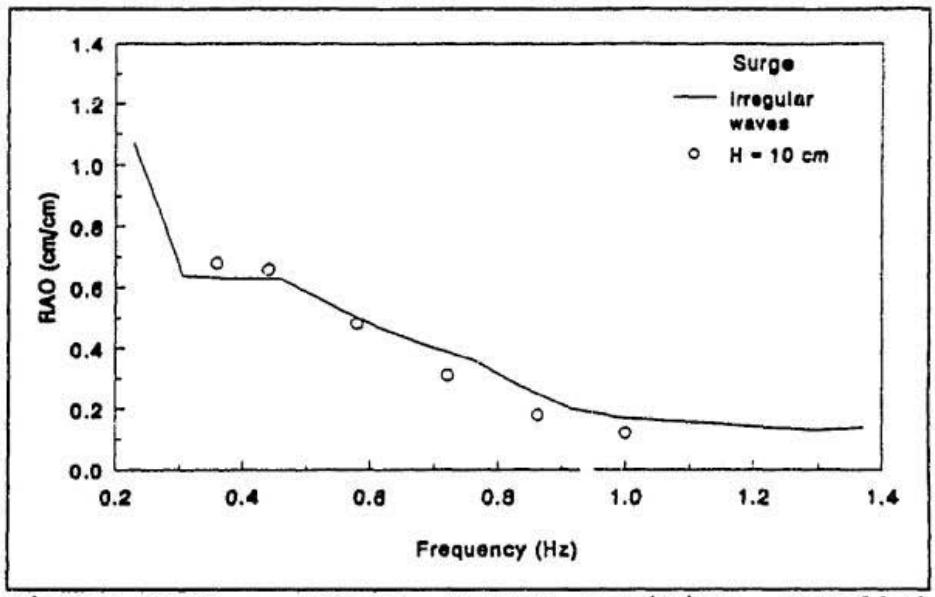

Figure D.35 - Surge: bottom position, parallel orientation, with stiffer mooring lines

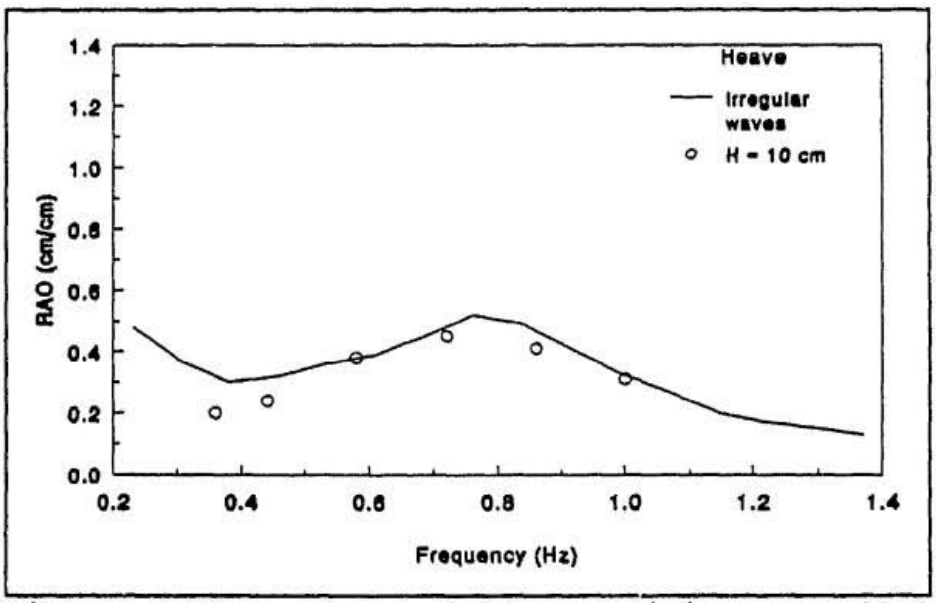

Figure D.36 - Heave: bottom position, parallel orientation, with stiffer mooring lines

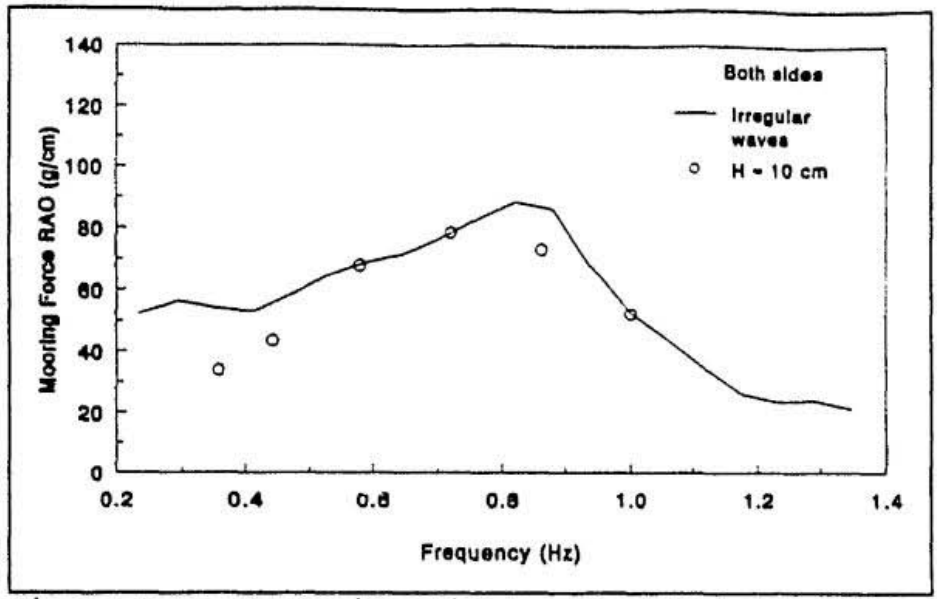

Figure D.37 - Mooring lines of both sides: bottom position, parallel orientation, with stiffer mooring lines

D.10 Middle Position, Perpendicular Orientation, with stiffer Mooring lines (K = 30 kg/m instead of K = 10 kg/m)

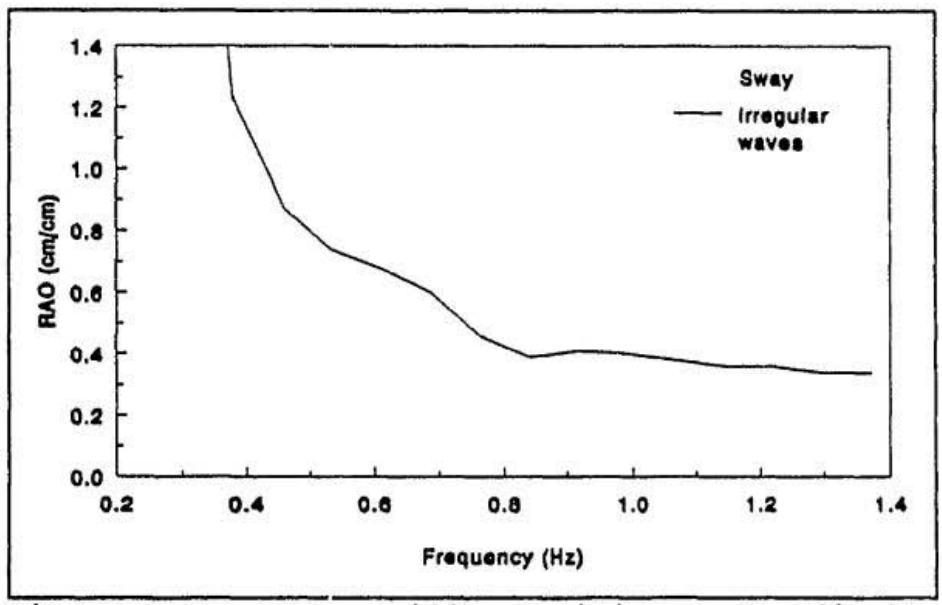

Figure D.38 - Sway: middle position, perpendicular orientation, with stiffer mooring lines

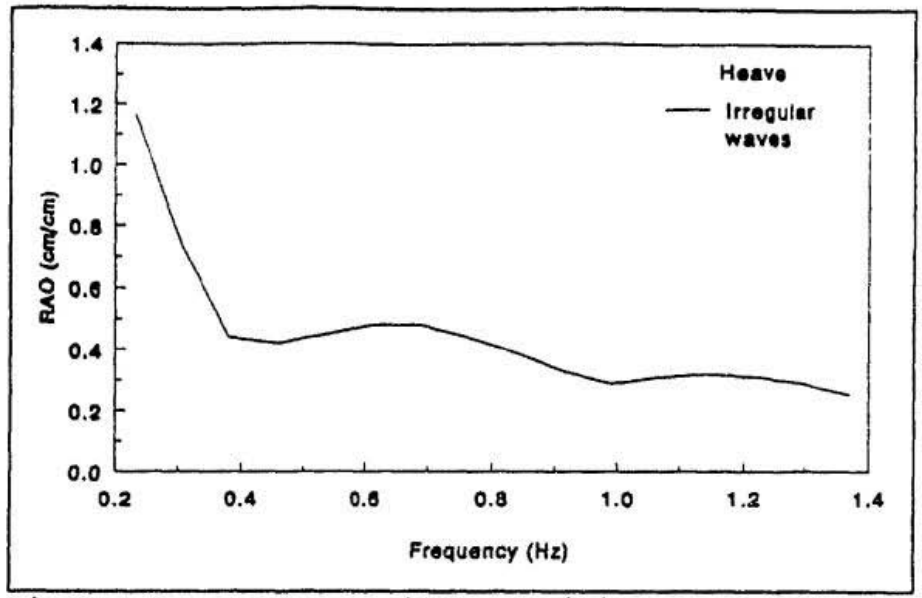

Figure D.39 - Heave: middle position, perpendicular orientation, with stiffer mooring lines

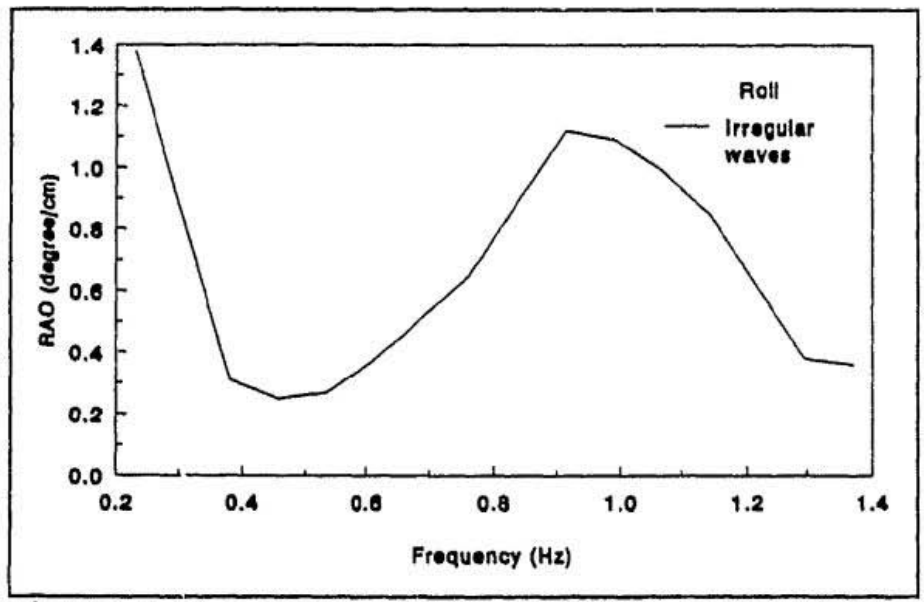

Figure D.40 - Roll: middle position, perpendicular orientation, with stiffer mooring lines

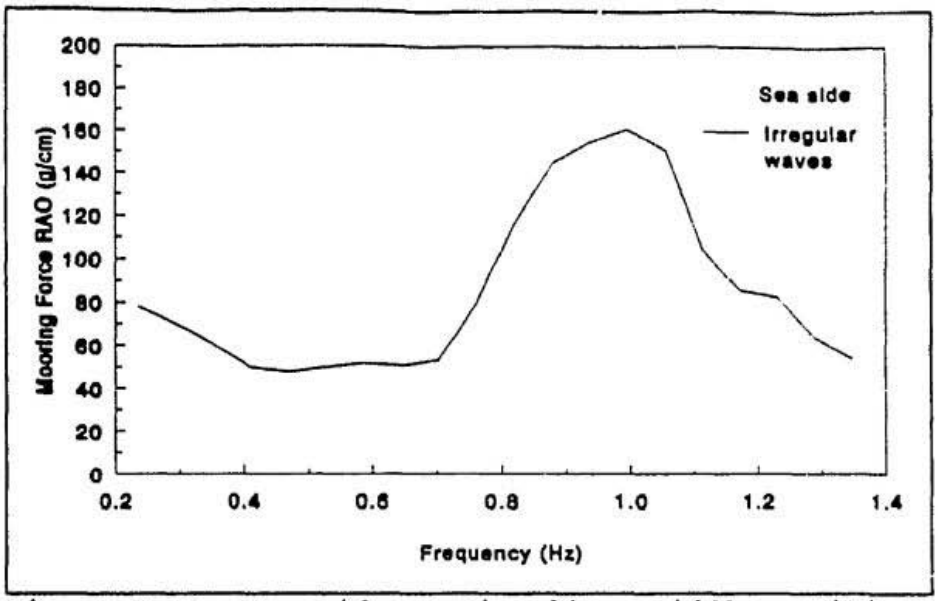

Figure D.41 - Sea side mooring line: middle position, perpendicular orientation, with stiffer mooring lines

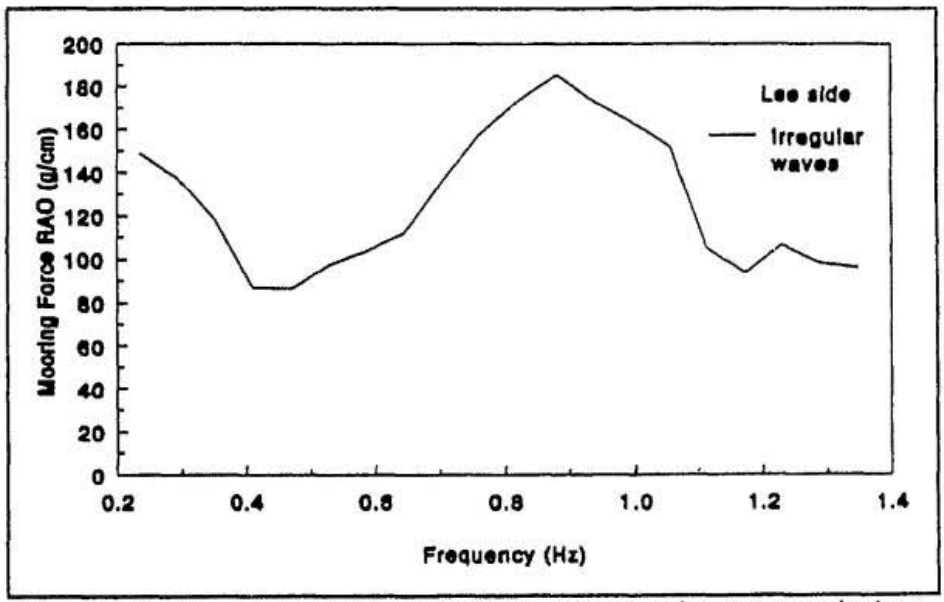

Figure D.42 - Lee side mooring line: middle position, perpendicular orientation, with stiffer mooring lines

D.11 Bottom Position, Perpendicular Orientation, with stiffer mooring lines (K = 30 kg/m instead of K = 10 kg/m)

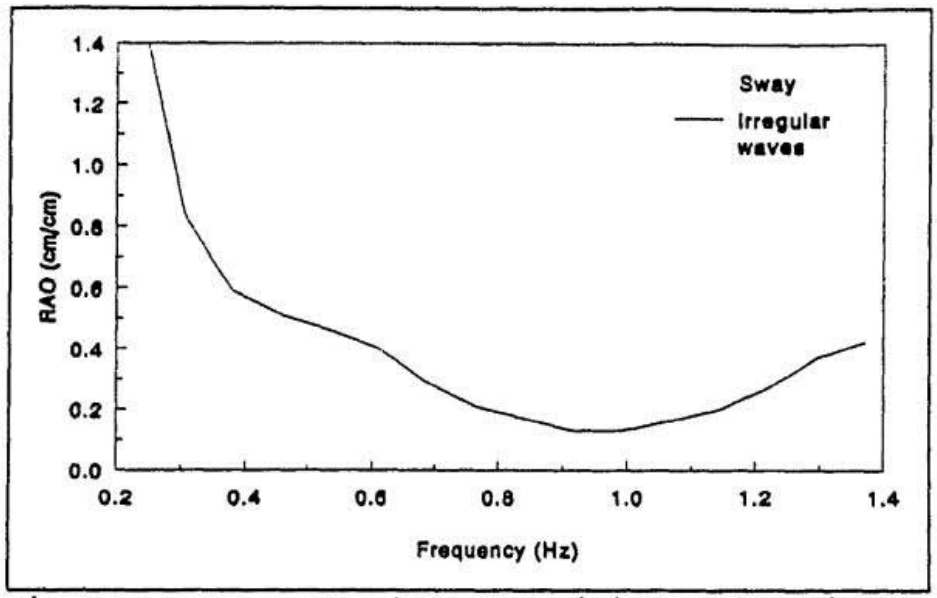

Figure D.43 - Sway: - bottom position, perpendicular orientation, with stiffer mooring lines

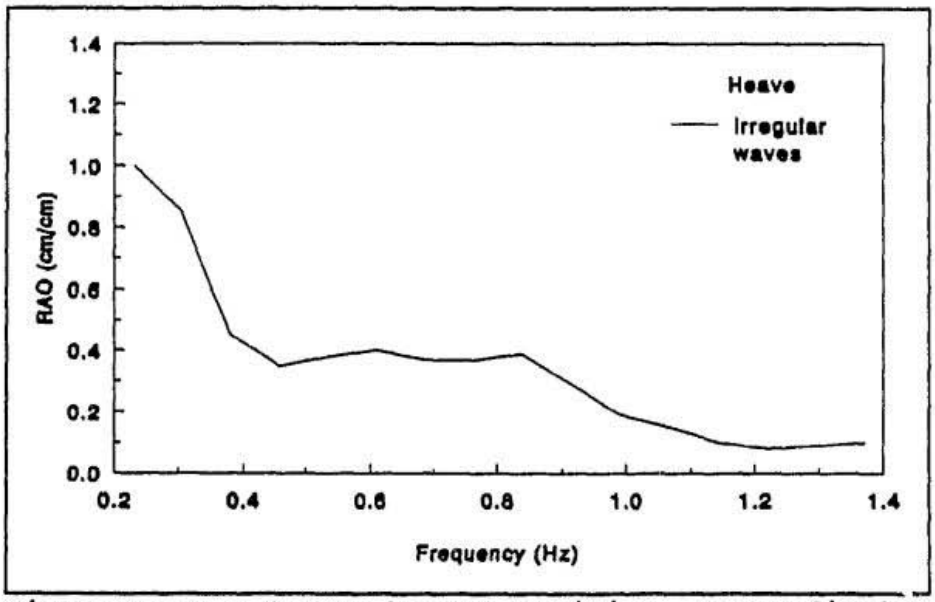

Figure D.44 - Heave: bottom position, perpendicular orientation, with stiffer mooring lines

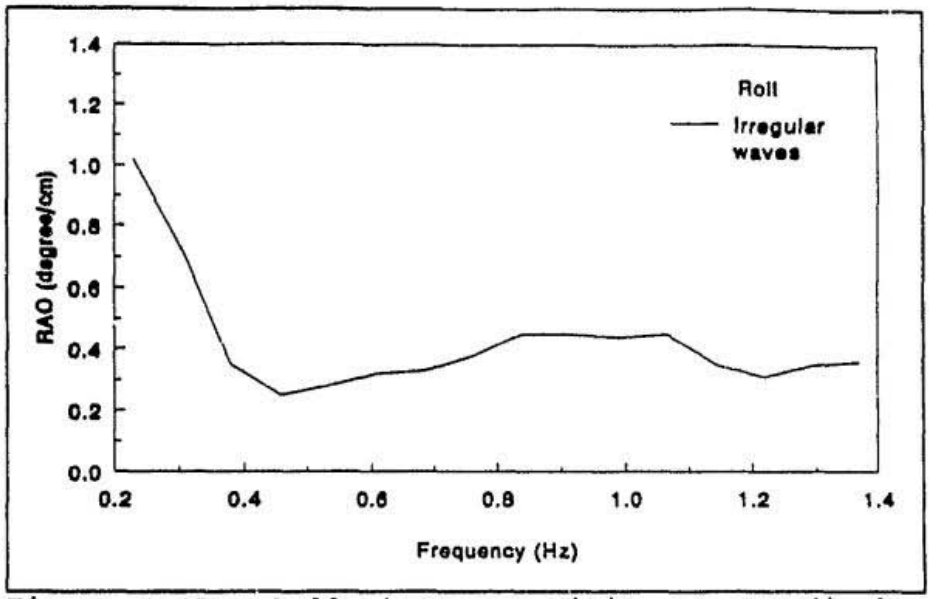

Figure D.45 - Roll: bottom position, perpendicular orientation, with stiffer mooring lines

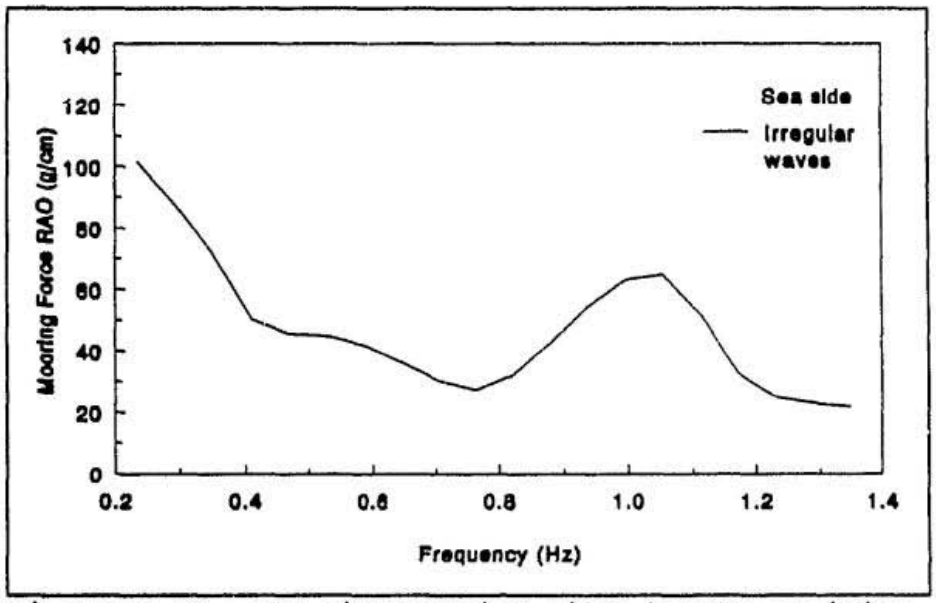

Figure D.46 - Sea side mooring line: bottom position, perpendicular orientation, with stiffer mooring lines

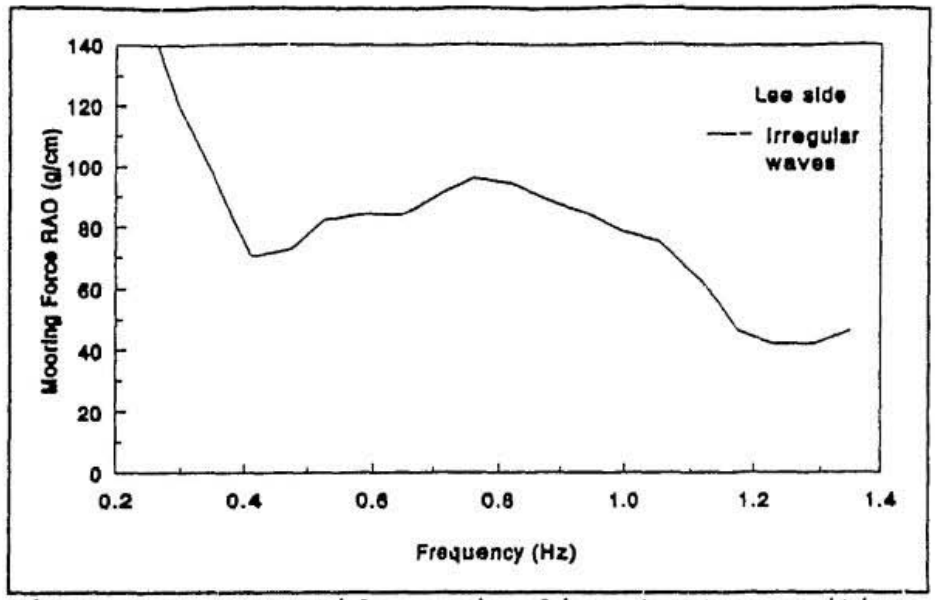

Figure D.47 - Lee side mooring line: bottom position, perpendicular orientation, with stiffer mooring lines

D.12 Middle Position, Parallel Orientation, with higher pretension (T ≈ 900 g instead of T ≈ 700 g)

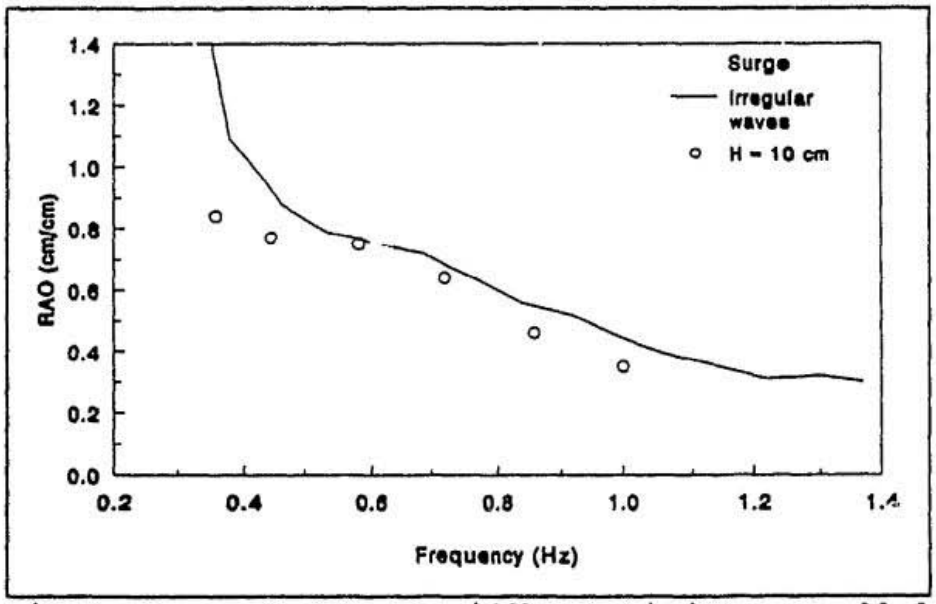

Figure D.48 - Surge: middle position, parallel orientation, with higher pretension

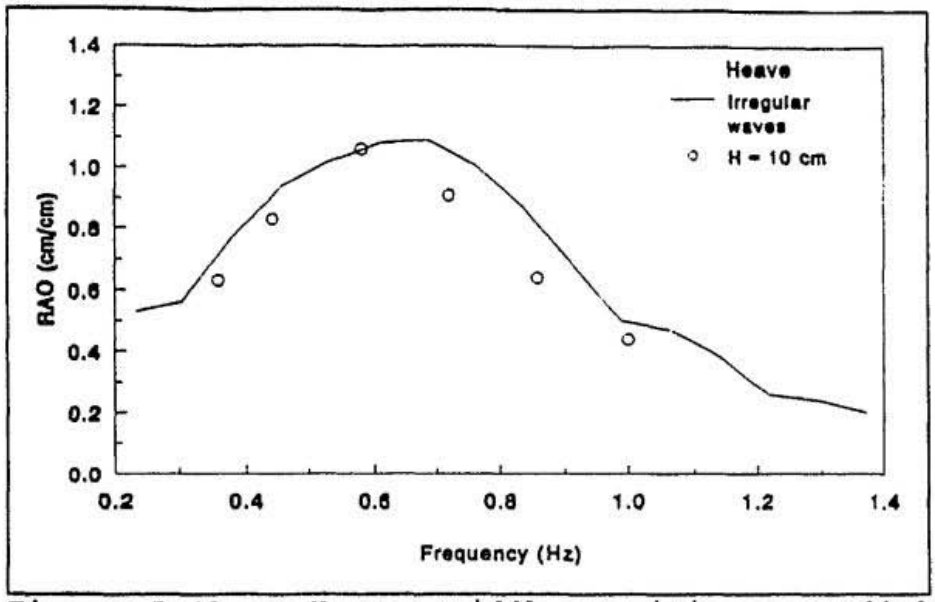

Figure D.49 - Heave: middle position, parallel orientation, with higher pretension

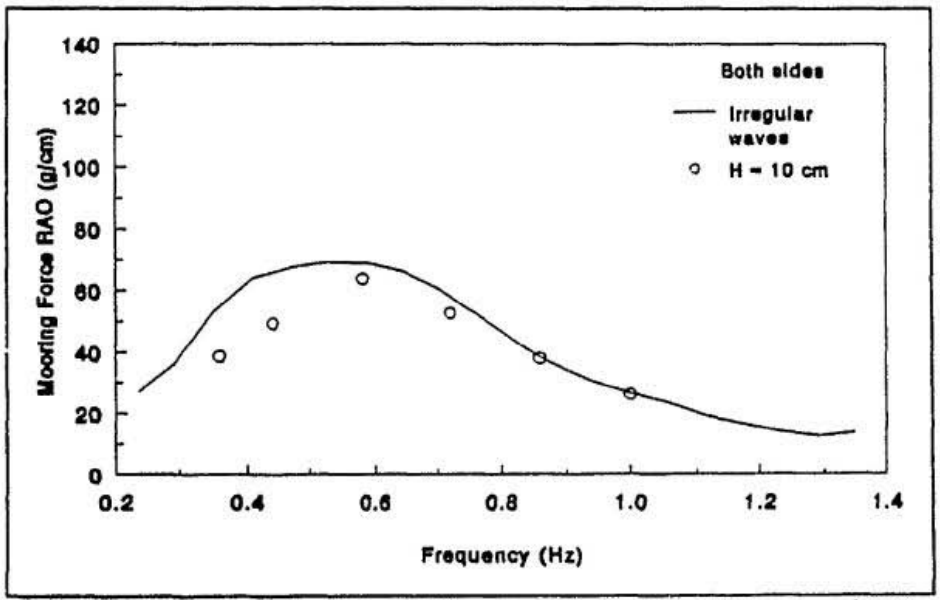

Figure D.50 - Mooring lines of both sides: middle position, parallel orientation, with higher pretension

D.13 Bottom Position, Parallel Orientation, with Higher Pretension (T ≈ 900 g instead of T ≈ 700 g)

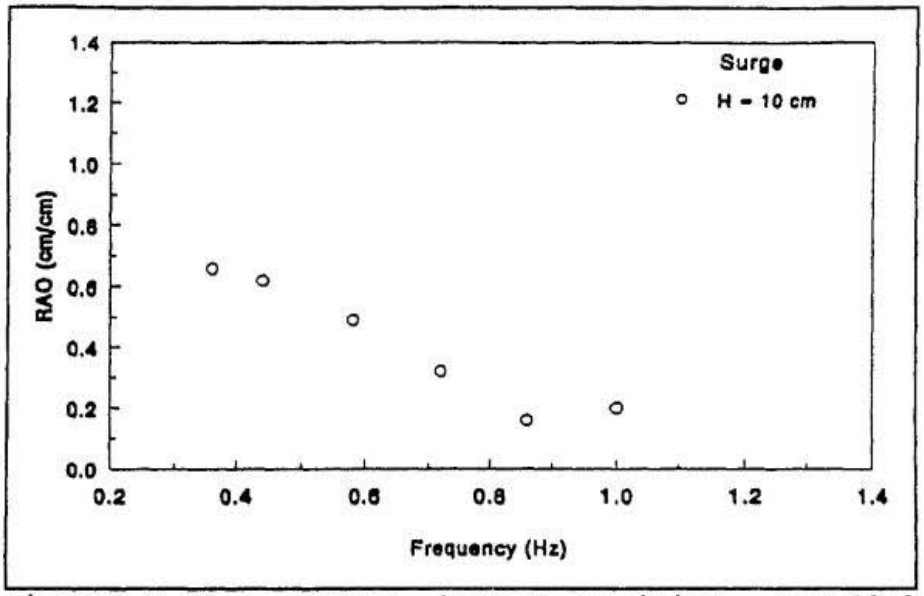

Figure D.51 - Surge: bottom position, parallel orientation, with higher pretension

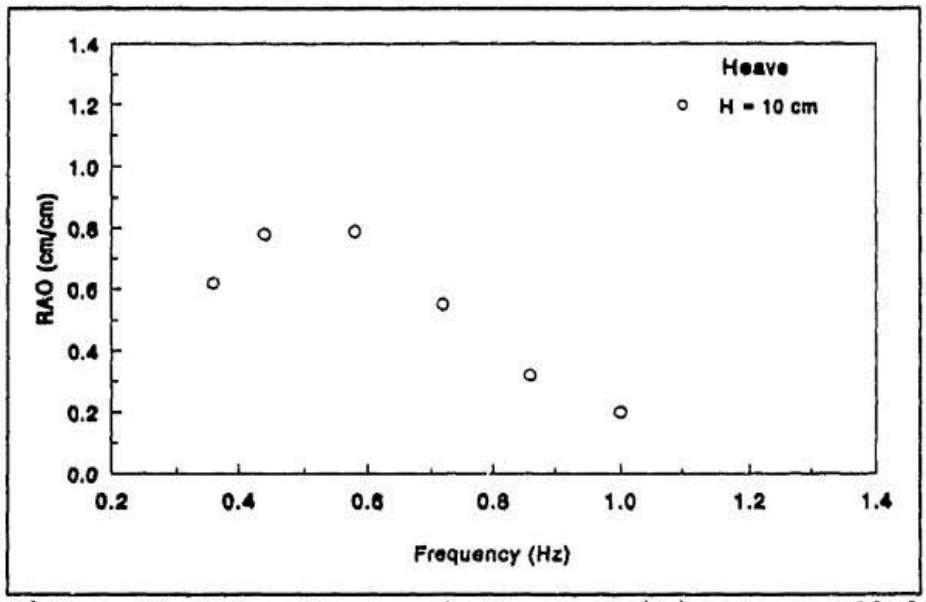

Figure D.52 - Heave: bottom position, parallel orientation, with higher pretension

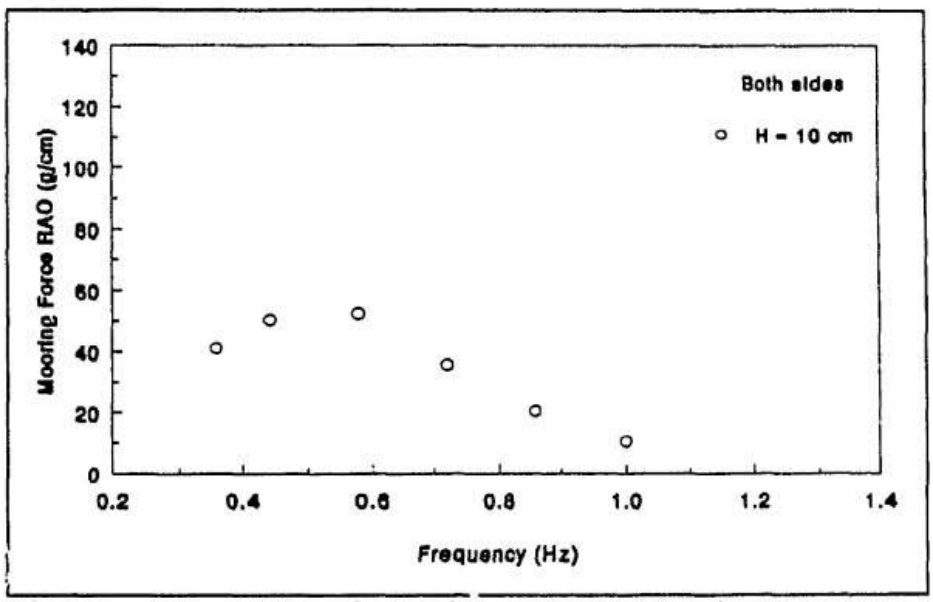

Figure D.53 - Mooring lines of both sides: bottom position, parallel orientation, with higher pretension